APPROACHES TO THE SYNTHESIS, MODELLING AND OPTIMISATION OF SPATIAL TRANSLATIONAL COMPLIANT PARALLEL MECHANISMS

Haiyang Li

Thesis submitted for the degree of

Doctor of Philosophy

NATIONAL UNIVERSITY OF IRELAND, CORK

SCHOOL OF ENGINEERING

ELECTRICAL AND ELECTRONIC ENGINEERING

November 2016

Head of School: Prof. Liam Marnane

Supervisors: Dr. Guangbo Hao and Dr. Richard C. Kavanagh

To my whole family

ABSTRACT

The main facets of designing compliant mechanisms are synthesis, modelling and optimization. This thesis focuses on these three aspects of designing compliant mechanisms with a particular emphasis on spatial translational compliant parallel mechanisms (XYZ CPMs).

In this thesis, a constraint and position identification (CPI) synthesis approach, a constraint-force-based (CFB) modelling approach and a position-space-reconfiguration (PSR) approach are proposed. Subsequently, two PSR-based optimization approaches are presented.

A large number of XYZ CPMs can be synthesized using the proposed CPI approach. Each of the synthesized XYZ CPMs can provide decoupled translations along the X-, Y- and Z-axes, and can be actuated by three ground-mounted linear actuators. Furthermore, the motion characteristics of a synthesized XYZ CPM can be analysed, based on an analytical model that can be derived using the proposed CFB approach. Such motion characteristics can include cross-axis coupling, lost motion, parasitic motion and actuation stiffness. If the motion characteristics of an XYZ CPM need to be improved, the XYZ CPM can be reconfigured using the PSR approach. For example, two PSR-based optimization approaches are detailed, which are used to reduce parasitic motions of XYZ CPMs and to reconfigure a non-symmetric XYZ CPM into a symmetric XYZ CPM, respectively. Such PSR-based optimization approaches can be employed to optimize both the geometrical dimension and the geometrical shape of an XYZ CPM. Therefore, an XYZ CPM can be synthesized using the CPI approach, modelled using the CFB approach, and then optimized using the PSR-based approaches.

In order to demonstrate the use of these proposed approaches, several examples of XYZ CPMs are synthesized, modelled and optimized. These design examples are also verified by FEA simulations and/or experimental tests. Several prototypes of the obtained XYZ CPMs are fabricated, and a control system for one of the prototypes is also presented.

It is important to note that the proposed CFB approach, PSR approach and PSR--based optimization approaches can also be employed to model, reconfigure and optimize other types of compliant mechanisms in addition to XYZ CPMs.

PUBLICATIONS ARISING FROM THIS THESIS

1. **Haiyang Li** and Guangbo Hao*, "A constraint and position identification (CPI) approach for the synthesis of decoupled spatial translational compliant parallel manipulators ", *Mechanism and Machine Theory*, vol. 90, pp. 59–83, 2015. (**This journal paper arises from Chapter 2 of this thesis**)
2. **Haiyang Li**, Guangbo Hao* and Richard Kavanagh, "A new XYZ compliant parallel mechanism for micro/nano manipulation: Design and Analysis," *Micromachines*, vol. 7, no. 2, pp. 23, 2016. (**This journal paper proposes an XYZ CPM which is systhesized using the CPI approach that is proposed in Chapter 2 of this thesis**)
3. **Haiyang Li** and Guangbo Hao*, "Constraint-Force-Based Approach of Modelling Compliant Mechanisms: Principle and Application," *Precision Engineering*, vol. 47, pp. 158-181, 2016. (**This journal paper arises from Chapter 3 of this thesis**)
4. **Haiyang Li**, Guangbo Hao* and Richard Kavanagh, "Position-space-based compliant mechanism reconfiguration approach and its application in the reduction of parasitic motion," *Journal of Mechanical Design (ASME Transactions)*, vol. 138, no. 9, pp. 092301, 10.1115/1.4033988, 2016. (**This journal paper arises from Chapter 4 of this thesis**)
5. **Haiyang Li**, Guangbo Hao* and Richard Kavanagh, "Synthesis of decoupled spatial translational compliant parallel mechanisms via freedom and actuation method (FAM)," in *ASME 2014 12th Biennial Conference on Engineering Systems Design and Analysis*, pp. V003T17A004–V003T17A004, Copenhagen, Denmark, June 25–27, 2014. (**This conference paper arises from Chapter 2 of this thesis**)
6. **Haiyang Li** and Guangbo Hao*, "Constraint-force-based (CFB) modelling of compliant mechanisms," in *ASME 2015 International Design Engineering Technical Conferences & Computers and Information in Engineering Conference*, pp. V05AT08A006, Boston, Massachusetts,

August 2–5, 2015. (**This conference paper arises from Chapter 3 of this thesis**)

7. **Haiyang Li** and Guangbo Hao*, "Compliant mechanism reconfiguration based on position space concept for reducing parasitic motion," in *ASME 2015 International Design Engineering Technical Conferences & Computers and Information in Engineering Conference*, pp. V05AT08A004, Boston, Massachusetts, August 2–5, 2015. (**This conference paper arises from Chapter 4 of this thesis, which was awarded the best interactive poster award in the MR-6 group of the IDETC/CIE 2015 conference**)
8. **Haiyang Li** and Guangbo Hao*, "Position-space-based symmetric compliant mechanism design approach and its application in the design of a high-performance spatial translational manipulator," in *ASME 2016 International Design Engineering Technical Conferences & Computers and Information in Engineering Conference*, Charlotte, North Carolina, August 21–24, 2016. (**This conference paper arises from Chapter 5 of this thesis**)

ACKNOWLEDGEMENTS

First and foremost I want to thank my primary supervisor Dr. Guangbo Hao, who gave me an opportunity to be a PhD student in University College Cork. It is my honour to be his first PhD student. He has taught me both consciously and unconsciously. I appreciate all his contributions of time, ideas and findings. Without his help, I could not get my PhD degree less than four years. I thank him for his help in both my studies and my life in Ireland.

I would like to thank my co-supervisor Dr. Richard Kavanagh, for his valuable comments on my publications including my PhD thesis and my papers. I also thank him for his valuable suggestions on how to deal with research issues properly.

Great appreciation goes to Mr. Timothy Power and Mr. Michael O'Shea. The fabrication of the prototypes, as shown in my thesis and papers, would have been impossible without their unconditional help.

For this thesis, I would like to thank my internal and external examiners: Dr. William Wright at University College Cork and Prof. Just Herder at Delft University of Technology. Because of their insightful questions and valuable comments, the thesis has been improved.

My time at University College Cork was made enjoyable in large part due to the many friends and colleagues. I would like to specially thank Alison O'Shea, Brian Michael Murphy, Megan Flanders, Oksana Semenova, Rehan Ahmed, Shima Gholinezhadasnefestani and Wentao Jiang, for their help, encouragement and friendship. They became an important part of my life, and the time spent with them will be in my memories forever.

My best thanks and wishes are given to my family members, my father Yunfu Li, my mother Guanghui Bai, my wife Jiao Meng, my brother Haitao Li, my sister in law Junjie Guo, my sister Xiaomin Li, my niece Shiyao Li and my

daughter Mengyin Li, for their love, support and care. A special thank goes to my wife because I would not have been able to come to this point in my life without her love and sacrifices.

Last but not the least, I gratefully acknowledge Irish Research Council (IRC) for awarding an IRCSET Embark PhD scholarship (RS/2012/361) to me, which made my PhD work possible.

DECLARATION

I hereby declare that this is entirely my own work and that it has not been submitted for another degree, either at University College Cork or elsewhere.

Signed:_____

Date:_____

Haiyang Li

University College Cork

LIST OF CONTENTS

List of Abbreviations and Acronyms

AFM	Atomic-force microscopy
AM	Actuated module
AS	Actuated stage
BCM	Basic compliant module
BS	Base stage
C-BCM	Combined-BCM
CFB	Constraint-force-based
CPI	Constraint and position identification
CPM	Compliant parallel mechanism
DOC	Degrees of constraint
DOF	Degrees of freedom
DTBCM	Double-two-beam compliant module
FACT	Freedom and constraint topologies
FBCM	Four-beam compliant module
FBD	Free-body-diagram
ICM	Independent compliant module
MEMS	Microelectromechanical system
MRS	Mobile rigid stage
MS	Motion stage
NBCM	Non-basic compliant module
PM	Passive module
PSR	Position-space-based reconfiguration
PSR-RPM	PSR-based approach to reduce parasitic motions
PSR-SCM	PSR-based approach to design symmetric compliant mechanisms
RL	Rigid linkage
TBCM	Two-beam compliant module
XYZ CPM	Spatial translational compliant parallel mechanism

LIST OF NOMENCLATURE

$\boldsymbol{\zeta}_{*}$	General wrench vector for representing forces
$\boldsymbol{f}_{\mathrm{T}*}$	Translational-force vector
$\boldsymbol{f}_{\mathrm{R}*}$	Rotational-force vector
$\boldsymbol{r}_{*}$	Wrench location vector
q_{*}	Wrench pitch
$\boldsymbol{\zeta}_{*\text{-tx}}$	Principal wrench along X-axis
$\boldsymbol{\zeta}_{*\text{-ty}}$	Principal wrench along Y-axis
$\boldsymbol{\zeta}_{*\text{-tz}}$	Principal wrench along Z-axis
$\boldsymbol{\zeta}_{*\text{-rx}}$	Principal wrench about X-axis
$\boldsymbol{\zeta}_{*\text{-ry}}$	Principal wrench about Y-axis
$\boldsymbol{\zeta}_{*\text{-rz}}$	Principal wrench about Z-axis
$\zeta_{*\text{-tx}}$	Principal wrench coefficient along X-axis
$\zeta_{*\text{-ty}}$	Principal wrench coefficient along Y-axis
$\zeta_{*\text{-tz}}$	Principal wrench coefficient along Z-axis
$\zeta_{*\text{-rx}}$	Principal wrench coefficient about X-axis
$\zeta_{*\text{-ry}}$	Principal wrench coefficient about Y-axis
$\zeta_{*\text{-rz}}$	Principal wrench coefficient about Z-axis
$\boldsymbol{\zeta}_{\mathrm{C}*}$	Special wrench vector for representing constrains
$\kappa_{*\text{-tx}}$	Constraint coefficient along X-axis
$\kappa_{*\text{-ty}}$	Constraint coefficient along Y-axis
$\kappa_{*\text{-tz}}$	Constraint coefficient along Z-axis
$\kappa_{*\text{-rx}}$	Constraint coefficient about X-axis
$\kappa_{*\text{-ry}}$	Constraint coefficient about Y-axis
$\kappa_{*\text{-rz}}$	Constraint coefficient about Z-axis
$j_{*\text{-tx}}$	Direction coefficient along X-axis

$j_{*\text{-ty}}$	Direction coefficient along Y-axis
$j_{*\text{-tz}}$	Direction coefficient along Z-axis
$j_{*\text{-rx}}$	Direction coefficient about X-axis
$j_{*\text{-ry}}$	Direction coefficient about Y-axis
$j_{*\text{-rz}}$	Direction coefficient about Z-axis
$\boldsymbol{\xi}_{*}$	General twist vector for representing displacements
$\boldsymbol{v}_{\text{T}*}$	Translational-motion vector
$\boldsymbol{v}_{\text{R}*}$	Rotational-motion vector
$\boldsymbol{c}_{*}$	Twist location vector
p_{*}	Twist pitch
$\boldsymbol{\xi}_{*\text{-tx}}$	Principal twist along X-axis
$\boldsymbol{\xi}_{*\text{-ty}}$	Principal twist along Y-axis
$\boldsymbol{\xi}_{*\text{-tz}}$	Principal twist along Z-axis
$\boldsymbol{\xi}_{*\text{-rx}}$	Principal twist about X-axis
$\boldsymbol{\xi}_{*\text{-ry}}$	Principal twist about Y-axis
$\boldsymbol{\xi}_{*\text{-rz}}$	Principal twist about Z-axis
$\xi_{*\text{-tx}}$	Principal twist coefficient along X-axis
$\xi_{*\text{-ty}}$	Principal twist coefficient along Y-axis
$\xi_{*\text{-tz}}$	Principal twist coefficient along Z-axis
$\xi_{*\text{-rx}}$	Principal twist coefficient about X-axis
$\xi_{*\text{-ry}}$	Principal twist coefficient about Y-axis
$\xi_{*\text{-rz}}$	Principal twist coefficient about Z-axis
$\mathbf{T}_{*}$	Coordinate transformation matrix
$\mathbf{R}_{*}$	Rotation matrix
$\mathbf{D}_{*}$	Location skew-symmetric matrix
$\left(x_{*}, y_{*}, z_{*}\right)$	Coordinates of a point in a coordinate system

E_*	Young's modulus
G_*	Shear modulus
J_*	Torsional constant
v_*	Poisson's ratio
I_*	Moment of inertia of cross-section area
L_*	Beam length
t_*	Normalized beam thickness
w_*	Normalized cube's width
$\mathrm{K}_*(\cdot)$	Variable vector
$\mathbf{k}_*$	Stiffness matrix
α_*, β_*, γ_*	Angles

Note that subscript "*" in each of the nomenclatures can be replaced by a number of characters or an empty string.

LIST OF FIGURES

LIST OF TABLES

1 INTRODUCTION

In this chapter, compliant mechanisms are introduced, and then existing approaches to the design of compliant mechanisms are reviewed. Based on the challenges of the existing approaches, the scope and aim of this thesis are proposed. Finally, the contributions of this thesis are summarized.

1.1 Compliant Mechanisms

A mechanism is a device which is designed to transform input forces and displacements into desired output forces and displacements. Traditionally, when designers needed a mechanism to achieve some mechanical tasks, they commonly employed mechanisms that are assemblies of rigid parts connected with rigid joints such as rigid sliding joints and rigid rolling joints. Such mechanisms are termed as the rigid-body mechanisms. The motions of a rigid-body mechanism are performed through the operation of the rigid joints. However, it can be seen that a large number of moving things in nature are flexible, and the movements are made through the bending of their compliant members. Our hearts are such moving things, which can work for every minute over our entire lives. A few other examples of living objects with compliant members include sea weed, bee wings, bat wings, eels and elephant trunks.

If a device transmits or transforms input forces and displacements into a required set of output forces and displacements by means of the elastic deformation of its flexible members rather than rigid joints, the device is termed a compliant mechanism [1-7]. Wire-beams are fundamental flexible members used in compliant mechanisms. The deformation of a wire-beam depends on

the boundary conditions and the applied forces. Taking a cantilever wire-beam as an example, the free end can easily perform two translations and three rotations about the three axes of a coordinate system located along the beam, under different applied forces (translational and rotational forces); however, it is hard to perform a translation along the wire-beam. If the stiffness along or about one axis is defined as the ratio of the applied force to the associated deformation along or about the axis, the stiffness of the cantilever wire-beam along the wire-beam is much larger compared with the stiffness along or about the other directions. Therefore, the direction along the wire-beam is regarded as the DOF (degree of freedom) direction, and the other directions are regarded as the DOC (degree of constraint) directions. In addition, the deformations of the free end of a wire-beam can be calculated on the basis of the Euler-Bernoulli beam equation.

The last decade has witnessed the rapid development of compliant mechanisms, because such mechanisms have many advantages compared with traditional rigid-body mechanisms. These advantages include reduced number of parts, reduced product weight, minimized assembly requirements, ability to miniaturize, no need for lubrication, no friction, no backlash and ease of fabrication [1-7]. In addition, a compliant mechanism can be constructed of any type of material including smart and active materials, and can be actuated by modern actuators such as piezoelectric, shape-memory alloy, electro-thermal, electrostatic, fluid pressure and electromagnetic actuators.

For example, Figure 1.1 shows one rigid-body clip and two compliant clips (termed compliant clip-I and compliant clip-II). The rigid-body clip, as shown in Figure 1.1(a), carries out its clamping motion through performing the rigid rolling joint. This rigid rolling joint can be replaced by a compliant rolling joint, and such design examples can be seen in Figure 1.1(b) and Figure 1.1(c). Note that the rigid rolling joints of the compliant clip-I are not employed to perform the clamping motion. Compared with the rigid-body clip, the compliant clips,

especially the one shown in Figure 1.1(c), have many advantages such as reduced number of parts, reduced product weight, minimized assembly requirements and ease of fabrication.

Due to their advantages, compliant mechanisms have been experiencing a rapid increase in use in various applications, and some typical applications can be seen in Table 1.1.

Table 1.1 Main applications of compliant mechanisms

Application fields	Application examples
Nano-/micro-manipulation [8-20]	An XY compliant mechanism for nano-positioning, as shown in Figure 1.2
Small-scale devices [21-28]	Microelectromechanical systems (MEMS), as shown in Figure 1.3
Energy harvesting and sensors [29-35]	An electromagnetic generator, as shown in Figure 1.4
Medical devices [36-41]	A smart knee brace, as shown in Figure 1.5
Smart materials [42-46]	A compliant wing, as shown in Figure 1.6 A compliant mechanism based material with negative Poisson's ratio, as shown in Figure 1.7
Robots [47-52]	A insect-scale flying robot, as shown in Figure 1.8
Consumer products [53]	Compliant clips, as shown in Figure 1.1

(a) (b) (c)

Figure 1.1 Rigid and compliant clips: (a) rigid-body clip, (b) compliant clip-I, and (c) compliant clip-II

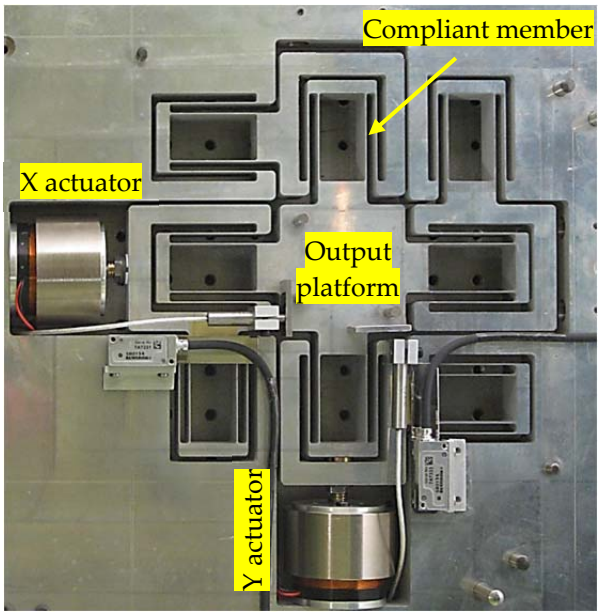

Figure 1.2 An XY compliant mechanism for nano-positioning [20]

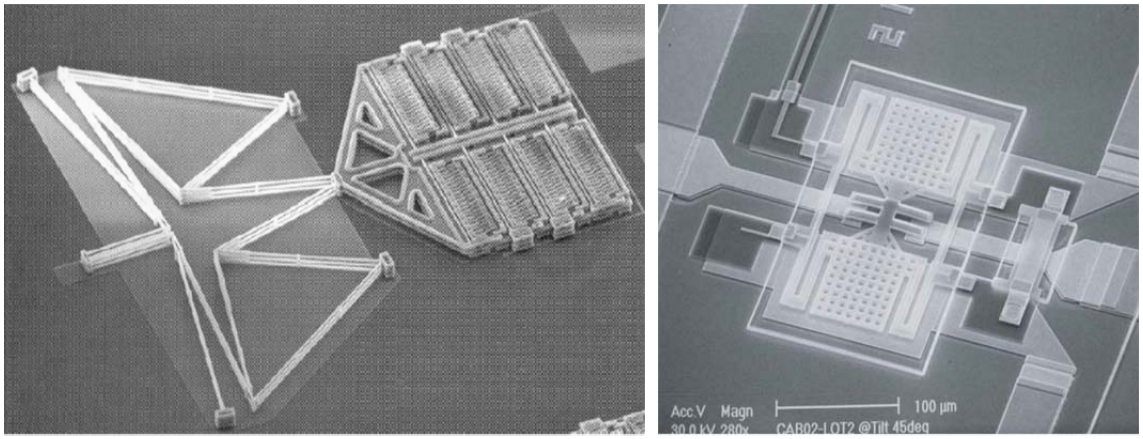

Figure 1.3 Applications of compliant mechanisms in MEMS: (a) a MEMS actuation system [22], and (b) a MEMS switch [26]

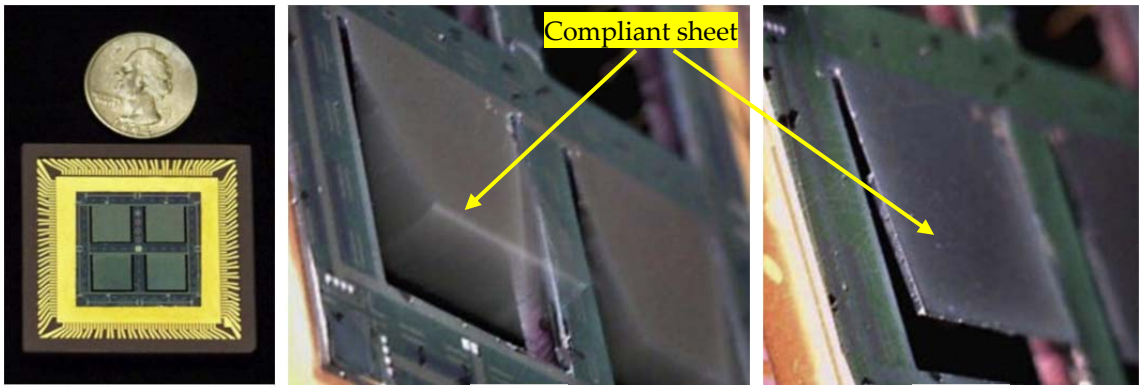

(a) (b) (c)

Figure 1.4 A compliant mechanism based vibration powered electromagnetic generator [32]: (a) electromagnetic generator, (b) and (c) the compliant sheets at different positions

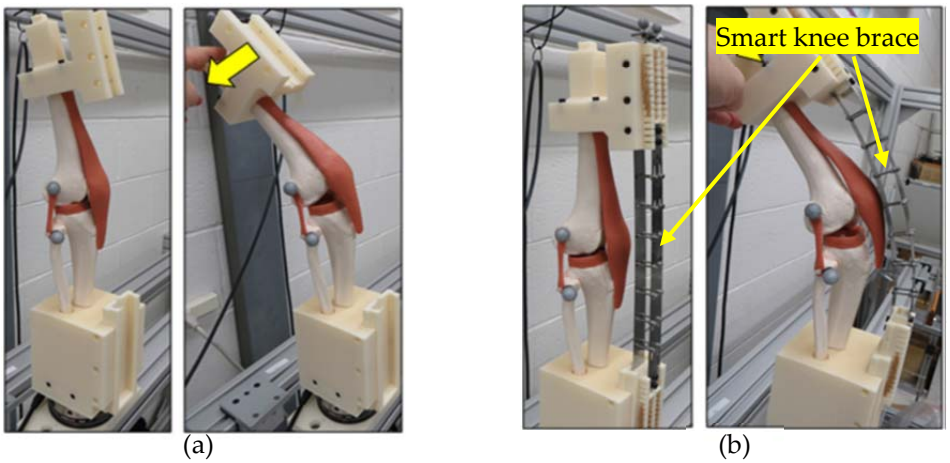

Figure 1.5 A compliant mechanism based smart knee brace [39]: (a) prototype model without brace, and (b) prototype model with brace

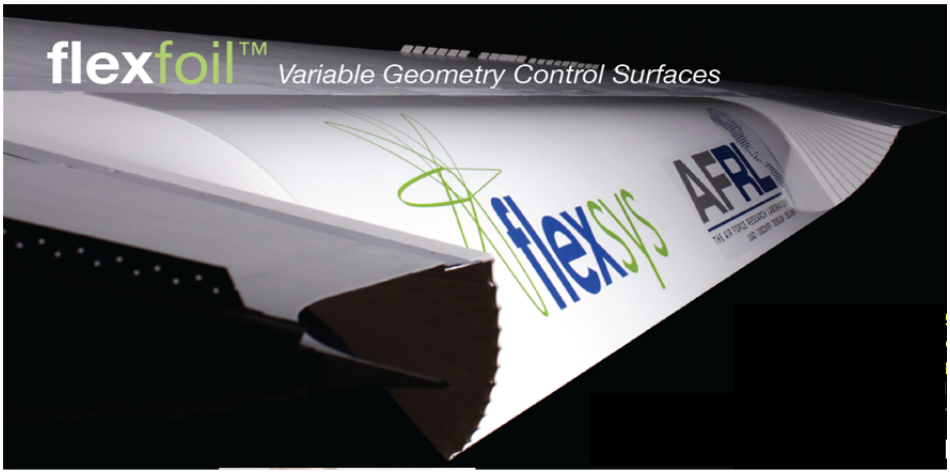

Figure 1.6 A compliant mechanism based smart aircraft wing

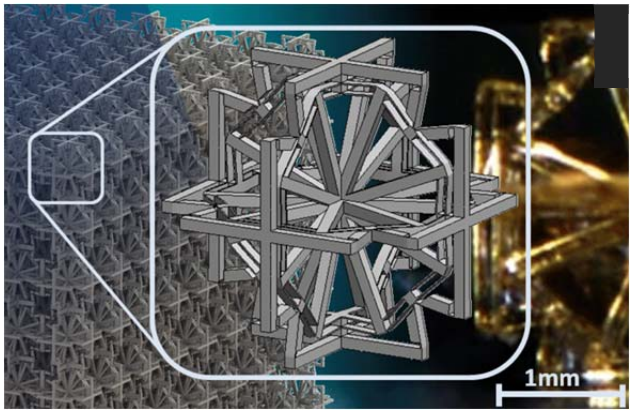

Figure 1.7 Compliant mechanism based material with negative Poisson's ratio (Courtesy of Prof. Jonathan B. Hopkins, in UCLA)

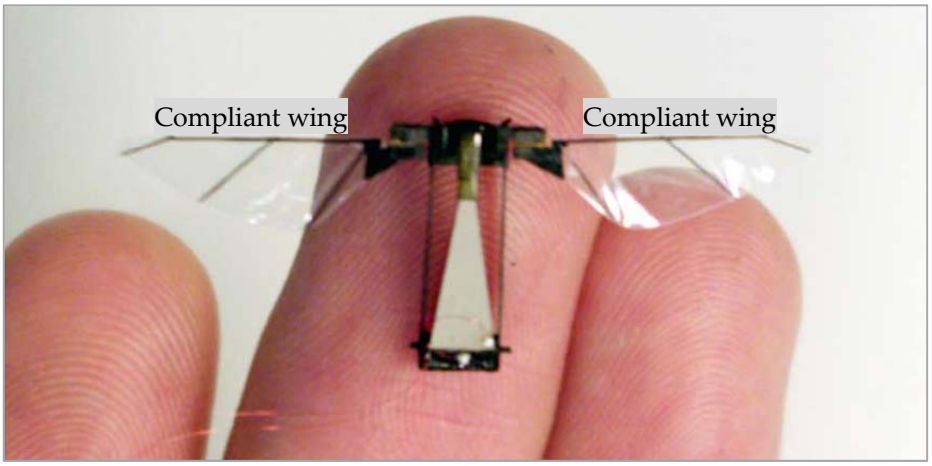

Figure 1.8 A compliant mechanism based insect-scale flying robot [51]

1.2 Review of Compliant Mechanism Design

1.2.1 Design process

As mentioned in Section 1.1, compliant mechanisms are widely used in many applications due to their advantages over traditional rigid-body mechanisms. However, it is difficult for designers to find enough resources to guide them to design compliant mechanisms [3, 7]. A rigid-body mechanism can accomplish its movements by its different rigid-body parts. However, a compliant mechanism should be able to achieve its complex tasks using its very few compliant parts, or even only one compliant part [7]. Moreover, it usually requires designers to consider motion and force behaviours simultaneously in the design of compliant mechanisms. Therefore, the design of compliant mechanisms is more difficult compared with that of rigid-body mechanisms.

A compliant mechanism should be designed under specific design requirements. The design requirements are different from case to case, while some general requirements for designing a compliant mechanism can be seen below [20].

i. The most important design requirement is to meet the required number and directions of DOF or DOC. In contrast to rigid-body mechanisms,

the stiffness of a compliant mechanism is neither zero in its DOF directions nor infinitely large in its DOC directions. Consequently, the design of a compliant mechanism requires that the stiffness of the compliant mechanism along the DOC directions should be much larger than that along the DOF directions.

ii. Another important design requirement is to meet the required motion accuracy within the required motion ranges. Compliant mechanisms can provide motions with high repeatability because they are free of backlash. However, due to the stiffness characteristics of compliant mechanisms mentioned above, compliant mechanisms always suffer from parasitic motions[1] which affect their motion accuracy. Therefore, when designing a compliant mechanism, the parasitic motions should be minimized or eliminated. Additionally, the cross-axis coupling[2] and lost motions[3] of the compliant mechanism should also be reduced, because the cross-axis coupling and lost motions also affect the motion accuracy of the compliant mechanism.

iii. Stiffness variation along the DOF and DOC directions, resulting from the displacement changes, should meet the static and dynamic design

---

[1] A parasitic motion of a compliant mechanism is a motion of the compliant mechanism along or about a DOC direction of the compliant mechanism.

[2] The cross-axis coupling of a compliant mechanism, in this thesis, refers to the motions in the DOF directions. This specifically means that a motion of a multi-axis output motion stage along one DOF direction is affected by that along the other DOF directions. For a nominal decoupled compliant mechanism, the cross-axis coupling results from the parasitic motions of the compositional compliant modules.

[3] A lost motion of a compliant mechanism, in this thesis, represents the difference between an input displacement and the associated output displacement. Such a lost motion of a nominal decoupled compliant mechanism results from the parasitic motions of the compositional compliant modules.

requirements. When designing a control system for a compliant mechanism, the control system should be robust against the stiffness variation of the compliant mechanism.

iv. Manufacturability and compactness should also meet the design requirements. It is desirable that a compliant mechanism can be designed and manufactured monolithically.

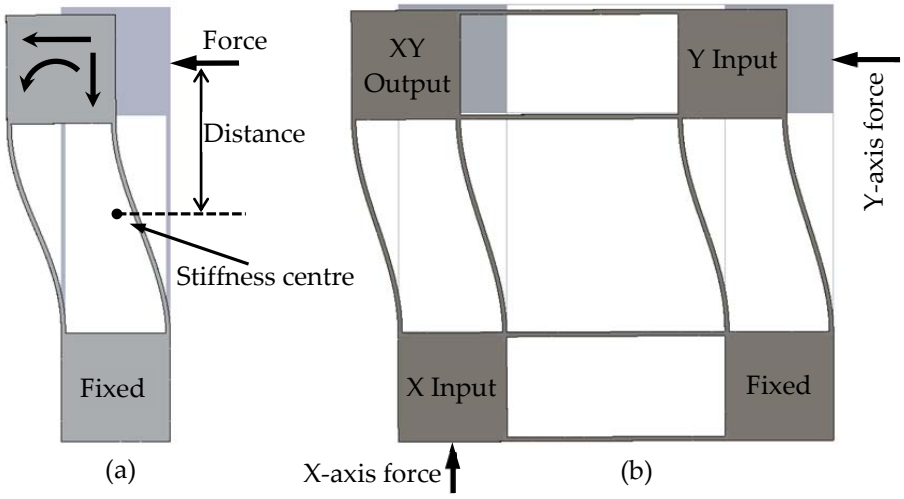

Figure 1.9 Deformation demonstration of compliant mechanisms: (a) deformation of a basic (planar) parallelogram compliant mechanism, and (b) deformation of an XY compliant mechanism

The above-mentioned parasitic motion, cross-axis coupling and lost motion can be demonstrated by an example, as shown in Figure 1.9. Figure 1.9(a) shows a basic parallelogram compliant mechanism. There is a point position in the beams' geometrical centre of the basic parallelogram compliant mechanism, as shown in Figure 1.9(a). If an actuation force, applied on the mobile stage, goes through this point, it will not produce a rotational displacement of the basic parallelogram compliant mechanism. The point position is termed the stiffness centre of the basic parallelogram compliant mechanism [54-56]. The force-displacement relationship of the basic parallelogram compliant mechanism with respect to the stiffness centre shows that the translations are decoupled from the rotation, which means the linear stiffness matrix with respect to the stiffness centre is a diagonal matrix.

If an actuation force is applied at another position shown in Figure 1.9(a), it will result in a torque relative to the stiffness centre, so that the mobile end of the basic parallelogram compliant mechanism will not only have a translation but also a rotation. The rotation is the parasitic rotation of the basic parallelogram compliant mechanism, because it is in the DOC direction of the parallelogram compliant mechanism. In addition, the vertical distance between the two ends of the basic parallelogram compliant mechanism decreases when the free end has a horizontal translation. In other words, the free end has a vertical translation and a horizontal translation at the same time. The vertical translation is the parasitic translation of the basic parallelogram compliant mechanism, because it is also in the DOC direction of the parallelogram compliant mechanism. The parasitic rotation and parasitic translation are parasitic motions of the basic parallelogram compliant mechanism, which are much smaller than the horizontal translation (the horizontal translation is usually termed as the primary translation).

Figure 1.9(b) shows a nominal decoupled XY compliant mechanism, whose primary motions are the translations of the XY output stage along the X- and Y-axes, the translation of the X input stage along the X-axis, and the translation of the Y input stage along the Y-axis. It can be seen that the XY compliant mechanism consists of four basic parallelogram compliant mechanisms. Because each of the basic parallelogram compliant mechanisms has a parasitic rotation and a parasitic translation, the XY compliant mechanism has parasitic motions including the rotations of both the input and output stages, the translation of the X input stage along the Y-axis, and the translation of the Y input stage along the X-axis.

If only a Y-axis actuation force is applied, the primary translation of the Y input stage is a little bit larger than the primary translation of the XY output stage along the Y-axis. The difference between the two translations is the lost motion of the XY compliant mechanism along the Y-axis. The lost motion happens due

to the fact that the compliant module located between the Y input stage and XY output stage has a parasitic translation along the Y-axis. Moreover, the XY output stage also has a tiny translation along the X-axis under the actuation of Y-axis actuation force only. That is to say, the X-axis and Y-axis motions of the XY output stage are coupled. This cross-axis coupling also results from the parasitic motions of the XY compliant mechanism. Therefore, both the lost motion and the cross-axis coupling are caused by the parasitic motions of the associated compositional compliant modules.

According to the general design requirements summarized above, the best available process for compliant mechanism design is probably a combination of synthesis, modelling and optimization [20]. Consequently, these topics have been active research areas in terms of compliant mechanism design.

1.2.2 Existing design approaches and their challenges

As mentioned in Section 1.2.1, the process of designing a compliant mechanism includes synthesis, modelling and optimization. Therefore, design approaches for implementing compliant mechanisms are the approaches to the synthesis, modelling and optimization of such mechanisms. The existing approaches and their challenges are introduced in this section.

1.2.2.1 Type synthesis: approaches and challenges

The constraint-based approach is widely used to synthesize compliant mechanisms [55, 57-59]. This approach is based on the concepts [57-59]: (a) the mobility of a given rigid stage is determined by the locations and orientations of the constraint elements, such as wire-beams, applied on it; and (b) one non-redundant 1-DOC constraint element removes one DOF from the given rigid stage. A compliant mechanism can be synthesized using the constraint-based approach by selecting appropriate constraint elements and identifying their locations and orientations [55]. Such selection and identification rely heavily on designers' creative thinking and experience [55], so it is hard for beginners to

synthesize new compliant mechanisms using the constraint-based approach.

The screw-theory-based approach, as proposed in [60-65], can mathematically identify the locations and orientations of the required constraint elements in a compliant mechanism. Moreover, this screw-theory-based approach does not require any design experience, so it can be used by both experts and beginners. However, if using the screw-theory-based approach to synthesize a complex compliant mechanism, the associated mathematical expressions can be complicated.

References [66, 67] introduce a synthesis approach called freedom and constraint topologies (FACT). The FACT approach represents the mathematics of screw theory by a comprehensive library of geometrical shapes which is shown in Figure 1.10. When synthesizing a compliant mechanism, the geometrical shapes show the possible permitted selections of constraint elements. The FACT approach enables designers to visualize and determine the general geometrical forms of the compliant mechanisms so as to accomplish required motions. However, the FACT approach usually does not take actuator isolation into account (actuator isolation is defined in [55]).

Optimization-based approaches, such as the topology-optimization-based approach and the module optimization approach, can also help designers to synthesize novel compliant mechanisms, even though the designers may not have any relevant design experience [68-74]. However, these optimization-based approaches often result in a narrow family of designs because of their specific design spaces [20].

When some basic compliant mechanisms have been synthesized using the approaches introduced above, one can adopt these basic compliant mechanisms to synthesize other compliant mechanisms using the rigid-body-replacement-based approach, as reported in [3, 75, 76]. If a rigid-body mechanism already exists, a compliant mechanism can be synthesized by replacing the rigid

components of the rigid-body mechanisms with corresponding basic compliant mechanisms designed previously, based on the rigid-body-replacement-based approach. The resulting compliant mechanism has the same DOF as the rigid-body mechanism. The rigid-body-replacement-based approach is a useful and practical approach for the synthesis of compliant mechanisms, but this approach usually leads designers to generate compliant mechanisms that are characterized by the associated rigid-body mechanisms.

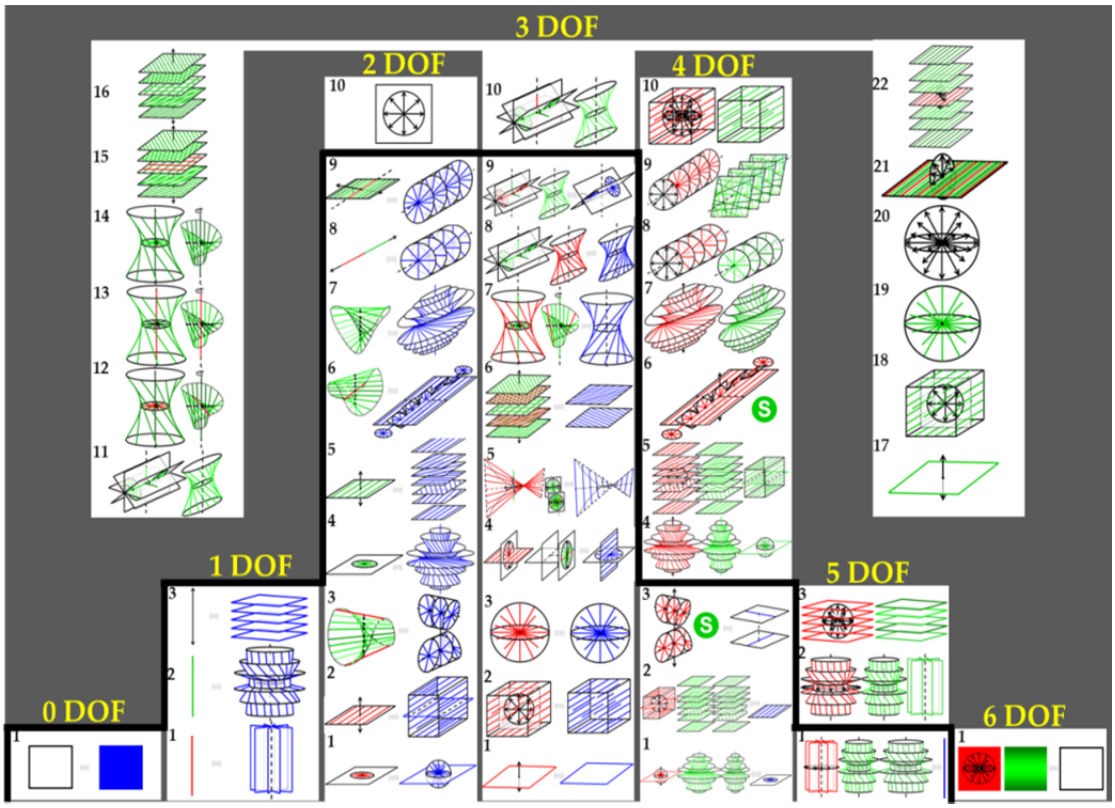

Figure 1.10 Library of freedom and constraint spaces in the FACT approach (Courtesy of Prof. Jonathan B. Hopkins, in UCLA)

1.2.2.2 Analytical modelling: approaches and challenges

Numerous works have been conducted on modelling compliant mechanisms [3, 55, 56, 77-84]. There are two main system-level approaches to model compliant mechanisms, one is the free-body-diagram (FBD)-based approach used in [55], and the other is the energy-based approach, using the virtual work principle employed in [79, 85]. Compared with the FBD-based modelling approach, the energy-based approach can simplify compliant mechanism modelling through

ignoring some internal variables. However, the ignored internal variables may be needed to estimate the motion characteristics of the modelled compliant mechanisms. Awtar [20] also claims that it is very difficult to derive an inverse relationship using the energy based approach. The analytical model of a compliant mechanism, derived using the FBD-based modelling approach, can be used not only to predict the motion characteristics but also to analyse the effects of all the variables (including the internal variables) on the motion characteristics.

When using the FBD-based modelling approach to model a compliant mechanism non-linearly, the deformed configuration of the compliant mechanism should be obtained. It is hard to model complex compliant mechanisms non-linearly using the FBD-based modelling approach, because it is difficult to obtain the deformed configuration and the associated mathematical expressions. The FBD-based modelling approach can be easily used to model a compliant mechanism linearly, because the deformed configuration of the compliant mechanism does not need to be known. However, the linear model of a compliant mechanism is valid only for very small displacements [77].

1.2.2.3 Structure optimization: approaches and challenges

The analytical model of a compliant mechanism can be used not only to predict the motion characteristics of the compliant mechanisms, but also to obtain the relationships between the geometrical parameters and the motion characteristics. Therefore, the analytical model of a compliant mechanism can be used to optimize the geometrical parameters so that the motion characteristics are improved. Both the geometrical dimension and the geometrical shape of a compliant mechanism can be optimized by optimizing the geometrical parameters. However, the author is unaware of an optimization approach that simultaneously allows consideration of the geometrical dimension and the geometrical shape of a compliant mechanism. Therefore, an

optimization approach which can optimize both geometrical dimensions and the geometrical shapes of compliant mechanisms is desired.

1.3 Scope and Aim of This Thesis

Compliant mechanisms can be classified into different types which should be designed based on different requirements. Therefore, it is better to use different design approaches (synthesis, modelling and optimization approaches) to design different types of compliant mechanisms. This thesis focuses on the design of spatial translational compliant parallel mechanisms (XYZ CPMs), and the main aim of this thesis is to develop approaches to the synthesis, modelling and optimization of XYZ CPMs.

1.3.1 Scope: XYZ CPMs

Serial kinematic configuration and parallel kinematic configuration are two well-known configurations used in the design of compliant mechanisms [20]. Each of the kinematic configurations has its own pros and cons. A serial kinematic compliant mechanism can be designed by stacking several compliant modules[4] in series, and each of the compliant modules achieves some of the required motions of the compliant mechanism. The compliant modules in a serial kinematic compliant mechanism are independent of each other, so they

[4] A compliant module is a compliant compositional part of a compliant mechanism (also known as a sub-compliant mechanism), which includes flexible members and their rigid linkages. Therefore, a compliant module can be a single wire beam, a single sheet, or a combination of wire beams, sheets, and their rigid linkages. In addition, compliant modules are divided into two types, basic compliant modules (BCMs) and non-basic compliant modules (NBCMs). If a compliant module contains only one basic compliant element, the compliant module is a BCM; otherwise, the compliant module is a NBCM. A wire beam, a sheet beam, a short beam, a notch hinge and a split tube are BCMs. A NBCM is composed of several BCMs in a serial, parallel or hybrid configuration.

can be designed separately [20]. Additionally, all the compliant modules of a serial kinematic compliant mechanism can be actuated by different actuators, so that the control system design can also be relatively simple. However, the most undesirable feature of a serial kinematic compliant mechanism is that most actuators of the serial kinematic compliant mechanism move with the associated compliant modules. Such moving actuators affect the dynamic performance of the compliant mechanism and the application of the compliant mechanism in some fields such as MEMS. Parallel kinematic compliant mechanisms (usually called compliant parallel mechanisms (CPM)) are free of this problem because actuators of CPMs can be mounted on the ground (the actuators are called ground-mounted actuators). However, it is a challenge to design a CPM with desired motion characteristics such as reduced cross-axis coupling, decreased lost motions and minimized parasitic motions. Therefore, this thesis focuses on the development of the approaches to the synthesis, modelling and optimization of CPMs rather than serial kinematic compliant mechanisms. XYZ CPMs are a type of CPMs, which are mainly studied in this thesis, because such CPMs are gaining more and more attention due to their successful applications.

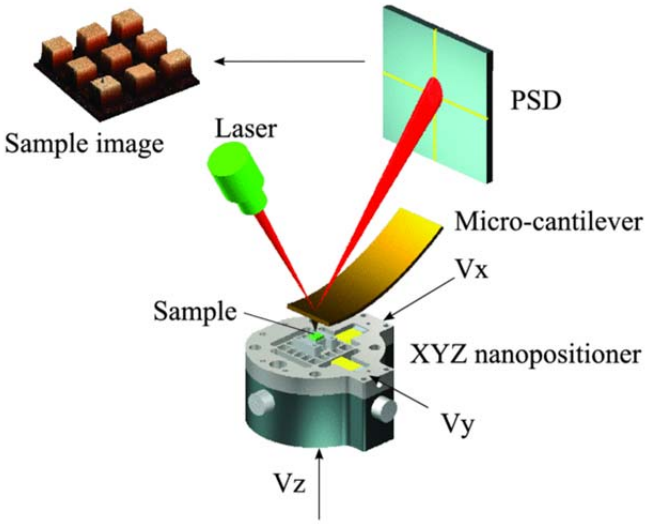

Figure 1.11 Operating principle of an AFM [18] (Courtesy of Prof. Y. K. Yong)

XYZ CPMs are suitable for a wide range of 2D and 3D nano- and micro-manipulation applications. They can be used in various applications such as

nano-/micro-assembly, optical component alignment, metrology applications, 3-axis force sensors, microscopy and spectroscopy applications [16, 77, 86, 87]. Some of the applications can be seen from Table 1.2. It is important to note that Atomic-force microscopy (AFM) is one of the most successful applications of XYZ CPMs [88]. The XYZ nanopositioner, as shown in Figure 1.11, can be designed using an XYZ CPM.

Table 1.2 Applications of XYZ CPMs

Application field	Application description	Company
Micro assembly	Assembly of micro components	Invenios
Nano-/micro-positioning	High accuracy nano-positioning along X-, Y- and Z-axes	nPoint, Thorlabs, Physik Instrument, Invenios, Piezosystem Jena, Newmark Systems Inc., SmarAct GmbH, Elliot Scientific, Mad City Labs, Nano Scan Tech, Polytec
Optics	Handling of small components and assemblies	Piezosystem Jena, Elliot Scientific, Edmund Optics, Queensgate Instruments
Optical tweezers and optical traps	Manipulating nano- and micro-meter sized electric particles	Thorlabs
Optical fibre alignment	Accurate motion and placement of individual fibres for alignment	Edmund Optics
Metrology	Accurate measurement of motion and placement	Nano Scan Technology, Carl Zeiss Microscopy
AFM/SPM/MFM/Reflectance	Accurate placement of specimen for examination	Nano Scan Technology, Siskiyou, Queensgate Instruments
Spectroscopy	Measurement of radiation intensity as a function of wavelength	Physik Instrument
Fluorescence microscopy and spectroscopy	Accurate placement of specimen for examination	Siskiyou
Super resolution microscopy	Accurate placement of specimen for examination	Physik Instrument
Photovoltaics	Component alignment	Newport Corporation
MEMS	Accurate handling of nano- and micro-electronic mechanical systems	Newport Corporation, Nano Scan Technology
Nano-fabrication, Nano-patterning and Nano-machining	Accurate positioning with precision motion is needed to manufacture small, detailed components	Mad City Labs, Newport Corporation
Magnetic tweezers, traps and manipulation	Scientific instruments for the manipulation of biomolecules	Elliot Scientific

1.3.2 Aim: effective approaches to the design of XYZ CPMs

Existing XYZ CPMs were designed using the existing synthesis, modelling and optimization approaches discussed in Section 1.2. However, these existing approaches have limitations. Therefore, this thesis will focus on new effective approaches to the synthesis, modelling and optimization of XYZ CPMs. The desired effective synthesis approach requires that a great number of XYZ CPMs with different geometrical structures can be synthesized by both experts and beginners; the desired effective modelling approach requires that the physical meaning of the mathematical expression can be understood easily; and the desired effective optimization approach requires that both the geometrical dimension and the geometrical shape of an XYZ CPM can be optimized simultaneously.

1.3.2.1 Desired synthesis approach

Most existing XYZ CPMs were synthesized using the constraint-based approach with qualitative arguments and rationale [87]. In recent years, many XYZ CPMs were also synthesized using the rigid-body-replacement-based approach [77, 80, 89]. This rigid-body-replacement-based approach often begins with a rigid-body mechanism which can provide the same motions as the desired XYZ CPM. The rigid-body mechanism can be converted to an XYZ CPM by replacing the rigid kinematic joints or chains with equivalent compliant modules [7]. The rigid-body-replacement-based approach is an efficient approach to the synthesis of XYZ CPMs. However, this approach is only suitable for those designers who are knowledgeable about rigid-body parallel mechanisms. Additionally, the rigid-body-replacement-based approach depends on the development of rigid-body mechanisms [7].

A constraint map for XYZ CPM synthesis was proposed by Awtar et al in [87]. This constraint map decomposes an XYZ CPM into rigid stages and compliant modules, and each compliant module is allocated specific constraints. In [87], all

compliant modules were designed based on the allocated constraints, and an XYZ CPM was presented by assembling the rigid stages and the compliant modules together. It is well known that different compliant modules can be designed on the basis of the specific constraints, so that new XYZ CPMs can be obtained through replacing the compliant modules of the XYZ CPM designed in [87] with other compliant modules with the same constraints. However, the constraint map is only suitable for certain types of XYZ CPMs. For example, the constraints of the compliant modules in the XYZ CPMs as shown in [77, 89] are beyond the range of the constraint map.

The existing approaches for synthesizing XYZ CPMs are often limited to some types of XYZ CPMs. Therefore, a more effective approach of synthesizing XYZ CPMs is desirable. The XYZ CPMs, designed using the desired synthesis approach, should be able to provide three highly-decoupled translations along three orthogonal axes (X-, Y- and Z-axes), while the rotational stiffness about the three axes should be much higher than the translational stiffness along the three axes [74, 78]. Furthermore, the three translations can be actuated by three ground-mounted linear actuators. In addition, the designed XYZ CPMs should have the potential of allowing diverse structures, which can be employed in different applications.

1.3.2.2 Desired analytical modelling approach

As mentioned in Section 1.2.2, there are two main approaches to model compliant mechanisms (including XYZ CPMs). One is the FBD-based modelling approach, and the other is the energy-based approach. In this thesis, the basic principle of the FBD-based modelling approach is followed to model XYZ CPMs, because all geometrical parameters/variables of an XYZ CPM can be taken into account in the FBD-based modelling approach.

The FBD-based modelling approach, as used in [55], decomposes a compliant mechanism into rigid stages and compliant modules, and then identifies the

deformed configuration of the compliant mechanism. According to the deformed configuration, the analytical model of the compliant mechanism is derived by resolving all the equations associated with the force equilibrium conditions, the geometrical compatibility conditions, and the force-displacement relationships of the compliant modules. The analytical model of a compliant mechanism, derived using the FBD-based modelling approach, can be used to estimate and optimize the motion characteristics of the compliant mechanism. However, the modelling of a complex XYZ CPM directly using the FBD-based modelling approach proves to be complicated, as demonstrated in [55], because (a) a designer must use his/her pattern recognition and visualization skills to identify the possible deformed configuration of the XYZ CPM in order to obtain the geometrical compatibility conditions, (b) the derivation of all the force equilibrium equations should be based on the visualized deformed configuration, and (c) the physical meaning of the expressions, in terms of the force-displacement relationships of the compliant modules, is not apparent.

In order to simplify the modelling process, XYZ CPMs are usually modelled linearly using the FBD-based modelling approach [77, 80]. In such a linear modelling process, both the associated geometrical compatibility conditions and the force-displacement equations are linearized and represented by linear matrices [80]. Therefore, the linear model of an XYZ CPM can be obtained via basic matrix operations such as matrix transformation, matrix addition and matrix subtraction. However, the linear model captures only instantaneous effects, which is suitable for very small displacements [55, 80, 90].

Therefore, a modelling approach, based on the same basic principle as the FBD-based modelling approach, is desired to effectively deal with both linear and nonlinear modelling of XYZ CPMs.

1.3.2.3 Desired optimization approach

The stiffness of a compliant joint is neither zero in DOF directions nor infinitely large in the DOC directions. Therefore, compliant mechanisms (with a particular emphasis on distributed-compliance) often suffer from undesired cross-axis couplings, lost motions and parasitic motions [2-5, 91, 92].

It is desirable to minimize such cross-axis couplings and the lost motions, while they can also be compensated by close-loop control systems [55]. However, most parasitic rotations of a compliant mechanism cannot be compensated by an active control system, so parasitic rotations of compliant mechanisms should be maximally reduced or eliminated through the associated structure optimization. Taking a basic parallelogram compliant mechanism shown in Figure 1.12(a) as an example, a force acting at the top mobile stage of the basic parallelogram compliant mechanism can produce not only a primary transverse motion, but also a small parasitic rotation [54, 93]. The parasitic rotation can affect the motion accuracy of the basic parallelogram compliant mechanism, and cannot be compensated by the actuation force [55, 87]. Therefore, this thesis focuses on the reduction of parasitic motions of compliant mechanisms, with consideration of reducing the cross-axis couplings and lost motions.

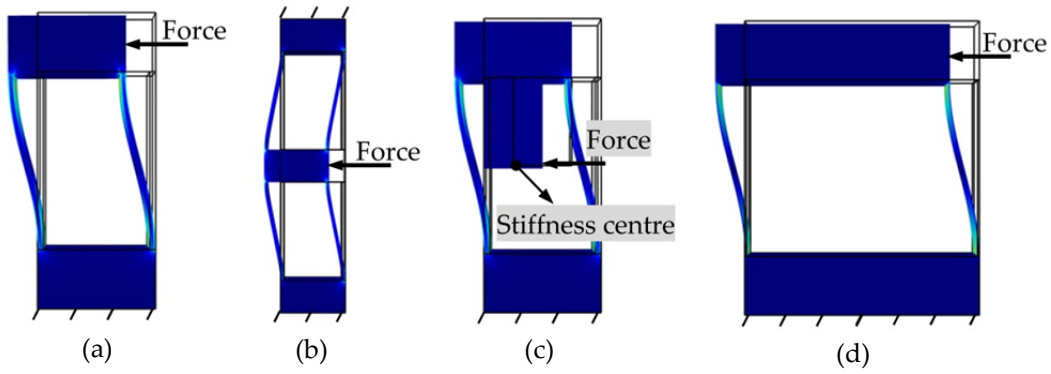

Figure 1.12 1-DOF translational compliant mechanisms: (a) basic parallelogram compliant mechanism, (b) compound basic parallelogram compliant mechanism, (c) basic parallelogram compliant mechanism being actuated at its stiffness centre, and (d) basic parallelogram compliant mechanism with smaller in-plane thickness and larger spanning size

The employment of a symmetric arrangement, as shown in Figure 1.12(b), is a widely-used approach to minimize parasitic motions of compliant mechanisms. Using such an approach can lead to a compliant mechanism with larger actuation stiffness (i.e., stiffness along the directions of the actuations), because of the additional (redundant) constraints.

Awtar [55] proposed a method of attenuating a parasitic motion of a compliant mechanism by using the concept of the stiffness centre of a parallelogram mechanism first reported in [1, 91] by R. V. Jones. For example, if an actuation force goes through the stiffness centre of the basic parallelogram compliant mechanism, as shown in Figure 1.12(c), the parasitic rotation of the basic parallelogram compliant mechanism will be significantly reduced [91]. However, this approach is suitable for only some compliant mechanisms.

The above mentioned optimization approaches are used to reduce a parasitic motion of a compliant mechanism by changing the geometrical shape of the compliant mechanism. A parasitic motion of a compliant mechanism can also be decreased by optimizing the geometrical dimension of the compliant mechanism [94]. For example, the parasitic rotation of the basic parallelogram compliant mechanism can be alleviated by decreasing the beam in-plane thickness and/or increasing the spanning size of the two beams, as illustrated in Figure 1.12(d). The optimization of a basic parallelogram compliant mechanism is easily achieved by optimizing the geometrical dimension. However, decreasing the beam in-plane thickness can significantly reduce the stiffness of the basic parallelogram compliant mechanism due to the cubic relationship that exists between the stiffness and the in-plane thickness, at the expense of increasing the difficulty of manufacturing. Increasing the spanning size can make the system bulky, as is clear by comparing Figure 1.12(d) with Figure 1.12(a).

Each of the optimization approaches introduced above has both pros and cons.

An XYZ CPM can be optimized using the above approaches, but none of the approaches can optimize an XYZ CPM by simultaneously changing both the geometrical dimension and the geometrical shape. Therefore, the desired approach of optimizing an XYZ CPM should be able to reduce a parasitic motion of the XYZ CPM via optimizing both the geometrical dimension and the geometrical shape simultaneously.

1.4 Main Contributions of This Thesis

Based on the scope and aim of this thesis, new approaches to the type synthesis, analytical modelling and structure optimization of XYZ CPMs are proposed in the following chapters. More specifically, a constraint and position identification (CPI) approach to the synthesis of XYZ CPM is proposed in Chapter 2; a constraint-force-based (CFB) approach of modelling XYZ CPMs is derived in Chapter 3; and a position-space-based reconfiguration (PSR) approach and two PSR-based approaches of optimizing XYZ CPMs are introduced in Chapter 4. Using the above approaches, some typical XYZ CPMs are synthesized, modelled and optimized in this thesis. Additionally, one of the optimized XYZ CPMs is fabricated, and a control system for this prototype is also presented.

The CPI synthesis approach, the CFB modelling approach and the PSR-based optimization approaches are the main contribution of this thesis. In the remainder of this section, these approaches are introduced briefly.

1.4.1 CPI synthesis approach

The CPI approach is proposed to synthesize decoupled XYZ CPMs, and each of these synthesized XYZ CPMs can be actuated by three ground-mounted linear actuators.

An XYZ CPM, in the CPI approach, is decomposed into compliant modules that are linked by rigid stages. Therefore, an XYZ CPM can be synthesized through

carrying out the following main tasks: (a) identifying the topological structure of the compliant modules and rigid stages, which shows the interconnection of the compliant modules and rigid stages, (b) obtaining the geometrical forms of compliant modules, and (c) arranging the positions of the compliant modules, and (d) linking the compliant modules using the rigid stages based on the topological structure.

Three-legged XYZ CPMs are basic XYZ CPMs. In the CPI approach, the topological structure of a three-legged XYZ is derived, and the *constraint spaces*[5] of the compliant modules are obtained using screw theory. The geometrical form of each of the compliant modules can be obtained based on any one of the possible permitted constraints in the constraint space of the compliant module. For any one possible permitted constraint of a compliant module, the compliant module has many possible permitted positions in the associated compliant mechanism. In this thesis, the set of all the possible permitted positions of a compliant module is termed *position space*[6] of the compliant module. The derivation of the position space of a compliant module is also introduced in the CPI approach.

Note that existing synthesis approaches such as the constraint-based approach [55], the screw-theory-based approach [61-65, 95] and the FACT approach [66, 67, 96-98] are not effective approaches for synthesizing XYZ CPMs. However,

---

[5] The set of all the possible permitted constraints of a compliant module is defined as the *constraint space* of the compliant module in the compliant mechanism. Note that the constraint of a compliant module is defined to represent both the number and the directions of the DOC of the compliant module.

[6] For one possible permitted constraint, a compliant module in a compliant mechanism can be placed at different positions. The set of the entire possible permitted positions of the compliant module is termed the *position space* of the compliant module in the compliant mechanism under the selected constraint of the compliant module.

they, especially the FACT approach, are suitable for synthesizing compliant modules. Therefore, in the CPI approach, the geometrical form of a compliant module can be obtained using these existing synthesis approaches.

It is clear in the CPI approach that one compliant module in a three-legged XYZ CPM has many possible permitted geometrical forms and positions, so the CPI approach can synthesize a large number of three-legged XYZ CPMs through assembling the possible permitted geometrical forms of compliant modules and rigid stages, based on the topological structure and the position spaces. Moreover, a three-legged XYZ CPM, that is synthesized using the CPI approach, can provide three decoupled translations. Additionally, XYZ CPMs with more than three legs can be synthesized through adding redundant legs to three-legged XYZ CPMs.

1.4.2 CFB modelling approach

In order to analyse the motion characteristics of an XYZ CPM that is synthesized using the CPI approach, it is better to model the XYZ CPM analytically. Therefore, the CFB approach is proposed, which can be used to effectively model XYZ CPMs both linearly and non-linearly. Additionally, the CFB approach can also be used to model other types of compliant mechanisms in addition to XYZ CPMs.

The CFB approach regards compliant modules as multi-DOF or multi-DOC springs, and a deformed compliant module stores potential energy which can produce elastic forces that act on the connected rigid stages. Such elastic forces are termed *variable constraint forces* in this thesis, because the elastic forces vary with the deformation of the compliant modules. Additionally, in this thesis, the external forces exerted on a compliant mechanism are regarded as *constant constraint forces*, because the external forces are independent of the deformation of the compliant mechanisms. If a compliant mechanism is in static equilibrium, the rigid stages are in static equilibrium under the influence of the variable

constraint forces and the applied constant constraint forces. Therefore, the constraint force equilibrium equations for the rigid stages can be represented by the associated variable and constant constraint forces. The analytical model of the compliant mechanism can be derived based on the constraint force equilibrium equations.

The variable constraint force of a BCM (basic compliant module, as defined in Section 1.3.1) can be derived from its previously-obtained force-displacement relationship. The variable constraint force of a NBCM (non-basic compliant module, as defined in Section 1.3.1) can also be derived from the force-displacement relationship of the NBCM, if this force-displacement relationship is already known. If the force-displacement relationship of a NBCM is not known, the variable constraint force of the NBCM can be derived based on the variable constraint forces of the associated BCM, because the NBCM can be further decomposed into BCMs.

Taking the XYZ CPM shown in Figure 1.13 (proposed in [99]) for example, the XYZ CPM has three NBCMs, Leg-X, Leg-Y, and Leg-Z. Each of the legs can be decomposed into an actuated module (AM) and a passive module (PM), and the AM and PM can also be further decomposed into BCMs, sheet beams and wire-beams, respectively. The variable constraint forces of Leg-X, Leg-Y and Leg-Z can be obtained from their own force-displacement relationships, or derived based on the variable constraint forces of the AMs and PMs. The variable constraint forces of the AMs and PMs can be obtained from their own force-displacement relationships, or derived based on the variable constraint forces of the sheet beams and wire-beams.

Based on the above, the CFB approach can model a compliant mechanism (the compliant mechanism can be an XYZ CPM) by following on the following steps: (a) decomposing the compliant mechanism into rigid stages and compliant modules, (b) obtaining the variable constraint forces of the compliant modules,

(c) obtaining the constraint force equilibrium equations for the rigid stages, and (d) deriving the model of the compliant mechanism by solving the constraint force equilibrium equations.

Compared with the traditional FBD-based modelling approach, use of the CFB approach eliminates the need to identify the possible deformed configuration of a compliant mechanism to obtain the geometrical compatibility conditions and the force equilibrium equations. Moreover, the mathematical expressions of the CFB approach have easily understood physical meanings. Therefore, the CFB approach can be regarded as a development of the FBD-based modelling approach.

A complex compliant mechanism can be regarded as a combination of several sub-compliant mechanisms. Therefore, the modelling process of a complex compliant mechanism can be divided into many modelling sub-processes.

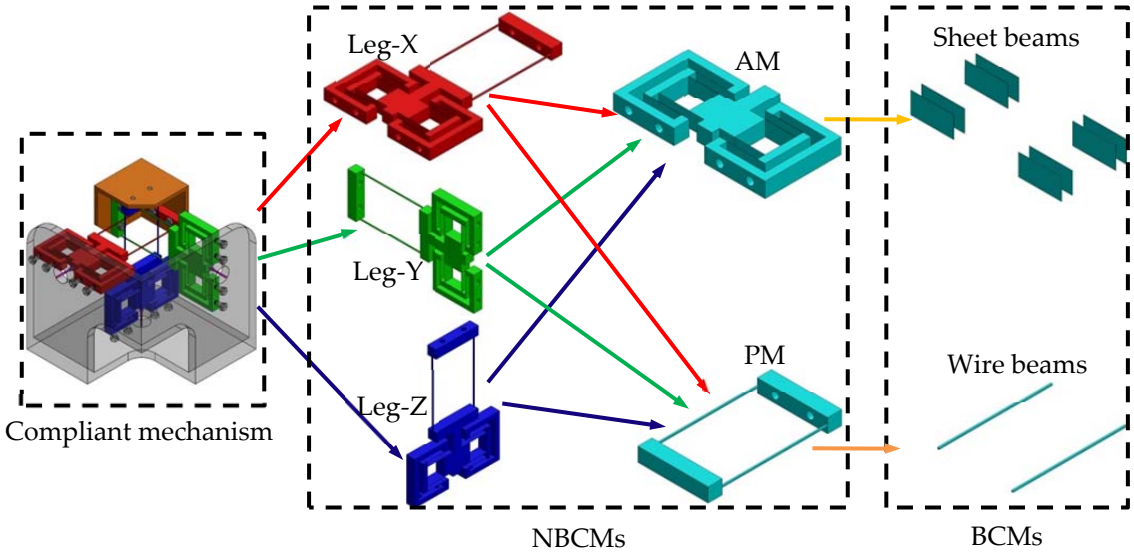

Figure 1.13 Decomposition of an XYZ CPM [99]

1.4.3 PSR-based optimization approaches

As discussed in Section 1.4.1, a compliant module in an XYZ CPM has many possible permitted positions within its position space. Therefore, an XYZ CPM can be reconfigured by rearranging the positions of the associated compliant modules within their position spaces. Such a reconfiguration approach is

termed the PSR approach. Note that the decomposition of an XYZ CPM in the PSR approach can be different from the decomposition in the CPI and CFB approaches. In addition, any compliant mechanisms (including XYZ CPMs) can be reconfigured using the PSR approach.

The PSR approach can be used to reconfigure any one compliant mechanism to change both the geometrical dimension and the geometrical shape of the compliant mechanism. For example, the original 1-DOF translational compliant mechanism, as shown in Figure 1.14(a), can be decomposed into an motion stage (MS), four base stages (BSs), and two double-two-beam compliant modules (DTBCMs), as shown in Figure 1.14(b). The two DTBCMs, with their BSs, can be moved to other permitted positions in the 1-DOF translational compliant mechanism system. It is clear that all the positions of the two DTBCMs, shown in Figure 1.14, are possible permitted positions, because the DOC or DOF of the 1-DOF translational compliant mechanism remains the same when the positions of the two DTBCMs change, as shown in Figure 1.14. When the positions of the two DTBCMs are changed, both the geometrical dimension and the geometrical shape can be changed, as seen in Figure 1.14(c) – Figure 1.14(e). Figure 1.14(c) shows that the spanning size between the two compliant modules is increased, via translating one of the DTBCMs along the X-axis and linking the compliant module to the MS using a rigid linkage (RL). Figure 1.14(d) shows that the geometrical shape of the compliant mechanism is changed through rotating one of the DTBCMs about the X-axis at 180°. The changes of both the geometrical dimension and the geometrical shape are illustrated in Figure 1.14(e).

In addition, from Figure 1.14(f), it can be seen that a permitted position of a compliant module is also a position to add a redundant copy of the compliant module. In Figure 1.14(f), three redundant copies of the DTBCM are added to the 1-DOF translational compliant mechanism, which does not affect the DOF of the compliant mechanism.

The motion characteristics of a compliant mechanism can be improved through optimizing the geometrical dimension and geometrical shape of the compliant mechanism. Therefore, the PSR can be used to improve the motion characteristics of a compliant mechanism through reconfiguring the compliant mechanism. Such motion characteristics can be parasitic motion, cross-axis coupling and lost motion. In this thesis, two PSR-based optimization approaches are proposed, which are employed to reduce parasitic motions (RPMs) of compliant mechanisms and to reconfigure non-symmetric compliant mechanisms into symmetric compliant mechanisms (SCMs), respectively. These two PSR-based optimization approaches are termed the PSR-RPM and PSR-SCM approaches, respectively.

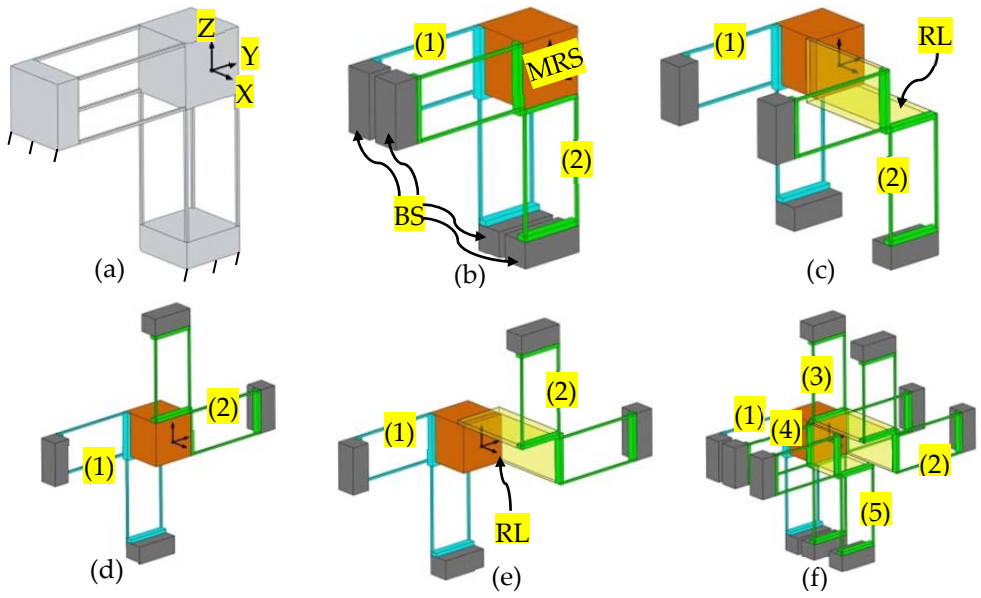

Figure 1.14 Position-space-based reconfiguration of a 1-DOF translational compliant mechanism: (a) original 1-DOF translational compliant mechanism, (b) decomposition of the 1-DOF translational compliant mechanism, (c) geometrical dimension change, (d) geometrical shape change, (e) changes of both geometrical dimension and geometrical shape, and (f) adding redundant compliant modules (RL: rigid linkage, MS: motion stage, BS: base stage)

The PSR-RPM approach is employed to reduce parasitic motions of a compliant mechanism by rearranging the compliant modules of the compliant mechanism, without adding redundant compliant modules. The PSR-SCM approach is

employed to reconfigure a non-symmetric compliant mechanism into a symmetric compliant mechanism, through rearranging the compliant modules of the compliant mechanism by adding a small number of redundant compliant modules. The derived symmetric compliant mechanism has desired motion characteristics such as reduced parasitic motions, due to its symmetric configuration.

This page is intentionally left blank.

2 CPI SYNTHESIS APPROACH

The CPI approach, proposed in this chapter, focuses on synthesizing three-legged XYZ CPMs which are basic XYZ CPMs. Other XYZ CPMs with more than three legs can be obtained through adding redundant legs on three-legged XYZ CPMs. Both the principle and the application of the CPI approach are detailed in this chapter. More specifically, the principle of the CPI approach is presented in Section 2.1. According to this principle, the suitable constraints and positions of the compliant modules of a three-legged XYZ CPM should be known. As defined in Chapter 1, the constraint of a compliant module represents both the number and the directions of the DOC of the compliant module. Possible permitted constraints and positions for the compliant modules in a three-legged XYZ CPM are derived in Sections 2.2 and 2.3. The synthesis procedure of the CPI approach is summarized in Section 2.4, followed by several detailed example demonstrations in Section 2.5. Summary is finally drawn in Section 2.6.

2.1 Principle

As is required in Chapter 1, an XYZ CPM synthesized using the CPI approach should be able to provide three translations along the X-, Y- and Z-axes. Additionally, the three translations should be decoupled, and can be actuated by three ground-mounted linear actuators. Therefore, a desired XYZ CPM has at least three non-redundant parallel legs. The three legs can be termed Leg-X, Leg-Y and Leg-Z (associated with the translations of the XYZ CPM along the X-, Y- and Z-axes, respectively).

A three-legged XYZ CPM has three non-redundant legs, Leg-X, Leg-Y and Leg-Z, so each of the legs should be able to transmit the translation of the associated linear actuator to the motion stage (MS) of the XYZ CPM. Furthermore, each of the legs should have an actuated stage (AS) on which the translation of the associated linear actuator can be exerted. The ASs of Leg-X, Leg-Y and Leg-Z can be termed AS-X, AS-Y and AS-Z, respectively. Moreover, base stages (BSs) of a three-legged XYZ CPM can be termed BS-X, BS-Y and BS-Z, and these BSs link the Leg-X, Leg-Y and Leg-Z to the ground, respectively. As a result, a three-legged XYZ CPM should have the following rigid stages: MS, AS-X, AS-Y, AS-Z, BS-X, BS-Y and BS-Z.

Based on the definition of a compliant module in Chapter 1, the components linking the MS, AS and BS in a leg of a three-legged XYZ CPM can be regarded as compliant modules. More specifically, the compliant modules between the MS and the ASs are called passive modules (PMs), and the compliant modules between the ASs and the BSs are called active modules (AMs). Therefore, a three-legged XYZ CPM has three PMs (PM-X, PM-Y and PM-Z) and three AMs (AM-X, AM-Y and AM-Z). Both the PMs and the AMs can be parallel, serial and hybrid compliant modules.

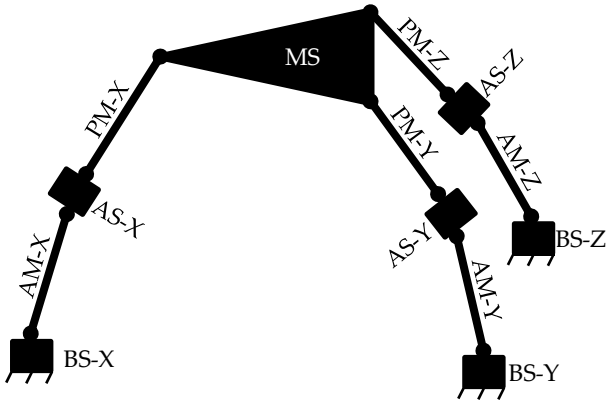

Figure 2.1 Illustration of the topological structure of a three-legged XYZ CPM

Therefore, the topological structure of a three-legged XYZ CPM can be seen in Figure 2.1, which shows the interconnection of the compliant modules and rigid stages.

It can be seen from the topological structure that a three-legged XYZ CPM is a combination of compliant modules (PMs and AMs) that are linked by rigid stages (MS, ASs and BSs). Therefore, synthesizing a three-legged XYZ CPM is to identify the geometrical forms and positions of the compliant modules in the topological structure, and then to link the compliant modules using the rigid stages based on the topological structure. The rigid stages can be synthesized easily, so the main work of synthesizing a three-legged XYZ CPM requires identification of the geometrical forms and positions of the compliant modules.

The geometrical forms and positions of the compliant modules of a three-legged XYZ CPM can be obtained based on the constraints of the compliant modules. Therefore, in order to identify the geometrical forms and positions of the compliant modules, it is better to firstly obtain all the possible permitted constraints of the compliant modules.

A three-legged XYZ CPM should provide three decoupled translations, which means the translations of the MS should be decoupled from each other. Additionally, it can be derived that each AS is permitted to translate only along the actuation direction of the associated actuator, because linear actuators cannot tolerate off-axis loads and displacements [87]. Additionally, the desired mobility of the MS and ASs is completely controlled by the PMs and AMs. Therefore, the constraint spaces of the compliant modules can be identified by the desired mobility of the MS and ASs. The constraint spaces of the PMs and AMs in a three-legged XYZ CPM are derived in Section 2.2.

For a specific synthesis process, the constraint of a PM or an AM can be selected from its constraint space. Based on the selected constraint, both the possible permitted geometrical forms and the position spaces of the PM or AM can be determined. As stated in Section 1.4.1, the possible permitted geometrical forms of the PMs and AMs can be obtained using the existing approaches such as the screw-theory-based method and the FACT method, based on the constraints of

the PMs and AMs. The derivation of the position spaces of the PMs and AMs in a three-legged XYZ CPM are described in Section 2.3.

2.2 Constraint Space

2.2.1 Analysis domains for constraint space identification

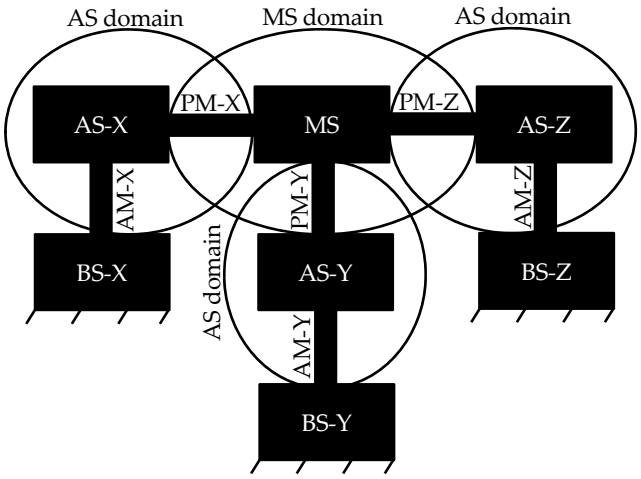

Figure 2.2 Illustration of rigid stages and compliant modules of a three-legged XYZ CPM in different analysis domains, MS domain and AS domains

It is derived in Section 2.1 that the constraint spaces of the PMs and AMs can be identified based on the desired mobility of the MS and ASs. In order to identify the constraint spaces of the PMs and AMs easily, the MS, ASs, PMs and AMs are assigned to different analysis domains as shown in Figure 2.2. The constraint spaces of the compliant modules in a domain are subject to the permitted motions of the rigid stage in the domain. It can be seen in Figure 2.2 that the MS is constrained by the total contribution of the constraints of the three PMs. Similarly, each AS is constrained by the total contribution of the constraints of the PM and the AM in the same leg. Note that the three PMs are included in the intersection fields between the MS domain and the AS domains, so that the constraint spaces of the PMs and those of the AMs interrelate with each other.

In order to simplify the CPI approach, it can be assumed that the PMs and AMs of a three-legged XYZ CPM are independent of each other. This assumption

means that one of the compliant modules, PMs and AMs, constrains a motion of a rigid stage completely depending on its own structure, without considering any contribution of the other compliant modules. Due to this assumption, a small number of XYZ CPMs, such as the one shown in Appendix A, cannot be synthesized using the CPI approach. However, they may be obtained via some appropriate modifications on XYZ CPMs that can be synthesized using the CPI approach.

2.2.2 Mathematical theory for constraint space identification

In this chapter, constraint spaces of compliant modules are derived using screw theory. Therefore, for a three-legged XYZ CPM, the constraints of the compliant modules and the motions of the rigid stages are represented by wrenches and twists, respectively, in screw theory. In other words, a twist can be used to represent a combination of linear and rotary motions, a wrench can be employed to describe a combination of linear and rotary forces, and screw theory combines them together. The constraint spaces of the compliant modules can be derived based on the relationships between the wrenches and the twists.

2.2.2.1 Wrenches and twists in screw theory

It is well known that forces and displacements can be represented by screw vectors, wrenches and twists, respectively [100]. Wrenches and twists can be represented as wrench lines and twist lines, with particular locations, orientations and pitches. Such a pitch refers to the coupling between the translational force and the rotational force in a wrench, and describes the translational displacement per rotation in a twist. Therefore, a wrench can be represented by Equation (2.1) and Figure 2.3(a), while a twist can be described by Equation (2.2) and Figure 2.3(b).

$$\zeta = \begin{bmatrix} \boldsymbol{f}_{\mathrm{T}} \\ \boldsymbol{f}_{\mathrm{R}} \end{bmatrix} = \begin{cases} \begin{bmatrix} \boldsymbol{f}_{\mathrm{T}} & \boldsymbol{r} \times \boldsymbol{f}_{\mathrm{T}} + q\boldsymbol{f}_{\mathrm{T}} \end{bmatrix}^{\mathrm{T}} & \text{force and moment} \\ \begin{bmatrix} \boldsymbol{f}_{\mathrm{T}} & \boldsymbol{r} \times \boldsymbol{f}_{\mathrm{T}} \end{bmatrix}^{\mathrm{T}} & q = 0, \text{pure force} \\ \begin{bmatrix} \boldsymbol{0} & \boldsymbol{f}_{\mathrm{R}} \end{bmatrix}^{\mathrm{T}} & q \to \infty, \text{pure moment} \end{cases} \tag{2.1}$$

where ζ is a wrench vector; and $\boldsymbol{f}_{\mathrm{T}}$ and $\boldsymbol{f}_{\mathrm{R}}$ are two three-dimensional vectors which represent translational and rotational loads, respectively. Additionally, $\boldsymbol{r}$ is a 3×1 location vector which points from the origin of the coordinate system to a point on the wrench line. The pitch is defined by $q = \left(\boldsymbol{f}_{\mathrm{T}} \cdot \boldsymbol{f}_{\mathrm{R}}\right) / \left(\boldsymbol{f}_{\mathrm{T}} \cdot \boldsymbol{f}_{\mathrm{T}}\right)$.

$$\xi = \begin{bmatrix} \boldsymbol{v}_{\mathrm{T}} \\ \boldsymbol{v}_{\mathrm{R}} \end{bmatrix} = \begin{cases} \begin{bmatrix} \boldsymbol{c} \times \boldsymbol{v}_{\mathrm{R}} + p\boldsymbol{v}_{\mathrm{R}} & \boldsymbol{v}_{\mathrm{R}} \end{bmatrix}^{\mathrm{T}} & \text{screw motion} \\ \begin{bmatrix} \boldsymbol{c} \times \boldsymbol{v}_{\mathrm{R}} & \boldsymbol{v}_{\mathrm{R}} \end{bmatrix}^{\mathrm{T}} & p = 0, \text{pure rotation} \\ \begin{bmatrix} \boldsymbol{v}_{\mathrm{T}} & \boldsymbol{0} \end{bmatrix}^{\mathrm{T}} & p \to \infty, \text{pure translation} \end{cases} \tag{2.2}$$

where ξ is a twist, $\boldsymbol{v}_{\mathrm{T}}$ and $\boldsymbol{v}_{\mathrm{R}}$ are two three-dimensional vectors which represent translational and rotational motions, respectively, while $\boldsymbol{c}$ is a 3×1 location vector which points from the origin of the coordinate system to a point on the twist line. The pitch is defined by $p = \left(\boldsymbol{v}_{\mathrm{R}} \cdot \boldsymbol{v}_{\mathrm{T}}\right) / \left(\boldsymbol{v}_{\mathrm{R}} \cdot \boldsymbol{v}_{\mathrm{R}}\right)$.

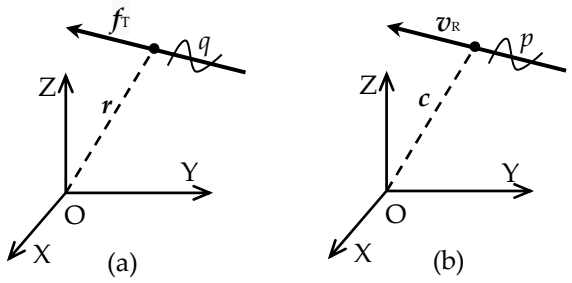

Figure 2.3 Illustration of a wrench and a twist: (a) a wrench ζ with a location vector *r*, an orientation vector f_{T}, and a scalar value of pitch *q*; and (b) a twist ξ with a location vector *c*, an orientation vector v_{R}, and a scalar value of pitch *p*

In a coordinate system, unit wrenches along and about the X-, Y- and Z-axes are defined as principal wrenches, as shown in Equation (2.3) and Figure 2.4(a) [64]. Any one wrench in this coordinate system can be described as a linear

combination of the principal wrenches, as shown in Equation (2.4) and Figure 2.4(b).

$$\begin{aligned}\boldsymbol{\zeta}_{tx} &= [1,0,0,0,0,0]^T, \boldsymbol{\zeta}_{ty} = [0,1,0,0,0,0]^T, \boldsymbol{\zeta}_{tz} = [0,0,1,0,0,0]^T \\ \boldsymbol{\zeta}_{rx} &= [0,0,0,1,0,0]^T, \boldsymbol{\zeta}_{ry} = [0,0,0,0,1,0]^T, \boldsymbol{\zeta}_{rz} = [0,0,0,0,0,1]^T\end{aligned} \tag{2.3}$$

$$\boldsymbol{\zeta} = \zeta_{tx}\boldsymbol{\zeta}_{tx} + \zeta_{ty}\boldsymbol{\zeta}_{ty} + \zeta_{tz}\boldsymbol{\zeta}_{tz} + \zeta_{rx}\boldsymbol{\zeta}_{rx} + \zeta_{ry}\boldsymbol{\zeta}_{ry} + \zeta_{rz}\boldsymbol{\zeta}_{rz} = [\zeta_{tx}, \zeta_{ty}, \zeta_{tz}, \zeta_{rx}, \zeta_{ry}, \zeta_{rz}]^T \tag{2.4}$$

where ζ_{tx}, ζ_{ty}, ζ_{tz}, ζ_{rx}, ζ_{ry} and ζ_{rz} are termed *principal wrench coefficients.* When using Equation (2.4) to represent a general force in a coordinate system, the principal wrench coefficients are the values of the general force along and about the X-, Y- and Z-axes.

Constraints can also be represented by wrenches. However, unlike a general force, a constraint is bidirectional in practice. For example, a translational constraint can restrict all translations along the constraint in two possible opposite directions. Therefore, if a wrench can be used to represent a constraint, the wrench should have two possible directions. This means that each of the principal wrench coefficients should have two possible values, one of which is the negation of the other. Consequently, the wrench $\boldsymbol{\zeta}$ in Equation (2.4) can be rewritten as a wrench $\boldsymbol{\zeta}_C$, as shown in Equation (2.5), when using the wrench to represent a constraint.

$$\boldsymbol{\zeta}_C = [\kappa_{tx} j_{tx}, \kappa_{ty} j_{ty}, \kappa_{tz} j_{tz}, \kappa_{rx} j_{rx}, \kappa_{ry} j_{ry}, \kappa_{rz} j_{rz}]^T \tag{2.5}$$

where κ_{tx}, κ_{ty}, κ_{tz}, κ_{rx}, κ_{ry} and κ_{rz} are termed *constraint coefficients*, while j_{tx}, j_{ty}, j_{tz}, j_{rx}, j_{ry} and j_{rz} are *direction coefficients*. The constraint and direction coefficients can be calculated using Equations (2.6) and (2.7), respectively.

$$\kappa_{tx} = |\zeta_{tx}|, \kappa_{ty} = |\zeta_{ty}|, \kappa_{tz} = |\zeta_{tz}|, \kappa_{rx} = |\zeta_{rx}|, \kappa_{ry} = |\zeta_{ry}|, \kappa_{rz} = |\zeta_{rz}| \tag{2.6}$$

$$j_{tx} = \pm 1, j_{ty} = \pm 1, j_{tz} = \pm 1, j_{rx} = \pm 1, j_{ry} = \pm 1, j_{rz} = \pm 1 \tag{2.7}$$

It is appropriate to define that a constraint coefficient equals one if the associated constraint is infinitely large, while the constraint coefficient equals zero if the associated constraint is infinitely small. In other words, if a constraint coefficient equals one, the direction associated with the constraint coefficient is a DOC direction; otherwise it is a DOF direction. Therefore, each of the constraint coefficients equals one or zero, for the synthesis of compliant mechanisms described in this chapter. In addition, a constraint wrench has two possible directions, while the instantaneous effective direction of a constraint wrench is always opposite to the direction of the motion constrained by this constraint wrench.

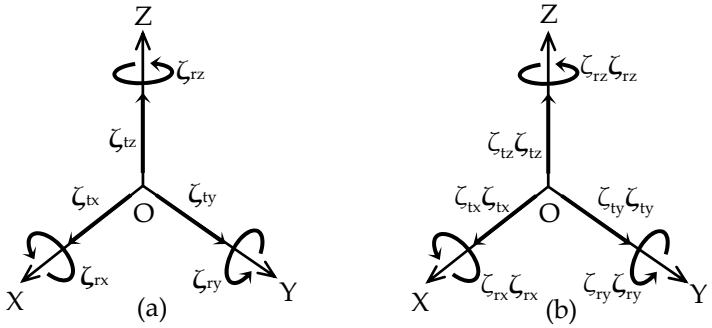

Figure 2.4 Principal wrenches and linear combination of the principal wrenches: (a) principal wrenches, and (b) linear combination of the principal wrenches

Similarly, unit twists along and about the three axes of a coordinate system, as shown in Figure 2.5(a) and Equation (2.8), can also be defined as principal twists. Any one twist ξ in a coordinate system can be described as a linear combination of the principal twists in the same coordinate system, as shown in Figure 2.5(b) and Equation (2.9).

$$\begin{aligned} &\xi_{tx} = [1,0,0,0,0,0]^T, \xi_{ty} = [0,1,0,0,0,0]^T, \xi_{tz} = [0,0,1,0,0,0]^T \\ &\xi_{rx} = [0,0,0,1,0,0]^T, \xi_{ry} = [0,0,0,0,1,0]^T, \xi_{rz} = [0,0,0,0,0,1]^T \end{aligned} \tag{2.8}$$

$$\boldsymbol{\xi} = \xi_{tx}\boldsymbol{\xi}_{tx} + \xi_{ty}\boldsymbol{\xi}_{ty} + \xi_{tz}\boldsymbol{\xi}_{tz} + \xi_{rx}\boldsymbol{\xi}_{rx} + \xi_{ry}\boldsymbol{\xi}_{ry} + \xi_{rz}\boldsymbol{\xi}_{rz} = \left[\xi_{tx}, \xi_{ty}, \xi_{tz}, \xi_{rx}, \xi_{ry}, \xi_{rz}\right]^{T} \tag{2.9}$$

where ξ_{tx}, ξ_{ty}, ξ_{tz}, ξ_{rx}, ξ_{ry} and ξ_{rz} are termed *principal twist coefficients*, which are the values of the displacements along and about the X-, Y- and Z-axes.

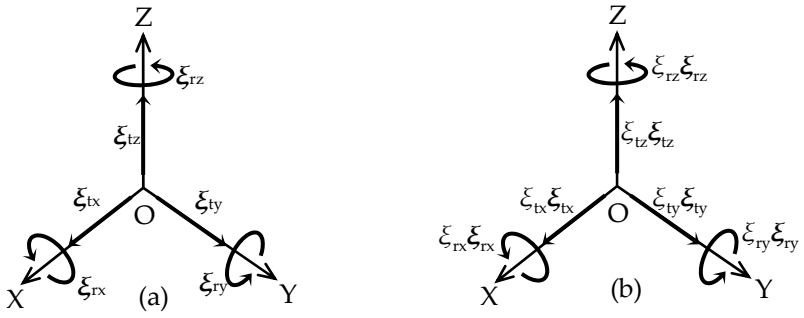

Figure 2.5 Principal twists and linear combination of the principal twists: (a) principal twists, and (b) linear combination of the principal twists

2.2.2.2 Relationship between a wrench and a twist

Assume that a rigid stage in a compliant mechanism is constrained by both constraints (provided by compliant members of the compliant mechanism) and external forces (such as actuation forces). A motion of the rigid stage can be represented by a twist, the constraints can be written as constraint wrenches, and the external forces can be denoted by force wrenches. If the twist is reciprocal to all the wrenches including both constraint wrenches and force wrenches, the direction of the twist is a DOF direction of the rigid stage; otherwise, the direction of the twist is a DOC direction [60, 100]. Note that if the dot product of a twist and a wrench equals zero (as shown in Equation (2.10)), the motion represented by the twist will not produce work under the action of the wrench and the twist is reciprocal to the wrench [60, 100].

For force wrenches:

$$\boldsymbol{\xi} \circ \boldsymbol{\zeta} = \left|\xi_{tx}\zeta_{tx}\right| + \left|\xi_{ty}\zeta_{ty}\right| + \left|\xi_{tz}\zeta_{tz}\right| + \left|\xi_{rx}\zeta_{rx}\right| + \left|\xi_{ry}\zeta_{ry}\right| + \left|\xi_{rz}\zeta_{rz}\right| = 0$$

For constraint wrenches:

$$\boldsymbol{\xi} \circ \boldsymbol{\zeta}_{C} = \left|\xi_{tx}\kappa_{tx}j_{tx}\right| + \left|\xi_{ty}\kappa_{ty}j_{ty}\right| + \left|\xi_{tz}\kappa_{tz}j_{tz}\right| + \left|\xi_{rx}\kappa_{rx}j_{rx}\right| + \left|\xi_{ry}\kappa_{ry}j_{ry}\right| + \left|\xi_{rz}\kappa_{rz}j_{rz}\right| = 0 \tag{2.10}$$

where operator '$\circ$' represents the dot product of a twist and a wrench.

2.2.2.3 Coordinate transformation of wrenches

A wrench, representing a force or a constraint, can be transformed from a coordinate system 'A' to another coordinate system 'B'. Equation (2.11) [60] shows that a coordinate transformation matrix **T**, which can be used to perform the transformation of a wrench from one coordinate system to another.

$$\mathbf{T}=\begin{bmatrix}\mathbf{R} & \mathbf{0}\\ \mathbf{D}\times\mathbf{R} & \mathbf{R}\end{bmatrix} \text{ where } \mathbf{D}=\begin{bmatrix}0 & -z & y\\ z & 0 & -x\\ -y & x & 0\end{bmatrix} \tag{2.11}$$

where the sub-matrix **R** is a 3×3 rotation matrix and the sub-matrix **D** is a 3×3 location skew-symmetric matrix. Based on this transformation matrix, a wrench in a coordinate system 'A' can be represented in another coordinate system 'B' by pre-multiplying the coordinate transformation matrix **T**. The entries x, y and z in the sub-matrix **D** are the coordinates of the origin of the coordinate system 'A' in the coordinate system 'B'.

2.2.3 Mobility of the rigid stages in the topological structure

As stated in Section 2.2.1, the constraint spaces of the compliant modules of a three-legged XYZ CPM can be determined by the mobility of the rigid stages. In this section, the mobility of the rigid stages in the topological structure of a three-legged XYZ CPM is obtained. Additionally, the transmission of the three actuation forces in the topological structure is also described in this section.

In a three-legged XYZ CPM system, the three translations of the MS are actuated by three ground-mounted linear actuators. The actuation forces of the actuators can be regarded as wrenches. A linear actuator can provide a translational force along the actuation axis, but cannot tolerate transverse forces and displacements [87]. Therefore, the actuation force of a linear actuator can be represented by a pure force wrench. This is also the reason why an AS is allowed to translate in one direction only. The actuation forces of the three actuators in a three-legged XYZ CPM system can be written as wrenches based

on Equation (2.1), as shown in Equation (2.12).

$$\zeta_{asx} = \begin{bmatrix} f_{Tasx} & \boldsymbol{r}_{asx} \times f_{Tasx} \end{bmatrix}^T, \zeta_{asy} = \begin{bmatrix} f_{Tasy} & \boldsymbol{r}_{asy} \times f_{Tasy} \end{bmatrix}^T \text{ and}$$
$$\zeta_{asz} = \begin{bmatrix} f_{Tasz} & \boldsymbol{r}_{asz} \times f_{Tasz} \end{bmatrix}^T \tag{2.12}$$

where ζ_{asx}, ζ_{asy} and ζ_{asz} are the three pure force wrenches in a global coordinate system O_{ms}-$X_{ms}Y_{ms}Z_{ms}$, while f_{Tasx}, f_{Tasy} and f_{Tasz} represent the directions of the three pure force wrenches, and $\boldsymbol{r}_{asx}$, $\boldsymbol{r}_{asy}$ and $\boldsymbol{r}_{asz}$ are the three location vectors. In the global coordinate system, the MS is permitted to translate along the X_{ms}-, Y_{ms}- and Z_{ms}-axes. Based on Equation (2.8), the mobility of the MS along the X_{ms}-, Y_{ms}- and Z_{ms}-axes can be described by three principal twists, $\xi_{ms\text{-}tx}$, $\xi_{ms\text{-}ty}$ and $\xi_{ms\text{-}tz}$, of the global coordinate system, as shown in Equation (2.13). As required by the decoupling characteristic, each actuator drives one of the three translations without influencing the other two translations, so that Equation (2.14) can be obtained based on Equation (2.10).

$$\xi_{ms\text{-}tx} = \begin{bmatrix} 1,0,0,0,0,0 \end{bmatrix}^T, \xi_{ms\text{-}ty} = \begin{bmatrix} 0,1,0,0,0,0 \end{bmatrix}^T, \xi_{ms\text{-}tz} = \begin{bmatrix} 0,0,1,0,0,0 \end{bmatrix}^T \tag{2.13}$$

$$\begin{aligned} &\xi_{ms\text{-}tx} \circ \zeta_{asx} \neq 0, \xi_{ms\text{-}tx} \circ \zeta_{asy} = 0, \xi_{ms\text{-}tx} \circ \zeta_{asz} = 0 \\ &\xi_{ms\text{-}ty} \circ \zeta_{asx} = 0, \xi_{ms\text{-}ty} \circ \zeta_{asy} \neq 0, \xi_{ms\text{-}ty} \circ \zeta_{asz} = 0 \\ &\xi_{ms\text{-}tz} \circ \zeta_{asx} = 0, \xi_{ms\text{-}tz} \circ \zeta_{asy} = 0, \xi_{ms\text{-}tz} \circ \zeta_{asz} \neq 0 \end{aligned} \tag{2.14}$$

It can be concluded from Equation (2.14) that: (a) f_{Tasx}, f_{Tasy} and f_{Tasz} should be parallel to the X_{ms}-, Y_{ms}- and Z_{ms}-axes, respectively; and (b) $\boldsymbol{r}_{asx}$, $\boldsymbol{r}_{asy}$ and $\boldsymbol{r}_{asz}$ can be any vectors. Consequently, the three actuation forces should be parallel to the X_{ms}-, Y_{ms}- and Z_{ms}-axes, respectively.

A PM is used to transmit the actuation force of an actuator from the AS to the MS without influencing the forces transmitted by the other two PMs, so that the PM cannot be compressed and elongated along the direction of the actuation force transmitted by the PM, i.e. the PM has a pure force wrench along the

actuation direction. A PM connects an MS and an AS using its two ends, so the force of the actuator inputs from the end connecting the AS and outputs from the end connecting the MS. Both the input force and the output force of a PM should be parallel to the axis of the global coordinate system, but the input force and the output force are not required to be collinear, as shown in Figure 2.6. According to the description above, three PM local coordinate systems (O_{pmx}-$X_{pmx}Y_{pmx}Z_{pmx}$, O_{pmy}-$X_{pmy}Y_{pmy}Z_{pmy}$ and O_{pmz}-$X_{pmz}Y_{pmz}Z_{pmz}$) and three AM local coordinate systems (O_{amx}-$X_{amx}Y_{amx}Z_{amx}$, O_{amy}-$X_{amy}Y_{amy}Z_{amy}$ and O_{amz}-$X_{amz}Y_{amz}Z_{amz}$) are defined, as shown in Figure 2.6.

Figure 2.6 shows that: (a) the MS is permitted to move in the X_{ms}-, Y_{ms}- and Z_{ms}-axes of the global coordinate system; (b) the PM local coordinate systems are located at the centre points of the interfaces between the MS and the three PMs, and are fixed to the MS; (c) each PM is represented as two parallel lines, a parallel line connector, and two small virtual rigid stages which are used to connect the PM to the MS and the AS. The two parallel lines indicate the input direction and the output direction of the actuation force transmitted by the PM; (d) each PM has a pure force wrench along the X-axis of the PM local coordinate system; (e) each AS is constrained to translate only along the X-axis of the PM coordinate system; (f) the AM local coordinate systems are located at the centre points of the interfaces between the ASs and the AMs, and fixed to the ASs; (g) each AM is expressed by one straight line and two virtual rigid stages which are used to connect the AM to the AS and the BS; and (h) each BS is bound to the ground, whose six DOF are completely constrained by the ground. In the next two sections, the constraint spaces and the position spaces will be identified based on the established coordinate systems.

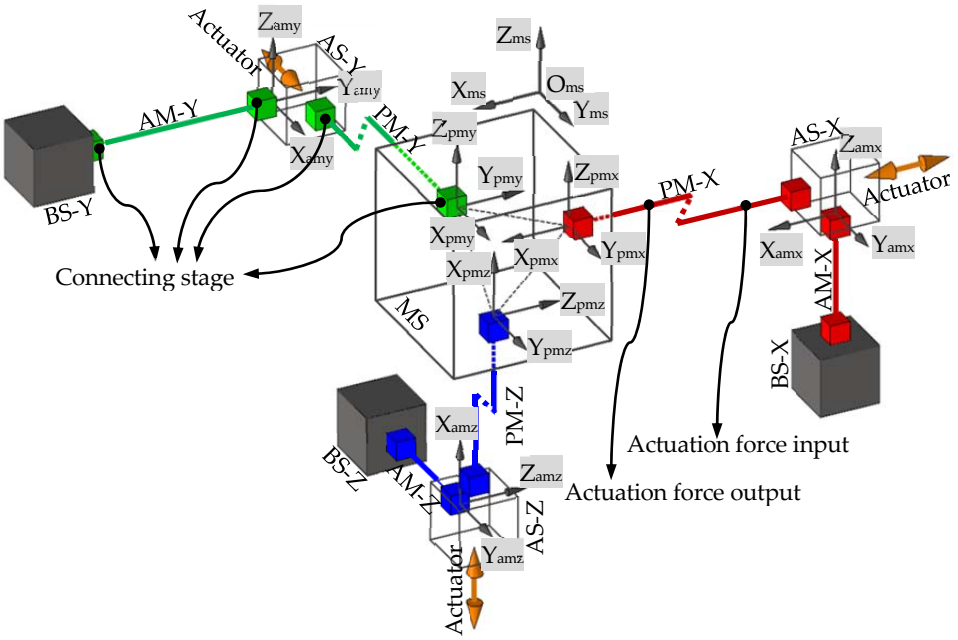

Figure 2.6 Illustration of rigid stages, compliant modules and actuators in a three-legged XYZ CPM system and representation of the defined coordinate systems (global coordinate system O_{ms}-$X_{ms}Y_{ms}Z_{ms}$; PM local coordinate systems O_{pmx}-$X_{pmx}Y_{pmx}Z_{pmx}$, O_{pmy}-$X_{pmy}Y_{pmy}Z_{pmy}$ and O_{pmz}-$X_{pmz}Y_{pmz}Z_{pmz}$; and AM local coordinate systems O_{amx}-$X_{amx}Y_{amx}Z_{amx}$, O_{amy}-$X_{amy}Y_{amy}Z_{amy}$ and O_{amz}-$X_{amz}Y_{amz}Z_{amz}$)

2.2.4 Constraint space identification

Table 2.1 The definitions of the motions of the rigid stages and the constraints of the compliant modules in a three-legged XYZ CPM

Item	Twist of motion	Wrench of constraint	Coordinate system
MS	$\xi_{ms\text{-}tx}$, $\xi_{ms\text{-}ty}$, $\xi_{ms\text{-}tz}$, $\xi_{ms\text{-}rx}$, $\xi_{ms\text{-}ry}$, $\xi_{ms\text{-}rz}$	/	O_{ms}-$X_{ms}Y_{ms}Z_{ms}$
PM-X	/	ζ_{Cpmx}	O_{pmx}-$X_{pmx}Y_{pmx}Z_{pmx}$
PM-Y	/	ζ_{Cpmy}	O_{pmy}-$X_{pmy}Y_{pmy}Z_{pmy}$
PM-Z	/	ζ_{Cpmz}	O_{pmz}-$X_{pz}Y_{pz}Z_{pz}$
AS-X	$\xi_{asx\text{-}tx}$, $\xi_{asx\text{-}ty}$, $\xi_{asx\text{-}tz}$, $\xi_{asx\text{-}rx}$, $\xi_{asx\text{-}ry}$, $\xi_{asx\text{-}rz}$	/	O_{pmx}-$X_{pmx}Y_{pmx}Z_{pmx}$
AS-Y	$\xi_{asy\text{-}tx}$, $\xi_{asy\text{-}ty}$, $\xi_{asy\text{-}tz}$, $\xi_{asy\text{-}rx}$, $\xi_{asy\text{-}ry}$, $\xi_{asy\text{-}rz}$	/	O_{pmy}-$X_{pmy}Y_{pmy}Z_{pmy}$
AS-Z	$\xi_{asz\text{-}tx}$, $\xi_{asz\text{-}ty}$, $\xi_{asz\text{-}tz}$, $\xi_{asz\text{-}rx}$, $\xi_{asz\text{-}ry}$, $\xi_{asz\text{-}rz}$	/	O_{pmz}-$X_{pmz}Y_{pmz}Z_{pmz}$
AM-X	/	ζ_{Camx}	O_{amx}-$X_{amx}Y_{amx}Z_{amx}$
AM-Y	/	ζ_{Camy}	O_{amy}-$X_{amy}Y_{amy}Z_{amy}$
AM-Z	/	ζ_{Camz}	O_{amz}-$X_{amz}Y_{amz}Z_{amz}$

For a decomposed three-legged XYZ CPM, the motions of each of the rigid

stages can be represented by the principal twists in the associated coordinate system, and the constraints of the compliant modules can be represented by wrenches in the associated coordinate systems. Such twists and wrenches are defined and shown in Table 2.1. Note that all the motions of the BSs are restricted by the ground, so the motions of the BSs are not represented by twists. The principal twists defined in Table 2.1 can be written as shown in Equations (2.13) and (2.15) – (2.18), based on Equation (2.8). The wrenches defined in Table 2.1 can be written as wrenches, as shown in Equations (2.19) – (2.24), based on Equation (2.5).

$$\xi_{\text{ms-rx}} = \left[0,0,0,1,0,0\right]^{\text{T}}, \xi_{\text{ms-ry}} = \left[0,0,0,0,1,0\right]^{\text{T}}, \xi_{\text{ms-rz}} = \left[0,0,0,0,0,1\right]^{\text{T}} \tag{2.15}$$

$$\begin{aligned} &\xi_{\text{asx-tx}} = \left[1,0,0,0,0,0\right]^{\text{T}}, \xi_{\text{asx-ty}} = \left[0,1,0,0,0,0\right]^{\text{T}}, \xi_{\text{asx-tz}} = \left[0,0,1,0,0,0\right]^{\text{T}}, \\ &\xi_{\text{asx-rx}} = \left[0,0,0,1,0,0\right]^{\text{T}}, \xi_{\text{asx-ry}} = \left[0,0,0,0,1,0\right]^{\text{T}}, \xi_{\text{asx-rz}} = \left[0,0,0,0,0,1\right]^{\text{T}} \end{aligned} \tag{2.16}$$

$$\begin{aligned} &\xi_{\text{asy-tx}} = \left[1,0,0,0,0,0\right]^{\text{T}}, \xi_{\text{asy-ty}} = \left[0,1,0,0,0,0\right]^{\text{T}}, \xi_{\text{asy-tz}} = \left[0,0,1,0,0,0\right]^{\text{T}}, \\ &\xi_{\text{asy-rx}} = \left[0,0,0,1,0,0\right]^{\text{T}}, \xi_{\text{asy-ry}} = \left[0,0,0,0,1,0\right]^{\text{T}}, \xi_{\text{asy-rz}} = \left[0,0,0,0,0,1\right]^{\text{T}} \end{aligned} \tag{2.17}$$

$$\begin{aligned} &\xi_{\text{asz-tx}} = \left[1,0,0,0,0,0\right]^{\text{T}}, \xi_{\text{asz-ty}} = \left[0,1,0,0,0,0\right]^{\text{T}}, \xi_{\text{asz-tz}} = \left[0,0,1,0,0,0\right]^{\text{T}}, \\ &\xi_{\text{asz-rx}} = \left[0,0,0,1,0,0\right]^{\text{T}}, \xi_{\text{asz-ry}} = \left[0,0,0,0,1,0\right]^{\text{T}}, \xi_{\text{asz-rz}} = \left[0,0,0,0,0,1\right]^{\text{T}} \end{aligned} \tag{2.18}$$

$$\zeta_{\text{Cpmx}} = \left[\kappa_{\text{pmx-tx}} j_{\text{pmx-tx}}, \kappa_{\text{pmx-ty}} j_{\text{pmx-ty}}, \kappa_{\text{pmx-tz}} j_{\text{pmx-tz}}, \kappa_{\text{pmx-rx}} j_{\text{pmx-rx}}, \kappa_{\text{pmx-ry}} j_{\text{pmx-ry}}, \kappa_{\text{pmx-rz}} j_{\text{pmx-rz}}\right]^{\text{T}} \tag{2.19}$$

$$\zeta_{\text{Cpmy}} = \left[\kappa_{\text{pmy-tx}} j_{\text{pmy-tx}}, \kappa_{\text{pmy-ty}} j_{\text{pmy-ty}}, \kappa_{\text{pmy-tz}} j_{\text{pmy-tz}}, \kappa_{\text{pmy-rx}} j_{\text{pmy-rx}}, \kappa_{\text{pmy-ry}} j_{\text{pmy-ry}}, \kappa_{\text{pmy-rz}} j_{\text{pmy-rz}}\right]^{\text{T}} \tag{2.20}$$

$$\zeta_{\text{Cpmz}} = \left[\kappa_{\text{pmz-tx}} j_{\text{pmz-tx}}, \kappa_{\text{pmz-ty}} j_{\text{pmz-ty}}, \kappa_{\text{pmz-tz}} j_{\text{pmz-tz}}, \kappa_{\text{pmz-rx}} j_{\text{pmz-rx}}, \kappa_{\text{pmz-ry}} j_{\text{pmz-ry}}, \kappa_{\text{pmz-rz}} j_{\text{pmz-rz}}\right]^{\text{T}} \tag{2.21}$$

$$\zeta_{\text{Camx}} = \left[\kappa_{\text{amx-tx}} j_{\text{amx-tx}}, \kappa_{\text{amx-ty}} j_{\text{amx-ty}}, \kappa_{\text{amx-tz}} j_{\text{amx-tz}}, \kappa_{\text{amx-rx}} j_{\text{amx-rx}}, \kappa_{\text{amx-ry}} j_{\text{amx-ry}}, \kappa_{\text{amx-rz}} j_{\text{amx-rz}}\right]^{\text{T}} \tag{2.22}$$

$$\zeta_{\text{Camy}} = \left[\kappa_{\text{amy-tx}} j_{\text{amy-tx}}, \kappa_{\text{amy-ty}} j_{\text{amy-ty}}, \kappa_{\text{amy-tz}} j_{\text{amy-tz}}, \kappa_{\text{amy-rx}} j_{\text{amy-rx}}, \kappa_{\text{amy-ry}} j_{\text{amy-ry}}, \kappa_{\text{amy-rz}} j_{\text{amy-rz}}\right]^{\text{T}} \quad (2.23)$$

$$\zeta_{\text{Camz}} = \left[\kappa_{\text{amz-tx}} j_{\text{amz-tx}}, \kappa_{\text{amz-ty}} j_{\text{amz-ty}}, \kappa_{\text{amz-tz}} j_{\text{amz-tz}}, \kappa_{\text{amz-rx}} j_{\text{amz-rx}}, \kappa_{\text{amz-ry}} j_{\text{amz-ry}}, \kappa_{\text{amz-rz}} j_{\text{amz-rz}}\right]^{\text{T}} \quad (2.24)$$

where κ's are constraint coefficients, and j's are direction coefficients.

For a three-legged XYZ CPM, the motions associated with $\xi_{\text{ms-tx}}$, $\xi_{\text{ms-ty}}$, $\xi_{\text{ms-tz}}$, $\xi_{\text{amx-tx}}$, $\xi_{\text{amy-tx}}$ and $\xi_{\text{amz-tx}}$ are permitted, while the others should be constrained. Moreover, the possible permitted constraints of the compliant modules can be identified in the different domains based on Equation (2.10). The wrench and the twist in Equation (2.10) should be in the same coordinate system, so the wrenches in Table 2.1 should be transformed to appropriate coordinate systems. More specifically, ζ_{Cpmx}, ζ_{Cpmy} and ζ_{Cpmz} should be transformed to the global coordinate system, because these wrenches are used to identify the motions associated with $\xi_{\text{ms-tx}}$, $\xi_{\text{ms-ty}}$, $\xi_{\text{ms-tz}}$, $\xi_{\text{ms-rx}}$, $\xi_{\text{ms-ry}}$ and $\xi_{\text{ms-rz}}$. Similarly, ζ_{Camx}, ζ_{Camy} and ζ_{Camz} should be transformed to the coordinate system O_{pmx}-$X_{\text{pmx}}Y_{\text{pmx}}Z_{\text{pmx}}$, O_{pmy}-$X_{\text{pmy}}Y_{\text{pmy}}Z_{\text{pmy}}$ and O_{pmz}-$X_{\text{pmz}}Y_{\text{pmz}}Z_{\text{pmz}}$, respectively. These coordinate transformation matrices can be derived as shown in Equations (2.25) – (2.30), based on Equation (2.11).

$$\mathbf{T}_{\text{pmx-m}} = \begin{bmatrix} 1 & 0 & 0 & 0 & 0 & 0 \\ 0 & 1 & 0 & 0 & 0 & 0 \\ 0 & 0 & 1 & 0 & 0 & 0 \\ 0 & -z_{\text{pmx}} & y_{\text{pmx}} & 1 & 0 & 0 \\ z_{\text{pmx}} & 0 & -x_{\text{pmx}} & 0 & 1 & 0 \\ -y_{\text{pmx}} & x_{\text{pmx}} & 0 & 0 & 0 & 1 \end{bmatrix} \quad (2.25)$$

$$\mathbf{T}_{\text{pmy-m}} = \begin{bmatrix} 0 & -1 & 0 & 0 & 0 & 0 \\ 1 & 0 & 0 & 0 & 0 & 0 \\ 0 & 0 & 1 & 0 & 0 & 0 \\ -z_{\text{pmy}} & 0 & y_{\text{pmy}} & 0 & -1 & 0 \\ 0 & -z_{\text{pmy}} & -x_{\text{pmy}} & 1 & 0 & 0 \\ x_{\text{pmy}} & y_{\text{pmy}} & 0 & 0 & 0 & 1 \end{bmatrix} \tag{2.26}$$

$$\mathbf{T}_{\text{pmz-m}} = \begin{bmatrix} 0 & 0 & -1 & 0 & 0 & 0 \\ 0 & 1 & 0 & 0 & 0 & 0 \\ 1 & 0 & 0 & 0 & 0 & 0 \\ y_{\text{pmz}} & -z_{\text{pmz}} & 0 & 0 & 0 & -1 \\ -x_{\text{pmz}} & 0 & -z_{\text{pmz}} & 0 & 1 & 0 \\ 0 & x_{\text{pmz}} & y_{\text{pmz}} & 1 & 0 & 0 \end{bmatrix} \tag{2.27}$$

$$\mathbf{T}_{\text{amx-pmx}} = \begin{bmatrix} 1 & 0 & 0 & 0 & 0 & 0 \\ 0 & 1 & 0 & 0 & 0 & 0 \\ 0 & 0 & 1 & 0 & 0 & 0 \\ 0 & -z_{\text{amx}} & y_{\text{amx}} & 1 & 0 & 0 \\ z_{\text{amx}} & 0 & -x_{\text{amx}} & 0 & 1 & 0 \\ -y_{\text{amx}} & x_{\text{amx}} & 0 & 0 & 0 & 1 \end{bmatrix} \tag{2.28}$$

$$\mathbf{T}_{\text{amy-pmy}} = \begin{bmatrix} 1 & 0 & 0 & 0 & 0 & 0 \\ 0 & 1 & 0 & 0 & 0 & 0 \\ 0 & 0 & 1 & 0 & 0 & 0 \\ 0 & -z_{\text{amy}} & y_{\text{amy}} & 1 & 0 & 0 \\ z_{\text{amy}} & 0 & -x_{\text{amy}} & 0 & 1 & 0 \\ -y_{\text{amy}} & x_{\text{amy}} & 0 & 0 & 0 & 1 \end{bmatrix} \tag{2.29}$$

$$\mathbf{T}_{\text{amz-pmz}} = \begin{bmatrix} 1 & 0 & 0 & 0 & 0 & 0 \\ 0 & 1 & 0 & 0 & 0 & 0 \\ 0 & 0 & 1 & 0 & 0 & 0 \\ 0 & -z_{\text{amz}} & y_{\text{amz}} & 1 & 0 & 0 \\ z_{\text{amz}} & 0 & -x_{\text{amz}} & 0 & 1 & 0 \\ -y_{\text{amz}} & x_{\text{amz}} & 0 & 0 & 0 & 1 \end{bmatrix} \tag{2.30}$$

where $\mathbf{T}_{\text{pmx-m}}$, $\mathbf{T}_{\text{pmy-m}}$ and $\mathbf{T}_{\text{pmz-m}}$ are the coordinate transformation matrices from the PM local coordinate systems to the global coordinate system.

$\left(x_{\text{pmx}}, y_{\text{pmx}}, z_{\text{pmx}}\right)$, $\left(x_{\text{pmy}}, y_{\text{pmy}}, z_{\text{pmy}}\right)$ and $\left(x_{\text{pmz}}, y_{\text{pmz}}, z_{\text{pmz}}\right)$ are the coordinates of the origins of the PM local coordinate systems in the global coordinate system, respectively, while $\mathbf{T}_{\text{amx-pmx}}$, $\mathbf{T}_{\text{amy-pmy}}$ and $\mathbf{T}_{\text{amz-pmz}}$ are the coordinate transformation matrices from the AM local coordinate systems O_{amx}-$X_{\text{amx}}Y_{\text{amx}}Z_{\text{amx}}$, O_{amy}-$X_{\text{amy}}Y_{\text{amy}}Z_{\text{amy}}$ and O_{amz}-$X_{\text{amz}}Y_{\text{amz}}Z_{\text{amz}}$ to the PM local coordinate systems O_{pmx}-$X_{\text{pmx}}Y_{\text{pmx}}Z_{\text{pmx}}$, O_{pmy}-$X_{\text{pmy}}Y_{\text{pmy}}Z_{\text{pmy}}$ and O_{pmz}-$X_{\text{pmz}}Y_{\text{pmz}}Z_{\text{pmz}}$, respectively. Also, $\left(x_{\text{amx}}, y_{\text{amx}}, z_{\text{amx}}\right)$, $\left(x_{\text{amy}}, y_{\text{amy}}, z_{\text{amy}}\right)$ and $\left(x_{\text{amz}}, y_{\text{amz}}, z_{\text{amz}}\right)$ are the coordinates of the origins of the AM local coordinate systems in the PM local coordinate systems.

Based on Equations (2.11) and (2.25) – (2.30), ζ_{Cpmx}, ζ_{Cpmy} and ζ_{Cpmz} can be transformed to the global coordinate system by pre-multiplying $\mathbf{T}_{\text{pmx-m}}$, $\mathbf{T}_{\text{pmy-m}}$ and $\mathbf{T}_{\text{pmz-m}}$, respectively, which are represented in Equations (2.31), (2.32) and (2.33). Similarly, ζ_{Camx}, ζ_{Camy} and ζ_{Camz} can be transformed to the PM local coordinate systems by pre-multiplying $\mathbf{T}_{\text{amx-pmx}}$, $\mathbf{T}_{\text{amy-pmy}}$ and $\mathbf{T}_{\text{amz-pmz}}$, respectively, as shown in Equations (2.34), (2.35) and (2.36).

$$\begin{aligned}\zeta_{\text{Cpmx}\rightarrow\text{m}} = \mathbf{T}_{\text{pmx-m}}\zeta_{\text{Cpmx}} = \Big[&\kappa_{\text{pmx-tx}} j_{\text{pmx-tx}}, \kappa_{\text{pmx-ty}} j_{\text{pmx-ty}}, \kappa_{\text{pmx-tz}} j_{\text{pmx-tz}}, \kappa_{\text{pmx-rx}} j_{\text{pmx-rx}}, \\ &\kappa_{\text{pmx-ry}} j_{\text{pmx-ry}} + z_{\text{pmx}} j_{\text{pmx-tx}}, \kappa_{\text{pmx-rz}} j_{\text{pmx-rz}} - y_{\text{pmx}} j_{\text{pmx-tx}}\Big]^{\text{T}}\end{aligned} \tag{2.31}$$

$$\begin{aligned}\zeta_{\text{Cpmy}\rightarrow\text{m}} = \mathbf{T}_{\text{pmy-m}}\zeta_{\text{Cpmy}} = \Big[&\kappa_{\text{pmy-ty}} j_{\text{pmy-ty}}, \kappa_{\text{pmy-tx}} j_{\text{pmy-tx}}, \kappa_{\text{pmy-tz}} j_{\text{pmy-tz}}, \\ &-\kappa_{\text{pmy-ry}} j_{\text{pmy-ry}} - z_{\text{pmy}} j_{\text{pmy-tx}}, \kappa_{\text{pmy-rx}} j_{\text{pmy-rx}}, \kappa_{\text{pmy-rz}} j_{\text{pmy-rz}} + x_{\text{pmy}} j_{\text{pmy-tx}}\Big]^{\text{T}}\end{aligned} \tag{2.32}$$

$$\begin{aligned}\zeta_{\text{Cpmz}\rightarrow\text{m}} = \mathbf{T}_{\text{pmz-m}}\zeta_{\text{Cpmz}} = \Big[&\kappa_{\text{pmz-tz}} j_{\text{pmz-tz}}, \kappa_{\text{pmz-ty}} j_{\text{pmz-ty}}, \kappa_{\text{pmz-tx}} j_{\text{pmz-tx}}, \\ &y_{\text{pmz}} j_{\text{pmz-tx}} - \kappa_{\text{pmz-rz}} j_{\text{pmz-rz}}, \kappa_{\text{pmz-ry}} j_{\text{pmz-ry}} - x_{\text{pmz}} j_{\text{pmz-tx}}, \kappa_{\text{pmz-rx}} j_{\text{pmz-rx}}\Big]^{\text{T}}\end{aligned} \tag{2.33}$$

$$\begin{aligned}\zeta_{\text{Camx}\rightarrow\text{pmx}} = \mathbf{T}_{\text{amx-pmx}}\zeta_{\text{Camx}} = \Big[&\kappa_{\text{amx-tx}} j_{\text{amx-tx}}, \kappa_{\text{amx-ty}} j_{\text{amx-ty}}, \kappa_{\text{amx-tz}} j_{\text{amx-tz}}, \kappa_{\text{amx-rx}} j_{\text{amx-rx}}, \\ &\kappa_{\text{amx-ry}} j_{\text{amx-ry}} + z_{\text{amx}} j_{\text{amx-tx}}, \kappa_{\text{amx-rz}} j_{\text{amx-rz}} - y_{\text{amx}} j_{\text{amx-tx}}\Big]^{\text{T}}\end{aligned} \tag{2.34}$$

$$\zeta_{\text{Camy}\rightarrow\text{pmy}} = \mathbf{T}_{\text{amy-pmy}}\zeta_{\text{Camy}} = \left[\kappa_{\text{amy-tx}}j_{\text{amy-tx}}, \kappa_{\text{amy-ty}}j_{\text{amy-ty}}, \kappa_{\text{amy-tz}}j_{\text{amy-tz}}, \kappa_{\text{amy-rx}}j_{\text{amy-rx}}, \kappa_{\text{amy-ry}}j_{\text{amy-ry}} + z_{\text{amy}}j_{\text{amy-tx}}, \kappa_{\text{amy-rz}}j_{\text{amy-rz}} - y_{\text{amy}}j_{\text{amy-tx}}\right]^{\text{T}} \quad (2.35)$$

$$\zeta_{\text{Camz}\rightarrow\text{pmz}} = \mathbf{T}_{\text{amz-pmz}}\zeta_{\text{Camz}} = \left[\kappa_{\text{amz-tx}}j_{\text{amz-tx}}, \kappa_{\text{amz-ty}}j_{\text{amz-ty}}, \kappa_{\text{amz-tz}}j_{\text{amz-tz}}, \kappa_{\text{amz-rx}}j_{\text{amz-rx}}, \kappa_{\text{amz-ry}}j_{\text{amz-ry}} + z_{\text{amz}}j_{\text{amz-tx}}, \kappa_{\text{amz-rz}}j_{\text{amz-rz}} - y_{\text{amz}}j_{\text{amz-tx}}\right]^{\text{T}} \quad (2.36)$$

As discussed in Section 2.1, the instantaneous direction of a constraint wrench is always in the opposite direction to the restricted motion. Therefore, the elements in an entry of the screw vectors, as shown in Equations (2.31) – (2.36), should have the same sign. Taking Equation (2.31) for example, the elements $\kappa_{\text{pmx-rz}}j_{\text{pmx-rz}}$ and $-y_{\text{pmx}}j_{\text{pmx-tx}}$ in the entry $\kappa_{\text{pmx-rz}}j_{\text{pmx-rz}} - y_{\text{pmx}}j_{\text{pmx-tx}}$ always have the same sign. Therefore, $\kappa_{\text{pmx-rz}}j_{\text{pmx-rz}} - y_{\text{pmx}}j_{\text{pmx-tx}}$ can be rewritten as ±1 multiplied by the sum of the absolute values of $\kappa_{\text{pmx-rz}}$ and $-y_{\text{pmx}}$, i.e. $\left|\kappa_{\text{pmx-rz}}\right| + \left|y_{\text{pmx}}\right|$. As a result, Equations (2.31) – (2.36) can be rewritten as

$$\zeta_{\text{Cpmx}\rightarrow\text{m}} = \left[\kappa_{\text{pmx-tx}}j_{\text{pmx-tx}}, \kappa_{\text{pmx-ty}}j_{\text{pmx-ty}}, \kappa_{\text{pmx-tz}}j_{\text{pmx-tz}}, \kappa_{\text{pmx-rx}}j_{\text{pmx-rx}}, \pm\left(\left|\kappa_{\text{pmx-ry}}\right| + \left|z_{\text{pmx}}\right|\right), \pm\left(\left|\kappa_{\text{pmx-rz}}\right| + \left|y_{\text{pmx}}\right|\right)\right]^{\text{T}} \quad (2.37)$$

$$\zeta_{\text{Cpmy}\rightarrow\text{m}} = \left[\kappa_{\text{pmy-ty}}j_{\text{pmy-ty}}, \kappa_{\text{pmy-tx}}j_{\text{pmy-tx}}, \kappa_{\text{pmy-tz}}j_{\text{pmy-tz}}, \pm\left(\left|\kappa_{\text{pmy-ry}}\right| + \left|z_{\text{pmy}}\right|\right), \kappa_{\text{pmy-rx}}j_{\text{pmy-rx}}, \pm\left(\left|\kappa_{\text{pmy-rz}}\right| + \left|x_{\text{pmy}}\right|\right)\right]^{\text{T}} \quad (2.38)$$

$$\zeta_{\text{Cpmz}\rightarrow\text{m}} = \left[\kappa_{\text{pmz-tz}}j_{\text{pmz-tz}}, \kappa_{\text{pmz-ty}}j_{\text{pmz-ty}}, \kappa_{\text{pmz-tx}}j_{\text{pmz-tx}}, \pm\left(\left|y_{\text{pmz}}\right| + \left|\kappa_{\text{pmz-rz}}\right|\right), \pm\left(\left|\kappa_{\text{pmz-ry}}\right| + \left|x_{\text{pmz}}\right|\right), \kappa_{\text{pmz-rx}}j_{\text{pmz-rx}}\right]^{\text{T}} \quad (2.39)$$

$$\zeta_{\text{Camx}\rightarrow\text{pmx}} = \left[\kappa_{\text{amx-tx}}j_{\text{amx-tx}}, \kappa_{\text{amx-ty}}j_{\text{amx-ty}}, \kappa_{\text{amx-tz}}j_{\text{amx-tz}}, \kappa_{\text{amx-rx}}j_{\text{amx-rx}}, \pm\left(\left|\kappa_{\text{amx-ry}}\right| + \left|z_{\text{amx}}\right|\right), \pm\left(\left|\kappa_{\text{amx-rz}}\right| + \left|y_{\text{amx}}\right|\right)\right]^{\text{T}} \quad (2.40)$$

$$\zeta_{\text{Camy}\rightarrow\text{pmy}} = \left[\kappa_{\text{amy-tx}}j_{\text{amy-tx}}, \kappa_{\text{amy-ty}}j_{\text{amy-ty}}, \kappa_{\text{amy-tz}}j_{\text{amy-tz}}, \kappa_{\text{amy-rx}}j_{\text{amy-rx}}, \pm\left(\left|\kappa_{\text{amy-ry}}\right| + \left|z_{\text{amy}}\right|\right), \pm\left(\left|\kappa_{\text{amy-rz}}\right| + \left|y_{\text{amy}}\right|\right)\right]^{\text{T}} \quad (2.41)$$

$$\zeta_{\text{Camz}\rightarrow\text{pmz}} = \Big[\kappa_{\text{amz-tx}} j_{\text{amz-tx}}, \kappa_{\text{amz-ty}} j_{\text{amz-ty}}, \kappa_{\text{amz-tz}} j_{\text{amz-tz}}, \kappa_{\text{amz-rx}} j_{\text{amz-rx}}, \pm\left(\left|\kappa_{\text{amz-ry}}\right| + \left|z_{\text{amz}}\right|\right), \pm\left(\left|\kappa_{\text{amz-rz}}\right| + \left|y_{\text{amz}}\right|\right)\Big]^{\text{T}} \tag{2.42}$$

According to the permitted motions of the MS, Equation (2.43) can be derived based on Equation (2.10) for the MS domain. The values of the constraint coefficients shown in Equation (2.44) can be identified based on Equations (2.37) – (2.39) and (2.43).

$$\begin{aligned}
&\text{(a) } \xi_{\text{ms-tx}} \circ \zeta_{\text{Cpmx}\rightarrow\text{m}} \neq 0 \text{ and } \xi_{\text{ms-tx}} \circ \zeta_{\text{Cpmy}\rightarrow\text{m}} = 0 \text{ and } \xi_{\text{ms-tx}} \circ \zeta_{\text{Cpmz}\rightarrow\text{m}} = 0 \\
&\text{(b) } \xi_{\text{ms-ty}} \circ \zeta_{\text{Cpmx}\rightarrow\text{m}} = 0 \text{ and } \xi_{\text{ms-ty}} \circ \zeta_{\text{Cpmy}\rightarrow\text{m}} \neq 0 \text{ and } \xi_{\text{ms-ty}} \circ \zeta_{\text{Cpmz}\rightarrow\text{m}} = 0 \\
&\text{(c) } \xi_{\text{ms-tz}} \circ \zeta_{\text{Cpmx}\rightarrow\text{m}} = 0 \text{ and } \xi_{\text{ms-tz}} \circ \zeta_{\text{Cpmy}\rightarrow\text{m}} = 0 \text{ and } \xi_{\text{ms-tz}} \circ \zeta_{\text{Cpmz}\rightarrow\text{m}} \neq 0 \\
&\text{(d) } \xi_{\text{ms-rx}} \circ \zeta_{\text{Cpmx}\rightarrow\text{m}} \neq 0 \text{ and/or } \xi_{\text{ms-rx}} \circ \zeta_{\text{Cpmy}\rightarrow\text{m}} \neq 0 \text{ and/or } \xi_{\text{ms-rx}} \circ \zeta_{\text{Cpmz}\rightarrow\text{m}} \neq 0 \\
&\text{(e) } \xi_{\text{ms-ry}} \circ \zeta_{\text{Cpmx}\rightarrow\text{m}} \neq 0 \text{ and/or } \xi_{\text{ms-ry}} \circ \zeta_{\text{Cpmy}\rightarrow\text{m}} \neq 0 \text{ and/or } \xi_{\text{ms-ry}} \circ \zeta_{\text{Cpmz}\rightarrow\text{m}} \neq 0 \\
&\text{(f) } \xi_{\text{ms-rz}} \circ \zeta_{\text{Cpmx}\rightarrow\text{m}} \neq 0 \text{ and/or } \xi_{\text{ms-rz}} \circ \zeta_{\text{Cpmy}\rightarrow\text{m}} \neq 0 \text{ and/or } \xi_{\text{ms-rz}} \circ \zeta_{\text{Cpmz}\rightarrow\text{m}} \neq 0
\end{aligned} \tag{2.43}$$

$$\begin{aligned}
&\text{(a) } \kappa_{\text{pmx-tx}} = 1 \text{ and } \kappa_{\text{pmx-ty}} = 0 \text{ and } \kappa_{\text{pmx-tz}} = 0 \\
&\text{(b) } \kappa_{\text{pmy-tx}} = 1 \text{ and } \kappa_{\text{pmy-ty}} = 0 \text{ and } \kappa_{\text{pmy-tz}} = 0 \\
&\text{(c) } \kappa_{\text{pmz-tx}} = 1 \text{ and } \kappa_{\text{pmz-ty}} = 0 \text{ and } \kappa_{\text{pmz-tz}} = 0 \\
&\text{(d) } \kappa_{\text{pmx-rx}} = 1 \text{ or/and } \kappa_{\text{pmy-ry}} = 1 \text{ or/and } \kappa_{\text{pmz-rz}} = 1 \\
&\text{(e) } \kappa_{\text{pmx-ry}} = 1 \text{ or/and } \kappa_{\text{pmy-rx}} = 1 \text{ or/and } \kappa_{\text{pmz-ry}} = 1 \\
&\text{(f) } \kappa_{\text{pmx-rz}} = 1 \text{ or/and } \kappa_{\text{pmy-rz}} = 1 \text{ or/and } \kappa_{\text{pmz-rx}} = 1
\end{aligned} \tag{2.44}$$

It should be noted that Equation (2.44) shows the completed solutions for the permitted constraints of the PMs in a three-legged XYZ CPM, including the exact constraints and redundant constraints. However, only independent constraints within each PM are considered in this thesis. The process of deriving the values of the constraint coefficients associated with the rotational DOF of the MS requires elaboration. Take $\xi_{\text{ms-rx}} \circ \zeta_{\text{Cpmx}\rightarrow\text{m}} \neq 0$ and/or $\xi_{\text{ms-rx}} \circ \zeta_{\text{Cpmy}\rightarrow\text{m}} \neq 0$ and/or $\xi_{\text{ms-rz}} \circ \zeta_{\text{Cpmz}\rightarrow\text{m}} \neq 0$ in Equation (2.43) for example, based on Equations (2.37) – (2.39), the following equations can be obtained: $\kappa_{\text{pmx-rx}} \neq 0$ or/and $\left|\kappa_{\text{pmy-ry}}\right| + \left|z_{\text{pmy}}\right| \neq 0$ or/and $\left|\kappa_{\text{pmz-rz}}\right| + \left|y_{\text{pmz}}\right| \neq 0$. Suppose that

$\kappa_{\text{pmx-rx}}=0,\ \kappa_{\text{pmy-ry}}=0$ and $\kappa_{\text{pmz-rz}}=0$, the motions associated with $\xi_{\text{ms-rx}}$ cannot be constrained if the global coordinate system is moved to the locations where $z_{\text{pmy}}=y_{\text{pmz}}=0$. In other words, if $\kappa_{\text{pmx-rx}}=0,\ \kappa_{\text{pmy-ry}}=0$ and $\kappa_{\text{pmz-rz}}=0$, there is still a line about which the MS can rotate. Therefore, at least one of the stiffness coefficients $\kappa_{\text{pmx-rx}}$, $\kappa_{\text{pmy-ry}}$ and $\kappa_{\text{pmz-rz}}$ cannot be zero as shown in the fourth row in Equation (2.44). Other stiffness coefficients in Equation (2.44) associated with the rotational DOF of the MS can also be obtained based on the process described as above. It should be pointed out that the results shown in Equation (2.44) are independent of the positions of the PM local coordinate systems (or the PMs).

In the same way, according to the permitted motions of the ASs in the AS domains, Equation (2.45) can be derived based on Equation (2.10) if the constraints of the PMs to the ASs are not considered. The values of the constraint coefficients can be identified as shown in Equation (2.46) based on Equations (2.40) – (2.42) and (2.45). The values of the stiffness coefficients in Equation (2.46) are also not subject to the positions of the AM local coordinate systems (or the AMs).

$$
\begin{aligned}
&\text{(a) } \xi_{\text{asx-tx}}\circ\zeta_{\text{Camx}\rightarrow\text{pmx}}=0 \text{ and } \xi_{\text{asx-ty}}\circ\zeta_{\text{Camx}\rightarrow\text{pmx}}\neq 0 \text{ and } \xi_{\text{asx-tz}}\circ\zeta_{\text{Camx}\rightarrow\text{pmx}}\neq 0 \text{ and}\\
&\quad \xi_{\text{asx-rx}}\circ\zeta_{\text{Camx}\rightarrow\text{pmx}}\neq 0 \text{ and } \xi_{\text{asx-ry}}\circ\zeta_{\text{Camx}\rightarrow\text{pmx}}\neq 0 \text{ and } \xi_{\text{asx-rz}}\circ\zeta_{\text{Camx}\rightarrow\text{pmx}}\neq 0\\
&\text{(b) } \xi_{\text{asy-tx}}\circ\zeta_{\text{Camy}\rightarrow\text{pmy}}=0 \text{ and } \xi_{\text{asy-ty}}\circ\zeta_{\text{Camy}\rightarrow\text{pmy}}\neq 0 \text{ and } \xi_{\text{asy-tz}}\circ\zeta_{\text{Camy}\rightarrow\text{pmy}}\neq 0 \text{ and}\\
&\quad \xi_{\text{asy-rx}}\circ\zeta_{\text{Camy}\rightarrow\text{pmy}}\neq 0 \text{ and } \xi_{\text{asy-ry}}\circ\zeta_{\text{Camy}\rightarrow\text{pmy}}\neq 0 \text{ and } \xi_{\text{asy-rz}}\circ\zeta_{\text{Camy}\rightarrow\text{pmy}}\neq 0\\
&\text{(c) } \xi_{\text{asz-tx}}\circ\zeta_{\text{Camz}\rightarrow\text{pmz}}=0 \text{ and } \xi_{\text{asz-ty}}\circ\zeta_{\text{Camz}\rightarrow\text{pmz}}\neq 0 \text{ and } \xi_{\text{asz-tz}}\circ\zeta_{\text{Camz}\rightarrow\text{pmz}}\neq 0 \text{ and}\\
&\quad \xi_{\text{asz-rx}}\circ\zeta_{\text{Camz}\rightarrow\text{pmz}}\neq 0 \text{ and } \xi_{\text{asz-ry}}\circ\zeta_{\text{Camz}\rightarrow\text{pmz}}\neq 0 \text{ and } \xi_{\text{asz-rz}}\circ\zeta_{\text{Camz}\rightarrow\text{pmz}}\neq 0
\end{aligned}
\tag{2.45}
$$

$$
\begin{aligned}
&\text{(a) } \kappa_{\text{amx-tx}}=0 \text{and} \kappa_{\text{amx-ty}}=1 \text{ and} \kappa_{\text{amx-tz}}=1 \text{and}\\
&\quad \kappa_{\text{amx-rx}}=1 \text{and} \kappa_{\text{amx-ry}}=1 \text{and} \kappa_{\text{amx-ry}}=1\\
&\text{(b) } \kappa_{\text{amy-tx}}=0 \text{and} \kappa_{\text{amy-ty}}=1 \text{ and} \kappa_{\text{amy-tz}}=1 \text{and}\\
&\quad \kappa_{\text{amy-rx}}=1 \text{and} \kappa_{\text{amy-ry}}=1 \text{and} \kappa_{\text{amy-ry}}=1\\
&\text{(c) } \kappa_{\text{amz-tx}}=0 \text{and} \kappa_{\text{amz-ty}}=1 \text{ and} \kappa_{\text{amz-tz}}=1 \text{and}\\
&\quad \kappa_{\text{amz-rx}}=1 \text{and} \kappa_{\text{amz-ry}}=1 \text{and} \kappa_{\text{amz-ry}}=1
\end{aligned}
\tag{2.46}
$$

Equation (2.44) shows that there are 27 (3×3×3=27) permitted constraint combinations for the PM-X, PM-Y and PM-Z if the redundant constraints from the three PMs to the MS are not considered. It can be seen from Equation (2.46) that each AM has five constraints in the AM local coordinate system if the constraints of the PM imposed on the AS are not considered.

At this part of the design, ASs are completely constrained by the AMs with the 27 permitted exact-constraint combinations for the PMs, which are shown in Table B.1 in Appendix B. The constraint combinations in Table B.1 form the basic constraint space of the compliant modules (i.e. B-constraint space), which is a subspace of the constraint spaces of the compliant modules.

As shown in Figure 2.2, each PM is included not only in the MS domain but also in the AS domain. Therefore, each AS can be constrained by both the PM and the AM. The following two conditions should be met if a PM can constrain an extra rotational DOF of the AS connecting to the PM: (a) the PM should have the constraint associated with the extra rotational DOF of the AS; and (b) this extra rotational DOF of the AS should be restricted by the other leg(s). Based on these two conditions, another subspace of the constraint space, termed the T-constraint space, can be obtained by transmitting some of the rotational constraints (each PM has one translational constraint which is used to actuate the MS, so the translational constraints of the PMs cannot be transmitted to the AMs) from the AMs to the PMs in the B-constraint space. One or more redundant constraints can be added to the PMs and AMs in the B-constraint space and the T-constraint space, and therefore the constraint space with redundant constraints is defined as the S-constraint space. Overall, the complete constraint space of the compliant modules consists of the B-constraint space, the T-constraint space and the S-constraint space, the relationships of which are represented in Figure 2.7.

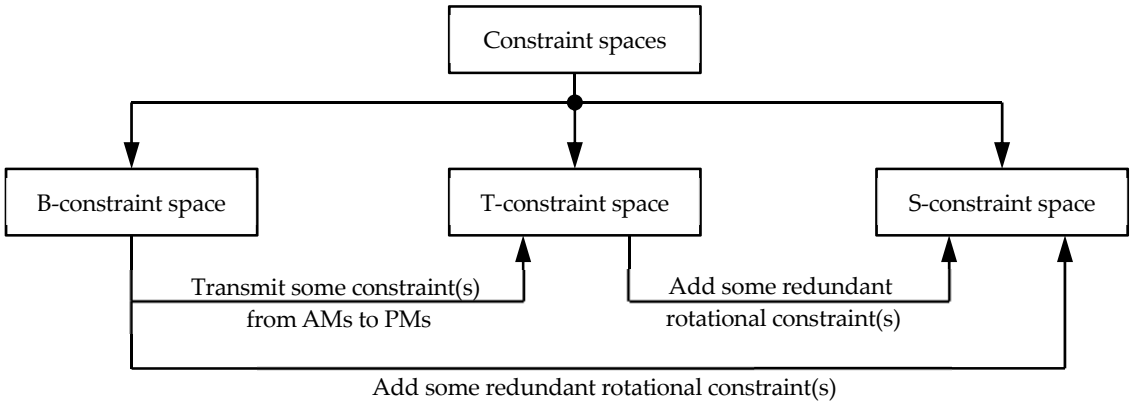

Figure 2.7 Relationships among the B-constraint space, T-constraint space and S-constraint space

2.3 Position Space

2.3.1 PM position space

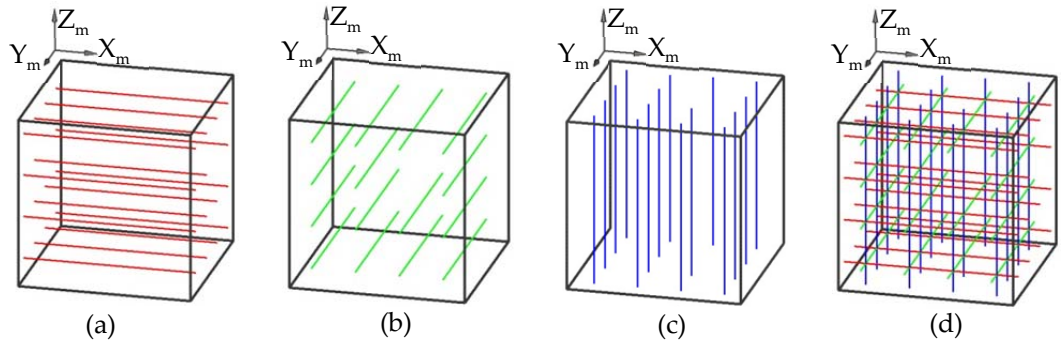

Figure 2.8 Permitted positions of the three PMs excluding considering the rotations about the X-axes of the three PM local coordinate systems: (a) permitted positions of the PM-X (red lines), (b) permitted positions of the PM-Y (green lines), (c) permitted positions of the PM-Z (blue lines), and (d) permitted position combination of the three PMs

From the discussion in Section 2.2.4, the results of the constraint coefficients shown in Equation (2.44) are independent of the positions of the PMs. Therefore, PMs can translate freely, and this cannot affect the constraints of the PMs to the XYZ CPM system. Moreover, each PM cannot rotate about the Y- and Z-axes of the PM local coordinate system, because the direction of the pure force wrench of the PM should be parallel to the local X-axis. If using three straight lines to represent the three PMs and ignoring considering the rotations of the three PMs

about the three X-axes of the three PM local coordinate systems, the permitted positions of the three PMs can be shown in Figure 2.8.

The following work is to identify if a PM can rotate about the X-axis of the PM local coordinate system, by taking PM-X as an example. Based on Table 2.1 and Equation (2.44), the constraint wrench of the PM-X can be written as

$$\zeta_{\text{Cpmx}} = \left[j_{\text{pmx-tx}}, 0, 0, \kappa_{\text{pmx-rx}} j_{\text{pmx-rx}}, \kappa_{\text{pmx-ry}} j_{\text{pmx-ry}}, \kappa_{\text{pmx-rz}} j_{\text{pmx-rz}} \right]^{\text{T}} \tag{2.47}$$

The coordinate transformation matrix, in terms of the rotation about the X-axis, is shown in Equation (2.48), based on Equation (2.11).

$$\mathbf{T}_{\text{pmx-Rx}} = \begin{bmatrix} 1 & 0 & 0 & 0 & 0 & 0 \\ 0 & \cos(\alpha_{\text{pmx}}) & -\sin(\alpha_{\text{pmx}}) & 0 & 0 & 0 \\ 0 & \sin(\alpha_{\text{pmx}}) & \cos(\alpha_{\text{pmx}}) & 0 & 0 & 0 \\ 0 & 0 & 0 & 1 & 0 & 0 \\ 0 & 0 & 0 & 0 & \cos(\alpha_{\text{pmx}}) & -\sin(\alpha_{\text{pmx}}) \\ 0 & 0 & 0 & 0 & \sin(\alpha_{\text{pmx}}) & \cos(\alpha_{\text{pmx}}) \end{bmatrix} \tag{2.48}$$

where α_{pmx} is the angle of the rotation about the X-axis of the PM local coordinate system O_{pmx}-$X_{\text{pmx}}Y_{\text{pmx}}Z_{\text{pmx}}$. After the rotation, the constraint wrench of the PM-X in the PM local coordinate system can be represented by $\zeta_{\text{Cpmx-Rx}}$ which can be written in Equation (2.49) based on Equations (2.47) and (2.48).

$$\zeta_{\text{Cpmx-Rx}} = \mathbf{T}_{\text{pmx-Rx}} \zeta_{\text{Cpmx}} = \begin{bmatrix} j_{\text{pmx-tx}} \\ 0 \\ 0 \\ \kappa_{\text{pmx-rx}} j_{\text{pmx-rx}} \\ \kappa_{\text{pmx-ry}} \cos(\alpha_{\text{pmx}}) j_{\text{pmx-ry}} - \kappa_{\text{pmx-rz}} \sin(\alpha_{\text{pmx}}) j_{\text{pmx-rz}} \\ \kappa_{\text{pmx-ry}} \sin(\alpha_{\text{pmx}}) j_{\text{pmx-ry}} + \kappa_{\text{pmx-rz}} \cos(\alpha_{\text{pmx}}) j_{\text{pmx-rz}} \end{bmatrix} = \begin{bmatrix} j_{\text{pmx-tx}} \\ 0 \\ 0 \\ \kappa_{\text{pmx-rx}} j_{\text{pmx-rx}} \\ \pm\left(\left| \kappa_{\text{pmx-ry}} \cos(\alpha_{\text{pmx}}) \right| + \left| \kappa_{\text{pmx-rz}} \sin(\alpha_{\text{pmx}}) \right| \right) \\ \pm\left(\left| \kappa_{\text{pmx-ry}} \sin(\alpha_{\text{pmx}}) \right| + \left| \kappa_{\text{pmx-rz}} \cos(\alpha_{\text{pmx}}) \right| \right) \end{bmatrix} \tag{2.49}$$

where $\kappa_{\text{pmx-ry}} \cos(\alpha_{\text{pmx}}) j_{\text{pmx-ry}} - \kappa_{\text{pmx-rz}} \sin(\alpha_{\text{pmx}}) j_{\text{pmx-rz}}$ is equivalent to

$\pm\left(\left|\kappa_{\text{pmx-ry}}\cos(\alpha_{\text{pmx}})\right|+\left|\kappa_{\text{pmx-rz}}\sin(\alpha_{\text{pmx}})\right|\right)$ because $\kappa_{\text{pmx-ry}}\cos(\alpha_{\text{pmx}})j_{\text{pmx-ry}}$ and $-\kappa_{\text{pmx-rz}}\sin(\alpha_{\text{pmx}})j_{\text{pmx-rz}}$ always have the same sign. Similarly, $\kappa_{\text{pmx-ry}}\sin(\alpha_{\text{pmx}})j_{\text{pmx-ry}}+\kappa_{\text{pmx-rz}}\cos(\alpha_{\text{pmx}})j_{\text{pmx-rz}}$ is equivalent to $\pm\left(\left|\kappa_{\text{pmx-ry}}\sin(\alpha_{\text{pmx}})\right|+\left|\kappa_{\text{pmx-rz}}\cos(\alpha_{\text{pmx}})\right|\right)$.

The PM-X is able to rotate about the X-axis of the PM local coordinate system if the wrenches ζ_{Cpmx} and $\zeta_{\text{Cpmx-Rx}}$ are equivalent. It can be concluded from Equation (2.49) that: (a) the PM-X can rotate about the X-axis if $\kappa_{\text{pmx-ry}}=\kappa_{\text{pmx-rz}}=0 \text{ or } 1$, and (b) the PM-X cannot rotate about the X-axis if $\kappa_{\text{pmx-ry}}\neq\kappa_{\text{pmx-rz}}$.

Overall, the position space of a PM is summarized as follows:

(a) The PM can translate freely, but cannot rotate about the Y- and Z-axes of the PM local coordinate system, which is represented in Figure 2.8.
(b) The PM can rotate about the X-axis of the PM local coordinate system, if both of the directions about the Y- and Z-axes in the PM local coordinate system are DOC directions or DOF directions of the PM.
(c) The PM cannot rotate about the X-axis of the PM local coordinate system if the PM can provide only one of the two rotational constraints about the Y- and Z-axes in the PM local coordinate system.

Note that in this section only the position space for a PM or an AM as a whole is considered. Actually, each PM or AM can be decomposed into several sub-compliant modules, and each of the sub-compliant modules has a position space. However, the position spaces of the sub-compliant modules are not considered in this chapter.

2.3.2 AM position space

According to Section 2.2.4, the results of the constraint coefficients as shown in

Equation (2.46) are independent of the positions of the AMs. Therefore, an AM can translate freely, which cannot affect the constraints of the AMs to the XYZ CPM system. Moreover, each AM cannot rotate about the Y- and Z-axes of the AM local coordinate system so that the DOF direction of the AM must be the same as that of the force provided by the actuator.

The following work is to identify whether an AM can rotate about the X-axis of the AM local coordinate system, by taking AM-X as an example. Based on Table 2.1 and the AM constraint space discussed in Section 2.2.4, the constraint wrench of the AM-X can be written as

$$\zeta_{\text{Camx}} = \left[0, j_{\text{amx-ty}}, j_{\text{amx-tz}}, \kappa_{\text{amx-rx}} j_{\text{amx-rx}}, \kappa_{\text{amx-ry}} j_{\text{amx-ry}}, \kappa_{\text{amx-rz}} j_{\text{amx-rz}}\right]^{\text{T}} \tag{2.50}$$

The coordinate transformation matrix in terms of the rotation about the X-axis is shown in Equation (2.51), based on Equation (2.11).

$$\mathbf{T}_{\text{amx-Rx}} = \begin{bmatrix} 1 & 0 & 0 & 0 & 0 & 0 \\ 0 & \cos(\alpha_{\text{amx}}) & -\sin(\alpha_{\text{amx}}) & 0 & 0 & 0 \\ 0 & \sin(\alpha_{\text{amx}}) & \cos(\alpha_{\text{amx}}) & 0 & 0 & 0 \\ 0 & 0 & 0 & 1 & 0 & 0 \\ 0 & 0 & 0 & 0 & \cos(\alpha_{\text{amx}}) & -\sin(\alpha_{\text{amx}}) \\ 0 & 0 & 0 & 0 & \sin(\alpha_{\text{amx}}) & \cos(\alpha_{\text{amx}}) \end{bmatrix} \tag{2.51}$$

where α_{amx} is the angle of the rotation about the X-axis of the AM local coordinate system. Additionally, ζ_{Camx} can be transformed to $\zeta_{\text{Camx-Rx}}$, as shown in Equation (2.52).

$$\zeta_{\text{Camx-Rx}} = \mathbf{T}_{\text{amx-Rx}} \zeta_{\text{Camx}} = \begin{bmatrix} 0 \\ \cos(\alpha_{\text{amx}}) j_{\text{amx-ty}} - \sin(\alpha_{\text{amx}}) j_{\text{amx-tz}} \\ \sin(\alpha_{\text{amx}}) j_{\text{amx-ty}} + \cos(\alpha_{\text{amx}}) j_{\text{amx-tz}} \\ \kappa_{\text{amx-rx}} j_{\text{amx-rx}} \\ \kappa_{\text{amx-ry}} \cos(\alpha_{\text{amx}}) j_{\text{amx-ry}} - \kappa_{\text{amx-rz}} \sin(\alpha_{\text{amx}}) j_{\text{amx-rz}} \\ \kappa_{\text{amx-ry}} \sin(\alpha_{\text{amx}}) j_{\text{amx-ry}} + \kappa_{\text{amx-rz}} \cos(\alpha_{\text{amx}}) j_{\text{amx-rz}} \end{bmatrix} = \begin{bmatrix} 0 \\ \pm\left(\left|\cos(\alpha_{\text{amx}})\right| + \left|\sin(\alpha_{\text{amx}})\right|\right) \\ \pm\left(\left|\sin(\alpha_{\text{amx}})\right| + \left|\cos(\alpha_{\text{amx}})\right|\right) \\ \kappa_{\text{amx-rx}} j_{\text{amx-rx}} \\ \pm\left(\left|\kappa_{\text{amx-ry}} \cos(\alpha_{\text{amx}})\right| + \left|\kappa_{\text{amx-rz}} \sin(\alpha_{\text{amx}})\right|\right) \\ \pm\left(\left|\kappa_{\text{amx-ry}} \sin(\alpha_{\text{amx}})\right| + \left|\kappa_{\text{amx-rz}} \cos(\alpha_{\text{amx}})\right|\right) \end{bmatrix} \tag{2.52}$$

On the basis of Equation (2.52), one can obtain the following: (a) the AM-X can rotate about the X-axis if $\kappa_{\text{amx-ry}} = \kappa_{\text{amx-rz}} = 0$ or 1, and (b) the AM-X cannot rotate about the X-axis if $\kappa_{\text{amx-ry}} \neq \kappa_{\text{amx-rz}}$.

Overall, the position space of an AM is summarized as follows:

(a) The AM can translate freely, but cannot rotate about the Y- and Z-axes of the AM local coordinate system.

(b) The AM can rotate about the X-axis of the AM local coordinate system if both of the directions about the Y- and Z-axes in the AM local coordinate system are DOC directions or DOF directions of the AM. The permitted rotations of the three AMs are illustrated in Figure 2.9.

(c) The AM cannot rotate about the X-axis of the AM local coordinate system if the AM can provide only one of the two rotational constraints about the Y- and Z-axes in the AM local coordinate system.

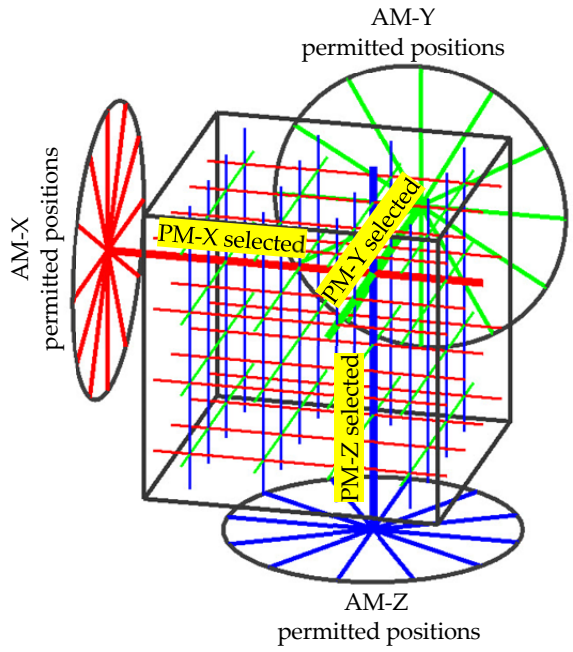

Figure 2.9 Permitted rotations of the AMs about the X-axes in the three AM local coordinate systems (PM-X and AM-X are shown by red lines; PM-Y and AM-Y are shown by green lines; and PM-Z and AM-Z are shown by blue lines)

Similar to the position space discussion for the PM in Section 2.3.1, if one AM is

comprised of several sub-compliant modules, the consideration of the position spaces of the sub-compliant modules is also out of the scope of this chapter.

2.4 Synthesis Procedure

The CPI approach is summarized as follows: once the constraint spaces and the position spaces of the compliant modules in the topological structure of a three-legged XYZ CPM are identified, the geometrical forms of the compliant modules can be derived based on the permitted constraints selected from the associated constraint spaces using the existing approaches such as the FACT approach, and then the compliant modules can be combined with the rigid stages based on the permitted positions selected from the position spaces. The selections of the permitted constraints and positions differ from case to case, depending on the requirements.

In practice, the final three-legged XYZ CPM is chosen from several potential three-legged XYZ CPMs synthesized based on different selections. Moreover, further modification may be needed to make the three-legged XYZ CPM have desired characteristics such as symmetric structure, compact configuration and easy fabrication. Additionally, the three-legged XYZ CPM may be modified into an XYZ CPM with more than three legs via adding redundant legs.

It should be emphasized that the CPI approach is based on a systematic arrangement of rigid stages and compliant modules using the constraint spaces and position spaces. The CPI approach based synthesis procedure is described in Figure 2.10.

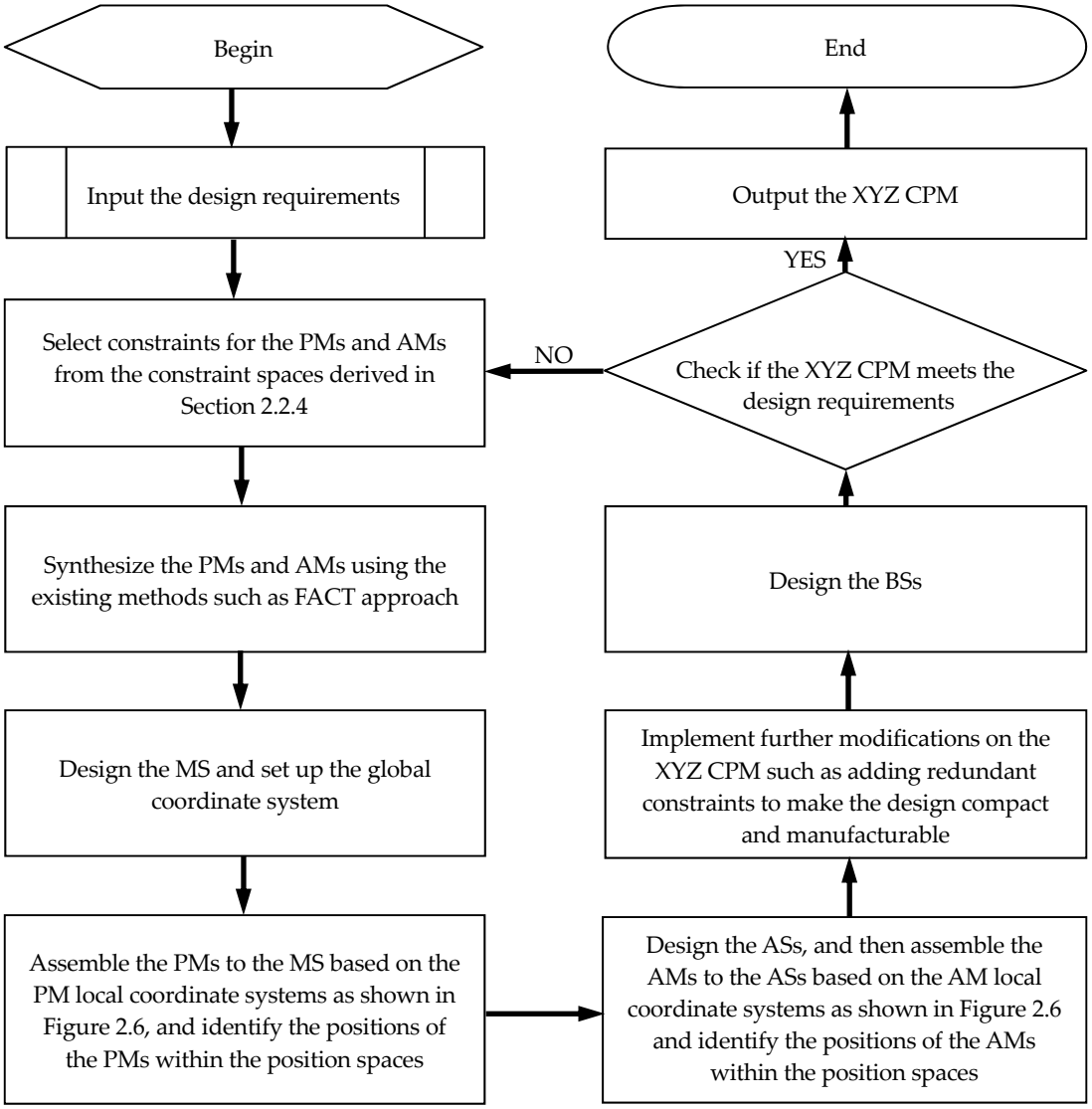

Figure 2.10 Flow chart for the CPI approach design procedure

2.5 Case Study

This section will use an example to demonstrate how to synthesize XYZ CPMs using the CPI approach. Suppose that the objective of the example is to synthesize XYZ CPMs with monolithic configurations such as the ones proposed in [87, 101]. The synthesis can be followed, based on Steps (i) to (ix) below.

i. Select constraints for the PMs and AMs from the constraint spaces shown in Appendix B. According to the design requirement, it is better to select the combination in which the PM-X, PM-Y and PM-Z have the same

constraint and the AM-X, AM-Y and AM-Z also have the same constraint, i.e., isotropic legs. The reason for this choice is that compliant modules can be designed with the same structure if the compliant modules have the same constraints. Therefore, Combination 16 in the B-constraint space (listed in Appendix B) is selected as the constraints of the compliant modules. In order to obtain more monolithic XYZ CPMs, a further three cases are derived based on Combination 16, which are shown in Table 2.2. In the table, Case 1 is Combination 16 listed in Appendix B. Case 2 is derived by selecting three redundant rotational constraints for the PMs used in Case 1, so that Case 2 belongs to the S-constraint space. Case 3 is determined by transmitting three rotational constraints (the underlined rotational constraints in Case 1) from the AMs to the PMs in Case 1, and then adding three redundant rotational constraints for the PMs, so Case 3 still belongs to the S-constraint space. If all redundant rotational constraints are selected for the PMs and AMs, Case 4 is generated, which is one case within the S-constraint space.

ii. Synthesize the structures of the PMs and AMs based on the constraints selected in Step i. In this example, several parallel compliant modules are synthesized using the FACT method [66] as shown in Figure 2.11. The compliant module in Figure 2.12(a), a 4-DOC parallel module, is designed by deleting two of the beams of the compliant module shown in Figure 2.11(c). The compliant module shown in Figure 2.12(b) and Figure 2.12(c), a 4-DOC serial module, is conceived by stacking the two compliant modules in Figure 2.11(d) together. These compliant modules include all the required compliant modules that are used in the 4 cases in Step i; however, other possible permitted geometrical forms of the compliant modules can be obtained based on the same constraints, if necessary.

iii. Choose cubes as the MSs (the dimensions can be ignored in this early-stage design) for these cases, and set up the global coordinate system, as

shown in Figure 2.6.

iv. Assemble the PMs based on the PM local coordinate systems, as shown in Figure 2.6, and the position spaces of the PMs, as illustrated in Figure 2.8(d). Here, the rotations of the PMs about the X-axes of the PM local coordinate systems should be identified based on the specific constraints of the PMs. The 2-DOC module in Figure 2.11(a) is selected as the PM for Case 1. The positions of the three PMs are identified as shown in Figure 2.13(a), and the orientations of the PMs should be subject to the PM local coordinate systems as illustrated in Figure 2.13(b). The three PMs cannot rotate about the three local X-axes due to their constraints based on the results in Section 2.3.1. Similarly, the PMs and their selected positions for Cases 2 to 4 are shown in Figure 2.14 to Figure 2.17, of which both Figure 2.16 and Figure 2.17 are correspond to Case 4.

v. Design ASs for the four cases. There are no specific requirements about the ASs.

vi. Identify the positions of the AMs in terms of the position spaces. For Case 1, the 5-DOC-1 module, shown in Figure 2.11(c), is selected as the AM. The permitted positions and selected positions of the AMs are represented in Figure 2.13(c) based on Figure 2.9, where the translations of the AMs are not considered in these cases. The positions for the three AMs, as shown in Figure 2.13(c), are selected to make the XYZ CPM compact. Similarly, the positions of the AMs for Cases 2 to 4 are shown in Figure 2.14 to Figure 2.17, of which both Figure 2.16 and Figure 2.17 are again correspond to Case 4.

vii. Make further modifications for the four cases. For example, an inactive module is added to the XYZ CPM in Case 1.

viii. Design BSs for the four cases. It should be noticed that the intermediate stages of the PMs of the XYZ CPMs as shown in Figure 2.15 and Figure 2.16 are selected as the equivalent BSs, because the intermediate stages can also provide the equivalent constraints to the ASs.

ix. Check if the final XYZ CPMs in the four cases meet the design requirements. The three novel XYZ CPMs, 4-4-XYZ CPM, 4-5-XYZ CPM-1 and 4-5-XYZ CPM-2, as shown in Figure 2.15 and Figure 2.16, are created in this chapter. The FEA results, shown in Figure 2.18 to Figure 2.20, validate the decoupled nature of the translational motions. The 2-5-XYZ CPM and 3-5-XYZ CPM, as shown in Figure 2.13 and Figure 2.14, were also proposed by Hao in [77] and [101]. A prototype for the 3-5-XYZ CPM is also demonstrated in Figure 2.21. The 4-5-XYZ CPM-3 illustrated in Figure 2.17 was already reported [87] by Awtar. These resulting XYZ CPMs can be manufactured easily by cutting in the three orthogonal directions.

Table 2.2 Four constraint combination cases for the PMs and AMs

Item	Module	Constraints in the PM and AM local coordinate systems		
		X	Y	Z
Case 1	PMs	$T_{px\text{-}tx}R_{px\text{-}rz}$	$T_{py\text{-}tx}R_{py\text{-}ry}$	$T_{pz\text{-}tx}R_{pz\text{-}ry}$
	AMs	$T_{ax\text{-}ty}T_{ax\text{-}tz}R_{ax\text{-}rx}\underline{R_{ax\text{-}ry}}R_{ax\text{-}rz}$	$T_{ay\text{-}ty}T_{ay\text{-}tz}R_{ay\text{-}rx}R_{ay\text{-}ry}\underline{R_{ay\text{-}rz}}$	$T_{az\text{-}ty}T_{az\text{-}tz}R_{az\text{-}rx}R_{az\text{-}ry}\underline{R_{az\text{-}rz}}$
Case 2	PMs	$T_{px\text{-}tx}R_{px\text{-}ry}R_{px\text{-}rz}$	$T_{py\text{-}tx}R_{py\text{-}ry}R_{py\text{-}rz}$	$T_{pz\text{-}tx}R_{pz\text{-}ry}R_{pz\text{-}rz}$
	AMs	$T_{ax\text{-}ty}T_{ax\text{-}tz}R_{ax\text{-}rx}R_{ax\text{-}ry}R_{ax\text{-}rz}$	$T_{ay\text{-}ty}T_{ay\text{-}tz}R_{ay\text{-}rx}R_{ay\text{-}ry}R_{ay\text{-}rz}$	$T_{az\text{-}ty}T_{az\text{-}tz}R_{az\text{-}rx}R_{az\text{-}ry}R_{az\text{-}rz}$
Case 3	PMs	$T_{px\text{-}tx}R_{px\text{-}rx}R_{px\text{-}ry}R_{px\text{-}rz}$	$T_{py\text{-}tx}R_{py\text{-}rx}R_{py\text{-}ry}R_{py\text{-}rz}$	$T_{pz\text{-}tx}R_{pz\text{-}rx}R_{pz\text{-}ry}R_{pz\text{-}rz}$
	AMs	$T_{ax\text{-}ty}T_{ax\text{-}tz}R_{ax\text{-}rx}R_{ax\text{-}rz}$	$T_{ay\text{-}ty}T_{ay\text{-}tz}R_{ay\text{-}rx}R_{ay\text{-}ry}$	$T_{az\text{-}ty}T_{az\text{-}tz}R_{az\text{-}rx}R_{az\text{-}ry}$
Case 4	PMs	$T_{px\text{-}tx}R_{px\text{-}rx}R_{px\text{-}ry}R_{px\text{-}rz}$	$T_{py\text{-}tx}R_{py\text{-}rx}R_{py\text{-}ry}R_{py\text{-}rz}$	$T_{pz\text{-}tx}R_{pz\text{-}rx}R_{pz\text{-}ry}R_{pz\text{-}rz}$
	AMs	$T_{ax\text{-}ty}T_{ax\text{-}tz}R_{ax\text{-}rx}R_{ax\text{-}ry}R_{ax\text{-}rz}$	$T_{ay\text{-}ty}T_{ay\text{-}tz}R_{ay\text{-}rx}R_{ay\text{-}ry}R_{ay\text{-}rz}$	$T_{az\text{-}ty}T_{az\text{-}tz}R_{az\text{-}rx}R_{az\text{-}ry}R_{az\text{-}rz}$

It can be concluded that all the resultant XYZ CPMs meet the early-stage design requirements and that they are compact and can be fabricated easily. Further comparisons can be made based on specific working conditions, non-linear kinematostatic analysis, dynamic analysis, etc. In addition, two non-monolithic designs, showing the PM rotations about the X-axes of the PM local coordinate systems, can be seen in Appendix C. Note that redundant legs can also be added to the synthesized three-legged XYZ CPMs.

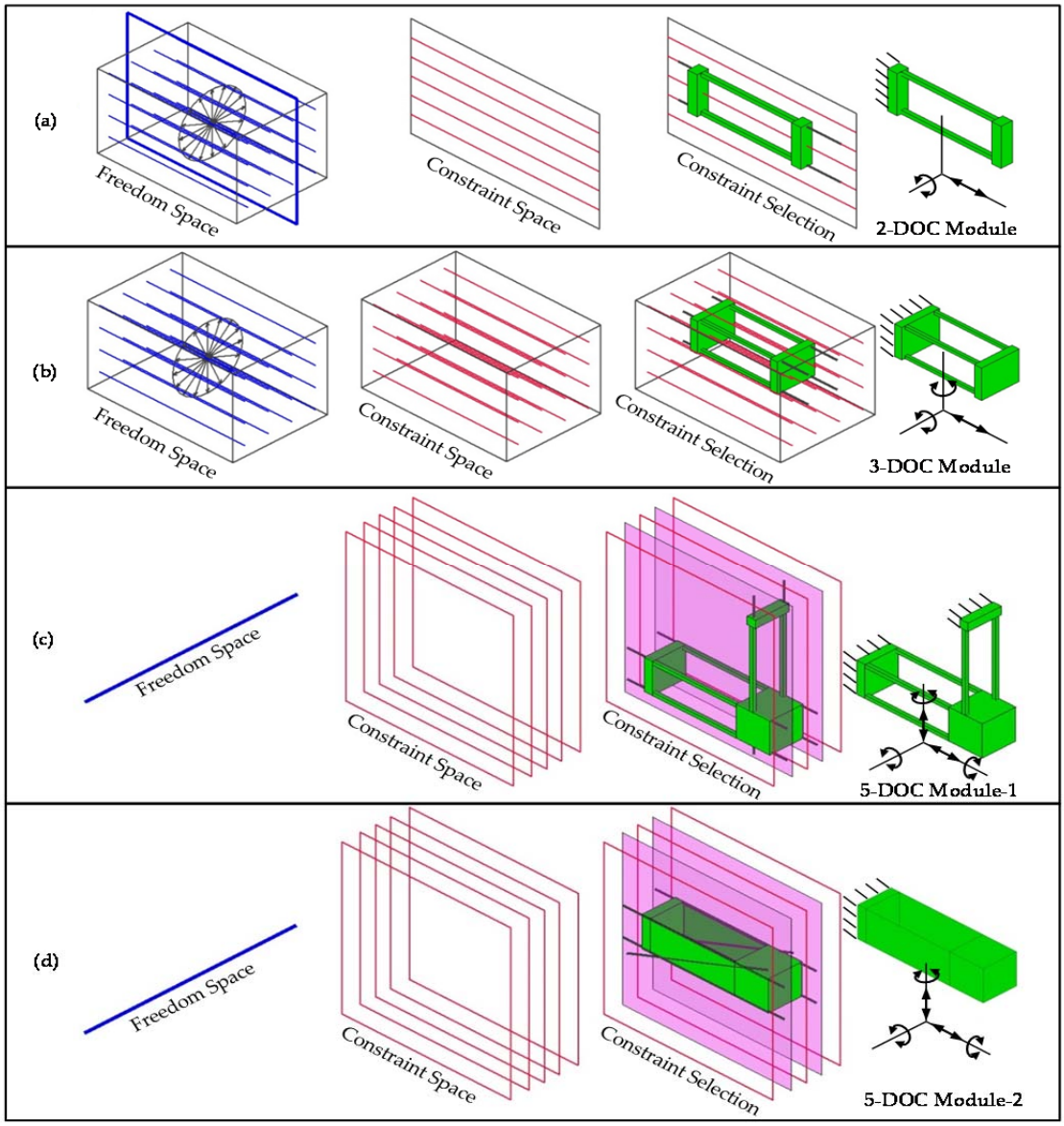

Figure 2.11 Parallel compliant modules with different DOC (or constraints) synthesized using the FACT method: (a) a 2-DOC module design, (b) a 3-DOC module design, (c) a 5-DOC module termed 5-DOC-1 module design, and (d) a 5-DOC module termed 5-DOC-2 module design

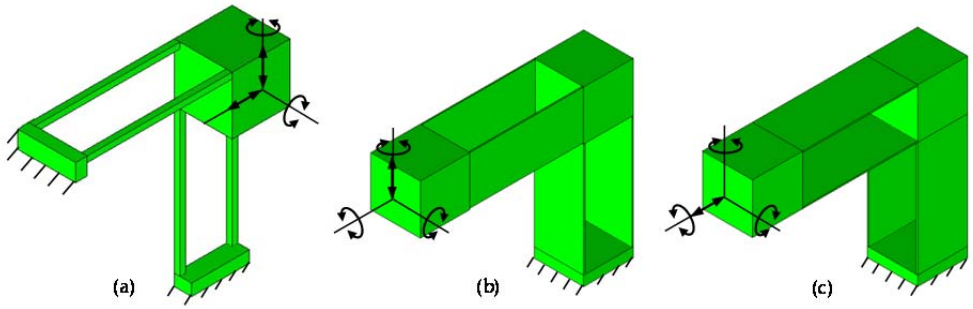

Figure 2.12 Compliant modules with different DOC (or constraints): (a) a 4-DOC module termed a 4-DOC-1 module, (b) a 4-DOC module termed a 4-DOC-2 module, and (c) a 4-DOC module termed a 4-DOC-3 module

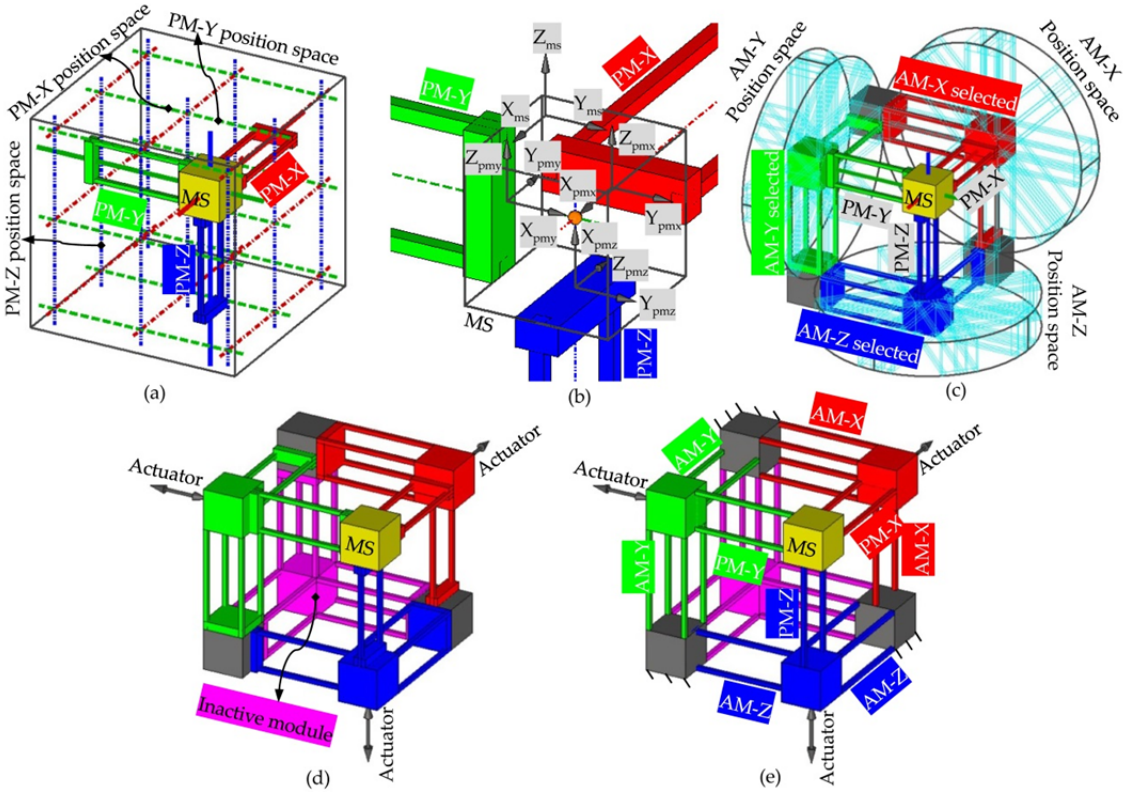

Figure 2.13 An XYZ CPM synthesized based on the constraints in the case 1: (a) determining the PM positions, (b) the orientations of the PMs in the PM local coordinate systems, (c) selecting the AM positions, (d) adding an inactive module, and (e) the final XYZ CPM termed 2-5-XYZ CPM (i.e. XYZ CPM with 2-DOC PM and 5-DOC AM)

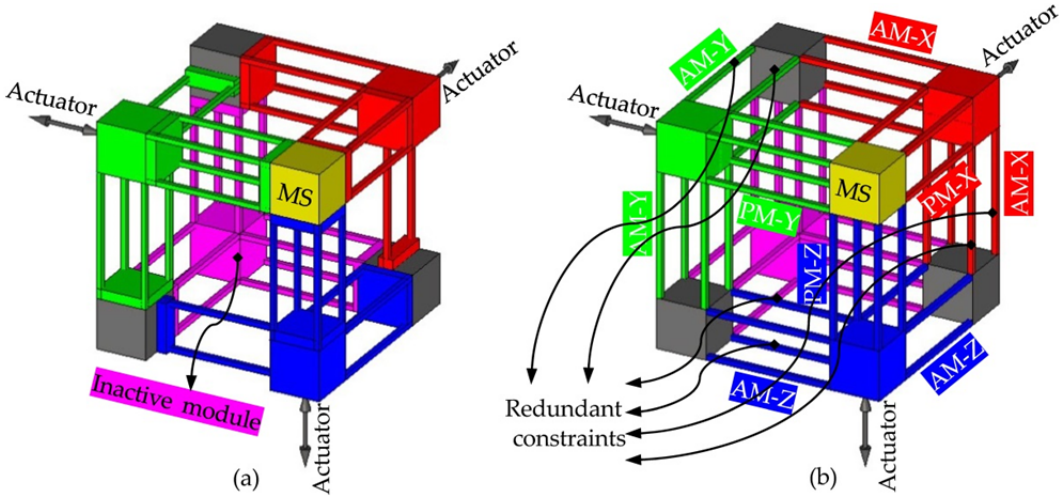

Figure 2.14 An XYZ CPM synthesized based on the constraints in the case 2: (a) replacing the PMs of the XYZ CPM shown in Figure 2.13(d) with the 3-DOC module in Figure 2.11(b), and (b) the final XYZ CPM termed the 3-5-XYZ CPM (i.e. an XYZ CPM with 3-DOC PMs and 5-DOC AMs) obtained by adding redundant constraints on the AMs of the XYZ CPM shown in Figure 2.14(a)

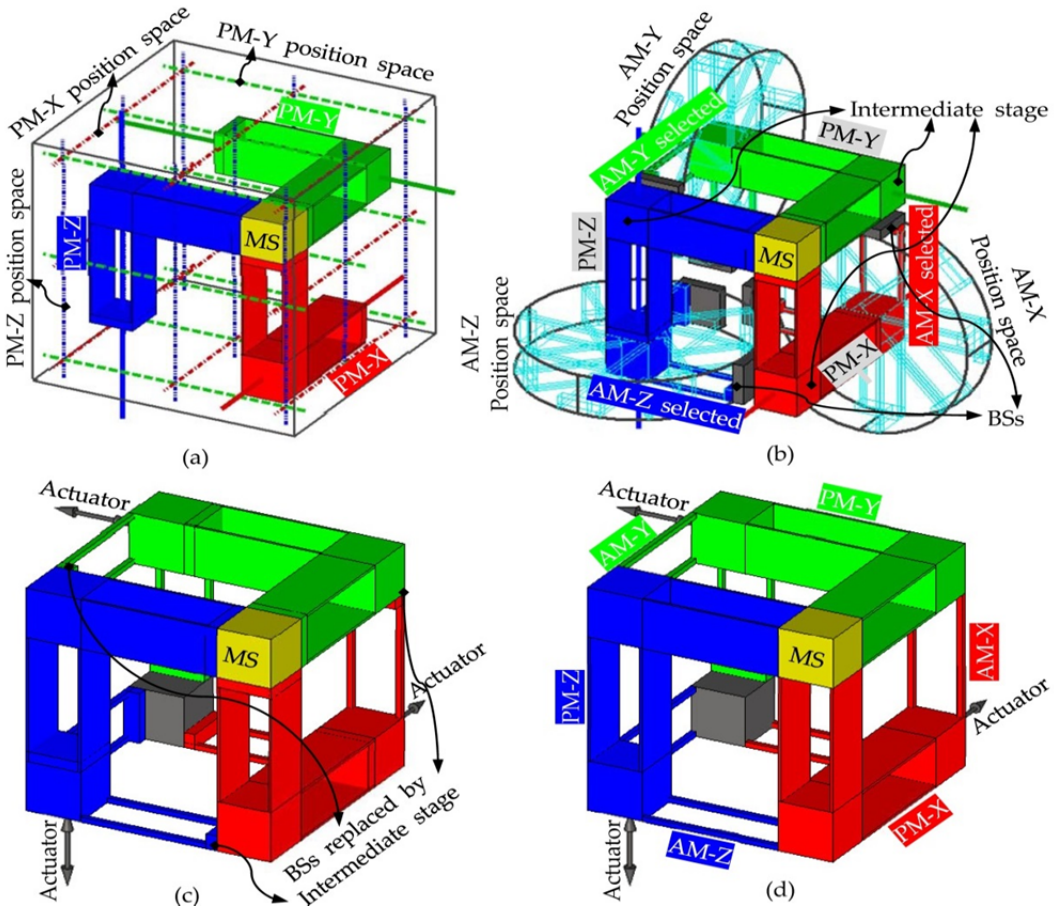

Figure 2.15 An XYZ CPM synthesized based on the constraints in the case 3: (a) determining the PM positions, (b) selecting the AM positions, (c) selecting the intermediate stages as the BSs (because the intermediate stages can provide the constraints which the BSs can offer), and (d) the final XYZ CPM termed 4-4-XYZ CPM (i.e. XYZ CPM with 4-DOC-2 PM and 4-DOC-1 AM)

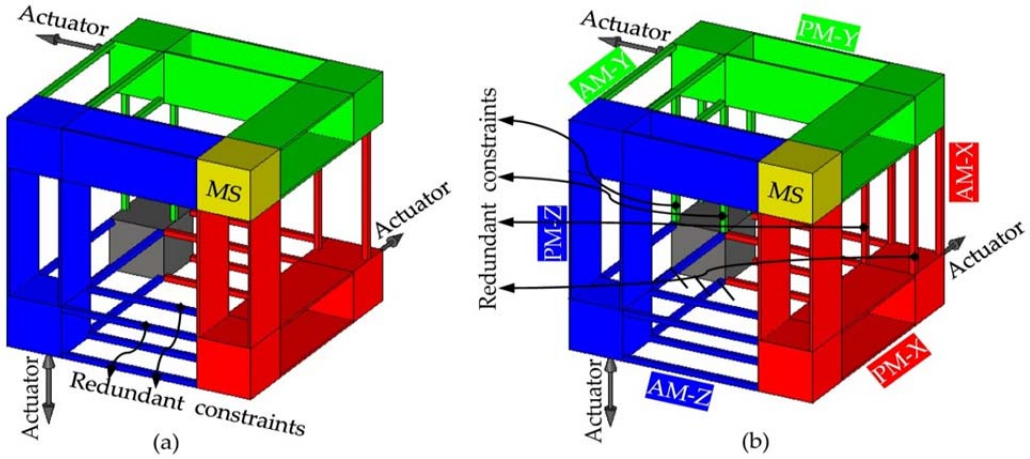

Figure 2.16 An XYZ CPM obtained by replacing the AMs of the 4-4-XYZ CPM with the 5-DOC-1 module and adding redundant constraints: (a) XYZ CPM termed 4-5-XYZ CPM-1 (i.e. XYZ CPM-1 with 4-DOC-2 PM and 5-DOC AM) through adding two wire-beams to the AM-Z, and (b) XYZ CPM termed 4-5-XYZ CPM-2 (i.e. XYZ CPM-2 with 4-DOC-2 PM and 5-DOC AM) by adding other four wire-beams to the AMs of the 4-5-XYZ CPM-1

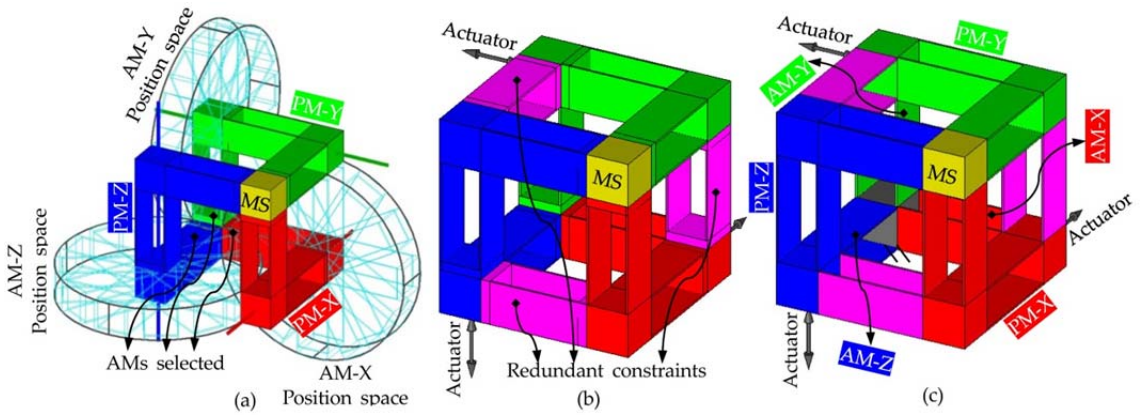

Figure 2.17 An XYZ CPM obtained by replacing the AMs of the 4-4-XYZ CPM with the 5-DOC-2 module based on the constraints in Case 4: (a) determining the AM positions, (b) adding redundant constraints, and (c) the final XYZ CPM termed 4-5-XYZ CPM-3 (i.e. XYZ CPM-3 with 4-DOC-2 PM and 5-DOC AM)

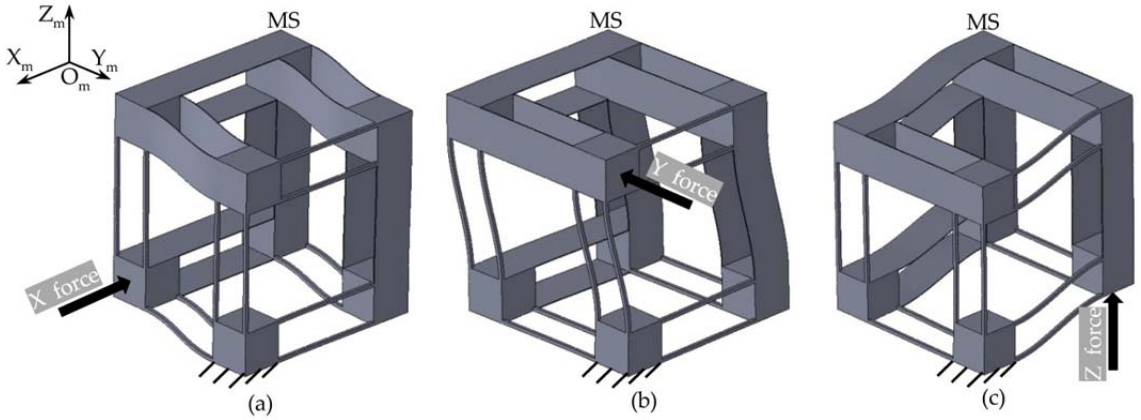

Figure 2.18 The FEA results of the 4-4-XYZ CPM: (a) X motion only, (b) Y motion only, and (c) Z motion only

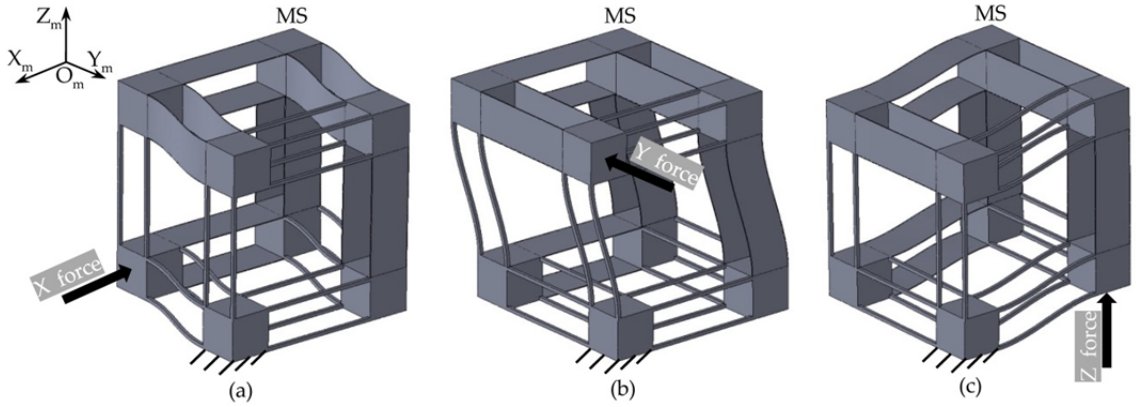

Figure 2.19 The FEA results of the 4-5-XYZ CPM-1: (a) X motion only, (b) Y motion only, and (c) Z motion only

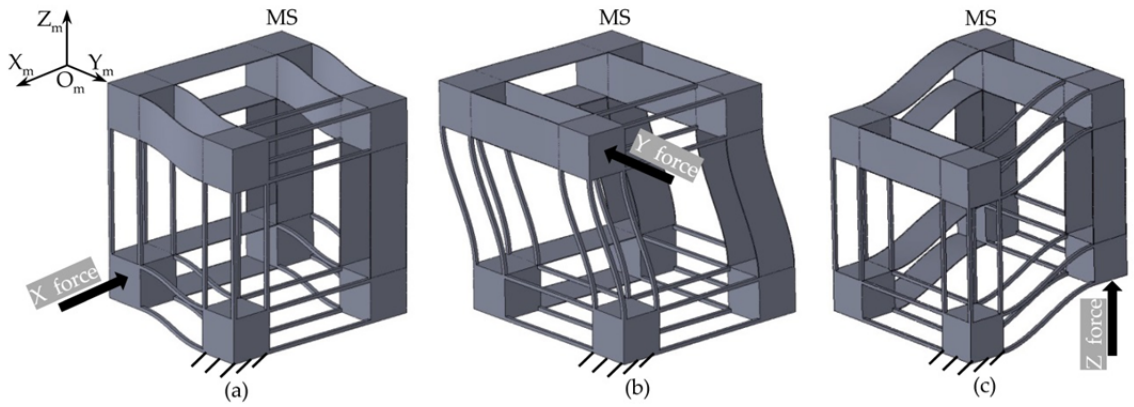

Figure 2.20 The FEA results of the 4-5-XYZ CPM-2: (a) X motion only, (b) Y motion only, and (c) Z motion only

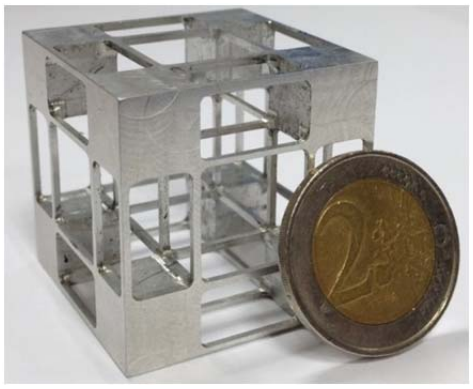

Figure 2.21 A prototype of the 3-5-XYZ CPM

2.6 Summary

A novel CPI approach for synthesizing decoupled XYZ CPMs, with consideration of actuation isolation, has been proposed. The XYZ CPMs, synthesized using the CPI approach, have the following characteristics:

(a) Each XYZ CPM has three non-redundant parallel legs between the MS and the BSs. Note that redundant legs can be added in the further modification design step to ensure a symmetrical arrangement.

(b) Each leg has an AS that can translate in one actuation direction only.

(c) The translational motion of each AS is transmitted to the MS without influencing the other two translations of the MS.

(d) Non-desired rotational motions of MSs are constrained by the three legs.

(e) The geometrical forms and positions of the legs can be adjusted under

the constraint spaces and the position spaces to meet a variety of design requirements and applications.

The CPI approach provides a systematic synthesis procedure for the compliant modules and rigid stages in an XYZ CPM system, according to the constraint spaces and the position spaces. The constraint spaces and the position spaces have been derived based on screw theory rather than design experience. The constraint spaces are classified into three different types (B-constraint space, T-constraint space, and S-constraint space), and the most frequently employed positions in the position spaces are illustrated by geometrical shapes. Additionally, the possible permitted geometrical forms of the compliant modules can be obtained using the existing approaches such as the FACT approach. Therefore, the CPI approach is an effective method that is accessible not only for experts, but also for beginners. The synthesis process has been demonstrated in a step by step fashion via several monolithic XYZ CPMs. The mobility of the XYZ CPMs synthesized is verified by FEA simulations.

The proposed constraint spaces contain a number of constraint combinations. Moreover, a number of XYZ CPMs can be synthesized based on only one of the combinations, because: (a) each compliant module in an XYZ CPM system has many permitted positions in its position space; and (b) each compliant module has many possible permitted geometrical forms such as a parallel geometrical form, serial geometrical form and hybrid geometrical form. Therefore, a variety of XYZ CPMs can be synthesized using the CPI approach.

It is noted that the CPI approach focuses on the early-stage conceptual design. Nonlinear characteristics such as parasitic motions are not considered. Additionally, coupled XYZ CPMs can be synthesized through further modifications of decoupled XYZ CPMs, as is detailed in Appendix D.

This page is intentionally left blank.

3 CFB MODELLING APPROACH

This chapter proposes a constraint-force-based (CFB) approach to model any compliant mechanisms with a particular emphasis on modelling complex compliant mechanisms such as XYZ CPMs. The principle of the CFB approach is presented in Section 3.1, followed by modelling examples in Section 3.2. In Section 3.3, the analytical results of the examples are validated by FEA simulations and experimental tests.

3.1 Principle

Similar to the CPI approach, in the CFB approach, a compliant mechanism is also regarded as a combination of the rigid stages and compliant modules. A compliant module can offer elastic forces due to its deformation. Such elastic forces are defined as variable constraint forces in the CFB approach, because the elastic forces vary with the displacements of the associated deformation. Additionally, the CFB approach defines external forces applied on a compliant mechanism as constant constraint forces that are independent of the deformation of the compliant mechanism. If a compliant mechanism is in static equilibrium, all the rigid stages are also in static equilibrium under the influence of the variable and constant constraint forces. Therefore, the constraint force equilibrium equations of the rigid stages can be obtained, and the analytical model of the compliant mechanism can be derived based on the constraint force equilibrium equations. As a result, the main work of modelling a compliant mechanism using the CFB approach is to derive the variable constraint forces and the constraint force equilibrium equations (including

deriving the geometrical compatibility conditions). The derivation of the variable constraint forces produced by compliant modules and constraint force equilibrium equations is demonstrated in Sections 3.1.1 and 3.1.2, respectively.

In this thesis, all geometrical length parameters and translational displacements are normalized by beam length L. Additionally, translational forces (including translational constraint forces) are normalized by EI/L^2, and the rotational forces (including rotational constraint forces) are normalized by EI/L. Here E is Young's modulus, I is moment of inertia of cross-section area of a beam, and L is the beam length.

3.1.1 Variable constraint forces

Compliant modules can be classified into BCMs (basic compliant modules, as defined in Section 1.3) and NBCMs (non-basic compliant modules, as defined in Section 1.3). The variable constraint force produced by a BCM can be obtained according to the force-displacement relationship of the BCM. This section takes a wire-beam with uniform cross-section (Figure 3.1) as an example BCM, so as to demonstrate the derivation of the variable constraint force produced by the wire-beam. As is well known, any one NBCM can be decomposed into rigid stages and BCMs. Therefore, the variable constraint force produced by a NBCM can be obtained based on the variable constraint forces of the associated BCMs.

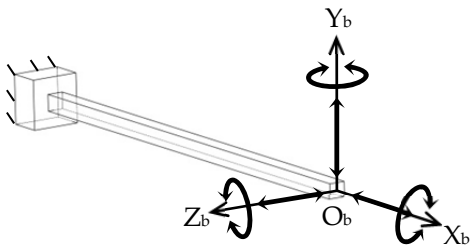

Figure 3.1 A wire-beam, its local coordinate system and the principal wrenches of the local coordinate system

In Chapter 1, constraints and motions of compliant modules are represented by

wrenches and twists, respectively, using screw theory in the CPI approach. In order to have a strong connection to the CPI approach, constraint forces (both variable and constant constraint forces) and motions are described as wrenches and twists, respectively, in the CFB approach. Note that constraint forces are actually forces, rather than constraints. Therefore, constraint forces can be represented by wrenches, based on Equation (2.4) rather than Equation (2.5).

A wrench, ζ_b, is used to represent the variable constraint force of the wire-beam (as depicted in Figure 3.1) in the coordinate system O_b-$X_bY_bZ_b$. A twist, ξ_b, is used to indicate the displacements of the beam free tip centre along and about the three axes of the coordinate system [61, 102]. The wrench ζ_b and the twist ξ_b can be written as shown below, based on Equations (2.4) and (2.9).

$$\zeta_b = \left[\zeta_{b\text{-}tx}, \zeta_{b\text{-}ty}, \zeta_{b\text{-}tz}, \zeta_{b\text{-}rx}, \zeta_{b\text{-}ry}, \zeta_{b\text{-}rz}\right]^T \tag{3.1}$$

$$\xi_b = \left[\xi_{b\text{-}tx}, \xi_{b\text{-}ty}, \xi_{b\text{-}tz}, \xi_{b\text{-}rx}, \xi_{b\text{-}ry}, \xi_{b\text{-}rz}\right]^T \tag{3.2}$$

where $\zeta_{b\text{-}tx}$, $\zeta_{b\text{-}ty}$, $\zeta_{b\text{-}tz}$, $\zeta_{b\text{-}rx}$, $\zeta_{b\text{-}ry}$ and $\zeta_{b\text{-}rz}$ are principal wrench coefficients, which represent the values of the variable constraint forces along and about the X_b-, Y_b- and Z_b-axes of the coordinate system O_b-$X_bY_bZ_b$, respectively. Additionally, $\xi_{b\text{-}tx}$, $\xi_{b\text{-}ty}$, $\xi_{b\text{-}tz}$, $\xi_{b\text{-}rx}$, $\xi_{b\text{-}ry}$ and $\xi_{b\text{-}rz}$ are principal twist coefficients, which represent the values of the displacements of the beam free tip centre along and about the three axes of the coordinate system O_b-$X_bY_bZ_b$.

If the displacement of a beam free tip centre is ξ_b, due to the influence of an applied external force represented by a wrench ζ_{bf}, the relationship between the ξ_b and the ζ_{bf} is the force-displacement relationship of the beam. The nonlinear force-displacement relationship of a wire-beam with uniform cross-section has been developed in [85], which is very accurate (for medium motion ranges, i.e., when the deflection is less than 0.1% of beam length), but complicated. A simplified force-displacement relationship of a wire-beam has been proposed in

[78], which is also sufficiently accurate when the rotations of the wire-beam are much smaller than the translations. The simplified force-displacement relationship proposed in [78] is adopted in this chapter, so the derived variable constraint force of a wire-beam is valid for modelling translational compliant mechanisms. Simplified force-displacement relationships are obtained, as shown in Equations (3.3) – (3.8).

$$\begin{aligned}
\xi_{\text{b-tx}} = {} & \frac{\zeta_{\text{bf-tx}} t_{\text{b}}^{\,2}}{12} + \xi_{\text{b-rz}}\left(\frac{\xi_{\text{b-ty}}}{20} - \frac{\xi_{\text{b-rz}}}{15}\right) + \left(\frac{\xi_{\text{b-rz}}}{20} - \frac{3\xi_{\text{b-ty}}}{5}\right)\xi_{\text{b-ty}} \\
& + \xi_{\text{b-rz}}\left(\frac{11\zeta_{\text{bf-tx}}\xi_{\text{b-rz}}}{6300} - \frac{\zeta_{\text{bf-tx}}\xi_{\text{b-ty}}}{1400}\right) + \xi_{\text{b-ty}}\left(\frac{\zeta_{\text{bf-tx}}\xi_{\text{b-ty}}}{700} - \frac{\zeta_{\text{bf-tx}}\xi_{\text{b-rz}}}{1400}\right) \\
& + \xi_{\text{b-rz}}\left(\frac{\zeta_{\text{bf-tx}}^2\xi_{\text{b-rz}}}{18000} - \frac{\zeta_{\text{bf-tx}}^2\xi_{\text{b-ty}}}{84000}\right) + \xi_{\text{b-ty}}\left(\frac{\zeta_{\text{bf-tx}}^2\xi_{\text{b-ty}}}{42000} - \frac{\zeta_{\text{bf-tx}}^2\xi_{\text{b-rz}}}{84000}\right) \\
& - \xi_{\text{b-ry}}\left(\frac{\xi_{\text{b-ry}}}{15} + \frac{\xi_{\text{b-tz}}}{20}\right) + \left(-\frac{\xi_{\text{b-ry}}}{20} - \frac{3\xi_{\text{b-tz}}}{5}\right)\xi_{\text{b-tz}} \\
& - \xi_{\text{b-ry}}\left(-\frac{11\zeta_{\text{bf-tx}}\xi_{\text{b-ry}}}{6300} - \frac{\zeta_{\text{bf-tx}}\xi_{\text{b-tz}}}{1400}\right) + \xi_{\text{b-tz}}\left(\frac{\zeta_{\text{bf-tx}}\xi_{\text{b-ry}}}{1400} + \frac{\zeta_{\text{bf-tx}}\xi_{\text{b-tz}}}{700}\right) \\
& - \xi_{\text{b-ry}}\left(-\frac{\xi_{\text{b-ry}}\zeta_{\text{bf-tx}}^2}{18000} - \frac{\xi_{\text{b-tz}}\zeta_{\text{bf-tx}}^2}{84000}\right) + \xi_{\text{b-tz}}\left(\frac{\xi_{\text{b-ry}}\zeta_{\text{bf-tx}}^2}{84000} + \frac{\xi_{\text{b-tz}}\zeta_{\text{bf-tx}}^2}{42000}\right)
\end{aligned} \tag{3.3}$$

$$\zeta_{\text{bf-ty}} = \frac{\xi_{\text{b-rz}}\zeta_{\text{bf-tx}}^2}{1400} - \frac{1}{700}\xi_{\text{b-ty}}\zeta_{\text{bf-tx}}^2 - \frac{\xi_{\text{b-rz}}\zeta_{\text{bf-tx}}}{10} + \frac{6\xi_{\text{b-ty}}\zeta_{\text{bf-tx}}}{5} - 6\xi_{\text{b-rz}} + 12\xi_{\text{b-ty}} \tag{3.4}$$

$$\zeta_{\text{bf-tz}} = -\frac{\xi_{\text{b-ry}}\zeta_{\text{bf-tx}}^2}{1400} - \frac{1}{700}\xi_{\text{b-tz}}\zeta_{\text{bf-tx}}^2 + \frac{\xi_{\text{b-ry}}\zeta_{\text{bf-tx}}}{10} + \frac{6\xi_{\text{b-tz}}\zeta_{\text{bf-tx}}}{5} + 6\xi_{\text{b-ry}} + 12\xi_{\text{b-tz}} \tag{3.5}$$

$$\xi_{\text{b-rx}} = \frac{\zeta_{\text{bf-rx}}}{\delta_{\text{b}}} + \frac{\zeta_{\text{bf-tx}}\left(\xi_{\text{ry}}\xi_{\text{ty}} + \xi_{\text{rz}}\xi_{\text{tz}}\right)}{10\delta_{\text{b}}} + \frac{6\left(\xi_{\text{ry}}\xi_{\text{ty}} + \xi_{\text{rz}}\xi_{\text{tz}}\right)}{\delta_{\text{b}}} \tag{3.6}$$

$$-\zeta_{\text{bf-ry}} = \frac{11\xi_{\text{b-ry}}\zeta_{\text{bf-tx}}^2}{6300} + \frac{\xi_{\text{b-tz}}\zeta_{\text{bf-tx}}^2}{1400} - \frac{2\xi_{\text{b-ry}}\zeta_{\text{bf-tx}}}{15} - \frac{\xi_{\text{b-tz}}\zeta_{\text{bf-tx}}}{10} - 4\xi_{\text{b-ry}} - 6\xi_{\text{b-tz}} \tag{3.7}$$

$$\zeta_{\text{bf-rz}} = -\frac{11\xi_{\text{b-rz}}\zeta_{\text{bf-tx}}^2}{6300} + \frac{\xi_{\text{b-ty}}\zeta_{\text{bf-tx}}^2}{1400} + \frac{2\xi_{\text{b-rz}}\zeta_{\text{bf-tx}}}{15} - \frac{\xi_{\text{b-ty}}\zeta_{\text{bf-tx}}}{10} + 4\xi_{\text{b-rz}} - 6\xi_{\text{b-ty}} \tag{3.8}$$

where t_{b} is the thickness of the wire-beam (square cross section), while

$\delta_b=G_bJ_b/E_bI_b \approx 27/32/(1+\upsilon_b)$, here G_b, J_b, E_b, I_b and υ_b are the shear modulus, torsional constant, Young's modulus, moment of inertia of cross-section area and Poisson's ratio, respectively [85]. Additionally, $\zeta_{bf\text{-}tx}$, $\zeta_{bf\text{-}ty}$, $\zeta_{bf\text{-}tz}$, $\zeta_{bf\text{-}rx}$, $\zeta_{bf\text{-}ry}$ and $\zeta_{bf\text{-}rz}$ are the principal wrench coefficients of the wrench $\boldsymbol{\zeta}_{bf}$, which represent the values of the external forces along and about the X_b-, Y_b- and Z_b-axes of the coordinate system O_b-$X_bY_bZ_b$, respectively. It can be seen from Equations (3.3) – (3.8) that the wrench $\boldsymbol{\zeta}_{bf}$ is a function of t_b, δ_b and the components of the twist $\boldsymbol{\xi}_b$. Therefore, the wrench $\boldsymbol{\zeta}_{bf}$ can be written as

$$\begin{aligned}\boldsymbol{\zeta}_{bf} = \mathrm{K}_{\mathrm{Beam}}\left(\boldsymbol{\xi}_b, t_b, \delta_b\right) = \Big[&\mathrm{K}_{\text{B-tx}}\left(\boldsymbol{\xi}_b, t_b, \delta_b\right), \mathrm{K}_{\text{B-ty}}\left(\boldsymbol{\xi}_b, t_b, \delta_b\right), \mathrm{K}_{\text{B-tz}}\left(\boldsymbol{\xi}_b, t_b, \delta_b\right), \\ &\mathrm{K}_{\text{B-rx}}\left(\boldsymbol{\xi}_b, t_b, \delta_b\right), \mathrm{K}_{\text{B-ry}}\left(\boldsymbol{\xi}_b, t_b, \delta_b\right), \mathrm{K}_{\text{B-rz}}\left(\boldsymbol{\xi}_b, t_b, \delta_b\right)\Big]^{\mathrm{T}}\end{aligned} \tag{3.9}$$

where $\mathrm{K}_{\mathrm{Beam}}(\cdot)$ is a 6×1 variable vector, whose six components are six functions, $\mathrm{K}_{\text{B-tx}}(\cdot)$, $\mathrm{K}_{\text{B-ty}}(\cdot)$, $\mathrm{K}_{\text{B-tz}}(\cdot)$, $\mathrm{K}_{\text{B-rx}}(\cdot)$, $\mathrm{K}_{\text{B-ry}}(\cdot)$ and $\mathrm{K}_{\text{B-rz}}(\cdot)$. The six functions can be obtained based on Equations (3.3) – (3.8), so that the values of the six functions are $\zeta_{bf\text{-}tx}$, $\zeta_{bf\text{-}ty}$, $\zeta_{bf\text{-}tz}$, $\zeta_{bf\text{-}rx}$, $\zeta_{bf\text{-}ry}$ and $\zeta_{bf\text{-}rz}$, respectively. When the beam is in a static equilibrium state, the resultant force represented by wrench $\boldsymbol{\zeta}_b$ is the reaction force to the resultant force represented by $\boldsymbol{\zeta}_{bf}$. According to Newton's third law, it can be derived that $\boldsymbol{\zeta}_b = -\boldsymbol{\zeta}_{bf}$. Therefore, the wrench $\boldsymbol{\zeta}_b$ can be written as

$$\boldsymbol{\zeta}_b = -\mathrm{K}_{\mathrm{Beam}}\left(\boldsymbol{\xi}_b, t_b, \delta_b\right) \tag{3.10}$$

Suppose that all rotational displacement components in $\boldsymbol{\xi}_b$ are much smaller than the translational displacement components, Equation (3.11) can be obtained based on Equations (3.3) – (3.8) and Equation (3.10).

$$\begin{aligned}\mathrm{K}_{\mathrm{Beam}}\left(\boldsymbol{\xi}_{\mathrm{b}}, t_{\mathrm{b}}, \delta_{\mathrm{b}}\right) &= \mathbf{k}_{\mathrm{Beam\text{-}L}}\boldsymbol{\xi}_{\mathrm{b}} + \mathrm{K}_{\mathrm{Beam\text{-}NL}}\left(\boldsymbol{\xi}_{\mathrm{b}}, t_{\mathrm{b}}, \delta_{\mathrm{b}}\right) \\ &= \begin{bmatrix} 12/t_{\mathrm{b}}^2 & 0 & 0 & 0 & 0 & 0 \\ 0 & 12 & 0 & 0 & 0 & -6 \\ 0 & 0 & 12 & 0 & 6 & 0 \\ 0 & 0 & 0 & \delta_{\mathrm{b}} & 0 & 0 \\ 0 & 0 & 6 & 0 & 4 & 0 \\ 0 & -6 & 0 & 0 & 0 & 4 \end{bmatrix} \boldsymbol{\xi}_{\mathrm{b}} + \begin{bmatrix} \sigma_{\mathrm{k\text{-}b1}} \\ \sigma_{\mathrm{k\text{-}b2}} \\ \sigma_{\mathrm{k\text{-}b3}} \\ \sigma_{\mathrm{k\text{-}b4}} \\ \sigma_{\mathrm{k\text{-}b5}} \\ \sigma_{\mathrm{k\text{-}b6}} \end{bmatrix}\end{aligned} \tag{3.11}$$

where

$$\sigma_{\mathrm{k\text{-}b1}} = \frac{36\left(35t_{\mathrm{b}}^2 - \xi_{\mathrm{b\text{-}tx}}\right)\left(\xi_{\mathrm{b\text{-}ty}}^2 + \xi_{\mathrm{b\text{-}tz}}^2\right)}{t_{\mathrm{b}}^2\left(175t_{\mathrm{b}}^2 + 3\xi_{\mathrm{b\text{-}ty}}^2 + 3\xi_{\mathrm{b\text{-}tz}}^2\right)},$$

$$\sigma_{\mathrm{k\text{-}b2}} = \frac{504\xi_{\mathrm{b\text{-}ty}}\left(5\xi_{\mathrm{b\text{-}tx}} + 3\left(\xi_{\mathrm{b\text{-}ty}}^2 + \xi_{\mathrm{b\text{-}tz}}^2\right)\right)}{175t_{\mathrm{b}}^2 + 3\xi_{\mathrm{b\text{-}ty}}^2 + 3\xi_{\mathrm{b\text{-}tz}}^2},$$

$$\sigma_{\mathrm{k\text{-}b3}} = \frac{504\xi_{\mathrm{b\text{-}tz}}\left(5\xi_{\mathrm{b\text{-}tx}} + 3\left(\xi_{\mathrm{b\text{-}ty}}^2 + \xi_{\mathrm{b\text{-}tz}}^2\right)\right)}{175t_{\mathrm{b}}^2 + 3\xi_{\mathrm{b\text{-}ty}}^2 + 3\xi_{\mathrm{b\text{-}tz}}^2},$$

$$\sigma_{\mathrm{k\text{-}b4}} = -\frac{6\left(\xi_{\mathrm{b\text{-}ry}}\xi_{\mathrm{b\text{-}ty}} + \xi_{\mathrm{b\text{-}rz}}\xi_{\mathrm{b\text{-}tz}}\right)\left(175t_{\mathrm{b}}^2 + 24\xi_{\mathrm{b\text{-}ty}}^2 + 24\xi_{\mathrm{b\text{-}tz}}^2 + 35\xi_{\mathrm{b\text{-}tx}}\right)}{175t_{\mathrm{b}}^2 + 3\xi_{\mathrm{b\text{-}ty}}^2 + 3\xi_{\mathrm{b\text{-}tz}}^2},$$

$$\sigma_{\mathrm{k\text{-}b5}} = \frac{42\xi_{\mathrm{b\text{-}tz}}\left(5\xi_{\mathrm{b\text{-}tx}} + 3\left(\xi_{\mathrm{b\text{-}ty}}^2 + \xi_{\mathrm{b\text{-}tz}}^2\right)\right)}{175t_{\mathrm{b}}^2 + 3\xi_{\mathrm{b\text{-}ty}}^2 + 3\xi_{\mathrm{b\text{-}tz}}^2},$$

$$\sigma_{\mathrm{k\text{-}b6}} = -\frac{42\xi_{\mathrm{b\text{-}ty}}\left(5\xi_{\mathrm{b\text{-}tx}} + 3\left(\xi_{\mathrm{b\text{-}ty}}^2 + \xi_{\mathrm{b\text{-}tz}}^2\right)\right)}{175t_{\mathrm{b}}^2 + 3\xi_{\mathrm{b\text{-}ty}}^2 + 3\xi_{\mathrm{b\text{-}tz}}^2}.$$

Note that $\mathrm{k}_{\mathrm{Beam\text{-}L}}$ is the linear stiffness matrix of the wire-beam, and $\mathrm{K}_{\mathrm{Beam\text{-}NL}}(\cdot)$ is a nonlinear stiffness variable vector about t_{b}, δ_{b} and the components of $\boldsymbol{\xi}_{\mathrm{b}}$.

The variable constraint force produced by a wire-beam can be calculated using Equations (3.3) – (3.10), or calculated using Equation (3.11) when the rotational displacements of the wire beam free tip centre are much smaller than the translational displacements.

In a similar way, the variable constraint forces produced by other BCMs can also be derived based on their force-displacement relationships. If the variable constraint forces of the BCMs which make up a NBCM are obtained, the variable constraint force produced by the NBCM can also be obtained, through transforming all the variable constraint forces of the BCMs to a common coordinate system and then adding these variable constraint force vectors in the common coordinate system; (two examples are shown in Sections 3.2.1 and 3.2.2). In addition, if the force-displacement relationship of a NBCM has existed already, the variable constraint force of the NBCM can also be calculated according to the force-displacement relationship of the NBCM.

3.1.2 Constraint force equilibrium equations

If a rigid body is balanced under the influence of n compliant modules and m external forces, the constraint force equilibrium equation for the rigid stage can be written as

$$\sum_{i=1}^{n}\left(\mathbf{T}_{\text{vc-}i}\zeta_{\text{vc-}i}\right)+\sum_{j=1}^{m}\left(\mathbf{T}_{\text{cc-}j}\zeta_{\text{cc-}j}\right)=\mathbf{0} \tag{3.12}$$

where wrenches $\zeta_{\text{vc-}i}$ (i=1, 2, 3 … n) and wrenches $\zeta_{\text{cc-}j}$ (j=1, 2, 3 … m) represent the variable constraint forces of the n compliant modules and m constant constraint forces applied on this rigid stage, respectively. $\mathbf{T}_{\text{vc-}i}$ (i=1, 2, 3 … n) and $\mathbf{T}_{\text{cc-}j}$ (j=1, 2, 3 … m) are transformation matrices, which can transform all the constraint forces to a common coordinate system.

When a compliant mechanism is in static equilibrium under the influence of a series of external forces (or constant constraint forces), all the rigid stages of the compliant mechanism are also in static equilibrium. As studied in Section 3.1.1, the variable constraint forces of the compliant modules can be derived. Therefore, the constraint force equilibrium equations for all the rigid stages can be represented by the variable and constant constraint forces. Moreover, the

analytical model of the compliant mechanism can be calculated based on the constraint force equilibrium equations.

The CFB approach can be used to model a compliant mechanism linearly and non-linearly. If all nonlinear contributions to the variable constraint forces are not considered and the transformation matrices are derived based on the undeformed configuration, the linear analytical model of the compliant mechanism can be obtained; otherwise, the nonlinear analytical model of the compliant mechanism can be derived.

3.2 Case Study

The CFB approach can be used to model any one compliant mechanism. Without loss of generality, a compact XYZ CPM (as shown in Figure 3.2 and Figure 2.14(b)) composed of identical wire-beams is modelled in this section using the CFB approach.

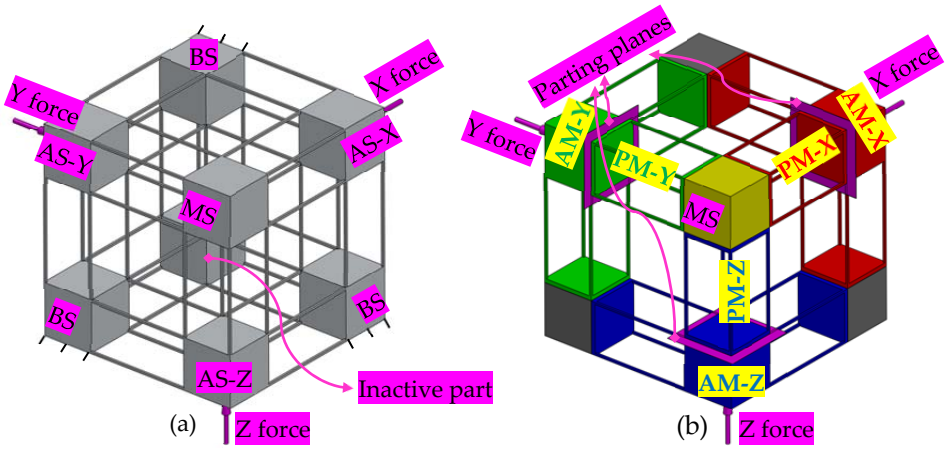

Figure 3.2 An XYZ CPM and its decomposition: (a) the rigid stages of the XYZ CPM, and (b) the compliant modules of the XYZ CPM

As studied in Chapter 2, this XYZ CPM can be decomposed into two types of NBCMs, which are termed four-beam NBCM and eight-beam NBCM. The four-beam NBCMs are PMs (PM-X, PM-Y and PM-Z), and the eight-beam NBCMs are AMs (AM-X, AM-Y and AM-Z). The rigid stages of the XYZ CPM are labelled in Figure 3.2(a), and the NBCMs are shown in Figure 3.2(b). Note that

the AS-X, AS-Y and AS-Z are ASs (actuated stages), and are also the rigid stages of the AM-X, AM-Y and AM-Z, respectively.

The BCMs of the NBCMs are wire-beams with uniform cross sections. The variable constraint force of such a wire-beam has been derived in Section 3.1.1, which is used to derive the variable constraint forces of the two NBCMs in Sections 3.2.1 and 3.2.2. Finally, the constraint force equilibrium equations and the analytical models of the XYZ CPM are derived in Section 3.2.3.

3.2.1 Variable constraint force of a four-beam NBCM

A four-beam NBCM of the XYZ CPM is shown in Figure 3.3. Suppose that the thickness of the mobile top plate is tiny compared with the length of the beams. Four wrenches, ζ_{fbi} (i=1, 2, 3 or 4), are used to represent the variable constraint forces of the four wire-beams in the local coordinate systems O_{fbi}-$X_{fbi}Y_{fbi}Z_{fbi}$ (i=1, 2, 3 or 4), respectively. Note that the local coordinate systems are placed at the tips of the four wire-beams, O_{fb1}, O_{fb2}, O_{fb3} and O_{fb4}, as shown in Figure 3.3. If the displacement of the four-beam NBCM is represented by a twist ξ_{fb} in the global coordinate system, the displacements of the tips of the four beams can be written as twists ξ_{fbi}, as shown in Equation (3.13).

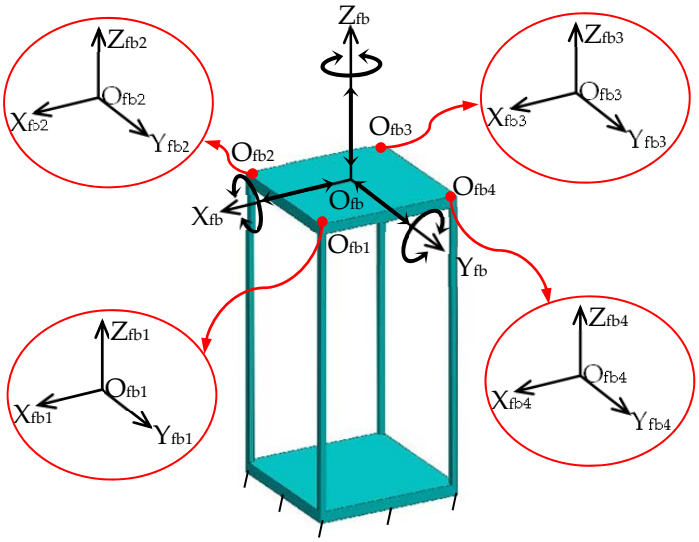

Figure 3.3 Illustration of a four-beam NBCM, the global coordinate system O_{fb}-$X_{fb}Y_{fb}Z_{fb}$, and the local coordinate systems O_{fb1}-$X_{fb1}Y_{fb1}Z_{fb1}$, O_{fb2}-$X_{fb2}Y_{fb2}Z_{fb2}$, O_{fb3}-$X_{fb3}Y_{fb3}Z_{fb3}$ and O_{fb4}-$X_{fb4}Y_{fb4}Z_{fb4}$

$$\boldsymbol{\xi}_{\mathrm{fb}i} = \left[\mathbf{T}_{\mathrm{fb}i\text{-}\mathrm{fb}}\right]^{\mathrm{T}} \boldsymbol{\xi}_{\mathrm{fb}} \quad i = 1, 2, 3 \text{ or } 4 \tag{3.13}$$

where $\mathbf{T}_{\mathrm{fb}i-\mathrm{fb}}$ (i=1, 2, 3 or 4) is the transformation matrix from the local coordinate systems $O_{\mathrm{fb}i}$-$X_{\mathrm{fb}i}Y_{\mathrm{fb}i}Z_{\mathrm{fb}i}$ to the global coordinate system O_{fb}-$X_{\mathrm{fb}}Y_{\mathrm{fb}}Z_{\mathrm{fb}}$. When the rotational displacements of the top plate are tiny compared with the translational displacements, the transformation matrices can be obtained as shown in Equation (3.14) based on Equation (2.11).

$$\mathbf{T}_{\mathrm{fb}i\text{-}\mathrm{fb}} = \begin{bmatrix} 1 & 0 & 0 & 0 & 0 & 0 \\ 0 & 1 & 0 & 0 & 0 & 0 \\ 0 & 0 & 1 & 0 & 0 & 0 \\ 0 & \sigma_{\mathrm{fb}i-1} & \sigma_{\mathrm{fb}i-2} & 1 & 0 & 0 \\ \sigma_{\mathrm{fb}i-3} & 0 & 0 & 0 & 1 & 0 \\ \sigma_{\mathrm{fb}i-4} & 0 & 0 & 0 & 0 & 1 \end{bmatrix} \tag{3.14}$$

where

$$\sigma_{\mathrm{fb}1-1} = \sigma_{\mathrm{fb}1-4} = \sigma_{\mathrm{fb}2-1} = \sigma_{\mathrm{fb}2-2} = \sigma_{\mathrm{fb}3-2} = \sigma_{\mathrm{fb}3-3} = \sigma_{\mathrm{fb}4-3} = \sigma_{\mathrm{fb}4-4} = \left(t_{\mathrm{fb}} - w_{\mathrm{fb}}\right)/2,$$
$$\sigma_{\mathrm{fb}1-2} = \sigma_{\mathrm{fb}1-3} = \sigma_{\mathrm{fb}2-3} = \sigma_{\mathrm{fb}2-4} = \sigma_{\mathrm{fb}3-1} = \sigma_{\mathrm{fb}3-4} = \sigma_{\mathrm{fb}4-1} = \sigma_{\mathrm{fb}4-2} = \left(w_{\mathrm{fb}} - t_{\mathrm{fb}}\right)/2.$$

where w_{fb} is the width of the square mobile plate of the four-beam NBCM, while t_{fb} is the thickness of the beam (in this example, all beams have the same thickness, i.e. $t_{\mathrm{fb}1} = t_{\mathrm{fb}2} = t_{\mathrm{fb}3} = t_{\mathrm{fb}4} = t_{\mathrm{fb}}$). Based on Equation (3.10), the variable constraint forces produced by the four beams can be obtained, as shown in Equation (3.15). The variable constraint force, $\boldsymbol{\zeta}_{\mathrm{fb}}$, of the four-beam NBCM is the vector sum of the variable constraint forces of the four beams, which can be written as Equation (3.16).

$$\boldsymbol{\zeta}_{\mathrm{fb}i} = -\mathrm{K}_{\mathrm{Beam}}\left(\boldsymbol{\xi}_{\mathrm{fb}i}, t_{\mathrm{fb}i}, \delta_{\mathrm{fb}i}\right) \; i = 1, 2, 3 \text{ or } 4 \tag{3.15}$$

$$\boldsymbol{\zeta}_{\mathrm{fb}} = \sum_{i=1}^{4}\left(\mathbf{T}_{\mathrm{fb}i\text{-}\mathrm{fb}}\boldsymbol{\zeta}_{\mathrm{fb}i}\right) \tag{3.16}$$

Combining Equations (3.3) – (3.10), (3.14), (3.15) and (3.16), the variable constraint force of the four-beam NBCM can be derived. Suppose that the

rotational displacements of the four-beam NBCM about the X_{fd}-, Y_{fd}- and Z_{fd}-axes are much smaller than the translational displacements along the X_{fd}-, Y_{fd}- and Z_{fd}-axes, the principal wrench coefficients, $\zeta_{fb\text{-}tx}$, $\zeta_{fb\text{-}ty}$, $\zeta_{fb\text{-}tz}$, $\zeta_{fb\text{-}rx}$, $\zeta_{fb\text{-}ry}$ and $\zeta_{fb\text{-}rz}$, of the wrench $\boldsymbol{\zeta}_{fb}$ can be simplified, as shown in Equations (3.17) – (3.22). For convenience, these equations can also be rewritten as Equation (3.23). If $\boldsymbol{\zeta}_{fbf}$ is a wrench representing an external force to balance the variable constraint force $\boldsymbol{\zeta}_{fb}$, wrench $\boldsymbol{\zeta}_{fbf}$ can be written as Equation (3.24), which is the force-displacement relationship of the four-beam NBCM.

$$\zeta_{fb-tx} = -\frac{1680\left(5\xi_{fb\text{-}tx} + 3\left(\xi_{fb\text{-}ty}^2 + \xi_{fb\text{-}tz}^2\right)\right)}{175t_{fb}^2 + 3\xi_{fb\text{-}ty}^2 + 3\xi_{fb\text{-}tz}^2} \tag{3.17}$$

$$\zeta_{fb-ty} = -\frac{48\xi_{fb\text{-}ty}\left(175t_{fb}^2 + 210\xi_{fb\text{-}tx} + 129\xi_{fb\text{-}ty}^2 + 129\xi_{fb\text{-}tz}^2\right)}{175t_{fb}^2 + 3\xi_{fb\text{-}ty}^2 + 3\xi_{fb\text{-}tz}^2} \tag{3.18}$$

$$\zeta_{fb-tz} = -\frac{48\xi_{fb\text{-}tz}\left(175t_{fb}^2 + 210\xi_{fb\text{-}tx} + 129\xi_{fb\text{-}ty}^2 + 129\xi_{fb\text{-}tz}^2\right)}{175t_{fb}^2 + 3\xi_{fb\text{-}ty}^2 + 3\xi_{fb\text{-}tz}^2} \tag{3.19}$$

$$\begin{aligned}\zeta_{fb\text{-}rx} = &\frac{840\left(5t_{fb}^2 - 3t_{fb}w_{fb} + 3w_{fb}^2\right)\left(\xi_{fb\text{-}ry}\xi_{fb\text{-}ty} + \xi_{fb\text{-}rz}\xi_{fb\text{-}tz}\right)}{3\xi_{fb\text{-}ty}^2 + 3\xi_{fb\text{-}tz}^2 + 175t_{fb}^2} \\ &- \frac{4\delta_{fb}\xi_{fb\text{-}rx}\left(3\xi_{fb\text{-}ty}^2 + 3\xi_{fb\text{-}tz}^2 + 175t_{fb}^2\right)}{3\xi_{fb\text{-}ty}^2 + 3\xi_{fb\text{-}tz}^2 + 175t_{fb}^2}\end{aligned} \tag{3.20}$$

$$\begin{aligned}\zeta_{fb\text{-}ry} = &-\frac{700\left(4t_{fb}^2 - 3t_{fb}w_{fb} + 3w_{fb}^2\right)\xi_{fb\text{-}ry}}{3\xi_{fb\text{-}ty}^2 + 3\xi_{fb\text{-}tz}^2 + 175t_{fb}^2} \\ &- \frac{24\xi_{fb\text{-}tz}\left(35\xi_{fb\text{-}tx} + 24\xi_{fb\text{-}ty}^2 + 24\xi_{fb\text{-}tz}^2 + 175t_{fb}^2\right)}{3\xi_{fb\text{-}ty}^2 + 3\xi_{fb\text{-}tz}^2 + 175t_{fb}^2}\end{aligned} \tag{3.21}$$

$$\begin{aligned}\zeta_{fb\text{-}rz} = &\frac{24\xi_{fb\text{-}ty}\left(35\xi_{fb\text{-}tx} + 24\xi_{fb\text{-}ty}^2 + 24\xi_{fb\text{-}tz}^2 + 175t_{fb}^2\right)}{3\xi_{fb\text{-}ty}^2 + 3\xi_{fb\text{-}tz}^2 + 175t_{fb}^2} \\ &- \frac{700\left(4t_{fb}^2 - 3t_{fb}w_{fb} + 3w_{fb}^2\right)\xi_{fb\text{-}rz}}{3\xi_{fb\text{-}ty}^2 + 3\xi_{fb\text{-}tz}^2 + 175t_{fb}^2}\end{aligned} \tag{3.22}$$

$$\boldsymbol{\zeta}_{\text{fb}} = -\mathrm{K}_{\text{FBeam}}\left(\boldsymbol{\xi}_{\text{fb}}, w_{\text{fb}}, t_{\text{fb}}, \delta_{\text{fb}}\right) = -\left[\zeta_{\text{fb-tx}}, \zeta_{\text{fb-ty}}, \zeta_{\text{fb-tz}}, \zeta_{\text{fb-rx}}, \zeta_{\text{fb-ry}}, \zeta_{\text{fb-rz}}\right]^{\mathrm{T}} \tag{3.23}$$

$$\boldsymbol{\zeta}_{\text{fbf}} = \mathrm{K}_{\text{FBeam}}\left(\boldsymbol{\xi}_{\text{fb}}, w_{\text{fb}}, t_{\text{fb}}, \delta_{\text{fb}}\right) \tag{3.24}$$

where $\delta_{\text{fb}} \approx 0.84375/\left(1+v_{\text{fb}}\right)$, with v_{fb} being the Poisson's ratio of the material (in this example, all beams are made of the same material, i.e. $\delta_{\text{fb1}} = \delta_{\text{fb2}} = \delta_{\text{fb3}} = \delta_{\text{fb4}} = \delta_{\text{fb}}$). When only the linear part of Equation (3.11) is considered (i.e. $\mathrm{K}_{\text{Beam}}\left(\boldsymbol{\xi}_{\text{b}}, t_{\text{b}}, \delta_{\text{b}}\right) \approx \mathbf{k}_{\text{Beam-L}}\boldsymbol{\xi}_{\text{b}}$ in Equation (3.11)), $\boldsymbol{\zeta}_{\text{fb}}$ can be simplified as

$$\begin{aligned}\boldsymbol{\zeta}_{\text{fb}} &= -\mathrm{K}_{\text{FBeam}}\left(\boldsymbol{\xi}_{\text{fb}}, w_{\text{fb}}, t_{\text{fb}}, \delta_{\text{fb}}\right) \\ &= -\mathbf{k}_{\text{FBeam-L}}\boldsymbol{\xi}_{\text{fb}} = -\begin{bmatrix} \sigma_{\text{k-fb1}} & 0 & 0 & 0 & 0 & 0 \\ 0 & 48 & 0 & 0 & 0 & -24 \\ 0 & 0 & 48 & 0 & 24 & 0 \\ 0 & 0 & 0 & \sigma_{\text{k-fb2}} & 0 & 0 \\ 0 & 0 & 24 & 0 & \sigma_{\text{k-fb3}} & 0 \\ 0 & -24 & 0 & 0 & 0 & \sigma_{\text{k-fb3}} \end{bmatrix}\boldsymbol{\xi}_{\text{fb}}\end{aligned} \tag{3.25}$$

$$\begin{aligned}\sigma_{\text{k-fb1}} &= 48/t_{\text{fb}}^2 \\ \sigma_{\text{k-fb2}} &= 4\left(6t_{\text{fb}}^2 - 12w_{\text{fb}}t_{\text{fb}} + 6w_{\text{fb}}^2 + \delta_{\text{fb}}\right) \\ \sigma_{\text{k-fb3}} &= 4\left(7t_{\text{fb}}^2 - 6w_{\text{fb}}t_{\text{fb}} + 3w_{\text{fb}}^2\right)/t_{\text{fb}}^2\end{aligned} \tag{3.26}$$

where $\mathbf{k}_{\text{FBeam-L}}$ is the linear stiffness matrix of the four-beam NBCM.

3.2.2 Variable constraint force of an eight-beam NBCM

An eight-beam NBCM, as shown in Figure 3.4(a), is comprised of one mobile rigid stage (MRS), two four-beam NBCMs termed CM-1 and CM-2, and base stages (BSs). CM-1 and CM-2 have the same dimension. The MRS, CM-1, CM-2 and BSs are illustrated in Figure 3.4(b). In this example, the eight-beam NBCM is decomposed into two four-beam NBCMs, because the variable constraint force of the four-beam NBCM has been obtained already in Section 3.2.1.

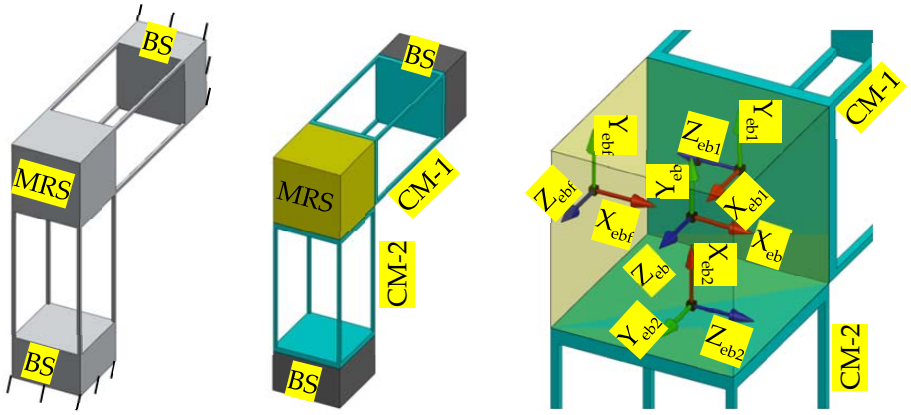

Figure 3.4 An eight-beam NBCM and the defined coordinate systems: (a) the eight-beam NBCM, (b) the decomposition of the eight-beam NBCM, and (c) the defined coordinate systems

A coordinate system O_{eb}-$X_{eb}Y_{eb}Z_{eb}$ is defined as the global coordinate system, which is located at the centre of the MRS. Coordinate systems O_{eb1}-$X_{eb1}Y_{eb1}Z_{eb1}$, O_{eb2}-$X_{eb2}Y_{eb2}Z_{eb2}$ and O_{ebf}-$X_{ebf}Y_{ebf}Z_{ebf}$ are defined as the local coordinate systems. The global and local coordinate systems can be seen in Figure 3.4(c). The origin of the coordinate system, O_{eb}-$X_{eb}Y_{eb}Z_{eb}$, is at the centre of the MRS, and the coordinate systems, O_{eb1}-$X_{eb1}Y_{eb1}Z_{eb1}$, O_{eb2}-$X_{eb2}Y_{eb2}Z_{eb2}$ and O_{ebf}-$X_{ebf}Y_{ebf}Z_{ebf}$, are placed at the centres of the three surfaces of the MRS, respectively. Note that the global coordinate system is fixed to the BSs, and the local coordinate systems are fixed to the MRS.

The displacement of the MRS in the global coordinate system can be written as a twist ξ_{eb}, as shown in Equation (3.27), and the displacements of CM-1 and CM-2 can be represented by twists ξ_{ef1} in the local coordinate system O_{eb1}-$X_{eb1}Y_{eb1}Z_{eb1}$ and ξ_{ef2} in the local coordinate system O_{eb2}-$X_{eb2}Y_{eb2}Z_{eb2}$, respectively. The twists ξ_{ef1} and ξ_{ef1} are shown in Equation (3.28).

$$\xi_{eb} = \left[\xi_{eb\text{-}tx}, \xi_{eb\text{-}ty}, \xi_{eb\text{-}tz}, \xi_{eb\text{-}rx}, \xi_{eb\text{-}ry}, \xi_{eb\text{-}rz}\right]^{T} \tag{3.27}$$

$$\xi_{eb1} = \left[\mathbf{T}_{eb1\text{-}eb}\right]^{T} \xi_{eb} \text{ and } \xi_{eb2} = \left[\mathbf{T}_{eb2\text{-}eb}\right]^{T} \xi_{eb} \tag{3.28}$$

where $\xi_{eb\text{-}tx}$, $\xi_{eb\text{-}ty}$, $\xi_{eb\text{-}tz}$, $\xi_{eb\text{-}rx}$, $\xi_{eb\text{-}ry}$ and $\xi_{eb\text{-}rz}$ are the principal twist coefficients, which represent the values of the displacements of the MRS along and about the X_{eb}-, Y_{eb}- and Z_{eb}-axes. In Equations (3.29) and (3.30), $\mathbf{T}_{eb1\text{-}eb}$ and $\mathbf{T}_{eb2\text{-}eb}$, obtained based on Equation (2.11), are the transformation matrices from the local coordinate systems O_{eb1}-$X_{eb1}Y_{eb1}Z_{eb1}$ and O_{eb2}-$X_{eb2}Y_{eb2}Z_{eb2}$ to the global coordinate system O_{eb}-$X_{eb}Y_{eb}Z_{eb}$, respectively. The transformation matrix from the local coordinate system O_{ebf}-$X_{ebf}Y_{ebf}Z_{ebf}$ to the global coordinate system is $\mathbf{T}_{ebf\text{-}eb}$, which is illustrated in Equation (3.31). Note that the effect of the MRS's rotations on the transformation matrices is ignored, because the rotational displacements are much smaller than the translational displacements of the MRS.

$$\mathbf{T}_{eb1\text{-}eb} = \begin{bmatrix} 0 & 0 & -1 & 0 & 0 & 0 \\ 0 & 1 & 0 & 0 & 0 & 0 \\ 1 & 0 & 0 & 0 & 0 & 0 \\ 0 & w_{eb}/2 & 0 & 0 & 0 & -1 \\ 0 & 0 & w_{eb}/2 & 0 & 1 & 0 \\ 0 & 0 & 0 & 1 & 0 & 0 \end{bmatrix} \tag{3.29}$$

$$\mathbf{T}_{eb2\text{-}eb} = \begin{bmatrix} 0 & 0 & 1 & 0 & 0 & 0 \\ 1 & 0 & 0 & 0 & 0 & 0 \\ 0 & 1 & 0 & 0 & 0 & 0 \\ 0 & -w_{eb}/2 & 0 & 0 & 0 & 1 \\ 0 & 0 & 0 & 1 & 0 & 0 \\ 0 & 0 & w_{eb}/2 & 0 & 1 & 0 \end{bmatrix} \tag{3.30}$$

$$\mathbf{T}_{ebf\text{-}eb} = \begin{bmatrix} 1 & 0 & 0 & 0 & 0 & 0 \\ 0 & 1 & 0 & 0 & 0 & 0 \\ 0 & 0 & 1 & 0 & 0 & 0 \\ 0 & 0 & 0 & 1 & 0 & 0 \\ 0 & 0 & w_{eb}/2 & 0 & 1 & 0 \\ 0 & -w_{eb}/2 & 0 & 0 & 0 & 1 \end{bmatrix} \tag{3.31}$$

where w_{eb} is the edge length of the MRS. Based on Equation (3.23), the variable constraint force produced by CM-1 and CM-2 can be obtained, as shown in

Equation (3.32).

$$\zeta_{\text{eb1}} = -\text{K}_{\text{FBeam}}\left(\xi_{\text{eb1}}, w_{\text{eb1}}, t_{\text{eb1}}, \delta_{\text{eb1}}\right) \text{ and } \zeta_{\text{eb2}} = -\text{K}_{\text{FBeam}}\left(\xi_{\text{eb2}}, w_{\text{eb2}}, t_{\text{eb2}}, \delta_{\text{eb2}}\right) \tag{3.32}$$

In this example, the CM-1 and CM-2 have the same dimension and material, so that $w_{\text{eb1}} = w_{\text{eb2}} = w_{\text{eb}}$, $t_{\text{eb1}} = t_{\text{eb2}} = t_{\text{eb}}$ and $\delta_{\text{eb1}} = \delta_{\text{eb2}} = \delta_{\text{eb}}$. It can be seen that the variable constraint force of the eight-beam NBCM is the vector sum of the variable constraint forces of the two four-beam NBCMs. Therefore, ζ_{eb} can be written as shown in Equation (3.33).

$$\zeta_{\text{eb}} = \mathbf{T}_{\text{eb1-eb}}\zeta_{\text{eb1}} + \mathbf{T}_{\text{eb2-eb}}\zeta_{\text{eb2}} \tag{3.33}$$

Combining Equations (3.23) and (3.29) – (3.33), the variable constraint force, ζ_{eb}, of the eight-beam NBCM can be obtained. Because the rotational displacements of the MRS are tiny compared with the translational displacements, the ζ_{eb} can be simplified as shown in Equations (3.34) – (3.39), which can also be rewritten as shown in Equation (3.40). If an external force represented by a wrench ζ_{ebf} is applied to the eight-beam parallel compliant module in the local coordinate system O_{ebf}-$X_{\text{ebf}}Y_{\text{ebf}}Z_{\text{ebf}}$, to balance ζ_{eb}, the force-displacement relationship of the eight-beam NBCM can be represented as shown in Equation (3.41).

$$\zeta_{\text{eb}-\text{tx}} = -\frac{96\xi_{\text{eb-tx}}\left(129\xi_{\text{eb-tx}}^2 + 35\left(5t_{\text{eb}}^2 + 3\xi_{\text{eb-ty}} + 3\xi_{\text{eb-tz}}\right)\right)}{175t_{\text{eb}}^2 + 3\xi_{\text{eb-tx}}^2} \tag{3.34}$$

$$\begin{aligned}\zeta_{\text{eb}-\text{ty}} = &-\frac{144\left(43\xi_{\text{eb-ty}} + 35\right)\xi_{\text{eb-tx}}^2}{175t_{\text{eb}}^2 + 3\xi_{\text{eb-tx}}^2} - \frac{1680\xi_{\text{eb-ty}}\left(5t_{\text{eb}}^2 + 6\xi_{\text{eb-tz}} + 5\right)}{175t_{\text{eb}}^2 + 3\xi_{\text{eb-tx}}^2} \\ &-\frac{24w_{\text{eb}}\xi_{\text{eb-rx}}\left(129\xi_{\text{eb-tx}}^2 + 35\left(5t_{\text{eb}}^2 + 6\xi_{\text{eb-tz}}\right)\right)}{175t_{\text{eb}}^2 + 3\xi_{\text{eb-tx}}^2}\end{aligned} \tag{3.35}$$

$$\begin{aligned}\zeta_{\text{eb}-\text{tz}} = &\frac{24w_{\text{eb}}\xi_{\text{eb-rx}}\left(129\xi_{\text{eb-tx}}^2 + 35\left(5t_{\text{eb}}^2 + 6\xi_{\text{eb-ty}}\right)\right)}{175t_{\text{eb}}^2 + 3\xi_{\text{eb-tx}}^2} \\ &-\frac{48\left(3\left(43\xi_{\text{eb-tz}} + 35\right)\xi_{\text{eb-tx}}^2 + 35\left(5t_{\text{eb}}^2 + 6\xi_{\text{eb-ty}} + 5\right)\xi_{\text{eb-tz}}\right)}{175t_{\text{eb}}^2 + 3\xi_{\text{eb-tx}}^2}\end{aligned} \tag{3.36}$$

$$\zeta_{\text{eb-rx}} = -\frac{4}{175t_{\text{eb}}^2+3\xi_{\text{eb-tx}}^2}\begin{pmatrix} 6\left(175\left(w_{\text{eb}}+1\right)t_{\text{eb}}^2+3\left(43w_{\text{eb}}+8\right)\xi_{\text{eb-tx}}^2\right)\left(\xi_{\text{eb-ty}}-\xi_{\text{eb-tz}}\right) \\ +\xi_{\text{eb-rx}}\begin{pmatrix} 18w_{\text{eb}}\left(43w_{\text{eb}}+8\right)\xi_{\text{eb-tx}}^2 \\ +35\begin{pmatrix} 10\left(\left(3w_{\text{eb}}^2+3w_{\text{eb}}+4\right)t_{\text{eb}}^2-3w_{\text{eb}}t_{\text{eb}}+3w_{\text{eb}}^2\right) \\ +3w_{\text{eb}}\left(6w_{\text{eb}}+1\right)\xi_{\text{eb-ty}}+3w_{\text{eb}}\left(6w_{\text{eb}}+1\right)\xi_{\text{eb-tz}}\end{pmatrix}\end{pmatrix}\end{pmatrix} \tag{3.37}$$

$$\zeta_{\text{eb-ry}} = -\frac{-4}{175t_{\text{eb}}^2+3\xi_{\text{eb-tx}}^2}\begin{pmatrix} 6\xi_{\text{eb-tx}}\begin{pmatrix} 3\left(43w_{\text{eb}}+8\right)\xi_{\text{eb-tx}}^2+35\left(5t_{\text{eb}}^2-3w_{\text{eb}}t_{\text{eb}}+3w_{\text{eb}}^2\right)\xi_{\text{eb-rx}} \\ +35\left(5\left(w_{\text{eb}}+1\right)t_{\text{eb}}^2+\left(6w_{\text{eb}}+1\right)\xi_{\text{eb-tz}}\right)\end{pmatrix} \\ -\xi_{\text{eb-ry}}\left(3\delta\xi_{\text{eb-tx}}^2+175\left(\left(\delta_{\text{eb}}+4\right)t_{\text{eb}}^2-3w_{\text{eb}}t_{\text{eb}}+3w_{\text{eb}}^2\right)\right)\end{pmatrix} \tag{3.38}$$

$$\zeta_{\text{eb-rz}} = -\frac{4}{175t_{\text{eb}}^2+3\xi_{\text{eb-tx}}^2}\begin{pmatrix} \xi_{\text{eb-rz}}\left(3\delta_{\text{eb}}\xi_{\text{eb-tx}}^2+175\left(\left(\delta_{\text{eb}}+4\right)t_{\text{eb}}^2-3w_{\text{eb}}t_{\text{eb}}+3w_{\text{eb}}^2\right)\right) \\ +6\xi_{\text{eb-tx}}\begin{pmatrix} 3\left(43w_{\text{eb}}+8\right)\xi_{\text{eb-tx}}^2-35\begin{pmatrix}5t_{\text{eb}}^2-3w_{\text{eb}}t_{\text{eb}} \\ +3w_{\text{eb}}^2\end{pmatrix}\xi_{\text{eb-rx}} \\ +35\left(5\left(w_{\text{eb}}+1\right)t_{\text{eb}}^2+\left(6w_{\text{eb}}+1\right)\xi_{\text{eb-ty}}\right)\end{pmatrix}\end{pmatrix} \tag{3.39}$$

$$\zeta_{\text{eb}} = -\text{K}_{\text{EBeam}}\left(\xi_{\text{eb}}, w_{\text{eb}}, t_{\text{eb}}, \delta_{\text{eb}}\right) = -\left[\zeta_{\text{eb-tx}}, \zeta_{\text{eb-ty}}, \zeta_{\text{eb-tz}}, \zeta_{\text{eb-rx}}, \zeta_{\text{eb-ry}}, \zeta_{\text{eb-rz}}\right]^{\text{T}} \tag{3.40}$$

$$\zeta_{\text{ebf}} = \left[\mathbf{T}_{\text{ebf-eb}}\right]^{-1}\text{K}_{\text{EBeam}}\left(\xi_{\text{eb}}, w_{\text{eb}}, t_{\text{eb}}, \delta_{\text{eb}}\right) \tag{3.41}$$

When only the linear part of the variable constraint force of the four-beam NBCM is considered (i.e. $\text{K}_{\text{FBeam}}\left(\xi_{\text{fb}}, w_{\text{fb}}, t_{\text{fb}}, \delta_{\text{fb}}\right) \approx \mathbf{k}_{\text{FBeam-L}}\xi_{\text{fb}}$ in Equation (3.25)), ζ_{eb} can be simplified as shown in Equation (3.42).

$$\begin{aligned}\zeta_{\text{eb}} &= -\text{K}_{\text{EBeam}}\left(\xi_{\text{eb}}, w_{\text{eb}}, t_{\text{eb}}, \delta_{\text{eb}}\right) = -\mathbf{k}_{\text{EBeam-L}}\xi_{\text{eb}} \\ &= -\begin{bmatrix} 96 & 0 & 0 & 0 & -\sigma_{\text{k-eb2}} & \sigma_{\text{k-eb2}} \\ 0 & \sigma_{\text{k-eb1}} & 0 & \sigma_{\text{k-eb2}} & 0 & 0 \\ 0 & 0 & \sigma_{\text{k-eb1}} & -\sigma_{\text{k-eb2}} & 0 & 0 \\ 0 & \sigma_{\text{k-eb2}} & -\sigma_{\text{k-eb2}} & \sigma_{\text{k-eb3}} & 0 & 0 \\ -\sigma_{\text{k-eb2}} & 0 & 0 & 0 & \sigma_{\text{k-eb4}} & 0 \\ \sigma_{\text{k-eb2}} & 0 & 0 & 0 & 0 & \sigma_{\text{k-eb4}} \end{bmatrix}\xi_{\text{eb}}\end{aligned} \tag{3.42}$$

where

$$\sigma_{\text{k-eb1}} = 48\left(1+1/t_{\text{eb}}^2\right)$$
$$\sigma_{\text{k-eb2}} = 24\left(w_{\text{eb}}+1\right)$$
$$\sigma_{\text{k-eb3}} = 8\left(\left(3w_{\text{eb}}^2+6w_{\text{eb}}+7\right)t_{\text{eb}}^2-6w_{\text{eb}}t_{\text{eb}}+3w_{\text{eb}}^2\right)/t_{\text{eb}}^2$$
$$\sigma_{\text{k-eb4}} = 4\left(6t_{\text{eb}}^4-12w_{\text{eb}}t_{\text{eb}}^3+\left(9w_{\text{eb}}^2+6w_{\text{eb}}+\delta_{\text{eb}}+7\right)t_{\text{eb}}^2-6w_{\text{eb}}t_{\text{eb}}+3w_{\text{eb}}^2\right)/t_{\text{eb}}^2$$

$\mathbf{k}_{\text{EBeam-L}}$ is the linear stiffness matrix of the eight-beam NBCM.

3.2.3 Modelling of the XYZ CPM

In this section, an XYZ CPM (Figure 3.2) is modelled using the CFB approach. The defined coordinate systems for the XYZ CPM are demonstrated in Figure 3.5. The global coordinate system O_{ms}-$X_{ms}Y_{ms}Z_{ms}$ is fixed to the ground, and the other local coordinate systems are fixed to the connected rigid stages, respectively. Each of the local coordinate systems can translate with the connected rigid stage, but cannot rotate with the connected rigid stage. When the XYZ CPM is in the undeformed configuration, the positions of the local coordinate systems are defined as the original positions of the local coordinate systems. Compared with these original positions, the displacements of the origins of the local coordinate systems O_{pmx}-$X_{pmx}Y_{pmx}Z_{pmx}$, O_{pmy}-$X_{pmy}Y_{pmy}Z_{pmy}$, O_{pmz}-$X_{pmz}Y_{pmz}Z_{pmz}$, O_{asx}-$X_{asx}Y_{asx}Z_{asx}$, O_{amx}-$X_{amx}Y_{amx}Z_{amx}$, O_{pax}-$X_{pax}Y_{pax}Z_{pax}$, O_{asy}-$X_{asy}Y_{asy}Z_{asy}$, O_{amy}-$X_{amy}Y_{amy}Z_{amy}$, O_{pay}-$X_{pay}Y_{pay}Z_{pay}$, O_{asz}-$X_{asz}Y_{asz}Z_{asz}$, O_{amz}-$X_{amz}Y_{amz}Z_{amz}$, and O_{paz}-$X_{paz}Y_{paz}Z_{paz}$ are represented as twists ξ_{pmx}, ξ_{pmy}, ξ_{pmz}, ξ_{asx}, ξ_{amx}, ξ_{pax}, ξ_{asy}, ξ_{amy}, ξ_{pay}, ξ_{asz}, ξ_{amz}, and ξ_{paz}, when the XYZ CPM is at a deformed configuration. Additionally, the displacement of the top centre of the MS is represented as a twist ξ_{ms} in the global coordinate system.

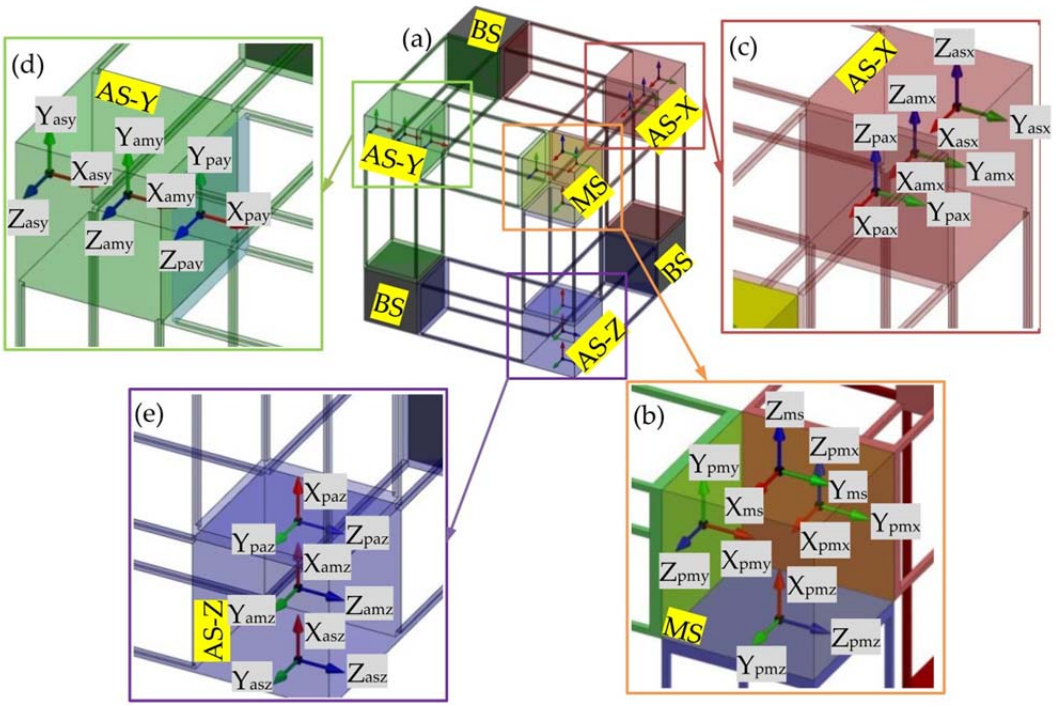

Figure 3.5 Coordinate system demonstration: (a) all the coordinate systems; (b) the coordinate systems, O_{ms}-$X_{ms}Y_{ms}Z_{ms}$, O_{pmx}-$X_{pmx}Y_{pmx}Z_{pmx}$, O_{pmy}-$X_{pmy}Y_{pmy}Z_{pmy}$ and O_{pmz}-$X_{pmz}Y_{pmz}Z_{pmz}$, fixed on the MS; (c) the coordinate systems, O_{asx}-$X_{asx}Y_{asx}Z_{asx}$, O_{amx}-$X_{amx}Y_{amx}Z_{amx}$ and O_{pax}-$X_{pax}Y_{pax}Z_{pax}$ fixed on the AS-X; (d) the coordinate systems, O_{asy}-$X_{asy}Y_{asy}Z_{asy}$, O_{amy}-$X_{amy}Y_{amy}Z_{amy}$ and O_{pay}-$X_{pay}Y_{pay}Z_{pay}$, fixed on the AS-Y; and (e) the coordinate systems, O_{asz}-$X_{asz}Y_{asz}Z_{asz}$, O_{amz}-$X_{amz}Y_{amz}Z_{amz}$ and O_{paz}-$X_{paz}Y_{paz}Z_{paz}$, fixed on the AS-Z

Based on Equation 2.11, the associated transformation matrices are defined as $\mathbf{T}_{pmx\text{-}ms}$, $\mathbf{T}_{pmy\text{-}ms}$, $\mathbf{T}_{pmz\text{-}ms}$, $\mathbf{T}_{pax\text{-}pmx}$, $\mathbf{T}_{pay\text{-}pmy}$, $\mathbf{T}_{paz\text{-}pmz}$, $\mathbf{T}_{pmx\text{-}pax}$, $\mathbf{T}_{pmy\text{-}pay}$, $\mathbf{T}_{pmz\text{-}paz}$, $\mathbf{T}_{pax\text{-}asx}$, $\mathbf{T}_{pay\text{-}asy}$, $\mathbf{T}_{paz\text{-}asz}$, $\mathbf{T}_{amx\text{-}asx}$, $\mathbf{T}_{amy\text{-}asy}$ and $\mathbf{T}_{amz\text{-}asz}$. The subscript of each of the transformation matrices shows the associated coordinate systems and the transformation between them. For instance, the subscript 'pmx-ms' in $\mathbf{T}_{pmx\text{-}ms}$ indicates that $\mathbf{T}_{pmx\text{-}ms}$ is the transformation matrix from the coordinate system O_{pmx}-$X_{pmx}Y_{pmx}Z_{pmx}$ to the coordinate system O_{ms}-$X_{ms}Y_{ms}Z_{ms}$. After deformation of the XYZ CPM, the transformation matrices can be written as Equations (E.1) – (E.15) in Appendix E. Note that all the tiny displacements such as the parasitic rotations in the transformation matrices are ignored.

On the basis of the conditions of geometrical compatibility [77], Equations (3.43)

– (3.46) can be obtained. It can be seen that ξ_{amx}, ξ_{amy} and ξ_{amz} are also represent the deformation displacements of AM-X, AM-Y and AM-Z, respectively. In addition, the deformation displacements of PM-X, PM-Y and PM-Z can also be derived. These can be represented as $\xi_{pmx\text{-}pax}$, $\xi_{pmy\text{-}pay}$ and $\xi_{pmz\text{-}paz}$ in the coordinate systems O_{pmx}-$X_{pmx}Y_{pmx}Z_{pmx}$, O_{pmy}-$X_{pmy}Y_{pmy}Z_{pmy}$ and O_{pmz}-$X_{pmz}Y_{pmz}Z_{pmz}$, respectively. The twists $\xi_{pmx\text{-}pax}$, $\xi_{pmy\text{-}pay}$ and $\xi_{pmz\text{-}paz}$ are shown in Equation (3.47).

$$\xi_{pmx} = \left[\mathbf{T}_{pmx\text{-}ms}\right]^{T} \xi_{ms}, \xi_{pmy} = \left[\mathbf{T}_{pmy\text{-}ms}\right]^{T} \xi_{ms}, \xi_{pmz} = \left[\mathbf{T}_{pmz\text{-}ms}\right]^{T} \xi_{ms} \tag{3.43}$$

$$\xi_{amx} = \left[\mathbf{T}_{amx\text{-}asx}\right]^{T} \xi_{asx} \text{ and } \xi_{pax} = \left[\mathbf{T}_{pax\text{-}asx}\right]^{T} \xi_{asx} \tag{3.44}$$

$$\xi_{amy} = \left[\mathbf{T}_{amy\text{-}asy}\right]^{T} \xi_{asy} \text{ and } \xi_{pay} = \left[\mathbf{T}_{pay\text{-}asy}\right]^{T} \xi_{asy} \tag{3.45}$$

$$\xi_{amz} = \left[\mathbf{T}_{amz\text{-}asz}\right]^{T} \xi_{asz} \text{ and } \xi_{paz} = \left[\mathbf{T}_{paz\text{-}asz}\right]^{T} \xi_{asz} \tag{3.46}$$

$$\begin{aligned} &\xi_{pmx\text{-}pax} = \xi_{pmx} - \left[\mathbf{T}_{pmx\text{-}pax}\right]^{T} \xi_{pax}, \xi_{pmy\text{-}pay} = \xi_{pmy} - \left[\mathbf{T}_{pmy\text{-}pay}\right]^{T} \xi_{pay} \text{ and} \\ &\xi_{pmz\text{-}paz} = \xi_{pmz} - \left[\mathbf{T}_{pmz\text{-}paz}\right]^{T} \xi_{paz} \end{aligned} \tag{3.47}$$

Suppose that the thicknesses of the beams (each assumed identical) and the edge lengths of the rigid stages can be represented as t and w, respectively, while v is the Poisson ratio of the material, and $\delta \approx 27/32/(1+v)$. Based on Equations (3.23) and (3.40), the variable constraint forces produced by the AM-X, AM-Y, AM-Z, PM-X, PM-Y and PM-Z can be written as shown in Equations (3.48) and (3.49).

$$\begin{aligned} &\zeta_{amx} = -\mathrm{K}_{EBeam}\left(\xi_{amx}, w, t, \delta\right), \\ &\zeta_{amy} = -\mathrm{K}_{EBeam}\left(\xi_{amy}, w, t, \delta\right), \\ &\zeta_{amz} = -\mathrm{K}_{EBeam}\left(\xi_{amz}, w, t, \delta\right) \end{aligned} \tag{3.48}$$

$$\zeta_{\text{pmx}} = -\text{K}_{\text{FBeam}}\left(\xi_{\text{pmx-pax}}, w, t, \delta\right),$$

$$\zeta_{\text{pmy}} = -\text{K}_{\text{FBeam}}\left(\xi_{\text{pmy-pay}}, w, t, \delta\right), \tag{3.49}$$

$$\zeta_{\text{pmz}} = -\text{K}_{\text{FBeam}}\left(\xi_{\text{pmz-paz}}, w, t, \delta\right)$$

where ζ_{amx}, ζ_{amy}, ζ_{amz}, ζ_{pmx}, ζ_{pmy} and ζ_{pmz} are wrenches representing the variable constraint forces of AM-X, AM-Y, AM-Z, PM-X, PM-Y and PM-Z in the coordinate systems O_{amx}-$X_{\text{amx}}Y_{\text{amx}}Z_{\text{amx}}$, O_{amy}-$X_{\text{amy}}Y_{\text{amy}}Z_{\text{amy}}$, O_{amz}-$X_{\text{amz}}Y_{\text{amz}}Z_{\text{amz}}$, O_{pmx}-$X_{\text{pmx}}Y_{\text{pmx}}Z_{\text{pmx}}$, O_{pmy}-$X_{\text{pmy}}Y_{\text{pmy}}Z_{\text{pmy}}$ and O_{pmz}-$X_{\text{pmz}}Y_{\text{pmz}}Z_{\text{pmz}}$, respectively. In addition, the ζ_{pmx}, ζ_{pmy} and ζ_{pmz} can also be represented in the coordinate systems O_{pax}-$X_{\text{pax}}Y_{\text{pax}}Z_{\text{pax}}$, O_{pay}-$X_{\text{pay}}Y_{\text{pay}}Z_{\text{pay}}$ and O_{paz}-$X_{\text{paz}}Y_{\text{paz}}Z_{\text{paz}}$, respectively, which can be written as ζ_{pmax}, ζ_{pmay} and ζ_{pmaz}, as shown in Equation (3.50).

$$\zeta_{\text{pmax}} = \mathbf{T}_{\text{pmx-apx}}\zeta_{\text{pmx}},\ \zeta_{\text{pmay}} = \mathbf{T}_{\text{pmy-apy}}\zeta_{\text{pmy}}\ \textbf{and}\ \zeta_{\text{pmaz}} = \mathbf{T}_{\text{pmz-apz}}\zeta_{\text{pmz}} \tag{3.50}$$

The actuation forces acting on the three ASs and the load force exerted on the MS are defined as constant constraint forces, which can be written as wrenches ζ_{asx}, ζ_{asy}, ζ_{asz} and ζ_{ms}, in the coordinate systems O_{asx}-$X_{\text{asx}}Y_{\text{asx}}Z_{\text{asx}}$, O_{asy}-$X_{\text{asy}}Y_{\text{asy}}Z_{\text{asy}}$, O_{asz}-$X_{\text{asz}}Y_{\text{asz}}Z_{\text{asz}}$ and O_{ms}-$X_{\text{ms}}Y_{\text{ms}}Z_{\text{ms}}$, respectively, as shown in Equations (3.51) – (3.54).

$$\zeta_{\text{asx}} = \left[\zeta_{\text{asx-tx}}, \zeta_{\text{asx-ty}}, \zeta_{\text{asx-tz}}, \zeta_{\text{asx-rx}}, \zeta_{\text{asx-ry}}, \zeta_{\text{asx-rz}}\right]^{\text{T}} \tag{3.51}$$

$$\zeta_{\text{asy}} = \left[\zeta_{\text{asy-tx}}, \zeta_{\text{asy-ty}}, \zeta_{\text{asy-tz}}, \zeta_{\text{asy-rx}}, \zeta_{\text{asy-ry}}, \zeta_{\text{asy-rz}}\right]^{\text{T}} \tag{3.52}$$

$$\zeta_{\text{asz}} = \left[\zeta_{\text{asz-tx}}, \zeta_{\text{asz-ty}}, \zeta_{\text{asz-tz}}, \zeta_{\text{asz-rx}}, \zeta_{\text{asz-ry}}, \zeta_{\text{asz-rz}}\right]^{\text{T}} \tag{3.53}$$

$$\zeta_{\text{ms}} = \left[\zeta_{\text{ms-tx}}, \zeta_{\text{ms-ty}}, \zeta_{\text{ms-tz}}, \zeta_{\text{ms-rx}}, \zeta_{\text{ms-ry}}, \zeta_{\text{ms-rz}}\right]^{\text{T}} \tag{3.54}$$

Based on Equation (3.12), the force equilibrium equations for the ASs and MS can be written in Equations (3.55) – (3.58).

$$\zeta_{\text{asx}} + \mathbf{T}_{\text{amx-asx}}\zeta_{\text{amx}} + \mathbf{T}_{\text{apx-asx}}\zeta_{\text{pmax}} = 0 \tag{3.55}$$

$$\zeta_{\text{asy}} + \mathbf{T}_{\text{amy-asy}}\zeta_{\text{amy}} + \mathbf{T}_{\text{apy-asy}}\zeta_{\text{pmay}} = 0 \tag{3.56}$$

$$\zeta_{\text{asz}} + \mathbf{T}_{\text{amz-asz}}\zeta_{\text{amz}} + \mathbf{T}_{\text{apz-asz}}\zeta_{\text{pmaz}} = 0 \tag{3.57}$$

$$\zeta_{\text{ms}} + \mathbf{T}_{\text{pmx-m}}\zeta_{\text{pmx}} + \mathbf{T}_{\text{pmy-m}}\zeta_{\text{pmy}} + \mathbf{T}_{\text{pmz-m}}\zeta_{\text{pmz}} = 0 \tag{3.58}$$

By combining Equations (3.43) – (3.58) and (E.1) – (E.15), the force equilibrium equations of the XYZ CPM can be obtained, which are elaborated in Equations (F.1) – (F.60) in Appendix F. The nonlinear force-displacement relationship of the XYZ CPM can be calculated from the force equilibrium equations using commercial software *Mathematica*. If only linear parts of the variable constraint forces of the PMs and AMs are considered, and by setting the primary translation displacements in the transformation matrices (in Appendix E) to zero, the linear model of the XYZ CPM can be derived, as shown in Equation (3.59).

$$\begin{aligned}
\xi_{\text{ms}} &= \boldsymbol{V}_{\text{m}}\left(\boldsymbol{W}_{\text{mx}}\zeta_{\text{asx}} + \boldsymbol{W}_{\text{my}}\zeta_{\text{asy}} + \boldsymbol{W}_{\text{mz}}\zeta_{\text{asz}} + \zeta_{\text{ms}}\right) \\
\xi_{\text{asx}} &= \boldsymbol{V}_{\text{x}}\left(\boldsymbol{W}_{\text{x}}\xi_{\text{ms}} + \zeta_{\text{asx}}\right) \\
\xi_{\text{asy}} &= \boldsymbol{V}_{\text{y}}\left(\boldsymbol{W}_{\text{y}}\xi_{\text{ms}} + \zeta_{\text{asy}}\right) \\
\xi_{\text{asz}} &= \boldsymbol{V}_{\text{z}}\left(\boldsymbol{W}_{\text{z}}\xi_{\text{ms}} + \zeta_{\text{asz}}\right)
\end{aligned} \tag{3.59}$$

where

$$\begin{aligned}
\boldsymbol{V}_{\text{m}} &= \left[\boldsymbol{U}_{\text{mx}} + \boldsymbol{U}_{\text{my}} + \boldsymbol{U}_{\text{mz}}\right]^{-1} \\
\boldsymbol{W}_{\text{mx}} &= \mathbf{T}_{\text{pmx-m}}\mathbf{k}_{\text{FBeam-L}}\left[\mathbf{T}_{\text{pmx-pax}}\right]^{\text{T}}\left[\mathbf{T}_{\text{pax-asx}}\right]^{\text{T}}\boldsymbol{V}_{\text{x}} \\
\boldsymbol{W}_{\text{my}} &= \mathbf{T}_{\text{pmy-m}}\mathbf{k}_{\text{FBeam-L}}\left[\mathbf{T}_{\text{pmy-pay}}\right]^{\text{T}}\left[\mathbf{T}_{\text{pay-asy}}\right]^{\text{T}}\boldsymbol{V}_{\text{y}} \\
\boldsymbol{W}_{\text{mz}} &= \mathbf{T}_{\text{pmz-m}}\mathbf{k}_{\text{FBeam-L}}\left[\mathbf{T}_{\text{pmz-paz}}\right]^{\text{T}}\left[\mathbf{T}_{\text{paz-asz}}\right]^{\text{T}}\boldsymbol{V}_{\text{z}}
\end{aligned}$$

$$\boldsymbol{U}_{\mathrm{mx}} = \mathbf{T}_{\mathrm{pmx\text{-}ms}}\mathbf{k}_{\mathrm{FBeam\text{-}L}}\left[\mathbf{T}_{\mathrm{pmx\text{-}ms}}\right]^{\mathrm{T}} - \mathbf{T}_{\mathrm{pmx\text{-}ms}}\mathbf{k}_{\mathrm{FBeam\text{-}L}}\left[\mathbf{T}_{\mathrm{pmx\text{-}pax}}\right]^{\mathrm{T}}\left[\mathbf{T}_{\mathrm{pax\text{-}asx}}\right]^{\mathrm{T}}\boldsymbol{V}_{\mathrm{x}}\boldsymbol{W}_{\mathrm{x}}$$
$$\boldsymbol{U}_{\mathrm{my}} = \mathbf{T}_{\mathrm{pmy\text{-}ms}}\mathbf{k}_{\mathrm{FBeam\text{-}L}}\left[\mathbf{T}_{\mathrm{pmy\text{-}ms}}\right]^{\mathrm{T}} - \mathbf{T}_{\mathrm{pmy\text{-}ms}}\mathbf{k}_{\mathrm{FBeam\text{-}L}}\left[\mathbf{T}_{\mathrm{pmy\text{-}pay}}\right]^{\mathrm{T}}\left[\mathbf{T}_{\mathrm{pay\text{-}asy}}\right]^{\mathrm{T}}\boldsymbol{V}_{\mathrm{y}}\boldsymbol{W}_{\mathrm{y}}$$
$$\boldsymbol{U}_{\mathrm{mz}} = \mathbf{T}_{\mathrm{pmz\text{-}ms}}\mathbf{k}_{\mathrm{FBeam\text{-}L}}\left[\mathbf{T}_{\mathrm{pmz\text{-}ms}}\right]^{\mathrm{T}} - \mathbf{T}_{\mathrm{pmz\text{-}ms}}\mathbf{k}_{\mathrm{FBeam\text{-}L}}\left[\mathbf{T}_{\mathrm{pmz\text{-}paz}}\right]^{\mathrm{T}}\left[\mathbf{T}_{\mathrm{paz\text{-}asz}}\right]^{\mathrm{T}}\boldsymbol{V}_{\mathrm{z}}\boldsymbol{W}_{\mathrm{z}}$$

$$\boldsymbol{U}_{\mathrm{x}} = \mathbf{T}_{\mathrm{amx\text{-}asx}}\mathbf{k}_{\mathrm{EBeam\text{-}L}}\left[\mathbf{T}_{\mathrm{amx\text{-}asx}}\right]^{\mathrm{T}} + \mathbf{T}_{\mathrm{pax\text{-}asx}}\mathbf{T}_{\mathrm{pmx\text{-}pax}}\mathbf{k}_{\mathrm{FBeam\text{-}L}}\left[\mathbf{T}_{\mathrm{pmx\text{-}pax}}\right]^{\mathrm{T}}\left[\mathbf{T}_{\mathrm{pax\text{-}asx}}\right]^{\mathrm{T}}$$
$$\boldsymbol{V}_{\mathrm{x}} = \left[\boldsymbol{U}_{\mathrm{x}}\right]^{-1}$$
$$\boldsymbol{W}_{\mathrm{x}} = \mathbf{T}_{\mathrm{pax\text{-}asx}}\mathbf{T}_{\mathrm{pmx\text{-}pax}}\mathbf{k}_{\mathrm{FBeam\text{-}L}}\left[\mathbf{T}_{\mathrm{pmx\text{-}ms}}\right]^{\mathrm{T}}$$

$$\boldsymbol{U}_{\mathrm{y}} = \mathbf{T}_{\mathrm{amy\text{-}asy}}\mathbf{k}_{\mathrm{EBeam\text{-}L}}\left[\mathbf{T}_{\mathrm{amy\text{-}asy}}\right]^{\mathrm{T}} + \mathbf{T}_{\mathrm{pay\text{-}asy}}\mathbf{T}_{\mathrm{pmy\text{-}pay}}\mathbf{k}_{\mathrm{FBeam\text{-}L}}\left[\mathbf{T}_{\mathrm{pmy\text{-}pay}}\right]^{\mathrm{T}}\left[\mathbf{T}_{\mathrm{pay\text{-}asy}}\right]^{\mathrm{T}}$$
$$\boldsymbol{V}_{\mathrm{y}} = \left[\boldsymbol{U}_{\mathrm{y}}\right]^{-1}$$
$$\boldsymbol{W}_{\mathrm{y}} = \mathbf{T}_{\mathrm{pay\text{-}asy}}\mathbf{T}_{\mathrm{pmy\text{-}pay}}\mathbf{k}_{\mathrm{FBeam\text{-}L}}\left[\mathbf{T}_{\mathrm{pmy\text{-}ms}}\right]^{\mathrm{T}}$$

$$\boldsymbol{U}_{\mathrm{z}} = \mathbf{T}_{\mathrm{amz\text{-}asz}}\mathbf{k}_{\mathrm{EBeam\text{-}L}}\left[\mathbf{T}_{\mathrm{amz\text{-}asz}}\right]^{\mathrm{T}} + \mathbf{T}_{\mathrm{paz\text{-}asz}}\mathbf{T}_{\mathrm{pmz\text{-}paz}}\mathbf{k}_{\mathrm{FBeam\text{-}L}}\left[\mathbf{T}_{\mathrm{pmz\text{-}paz}}\right]^{\mathrm{T}}\left[\mathbf{T}_{\mathrm{paz\text{-}asz}}\right]^{\mathrm{T}}$$
$$\boldsymbol{V}_{\mathrm{z}} = \left[\boldsymbol{U}_{\mathrm{z}}\right]^{-1}$$
$$\boldsymbol{W}_{\mathrm{z}} = \mathbf{T}_{\mathrm{paz\text{-}asz}}\mathbf{T}_{\mathrm{pmz\text{-}paz}}\mathbf{k}_{\mathrm{FBeam\text{-}L}}\left[\mathbf{T}_{\mathrm{pmz\text{-}ms}}\right]^{\mathrm{T}}$$

The following results can be derived from the linear and nonlinear analytical models of the XYZ CPM: (a) the displacements of the MS under the influence of specific external forces, (b) the displacements of the AS-X, AS-Y and AS-Z under the influence of specific external forces, (c) the lost motions between the displacements of the MS and the displacements of AS-X, AS-Y and AS-Z, (d) the actuation stiffness along the X_{ms}-, Y_{ms}- and Z_{ms}-axes, and (e) the relationships between the displacements and the geometrical parameters. Note that the linear analytical model is valid only over a very small motion range.

3.3 Model Comparisons

In this section, a series of FEA simulations and experimental tests are carried out to validate the linear and nonlinear analytical models of the XYZ CPM already proposed in Section 3.2.

3.3.1 FEA comparisons

For the FEA model of the XYZ CPM, let the beam length be 50mm, the beam thickness be 1mm, the edge length of the rigid stages be 25mm, the Poisson's ratio be 0.33, and the Young's modulus be 6.9×10^{10} Pa. Commercial software, COMSOL MULTIPHYSICS, is selected for the nonlinear FEA simulations, using the 10-node tetrahedral element and extra fine meshing technology (maximum element size 3.5mm, minimum element size 0.15mm, maximum element growth rate 1.35, curvature factor 0.3, and resolution of narrow regions 0.85). The XYZ CPM is actuated by three linear translational actuators without considering the mass of the XYZ CPM. Therefore, the constant constraint forces, ζ_{asx}, ζ_{asy}, ζ_{asz} and ζ_{ms}, can be simplified, as shown in Equation (3.60).

$$\begin{aligned}
\zeta_{\text{asx}} &= \left[\zeta_{\text{asx-tx}}, 0, 0, 0, 0, 0\right]^{\text{T}} \\
\zeta_{\text{asy}} &= \left[\zeta_{\text{asy-tx}}, 0, 0, 0, 0, 0\right]^{\text{T}} \\
\zeta_{\text{asz}} &= \left[\zeta_{\text{asz-tx}}, 0, 0, 0, 0, 0\right]^{\text{T}} \\
\zeta_{\text{ms}} &= \left[0, 0, 0, 0, 0, 0\right]^{\text{T}}
\end{aligned} \tag{3.60}$$

In order to achieve a $\pm0.1L$ motion range per axis (the motion range can be considered as a medium to large motion range compared with the length of the beam [103]), the actuation force per axis varies from -40N to $+40\text{N}$ (normalized actuation force per axis varies from −17.4 to +17.4). The designed XYZ CPM has an isotropic configuration, so the model associated with the motions of the MS and AS-X, is validated under the following conditions: (a) $\zeta_{\text{asx-tx}}$ varies from −17.4 to +17.4 when $\zeta_{\text{asy-tx}}=0$ and $\zeta_{\text{asz-tx}}=0$, (b) $\zeta_{\text{asx-tx}}$ varies from −17.4 to +17.4 when $\zeta_{\text{asy-tx}}=17.4$ and $\zeta_{\text{asz-tx}}=0$, and (c) $\zeta_{\text{asx-tx}}$ varies from −17.4 to +17.4 when $\zeta_{\text{asy-tx}}=17.4$ and $\zeta_{\text{asz-tx}}=17.4$. The nonlinear FEA results, nonlinear analytical results and linear analytical results can are shown in Figure 3.6 and

Figure 3.7.

It can be seen from Figure 3.6 that the nonlinear analytical results match the FEA results well, and that the linear analytical results have small difference compared with the FEA results within small motion ranges. For the translations of the MS, the difference between the FEA results and the nonlinear results is less than 3.25% in the translations along the X_{ms}- and Y_{ms}-axes (Figure 3.6 (a) and Figure 3.6 (b)), and less than 4.92% in the translation along the Z_{ms}-axis (Figure 3.6 (c)). The difference between the FEA results and the linear results is less than 6.59% in the translations along the X_{ms}- and Y_{ms}-axes (Figure 3.6 (a) and Figure 3.6 (b)), and less than 13.48% in the translation along the Z_{ms}-axis (Figure 3.6 (c)). For the results of the MS's rotations about the Y_{ms}- and Z_{ms}-axes, as shown in Figure 3.6 (e) and Figure 3.6 (f), the maximum difference between the FEA results and the nonlinear results is less than 2.7% under all the conditions, while the maximum difference between the FEA results and the linear results is about 16.3%. Compared with the FEA results, the linear and nonlinear results of the rotations about the X_{ms}-axis, as shown in Figure 3.6 (d), have larger differences, because the results (of the order of 10^{-4} rad) shown in this figure are comparable to the simulation accuracy and the analytical approximations. However, the analytical results of the rotations about the X_{ms}-axis still have similar trends as those of the associated FEA results.

Figure 3.6 (a) also shows that the translations of the MS along the X_{ms}-axis under the various conditions have small differences, which means that the translation of the MS along the X_{ms}-axis is almost decoupled from the translations of the MS along the other two directions. Figure 3.6 (b) and Figure 3.6 (c) illustrate that the translations of the MS along the Y_{ms}- and Z_{ms}-axes are insensitive to the force along the X_{ms}-axis, which also validates the cross-axis decoupling motion characteristics. Other motion characteristics of the XYZ CPM, such as lost motion and actuation stiffness, can also be captured from the linear and nonlinear models.

Figure 3.7 illustrates that the linear results have relative large differences to the FEA results, because the linear results cannot capture the elastokinematic effects [55]. It can be seen that the nonlinear analytical results of the AS-X's translations exhibit small differences to the FEA results. These differences are less than 2.74% in the translation along the X_{ms}-axis (Figure 3.7(a)), less than 5.33% in the translation along the Y_{ms}-axis (Figure 3.7(b)), and less than 4.55% in the translation along the Z_{ms}-axis (Figure 3.7(c)). The parasitic rotations of the AS-X about the Y_{ms}- and Z_{ms}-axes can be seen from Figure 3.7(e) – Figure 3.7(f), showing that the nonlinear results have a maximum deviation from the FEA results of approximately 7%.

However, Figure 3.7 (d) shows that the nonlinear results of the AS-X's X_{ms}-axis rotation have larger differences compared with the FEA results. The difference occurs mainly due to the following two reasons: (a) the rotational displacements about the X_{ms}-axis (in the order of 10^{-5} rad) are much smaller than the rotational displacements about the Y_{ms}- and Z_{ms}-axes (in the order of 10^{-3} rad), so the rotation results about the X_{ms}-axis are more sensitive to the pre-set relative tolerance of the FEA software (in the order of 10^{-6}); (b) approximation has been made when deriving the nonlinear analytical models of the XYZ CPM, and the tiny rotation results about the X_{ms}-axis are also dependent on the approximation. However, it can be seen that the nonlinear analytical and FEA results of the AS-X's rotation about the X_{ms}-axis show similar trends, so the nonlinear analytical results can still be employed to predict the X_{ms}-axis rotation of the AS-X.

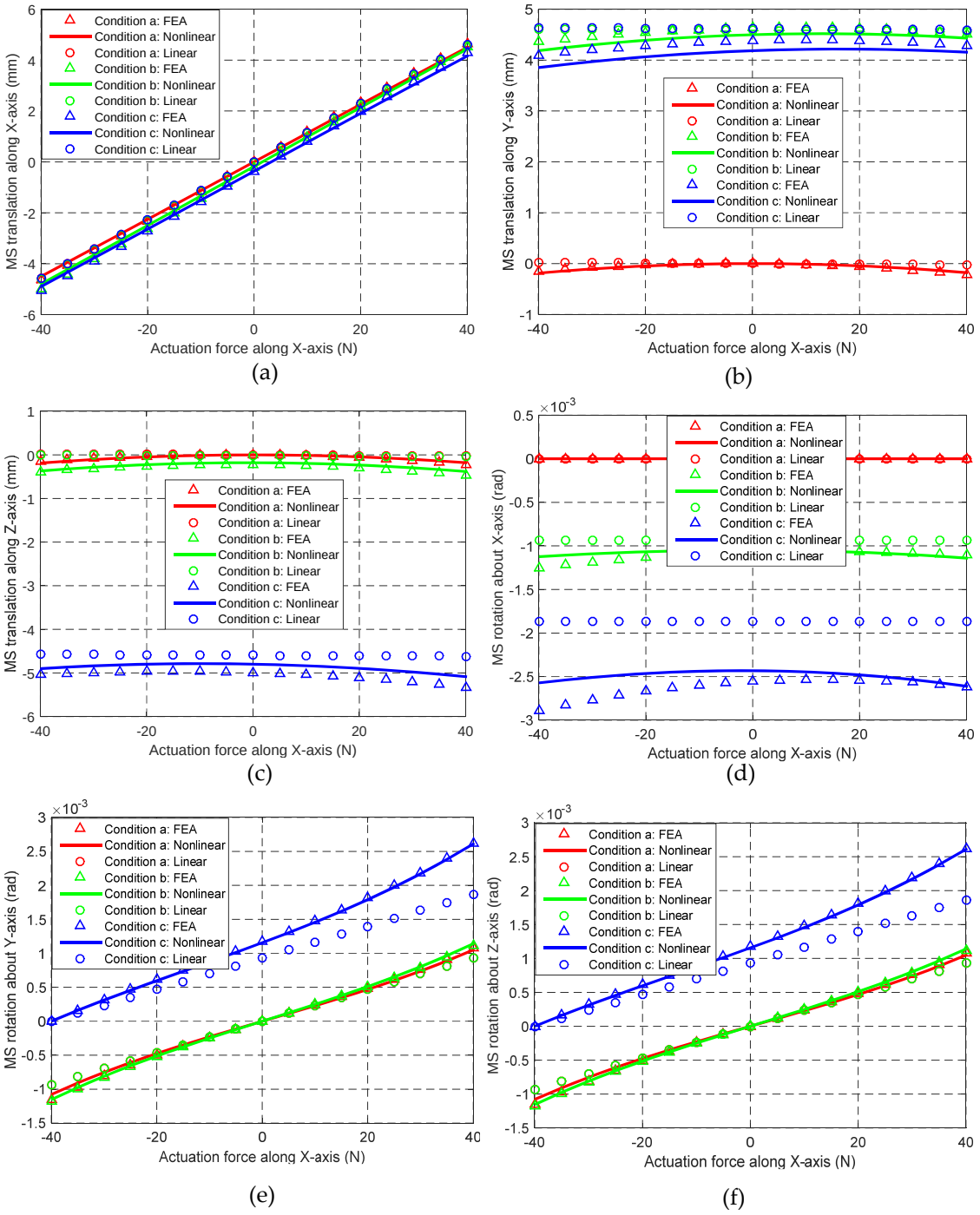

Figure 3.6 Comparison of FEA, nonlinear and linear results in terms of the MS's motion: (a) translations along the X_{ms}-axis, (b) translations along the Y_{ms}-axis, (c) translations along the Z_{ms}-axis, (d) rotations about the X_{ms}-axis, (e) rotations about the Y_{ms}-axis, and (f) rotations about the Z_{ms}-axis, all under the same predefined conditions

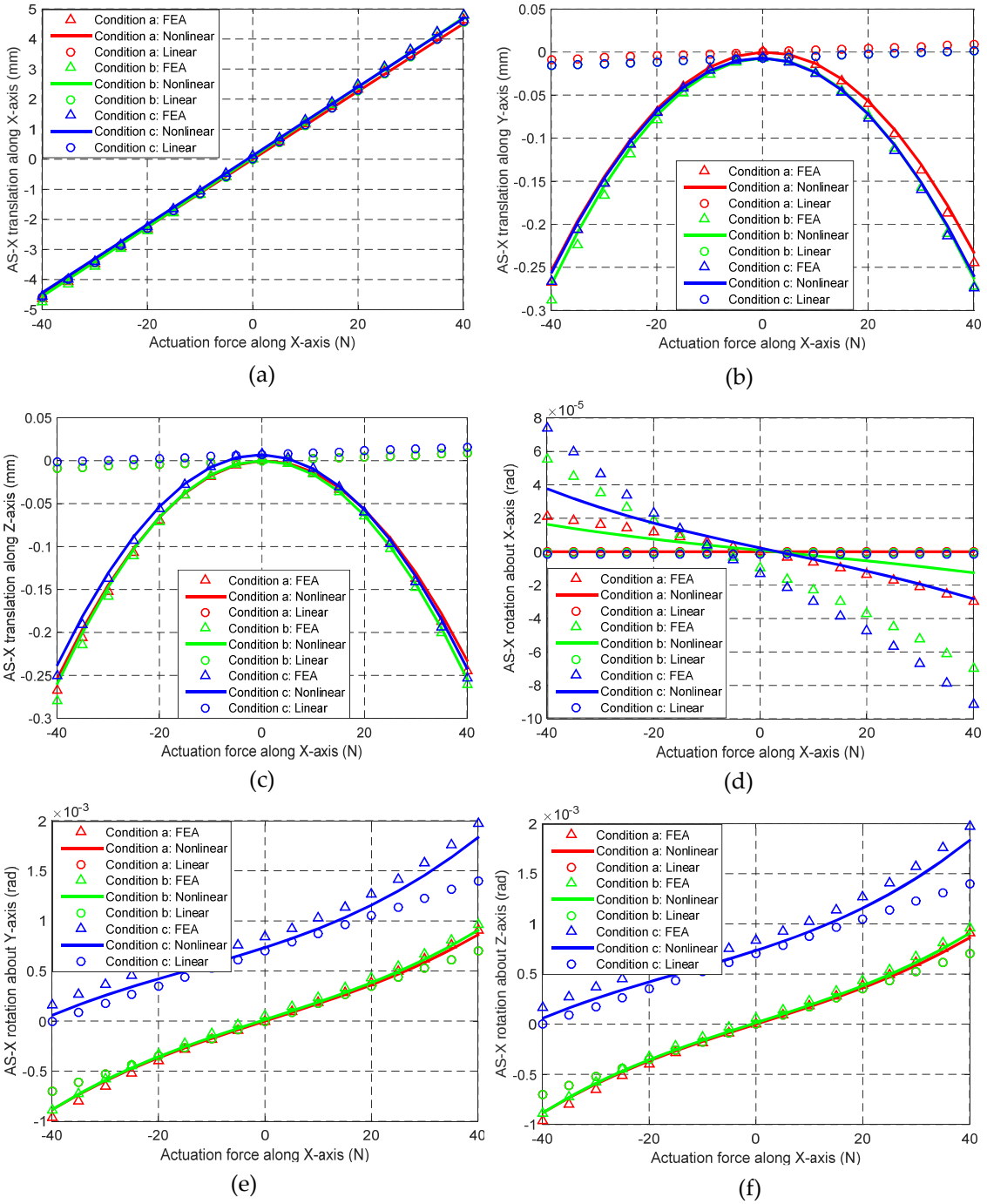

Figure 3.7 Comparison of FEA, nonlinear and linear results in terms of the AS-X's motion: (a) translations along the X_{ms}-axis, (b) translations along the Y_{ms}-axis, (c) translations along the Z_{ms}-axis, (d) rotations about the X_{ms}-axis, (e) rotations about the Y_{ms}-axis, and (f) rotations about the Z_{ms}-axis, , all under the same predefined conditions

3.3.2 Experimental tests

A prototype of the XYZ CPM is fabricated, as shown in Figure 3.8. The prototype is made of Aluminium 99.5, whose Poisson's ratio, Young's modulus

and Yield strength are approximately 0.33, about 6.9×10^{10} Pa and about 105MPa, respectively. The size of the prototype is the same as the FEA model. The maximum motion range per axis should be less than 0.634mm (normalized actuation force per axis is approximately 43.5) as calculated in Equation (3.61) based on [104]. The following conditions are considered in this experimental validation: (a) $\zeta_{\text{asx-tx}}$ varies from 0 to 2.2 when $\zeta_{\text{asy-tx}}=0$ and $\zeta_{\text{asz-tx}}=0$, (b) $\zeta_{\text{asx-tx}}$ varies from 0 to 2.2 when $\zeta_{\text{asy-tx}}=1.9$ and $\zeta_{\text{asz-tx}}=0$, and (c) $\zeta_{\text{asx-tx}}$ varies from 0 to 2.2 when $\zeta_{\text{asy-tx}}=1.9$ and $\zeta_{\text{asz-tx}}=-2.1$.

$$\text{Motion Range}\le 0.1667\times\frac{1.05\times10^{8}\times50}{6.9\times10^{10}\times\frac{1}{50}}=0.634\text{mm} \tag{3.61}$$

The displacements of the MS along the X_{ms}- and Y_{ms}-axes are measured by two digital dial gauges with 0.001mm resolution. The actuation forces are conducted by mass blocks, the mass of which are measured by an electronic scale with 0.001g resolution. Note that the displacements of the MS along the X_{ms}- and Y_{ms}-axes are not measured on the top centre of the MS, but on the surfaces, as shown in Figure 3.8. Additionally, only the rotational displacement of the MS about the Z_{ms}-axis is considered in this experimental test. A low-cost method of measuring this tiny rotational displacement is described in this chapter, the principle of which is indicated in Figure 3.9.

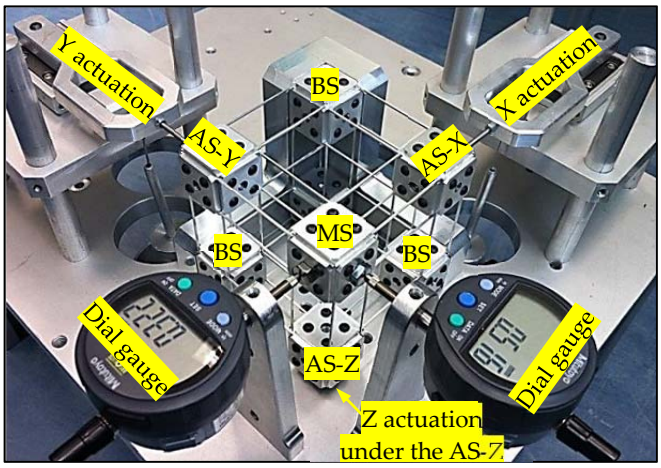

Figure 3.8 A prototype of the XYZ CPM with actuation and translational displacement measurement

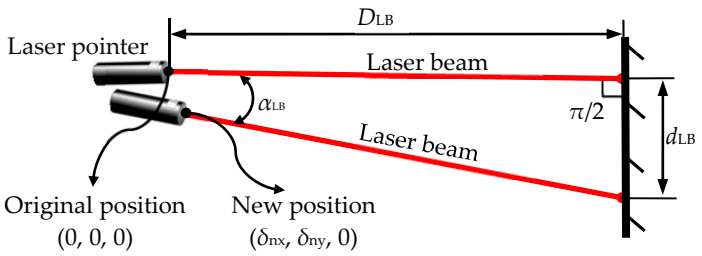

Figure 3.9 Principle of measuring the small rotation angle of the MS

As shown in Figure 3.9, the rotation angle can be calculated using Equation (3.62). If δ_{ny} are much smaller than D_{LB}, Equation (3.62) can be simplified to Equation (3.63).

$$\alpha_{LB} = \arctan\left(\frac{d_{LB} - \delta_{nx}}{D_{LB} - \delta_{ny}}\right) \tag{3.62}$$

$$\alpha_{LB} \approx \arctan\left(\frac{d_{LB} - \delta_{nx}}{D_{LB}}\right) \tag{3.63}$$

In this experimental test, the rotational displacement of the MS about the Z_{ms}-axis is obtained based on the equation above. More specifically, as shown in Figure 3.10(a), a laser pointer is fixed on the MS, so the laser pointer has the same displacements as the MS. At a long distance away from the laser pointer (6800mm in this case), a screen shown in Figure 3.10(b) is pasted onto a wall. At first, the laser beam is set vertical to the screen, and the position of the original laser spot on the screen is marked using a HD camera, as shown in Figure 3.10(b). When the MS moves to new positions under actuation forces, the HD camera records the new positions of the laser spots. Therefore, a series of pictures of the laser spots, such as the pictures shown in Figure 3.10(c) – Figure 3.10(h), are obtained. The positions of the laser spots on the pictures are determined using the image processing function of MATLAB software. Based on the positions and Equation (3.63), the rotational angles of the MS about the Z_{ms}-axis are obtained over the different conditions.

Figure 3.11(a) is obtained by considering the translations of the MS along the X_{ms}-

axis in the different conditions. The nonlinear analytical results differ little from the FEA results (less than 2.73%), and have acceptable differences to the experiment results (less than 8.98%). It can be seen from **Figure** 3.11(c) and **Figure** 3.11(d) that the nonlinear analytical results are close to the FEA results and the experimental results, with the maximum difference being approximately 2.79%. **Figure** 3.11(b) shows that the analytical results exhibit larger differences between the FEA and experimental results, because the displacements shown in this figure are close to the manufacturing and experimental errors and the simulation accuracy. However, the analytical, FEA and experimental results exhibit the similar trends.

The rotations of the MS about the Z_{ms}-axis under the different conditions are illustrated in Figure 3.12. It can be seen that the nonlinear analytical results match the FEA results well, with the maximum difference being less than 5.2%. The difference between the nonlinear analytical results and the experiment results is a little larger mainly due to the manufacturing and experimental errors, but the nonlinear analytical results and the experiment results again follow similar trends. The difference among the FEA, analytical and experimental results arises mainly from the following issues: FEA simulation error, manufacturing error, assembly error, experimental error, and data processing error (i.e. the positioning errors of the laser spots on the screen identified using the MATLAB image processing function).

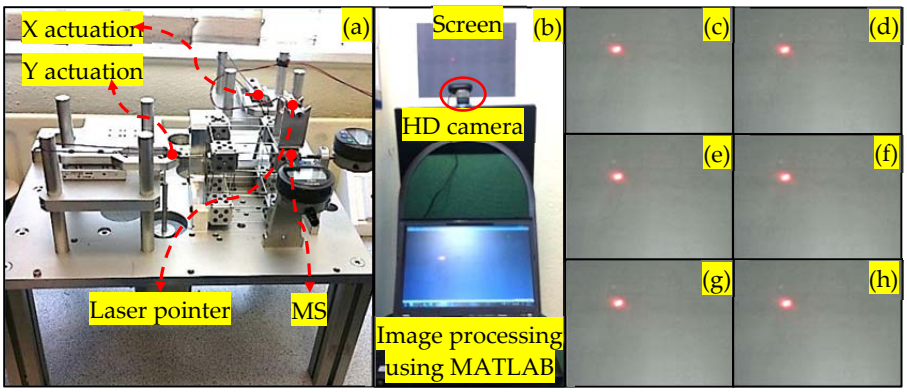

Figure 3.10 MS's rotation angle measurement: (a) experimental test system, (b) screen and image capture facilities, and (c)–(h) captured images of the laser spots at different positions

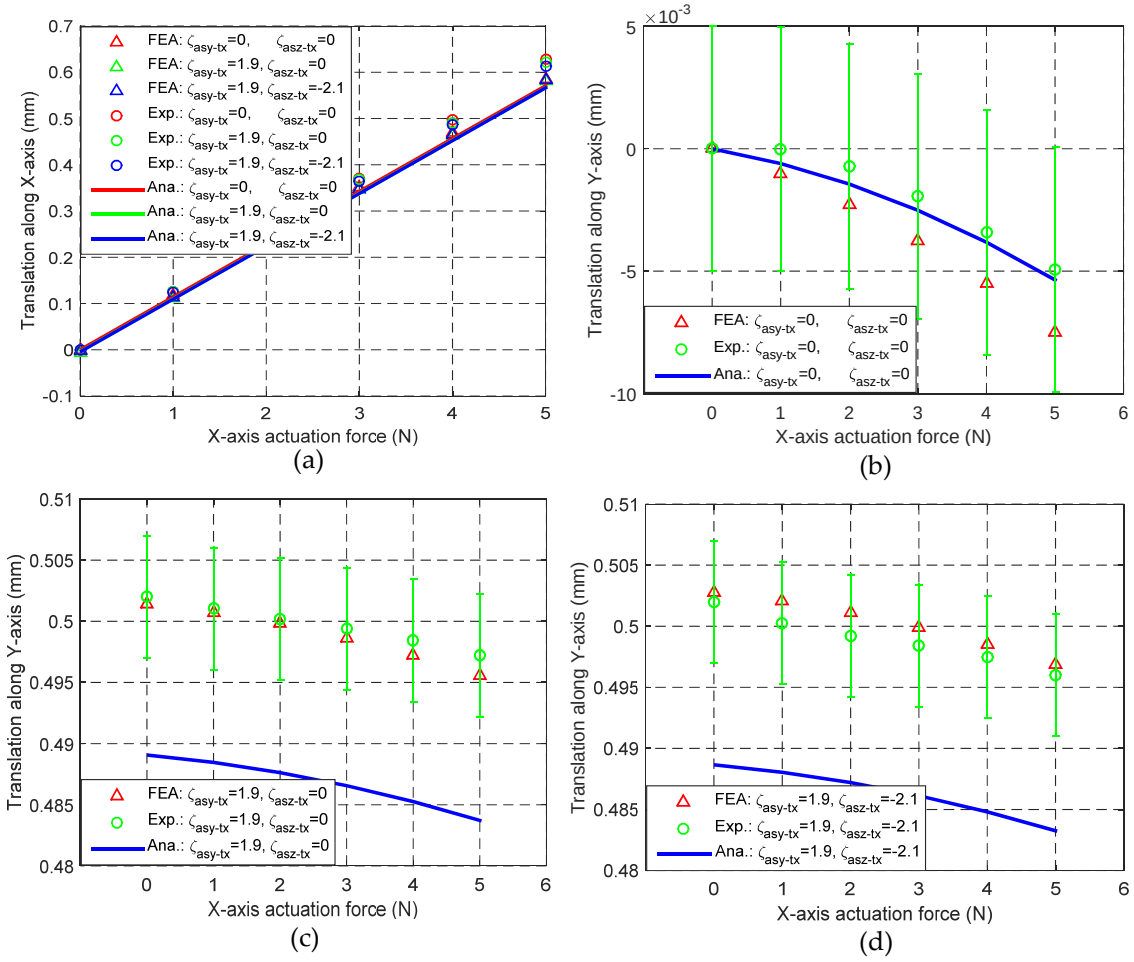

Figure 3.11 Comparison of analytical results, FEA results and experimental results with regard to the translations of the MS: (a) along the X_{ms}-axis under the different conditions, (b) along the Y_{ms}-axis when $\zeta_{asy\text{-}tx}$=0 and $\zeta_{asz\text{-}tx}$=0, (c) along the Y_{ms}-axis when $\zeta_{asy\text{-}tx}$=1.9 and $\zeta_{asz\text{-}tx}$=0, and (d) translations along the Y_{ms}-axis when $\zeta_{asy\text{-}tx}$=1.9 and $\zeta_{asz\text{-}tx}$=−2.1

3.4 Summary

This chapter has proposed a CFB approach to the modelling of compliant mechanisms (including XYZ CPMs) both linearly and nonlinearly. The proposed CFB approach is an improved FBD-based modelling method. Compared with the FBD approach, the mathematical expressions in the CFB approach have easily understood physical meanings.

The CFB technique involves decomposition of a compliant mechanism into rigid stages and compliant modules. The compliant modules (BCMs and/or NBCMs) can produce elastic forces due to their deformation. Such elastic forces are termed variable constraint forces. The derivation of the variable constraint

forces produced by BCMs and NBCMs is introduced. External forces applied on a compliant mechanism, such as actuation forces, are defined as constant constraint forces. The constraint force equilibrium equations of a balanced compliant mechanism can be represented by the variable constraint forces and the constant constraint forces. The analytical model of the compliant mechanism can be further derived from the constraint force equilibrium equations.

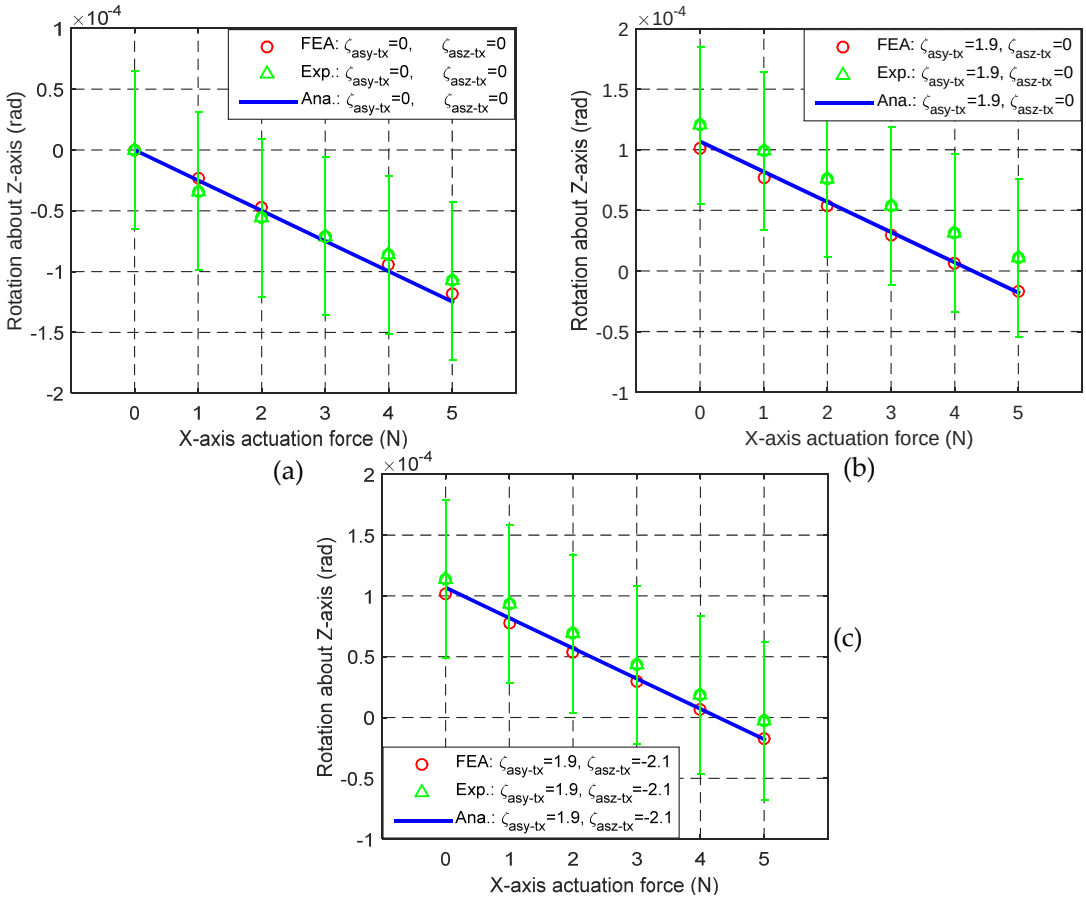

Figure 3.12 Comparison of analytical results, FEA results and experimental results under the different conditions with regard to the rotation of the MS about the Z-axis: (a) when $\zeta_{asy\text{-}tx}$=0 and $\zeta_{asz\text{-}tx}$=0, (b) when $\zeta_{asy\text{-}tx}$=1.9 and $\zeta_{asz\text{-}tx}$=0, and (c) when $\zeta_{asy\text{-}tx}$=1.9 and $\zeta_{asz\text{-}tx}$=−2.1

In this chapter, the variable constraint force produced by a wire-beam is obtained. This is used to derive the variable constraint forces of a four-beam NBCM and an eight-beam NBCM. Moreover, an XYZ CPM is analytically modelled based on the derived variable constraint forces of the two types of NBCMs using the CFB approach. The analytical model of the XYZ CPM is

validated by both FEA simulations and experimental tests.

In the CFB approach, the variable constraint forces and the constant constraint forces, are all represented by wrenches in screw theory, which may extend the CFB approach to a development of the screw-theory-based design approach reported in [61]. In the screw-theory-based design approach, compliant modules are regarded as constraints represented by wrenches [60, 61, 100, 105-107]. The wrenches can represent the directions and positions of the constraints of the compliant modules, while the exact values of constraint forces are not taken into account. In other words, the screw-theory-based design approach is actually a method of arranging the directions and positions of compliant modules under the design requirements. Under this approach, the constraint force provided by a compliant module is always represented by the binary number zero or one. A constraint force equals zero if the associated direction is a DOF direction; otherwise it equals one. However, the CFB approach not only takes the direction and position of the constraint of a compliant module into account, but also quantifies the constraints as exact constraint forces.

The CFB approach can be further extended to an approach for optimizing compliant mechanisms. As studied in Chapter 2, each compliant module in a compliant mechanism has a great number of permitted positions in its position space. Based on this position space concept, a compliant mechanism can be reconfigured into a series of new compliant mechanisms. If a compliant mechanism termed 'Compliant Mechanism-Original' is modelled using the CFB approach, the compliant mechanisms reconfigured from the Compliant Mechanism-Original can also be modelled easily, by only modifying the transformation matrices. On the other hand, a compliant mechanism with desired motion performance can be obtained through the optimization of the transformation matrices (in the same manner that the positions of the compliant modules are optimized). Therefore, the CFB modelling method can also be easily employed to optimize compliant mechanisms.

This page is intentionally left blank.

4 PSR-BASED OPTIMIZATION APPROACH FOR THE REDUCTION OF PARASITIC MOTIONS

Each of the compliant modules in a compliant mechanism can be placed at any one permitted position within its position space, which does not change the constraint imposed by the compliant module on the compliant mechanism. Therefore, a compliant mechanism can be reconfigured through selecting different permitted positions for the compliant modules from the associated position spaces. In this thesis, such a reconfiguration is termed a position-space-based reconfiguration (PSR). The PSR approach can be used to reconfigure a compliant mechanism so as to change both the geometrical dimension and the geometrical shape of the compliant mechanism.

Compliant mechanisms often suffer from undesired parasitic motions, cross-axis couplings and lost motions [2-5, 91, 92], due to the nature of their deformation. The cross-axis couplings and lost motions should be minimized in order to avoid complex control [55]. The parasitic motions should be maximally reduced, since they cannot be compensated by improving the control algorithm. The undesired motion characteristics of a compliant mechanism can be reduced through adjusting the geometrical dimension and geometrical shape of the compliant mechanism. Therefore, the PSR approach can be employed to reduce the undesired motion characteristics of a compliant mechanism.

In this thesis, two PSR-based approaches to the optimization of compliant mechanisms are proposed in Chapters 4 and 5, respectively. One PSR-based approach is used for the reduction of parasitic motions (RPM) of compliant

mechanisms (this approach is termed the PSR-RPM approach, which is studied in Chapter 4). The other PSR-based approach is used for the design of symmetric compliant mechanisms (SCMs) (this approach is termed the PSR-SCM approach, which is to be studied in Chapter 5).

4.1 Principle and Procedure of PSR-RPM Approach

The parasitic motions of a compliant mechanism can be reduced if the compliant modules are placed at appropriate positions. For example, the parallelogram compliant mechanism, as shown in Figure 4.1(a), can be decomposed into an MRS, two wire-beams and two BSs, as shown in Figure 4.1(b). The parasitic rotation of the MRS can be reduced through optimizing the positions of the two wire-beams. Two optimized parallelogram compliant mechanisms can be seen in Figure 4.1(c) and Figure 4.1(d). The spanning size of the compliant mechanism shown in Figure 4.1(c) is increased compared with the one in Figure 4.1(a), and the actuation force of the compliant mechanism shown in Figure 4.1(d) can pass through the stiffness centre [1, 55, 91] of the compliant mechanism. Therefore, the PSR-RPM approach can be used to reduce parasitic motions of a compliant mechanism by optimizing the positions of the associated compliant modules. In order to ensure that the DOF of the compliant mechanism remains unchanged, the positions of the compliant modules should be selected from the position spaces of the compliant modules.

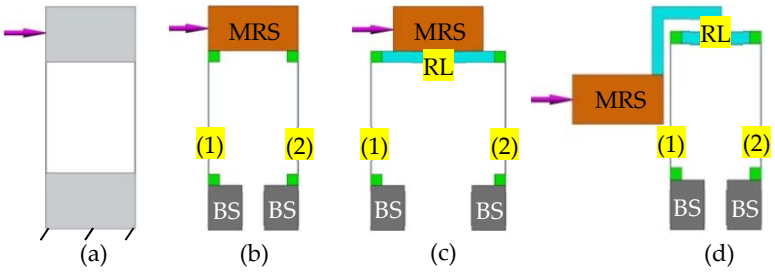

Figure 4.1 Optimization of a compliant mechanism for reducing the parasitic rotation: (a) the original parallelogram compliant mechanism, (b) decomposition of the parallelogram compliant mechanism, (c) and (d) optimization through changing the positions of the compliant modules

In order to find the appropriate positions for the compliant modules of a compliant mechanism, the parasitic motions of the compliant mechanism are analytically modelled in the PSR-RPM approach, using the position variables. Such position variables can represent any possible permitted positions of the compliant modules in the compliant mechanism. Subsequently, the positions of the compliant modules are optimized based on the analytical models of the parasitic motions. Finally, a new compliant mechanism with reduced parasitic motions can be rebuilt by placing all the compliant modules at the optimized positions.

In order to employ the PSR-RPM approach to reduce the parasitic motions of a compliant mechanism, the following tasks should be conducted: (a) decomposing the compliant mechanism into compliant modules and rigid stages, (b) identifying the position spaces of the compliant modules, (c) modelling the parasitic motions of the compliant mechanism using the position variables that represent any possible permitted positions of the compliant modules, (d) obtaining the values for the position variables which can reduce the parasitic motions to minima or acceptable levels, and (e) reconfiguring the compliant mechanism based on the optimized values of the position variables.

According to the tasks above, if the parasitic motions of a compliant mechanism are to be reduced, the PSR-RPM approach can be used based on the following steps:

1. Decompose the original compliant mechanism into ICMs and rigid stages. The optimization of a compliant mechanism using the PSR-RPM approach depends on the decomposition of the compliant mechanism, i.e., different decomposition patterns may have different optimization results. A compliant mechanism can be decomposed into rigid stages and compliant modules in different ways, and each compliant module has a great number of permitted positions within its position space.

Therefore, a compliant mechanism can be reconfigured in a great number of ways. However, to avoid complexity and reduce the difficulty in identifying the position spaces of compliant modules, the PSR-RPM approach limits the possible compliant modules to independent compliant modules (ICMs), i.e., a compliant mechanism can only be decomposed into rigid stages and ICMs.

An ICM is defined as a compliant module that produces a constraint in the associated compliant mechanism which is completely based on its own structure rather than needing cooperation with other compliant modules. According to the definition of the ICM, a strategy for identifying ICMs in a compliant mechanism and decomposing the compliant mechanism into rigid stages and the ICMs is introduced below.

a) Decompose the compliant mechanism into BCMs (BCMs, as defined in Chapter 1) and rigid stages.

b) Identify controllable rigid stages and non-controllable rigid stages in the compliant mechanism decomposed in Step (a). Any one rigid stage has six DOF along and about the X-, Y-and Z-axes in a 3D coordinate system, if no constraint is applied to it. Under the condition that each actuation displacement of the compliant mechanism is kept at a certain value within the motion range, if all the six DOF of a rigid stage are constrained, the rigid stage is called a controllable rigid stage; otherwise, it is called a non-controllable rigid stage. The input and output stages are all the controllable stages of a multi-DOF compliant parallel system. The secondary stage of a double parallelogram compliant mechanism, as reported in [55], is a non-controllable rigid stage.

c) Combine all the BCMs and non-controllable rigid stages (if these exist) between any two adjacent controllable rigid stages, through designing new rigid linkages. The combined compliant modules in this step are called combined-BCMs (C-BCMs). Therefore, each C-BCM is adjacent to two controllable rigid stages, and each of the controllable rigid stages is

constrained by one or more C-BCMs.

d) Identify the basic ICMs of the compliant mechanism. Assume that a controllable rigid stage is adjacent to n (n 1) C-BCMs, and assume that m (0 (m (06) DOF of the controllable rigid stages are constrained by the n C-BCMs (the other 6-m DOF is (are) constrained by the actuators or the ground). If one of the m DOF has to be constrained by h (2 20h 20n and n nd2) of the n C-BCMs together, the h C-BCMs together with their rigid linkages is a basic ICM. If one of the n C-BCMs is needed to constrain g (0 (g (0m) of the m DOF, and the g DOF can be constrained by the ICM without cooperating with the other C-BCMs, the single C-BCM is a basic ICM. Therefore, all the basic ICMs of the compliant mechanism can be identified in this step.

e) Assemble adjacent basic ICMs to form non-basic ICMs. If two or more adjacent basic ICMs are assembled together as a new compliant module, it can be shown that the new compliant module is also an ICM (termed a non-basic ICM), because each non-basic ICM is also independent from other basic ICMs and non-basic ICMs.

f) Decompose the compliant mechanism again into ICMs and rigid stages. Since the basic ICMs and the non-basic ICMs of the compliant mechanism are all identified in the above steps, one can decompose the compliant mechanism into ICMs (basic or non-basic), and rigid stages. If all the ICMs are basic ICMs, the decomposition is called the basic decomposition pattern; otherwise, it is called a non-basic decomposition pattern. One compliant mechanism has only one basic decomposition pattern, but can have several non-basic decomposition patterns. If one BS (base stage) links to more than one ICM, the BS should be decomposed so that each of the ICMs has its own BS.

The more ICMs a compliant mechanism has, the more new compliant mechanisms can be derived. Therefore, it is better to decompose a compliant mechanism into basic ICMs rather than non-basic ICMs, when

one wishes to minimize the parasitic motions of the compliant mechanism.

2. Set global and local coordinate systems. A global coordinate system is fixed to the ground. The MS remains at its original position in the global coordinate system over the entire reconfiguration procedure. Between the MS and a BS, there is an ICM chain (or leg). Therefore, there are one or more ICM chains between the MS and the BSs. In each of the ICM chains, an ICM is adjacent to two or more rigid stages. The local coordinate system of this ICM is located at the adjacent rigid stage, which is the MS of the compliant mechanism or that closer to the MS in the associated ICM chain. The other adjacent rigid stages of the ICM should be moved (rotated and translated) with the ICM relative to the ICM's local coordinate system. Note that if one BS is adjacent to several ICMs, the BS should be decomposed into several new BSs, so that each of the new BSs is adjacent to only one of the ICMs, which allows each of the new BSs to move together with its adjacent ICM.
3. Identify the position spaces of the ICMs in its local coordinate system. The position space of an ICM is identified based on the screw theory. This is demonstrated below.

   The constraint of an ICM on the associated compliant mechanism is not affected when the ICM translates to another position, because the ICM is independent of other ICMs in the compliant mechanism. Taking the well-known basic parallelogram compliant mechanism shown in Figure 4.1(a) as an example, this basic parallelogram compliant mechanism can be decomposed into an ICM (parallelogram compliant module) and an MS. When the parallelogram compliant module translates only (no rotation), the constraint of the parallelogram compliant module to the parallelogram compliant mechanism remains unchanged when the tip of the parallelogram compliant module connects the MS with a rigid body. Therefore, an ICM can translate to any other positions without changing

its orientation, i.e., the positions derived through the ICM's translation are the possible permitted positions of the ICM pertaining to its position space. The following part in this step identifies if an ICM can rotate about the axes of a coordinate system.

Based on Equation (2.5), the constraint of an ICM in a coordinate system O-XYZ can be denoted by a wrench based on Equation (2.5), as shown in Equation (4.1).

$$\zeta_{\mathrm{Ccm}} = \left[\kappa_{\mathrm{cm-tx}} j_{\mathrm{cm-tx}}, \kappa_{\mathrm{cm-ty}} j_{\mathrm{cm-ty}}, \kappa_{\mathrm{cm-tz}} j_{\mathrm{cm-tz}}, \kappa_{\mathrm{cm-rx}} j_{\mathrm{cm-rx}}, \kappa_{\mathrm{cm-ry}} j_{\mathrm{cm-ry}}, \kappa_{\mathrm{cm-rz}} j_{\mathrm{cm-rz}}\right]^{\mathrm{T}} \quad (4.1)$$

where $\kappa_{\mathrm{cm\text{-}tx}}$, $\kappa_{\mathrm{cm\text{-}ty}}$, $\kappa_{\mathrm{cm\text{-}tz}}$, $\kappa_{\mathrm{cm\text{-}rx}}$, $\kappa_{\mathrm{cm\text{-}ry}}$ and $\kappa_{\mathrm{cm\text{-}rz}}$ are constraint coefficients, and $j_{\mathrm{cm\text{-}tx}}$, $j_{\mathrm{cm\text{-}ty}}$, $j_{\mathrm{cm\text{-}tz}}$, $j_{\mathrm{cm\text{-}rx}}$, $j_{\mathrm{cm\text{-}ry}}$ and $j_{\mathrm{cm\text{-}rz}}$ are direction coefficients. If the wrench ζ_{Ccm} rotates about the X-, Y- and Z-axes at the angles α_{cm}, β_{cm} and γ_{cm}, respectively, the wrench ζ_{Ccm} will be transferred to wrenches $\zeta_{\mathrm{Ccm\text{-}Rx}}$, $\zeta_{\mathrm{Ccm\text{-}Ry}}$ and $\zeta_{\mathrm{Ccm\text{-}Rz}}$ by pre-multiplying the transformation matrices as denoted in Equation (4.3) [60].

$$\zeta_{\mathrm{Ccm\text{-}Rx}} = \mathbf{T}_{\mathrm{cm\text{-}rx}} \zeta_{\mathrm{Ccm}},\ \zeta_{\mathrm{Ccm\text{-}Ry}} = \mathbf{T}_{\mathrm{cm\text{-}ry}} \zeta_{\mathrm{Ccm}} \text{ and } \zeta_{\mathrm{Ccm\text{-}Rz}} = \mathbf{T}_{\mathrm{cm\text{-}Rz}} \zeta_{\mathrm{Ccm}} \quad (4.2)$$

where $\mathbf{T}_{\mathrm{cm\text{-}Rx}}$, $\mathbf{T}_{\mathrm{cm\text{-}Ry}}$ and $\mathbf{T}_{\mathrm{cm\text{-}Rz}}$ are the transformation matrices corresponding to the rotations about the X-, Y- and Z-axes at α_{cm}, β_{cm} and γ_{cm}, respectively.

$$\mathbf{T}_{\mathrm{cm\text{-}Rx}} = \begin{bmatrix} \mathbf{R}_{\mathrm{x}}(\alpha_{\mathrm{cm}}) & \mathbf{0}_{3\times3} \\ \mathbf{0}_{3\times3} & \mathbf{R}_{\mathrm{x}}(\alpha_{\mathrm{cm}}) \end{bmatrix},\ \mathbf{T}_{\mathrm{cm\text{-}Ry}} = \begin{bmatrix} \mathbf{R}_{\mathrm{y}}(\beta_{\mathrm{cm}}) & \mathbf{0}_{3\times3} \\ \mathbf{0}_{3\times3} & \mathbf{R}_{\mathrm{y}}(\beta_{\mathrm{cm}}) \end{bmatrix}$$
$$\text{and } \mathbf{T}_{\mathrm{cm\text{-}Rz}} = \begin{bmatrix} \mathbf{R}_{\mathrm{z}}(\gamma_{\mathrm{cm}}) & \mathbf{0}_{3\times3} \\ \mathbf{0}_{3\times3} & \mathbf{R}_{\mathrm{z}}(\gamma_{\mathrm{cm}}) \end{bmatrix} \quad (4.3)$$

where $\mathbf{R}_{\mathrm{x}}(\alpha_{\mathrm{cm}})$, $\mathbf{R}_{\mathrm{y}}(\beta_{\mathrm{cm}})$ and $\mathbf{R}_{\mathrm{z}}(\gamma_{\mathrm{cm}})$ are the three basic sub-rotation matrices about the X-, Y- and Z-axes at angles α_{cm}, β_{cm} and γ_{cm},

respectively.

On the basis of the results in Equations (4.1) – (4.3), It is clear that if the wrench $\zeta_{Ccm\text{-}Rx}$, $\zeta_{Ccm\text{-}Ry}$ or $\zeta_{Ccm\text{-}Rz}$ is equivalent to the original wrench ζ_{Ccm}, the positions derived by the rotation about the X-, Y- or Z-axis, are the new possible permitted positions of the wrench ζ_{Ccm}, and vice versa. Therefore, all the possible permitted positions of an ICM derived through either translations or rotations constitute the position space of the ICM.

4. Model the parasitic motions of the compliant mechanism using the position variables that represent any permitted positions of the ICMs within their position spaces.
5. Optimize the positions of the ICMs within their position spaces to minimize the parasitic motions, based on the analytical models of the parasitic motions derived in Step (4).
6. Place the ICMs at the optimized positions in the local coordinate systems.
7. Design rigid linkages to link each of the ICMs to the rigid stage at which the ICM's local coordinate system is located.
8. Re-design the BSs and modify the compliant mechanism for easy manufacture.

The PSR-RPM approach can be used to optimize any one compliant mechanism. In this chapter, an XYZ CPM is taken as an example to demonstrate the above steps in Section 4.2.

4.2 Case Study

In this section, an XYZ CPM (shown in Figure 4.2(a)) is optimized using the PSR-RPM approach so as to reduce the parasitic rotations (these rotations are some of the possible parasitic motions) of the XYZ CPM. The XYZ CPM is decomposed into rigid stages and ICMs in Section 4.2.1. This decomposition may be different from the decomposition of an XYZ CPM in the CPI and CFB

approaches. The position spaces of the ICMs are identified in Section 4.2.2. The positions of the ICMs are finally optimized, and a new XYZ CPM is obtained in Section 4.2.3.

4.2.1 XYZ CPM decomposition

The original XYZ CPM shown in Figure 4.2(a) can be decomposed based on Sub-Steps (a) – (f) of Step (2) in Section 4.1. To begin with, the XYZ CPM is decomposed into BCMs and rigid stages based on Step (a), as shown in Figure 4.2(b). The BCMs of the XYZ CPM are wire-beams. If the three actuation displacements of the XYZ CPM are kept at their zero points, all the six DOF of each of the seven rigid stages (the MS, the AS-X, the AS-Y, the AS-Z, and the three BSs) are constrained. It can be derived from Step (b) that the seven rigid stages are all controllable rigid stages. According to Step (c), all four BCMs (wire-beams) between any two adjacent rigid stages should be combined together as C-BCMs, using newly designed rigid linkages. There are a total of nine C-BCMs of the XYZ CPM, as illustrated in Figure 4.2(c).

The 24 DOF of the four rigid stages, the MS, the AS-X, the AS-Y and the AS-Z, are constrained by the nine C-BCMs, which is detailed in Table 1. It can be seen that any one of the 24 DOF can be constrained by one of the nine C-BCMs, or constrained by two of the nine C-BCMs separately. None of the nine C-BCMs needs to cooperate with the other C-BCMs in order to constrain any one of the 24 DOF. Therefore, each of the nine C-BCMs is independent of the others, i.e., all of them are basic ICMs.

Based on the identified basic ICMs, the basic decomposition pattern of the XYZ CPM is obtained, as shown in Figure 4.2(d). Figure 4.2(d) also shows that each of the three BSs is decomposed into two BSs, based on Step (d). According to the step (e), the basic ICMs, labelled with numbers 1, 2 and 3 in Figure 4.2(d), can be combined together as a new non-basic ICM labelled as ‘123’ shown in Figure 4.2(e). Therefore, Figure 4.2(e) illustrates a non-basic decomposition

pattern. Similarly, the decomposition pattern shown in Figure 4.2(f) is also a non-basic decomposition pattern with isotropic decomposition in each leg. In Figure 4.2(f), the three non-basic ICMs labelled as '123', '456' and '789' are Leg-X, Leg-Y and Leg-Z, as also shown in Figure 4.3.

For the non-basic decomposition pattern shown in Figure 4.2(f), the global and local coordinate systems can be set as shown in Figure 4.3. The global coordinate system, O_{ms}-$X_{ms}Y_{ms}Z_{ms}$, is fixed to the ground, and the MS cannot move in the global coordinate system over the entire procedure of the PSR-based reconfiguration. Local coordinate systems, O_x-$X_xY_xZ_x$, O_y-$X_yY_yZ_y$ and O_z-$X_zY_zZ_z$, are defined for Leg-X, Leg-Y and Leg-Z, respectively, as shown in Figure 4.3. Each of the three non-basic ICMs (Leg-X, Leg-Y and Leg-Z) can move in its local coordinate system within its position space. When the three non-basic ICMs move in their local coordinate systems, the BSs should be moved with the three non-basic ICMs, as stated in Step (2) in Section 4.1.

Table 4.1 The C-BCM(s) or actuation force that constrains each of the six DOF of the MS, the AS-X, the AS-Y and the AS-Z (C-BCMs 1, 4 and 7 are also the PMs of the XYZ CPM)

	The C-BCM(s) or actuation force			
6 DOF	**Constraining MS**	**Constraining AS-X**	**Constraining AS-Y**	**Constraining AS-Z**
X-translation DOF	C-BCM 1	X-actuator	C-BCM 5	C-BCM 9
Y-translation DOF	C-BCM 4	C-BCM 2	Y-actuator	C-BCM 8
Z-translation DOF	C-BCM 7	C-BCM 3	C-BCM 6	Z-actuator
X-rotation DOF	C-BCMs 4 and 7, separately	C-BCMs 2 and 3, separately	C-BCMs 4 and 6, separately	C-BCMs 7 and 8, separately
Y-rotation DOF	C-BCMs 1 and 7	C-BCMs 1 and 3, separately	C-BCMs 5 and 6, separately	C-BCMs 7 and 9, separately
Z-rotation DOF	C-BCMs 1 and 4	C-BCMs 1 and 2, separately	C-BCMs 4 and 5, separately	C-BCMs 8 and 9, separately

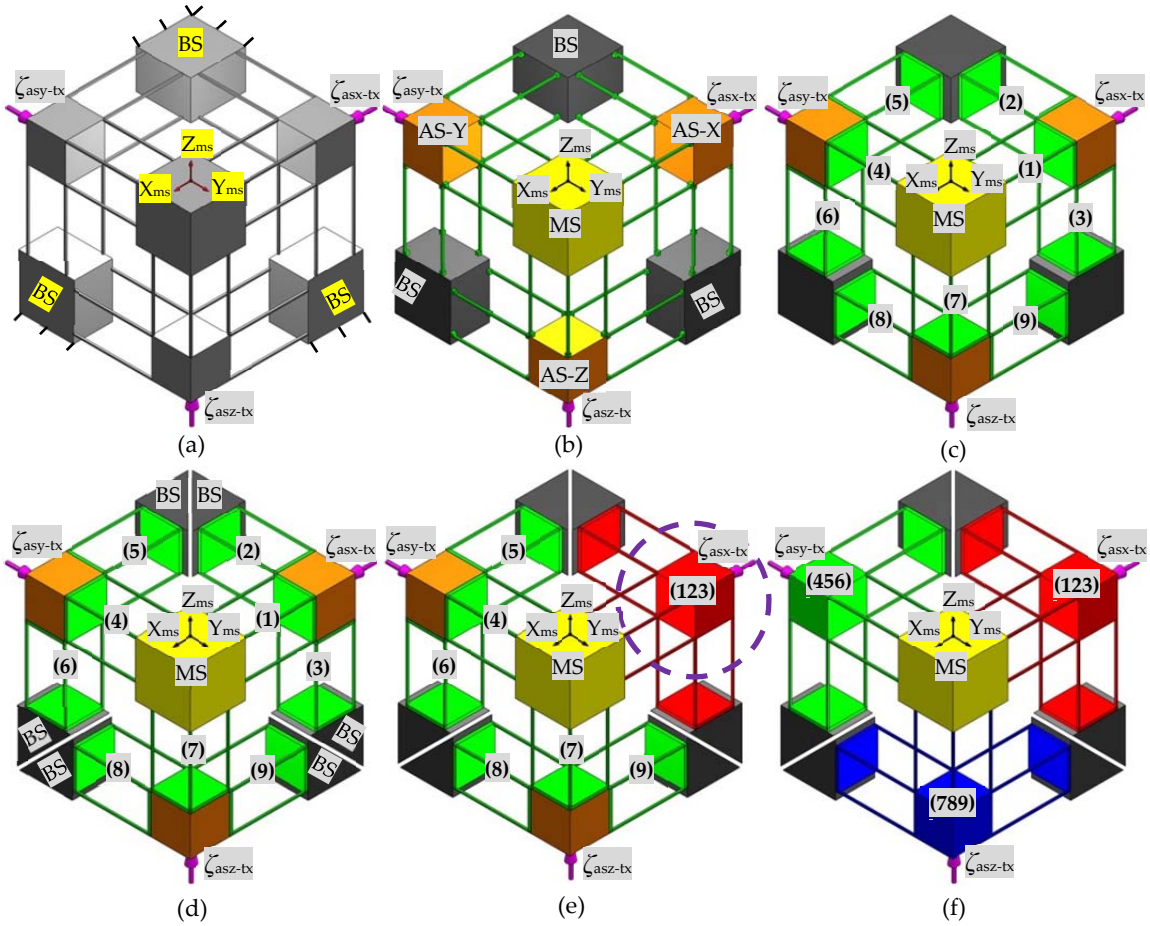

Figure 4.2 An XYZ CPM and its decomposition: (a) XYZ CPM, (b) BCMs and their rigid stages, (c) C-BCMs and their rigid stages, (d) basic decomposition pattern, (e) non-basic decomposition pattern-1, and (f) non-basic decomposition pattern-2

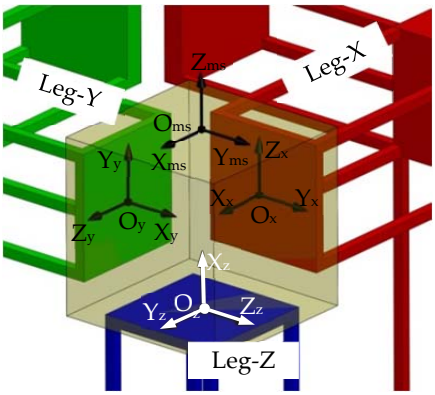

Figure 4.3 The global and local coordinate systems of the decomposed XYZ CPM

4.2.2 ICM position spaces

The position spaces of the ICMs in the XYZ CPM, obtained based on screw theory, are derived in this section. The three ICMs of the XYZ CPM, as shown in

Figure 4.2(f), are identical, as are the position spaces of the ICMs, in terms of their own local coordinate systems. Therefore, it is appropriate to take Leg-X as an example to derive the position spaces of the three ICMs.

Leg-X has four DOF, which are the translations along the X_x-, Y_x-, and Z_x-axes and the rotation about the X_x-axis. The wrench of the constraint of this 4-DOF ICM can be represented as

$$\zeta_{Cx} = \left[\kappa_{x-tx} j_{x-tx}, \kappa_{x-ty} j_{x-ty}, \kappa_{x-tz} j_{x-tz}, \kappa_{x-rx} j_{x-rx}, \kappa_{x-ry} j_{x-ry}, \kappa_{x-rz} j_{x-rz}\right]^T \tag{4.4}$$

Based on the DOF of Leg-X, stiffness coefficients $\kappa_{x\text{-}tx}$, $\kappa_{x\text{-}ty}$, $\kappa_{x\text{-}tz}$ and $\kappa_{x\text{-}rx}$ can be assigned zero, while $\kappa_{x\text{-}ry}$ and $\kappa_{x\text{-}rz}$ are assigned one. Therefore, Equation (4.4) can be rewritten as

$$\zeta_{Cx} = \left[0, 0, 0, 0, \pm 1, \pm 1\right]^T \tag{4.5}$$

According to Equations (4.2) and (4.3), after the rotations about the X_x-, Y_x-, and Z_x-axes of α_x, β_x and γ_x, respectively, the wrench ζ_{Cx} can be transferred to $\zeta_{Cx\text{-}Rx}$, $\zeta_{Cx\text{-}Ry}$ or $\zeta_{Cx\text{-}Rz}$, which can be written as

$$\zeta_{Cx\text{-}Rx} = \left[0, 0, 0, 0, \pm\left(\left|\cos\left(\alpha_x\right)\right| + \left|\sin\left(\alpha_x\right)\right|\right), \pm\left(\left|\sin\left(\alpha_x\right)\right| + \left|\cos\left(\alpha_x\right)\right|\right)\right]^T \tag{4.6}$$

$$\zeta_{Cx\text{-}Ry} = \left[0, 0, 0, \pm\left|\sin\left(\gamma_x\right)\right|, \pm\left|\cos\left(\gamma_x\right)\right|, \pm 1\right]^T \tag{4.7}$$

$$\zeta_{Cx\text{-}Rz} = \left[0, 0, 0, \pm\left|\sin\left(\beta_x\right)\right|, \pm 1, \pm\left|\cos\left(\beta_x\right)\right|\right]^T \tag{4.8}$$

It can be seen from Equations (4.5) and (4.6) – (4.8) that $\zeta_{Cx\text{-}Rx}$ is equivalent to ζ_{Cx} no matter what value of α_x has (it is well known that the sum of the absolute values of $\sin\left(\alpha_x\right)$ and $\cos\left(\alpha_x\right)$ is equal to or greater than one), but $\zeta_{Cx\text{-}Ry}$ or $\zeta_{Cx\text{-}Rz}$ are not equivalent to ζ_{Cx} if β_x and γ_x do not equal zero. Therefore, the positions derived by the rotation of the wrench ζ_{Cx} about X_x-axis are the possible

permitted positions of Leg-X.

In addition, the positions derived through any translations of Leg-X are also the possible permitted positions of Leg-X. Therefore, the position space of each of the three ICMs (Leg-X, Leg-Y and Leg-Z) includes the possible positions derived by (a) the translations along the local X-, Y- and Z-axes at any distance, and (b) the rotation about the local X-axis at any angle.

4.2.3 ICM position optimization

As mentioned earlier, a number of new compliant mechanisms can be derived by reconfiguring a compliant mechanism using the PSR-RPM approach. This section shows how a compliant mechanism with minimized parasitic motions can be obtained, through a modelling and optimization process. The XYZ CPM, shown in Figure 4.2(f), is taken as an example to demonstrate this process.

The modelling of the XYZ CPM is based on the CFB approach described in Chapter 3. As derived in Section 4.2.2, each of the ICMs of the XYZ CPM can be moved along the three axes of the local coordinate system, and can also be rotated about the local X-axis. However, this example only considers the rotations of the ICMs about the local X-axes, which are shown in Figure 4.4. The rotations of the ICMs should be considered in the modelling of the XYZ CPM.

The case study of the XYZ CPM with identical beams uses the following parameters: the beam length is 50mm, the cross sectional dimension of each beam is 2mm × 2mm, the dimension of the MS is 35mm × 35mm × 35mm, and the dimension of any one of the other identical rigid stages is 25mm × 25mm × 25mm. Aluminium alloy 6061 is selected as material (Young's modulus is 69000MPa, Poisson's ratio is 0.33). The displacement vectors of the three ICMs, Leg-X, Leg-Y and Leg-Z, in the origins of the defined local coordinate systems O_x-$X_xY_xZ_x$, O_y-$X_yY_yZ_y$ and O_z-$X_zY_zZ_z$ can be represented as twists ξ_x, ξ_y and ξ_z, respectively, as shown in Equations (4.9) – (4.11).

$$\boldsymbol{\xi}_{x} = \left[\xi_{x\text{-}tx}, \xi_{x\text{-}ty}, \xi_{x\text{-}tz}, \xi_{x\text{-}rx}, \xi_{x\text{-}ry}, \xi_{x\text{-}rz}\right]^{T} \tag{4.9}$$

$$\boldsymbol{\xi}_{y} = \left[\xi_{y\text{-}tx}, \xi_{y\text{-}ty}, \xi_{y\text{-}tz}, \xi_{y\text{-}rx}, \xi_{y\text{-}ry}, \xi_{y\text{-}rz}\right]^{T} \tag{4.10}$$

$$\boldsymbol{\xi}_{z} = \left[\xi_{z\text{-}tx}, \xi_{z\text{-}ty}, \xi_{z\text{-}tz}, \xi_{z\text{-}rx}, \xi_{z\text{-}ry}, \xi_{z\text{-}rz}\right]^{T} \tag{4.11}$$

where the subscripts -tx, -ty and -tz indicate the translational displacements along the local axes, and the subscripts -rx, -ry and -rz indicate the rotational displacements about the local axes. Based on Equation (2.4), the variable constraint forces of the three ICMs can be written as wrenches that are shown in Equation (4.12), and the actuation forces can be written as wrenches as shown in Equation (4.13).

$$\begin{aligned} \boldsymbol{\zeta}_{x} &= \left[\zeta_{x\text{-}tx}, \zeta_{x\text{-}ty}, \zeta_{x\text{-}tz}, \zeta_{x\text{-}rx}, \zeta_{x\text{-}ry}, \zeta_{x\text{-}rz}\right]^{T}, \boldsymbol{\zeta}_{y} = \left[\zeta_{y\text{-}tx}, \zeta_{y\text{-}ty}, \zeta_{y\text{-}tz}, \zeta_{y\text{-}rx}, \zeta_{y\text{-}ry}, \zeta_{y\text{-}rz}\right]^{T} \\ \boldsymbol{\zeta}_{z} &= \left[\zeta_{z\text{-}tx}, \zeta_{z\text{-}ty}, \zeta_{z\text{-}tz}, \zeta_{z\text{-}rx}, \zeta_{z\text{-}ry}, \zeta_{z\text{-}rz}\right]^{T} \end{aligned} \tag{4.12}$$

$$\boldsymbol{\zeta}_{asx} = \left[\zeta_{asx\text{-}tx}, 0, 0, 0, 0, 0\right]^{T}, \boldsymbol{\zeta}_{asy} = \left[\zeta_{asy\text{-}tx}, 0, 0, 0, 0, 0\right]^{T}, \boldsymbol{\zeta}_{asz} = \left[\zeta_{asz\text{-}tx}, 0, 0, 0, 0, 0\right]^{T} \tag{4.13}$$

where wrenches $\boldsymbol{\zeta}_{x}$, $\boldsymbol{\zeta}_{y}$ and $\boldsymbol{\zeta}_{z}$ represent the variable constraint forces produced by the three ICMs. Wrenches $\boldsymbol{\zeta}_{asx}$, $\boldsymbol{\zeta}_{asy}$ and $\boldsymbol{\zeta}_{asz}$ represent the three actuation forces exerted on the three ASs, as illustrated in Figure 4.4. For the linear modelling adopted in this example, the wrenches, $\boldsymbol{\zeta}_{x}$, $\boldsymbol{\zeta}_{y}$ and $\boldsymbol{\zeta}_{z}$, can be calculated using Equation (4.14) based on the studies in Chapter 3.

$$\boldsymbol{\zeta}_{x} = -\mathbf{k}_{x}\boldsymbol{\xi}_{x}, \boldsymbol{\zeta}_{y} = -\mathbf{k}_{y}\boldsymbol{\xi}_{y} \text{ and } \boldsymbol{\zeta}_{z} = -\mathbf{k}_{z}\boldsymbol{\xi}_{z} \tag{4.14}$$

where $\mathbf{k}_{x}$, $\mathbf{k}_{y}$ and $\mathbf{k}_{z}$ are the stiffness matrices of the ICMs in their own local coordinate systems. The stiffness matrices using the given parameters mentioned above can be derived as shown below, based on the results in [77].

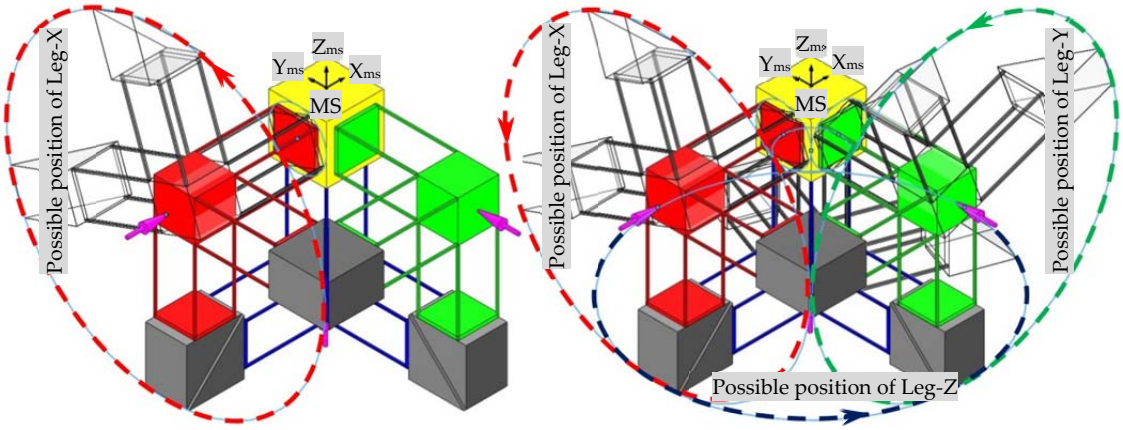

Figure 4.4 Demonstration of the possible permitted positions of the three non-basic ICMs through the rotations about the local X-axes: (a) the rotation of Leg-X about the local X-axis, and (b) the rotations of Leg-X, Leg-Y and Leg-Z about the local X-axes

$$\mathbf{k}_x = \mathbf{k}_y = \mathbf{k}_z$$

$$= \begin{bmatrix} 94.90 & 0.40 & 0.40 & -8.47\times10^{-22} & -17.40 & 17.40 \\ 0.40 & 47.53 & -4.29\times10^{-6} & 1.42\times10^{-4} & 2.32\times10^{-4} & -41.39 \\ 0.40 & -4.29\times10^{-6} & 47.53 & -1.42\times10^{-4} & 41.39 & -2.32\times10^{-4} \\ -8.47\times10^{-22} & 1.42\times10^{-4} & -1.42\times10^{-4} & 8.066 & -1.24\times10^{-4} & -1.24\times10^{-4} \\ -17.40 & 2.32\times10^{-4} & 41.40 & -1.24\times10^{-4} & 8.40\times10^{2} & 1.01\times10^{-2} \\ 17.40 & -41.39 & -2.32\times10^{-4} & -1.24\times10^{-4} & 1.01\times10^{-2} & 8.40\times10^{2} \end{bmatrix} \quad (4.15)$$

Using Equation (3.13), the constraint force equilibrium equation for the MS can be written as

$$\mathbf{T}_{x\text{-}m}\zeta_{asx} + \mathbf{T}_{y\text{-}m}\zeta_{asy} + \mathbf{T}_{z\text{-}m}\zeta_{asz} + \mathbf{T}_{x\text{-}m}\zeta_{x} + \mathbf{T}_{y\text{-}m}\zeta_{y} + \mathbf{T}_{z\text{-}m}\zeta_{z} = \mathbf{0} \quad (4.16)$$

where $\mathbf{T}_{x\text{-}m}$, $\mathbf{T}_{y\text{-}m}$ and $\mathbf{T}_{z\text{-}m}$ are the transformation matrices from the local coordinate systems, O_x-$X_xY_xZ_x$, O_y-$X_yY_yZ_y$, and O_z-$X_zY_zZ_z$, to the global coordinate system, O_{ms}-$X_{ms}Y_{ms}Z_{ms}$, respectively. Based on Equation (2.11), the transformation matrices can be written as shown in Equations (4.17) – (4.19), with consideration of the rotations of the ICMs about the local X-axes.

$$\mathbf{T}_{\text{x-m}} = \begin{bmatrix} 1 & 0 & 0 & 0 & 0 & 0 \\ 0 & \cos(\alpha_x) & -\sin(\alpha_x) & 0 & 0 & 0 \\ 0 & \sin(\alpha_x) & \cos(\alpha_x) & 0 & 0 & 0 \\ 0 & 7\cos(\alpha_x)/20 & -7\sin(\alpha_x)/20 & 1 & 0 & 0 \\ -7/20 & 7\sin(\alpha_x) & 7\cos(\alpha_x)/20 & 0 & \cos(\alpha_x) & -\sin(\alpha_x) \\ 0 & -7\cos(\alpha_x)/20 & 7\sin(\alpha_x)/20 & 0 & \sin(\alpha_x) & \cos(\alpha_x) \end{bmatrix} \tag{4.17}$$

$$\mathbf{T}_{\text{y-m}} = \begin{bmatrix} 0 & \sin(\alpha_y) & \cos(\alpha_y) & 0 & 0 & 0 \\ 1 & 0 & 0 & 0 & 0 & 0 \\ 0 & \cos(\alpha_y) & -\sin(\alpha_y) & 0 & 0 & 0 \\ 7/20 & -7\cos(\alpha_y)/20 & 7\sin(\alpha_y)/20 & 0 & \sin(\alpha_y) & \sin(\alpha_y) \\ 0 & -7\sin(\alpha_y)/20 & -7\cos(\alpha_y)/20 & 1 & 0 & 0 \\ 0 & 7\sin(\alpha_y)/20 & 7\cos(\alpha_y)/20 & 0 & \cos(\alpha_y) & -\sin(\alpha_y) \end{bmatrix} \tag{4.18}$$

$$\mathbf{T}_{\text{z-m}} = \begin{bmatrix} 0 & \cos(\alpha_z) & -\sin(\alpha_z) & 0 & 0 & 0 \\ 0 & \sin(\alpha_z) & \cos(\alpha_z) & 0 & 0 & 0 \\ 1 & 0 & 0 & 0 & 0 & 0 \\ 0 & 7\sin(\alpha_z)/10 & 7\cos(\alpha_z)/10 & 0 & \cos(\alpha_z) & -\sin(\alpha_z) \\ 0 & -7\cos(\alpha_z)/10 & 7\sin(\alpha_z)/10 & 0 & \sin(\alpha_z) & \cos(\alpha_z) \\ 0 & 0 & 0 & 1 & 0 & 0 \end{bmatrix} \tag{4.19}$$

where α_x, α_y and α_z are the rotation angles of the three ICMs about the X-axes of the local coordinate systems. In addition, the relationships among the twists, $\boldsymbol{\xi}_{ms}$, $\boldsymbol{\xi}_x$, $\boldsymbol{\xi}_y$ and $\boldsymbol{\xi}_z$, can be represented by Equation (4.20).

$$\boldsymbol{\xi}_x = \left(\mathbf{T}_x\right)^T \boldsymbol{\xi}_{ms},\ \boldsymbol{\xi}_y = \left(\mathbf{T}_y\right)^T \boldsymbol{\xi}_{ms} \text{ and } \boldsymbol{\xi}_z = \left(\mathbf{T}_z\right)^T \boldsymbol{\xi}_{ms} \tag{4.20}$$

where $\boldsymbol{\xi}_{ms}$ is a twist representing the displacement of the MS in the global coordinate system O_{ms}-$X_{ms}Y_{ms}Z_{ms}$, as shown in Equation (4.21).

$$\boldsymbol{\xi}_{ms} = \left[\xi_{ms\text{-}tx}, \xi_{ms\text{-}ty}, \xi_{ms\text{-}tz}, \xi_{ms\text{-}rx}, \xi_{ms\text{-}ry}, \xi_{ms\text{-}rz}\right]^T \tag{4.21}$$

where $\xi_{ms\text{-}tx}$, $\xi_{ms\text{-}ty}$, $\xi_{ms\text{-}tz}$, $\xi_{ms\text{-}rx}$, $\xi_{ms\text{-}ry}$ and $\xi_{ms\text{-}rz}$ are the values of the displacements of the MS along and about the X_{ms}-, Y_{ms}- and Z_{ms}-axes. Additionally, $\xi_{ms\text{-}tx}$, $\xi_{ms\text{-}ty}$, and $\xi_{ms\text{-}tz}$ represent the values of the primary translations of the MS, while $\xi_{ms\text{-}rx}$,

$\xi_{ms\text{-}ry}$ and $\xi_{ms\text{-}rz}$ represent the values of the parasitic rotations of the MS. Using Equations (4.9) – (4.21), the twist $\boldsymbol{\xi}_{ms}$ can be derived as shown in Equation (4.22).

$$\boldsymbol{\xi}_{ms} = \left(\mathbf{T}_{x\text{-}m}\mathbf{k}_x \left(\mathbf{T}_{x\text{-}m}\right)^T + \mathbf{T}_{y\text{-}m}\mathbf{k}_y \left(\mathbf{T}_{y\text{-}m}\right)^T + \mathbf{T}_{z\text{-}m}\mathbf{k}_z \left(\mathbf{T}_{z\text{-}m}\right)^T \right)^{-1} \boldsymbol{\zeta}_{xyz} \tag{4.22}$$

where $\boldsymbol{\zeta}_{xyz} = \mathbf{T}_{x\text{-}m}\boldsymbol{\zeta}_x + \mathbf{T}_{y\text{-}m}\boldsymbol{\zeta}_y + \mathbf{T}_{z\text{-}m}\boldsymbol{\zeta}_z$.

The PSR-RPM approach described in this example is designed to reduce the sum of the absolute values, $\xi_{m\text{-}rxyz}$, of the three parasitic rotations of the MS of the XYZ CPM, without considering the parasitic rotations of the ASs. When $\alpha_y = 0$ and $\alpha_z = 0$, the relationship between $\xi_{m\text{-}rxyz}$ and α_x can be seen in Figure 4.5, which shows that: (a) $\xi_{m\text{-}rxyz}$ will be minimized only when $\alpha_x = \pm\pi$ and the X-direction external force is applied, and (b) changing the rotation angle α_x cannot considerably affect $\xi_{m\text{-}rxyz}$, when only a Y- or Z-direction external force is exerted.

Because of the isotropic design of the XYZ CPM, the sum of the absolute parasitic rotation values, $\xi_{m\text{-}rxyz}$, of the MS can be minimized if $\alpha_x = \pm\pi$, $\alpha_y = \pm\pi$ and $\alpha_z = \pm\pi$, no matter which actuation force is applied. This conclusion is also validated in Figure 4.6. Using $\alpha_x = \pm\pi$, $\alpha_y = \pm\pi$ and $\alpha_z = \pm\pi$, the XYZ CPM shown in Figure 4.2(a) can be reconfigured (optimized) to a new XYZ CPM illustrated in Figure 4.7.

In order to compare the parasitic rotations of the two XYZ CPMs, FEA simulations are carried out. The commercial software, COMSOL MULTIPHYSICS, is selected for the nonlinear FEA simulations, using the 10-node tetrahedral element and extra fine meshing technology. As shown in Figure 4.8, the analytical results and the FEA results have almost the same trends with less than 7% difference over the motion range. It can also be seen that the sum of the absolute parasitic rotation values, $\xi_{m\text{-}rxyz}$, is reduced by approximately 50%.

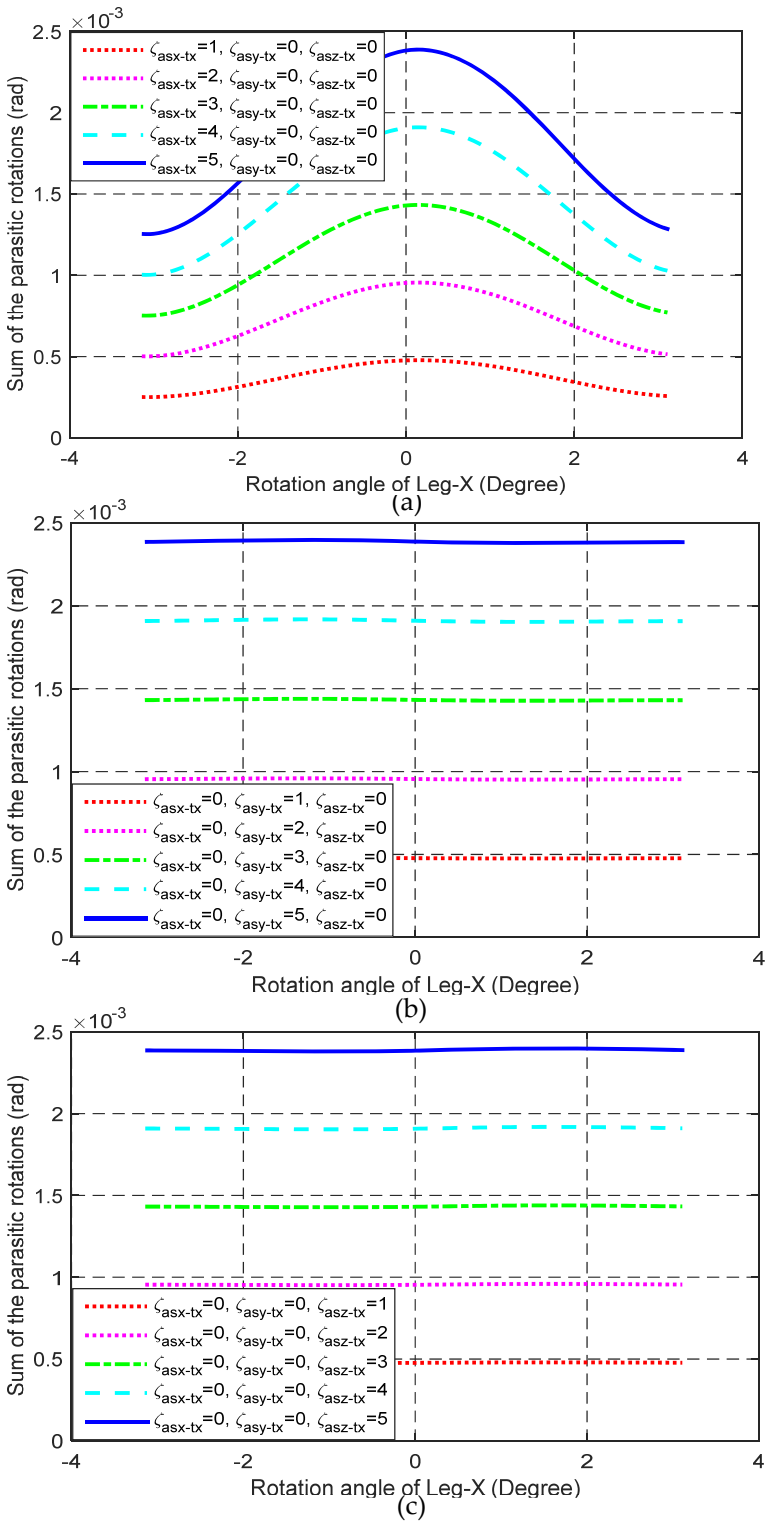

Figure 4.5 Sum of the absolute values of the parasitic rotations, $\xi_{m\text{-}rxyz}$, plotted against the rotation angle α_x: (a) only X direction force applied, (b) only Y direction force applied, and (c) only Z direction force applied

As mentioned in this section, $\xi_{m\text{-}rxyz}$ is the sum of the absolute values of the three parasitic rotations of the MS about the X_{ms}-, Y_{ms}- and Z_{ms}-axes. For Figure

4.8(b), when $\zeta_{asx\text{-}tx}$ varies from 0 to 1, while $\zeta_{asy\text{-}tx}$ =1 and $\zeta_{asz\text{-}tx}$ =0, some of the three parasitic rotations increase, but others decrease. Therefore, there is a flat region in Figure 4.8(b), and $\xi_{m\text{-}rxyz}$ remains unchanged in the region. This flat region cannot be predicted through consideration only of the geometrical shape, but can be derived and verified from the analytical models and the FEA simulations. That is the reason why the positions of the compliant modules should be optimized through analytical modelling.

A CAD prototype design based on the optimized XYZ CPM is illustrated in Figure 4.9. It can be seen from Figure 4.9 that the parasitic rotations produced by the AM of a leg can be compensated by the parasitic rotations produced by the two PMs of the other two legs. That is the physical reason why the parasitic rotations of the XYZ CPM are reduced.

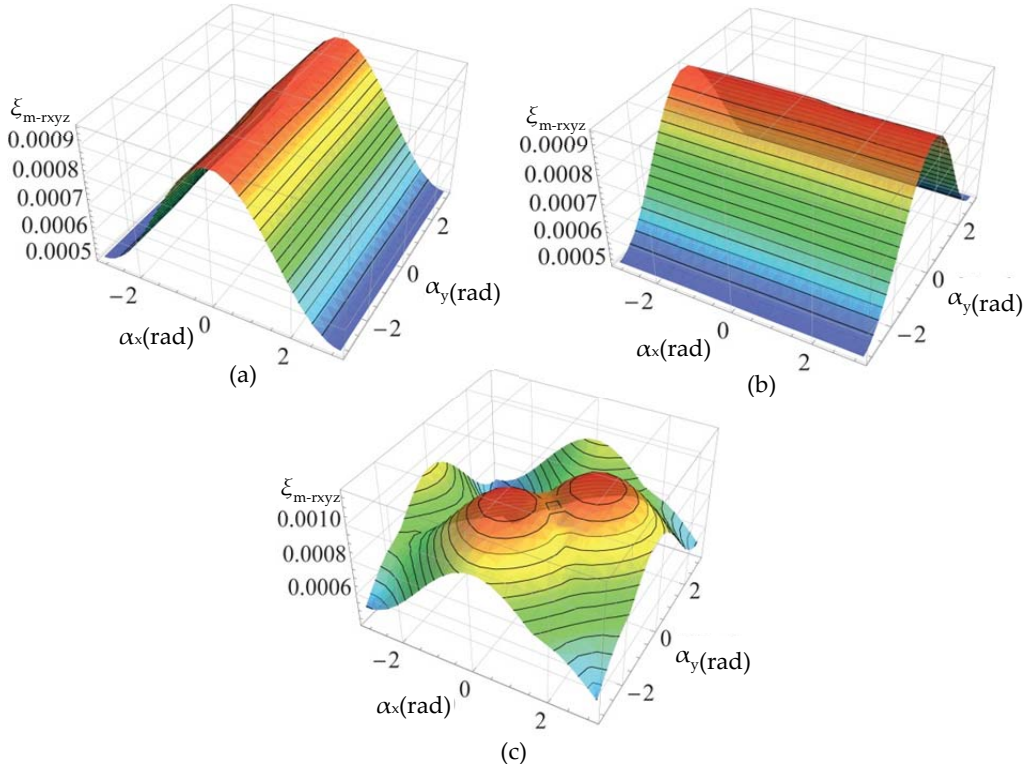

Figure 4.6 Sum of the absolute values of the parasitic rotations, $\xi_{m\text{-}rxyz}$, with the rotation angles α_x and α_y: (a) only X-direction force applied ($\zeta_{asx\text{-}tx}$ = 2, $\zeta_{asy\text{-}tx}$ = 0 and $\zeta_{asz\text{-}tx}$ = 0), (b) only Y-direction force applied ($\zeta_{asx\text{-}tx}$ = 0, $\zeta_{asy\text{-}tx}$ = 2 and $\zeta_{asz\text{-}tx}$ = 0), and (c) forces in X-and Y-directions applied ($\zeta_{asx\text{-}tx}$ = 2, $\zeta_{asy\text{-}tx}$ = 2 and $\zeta_{asz\text{-}tx}$ = 0)

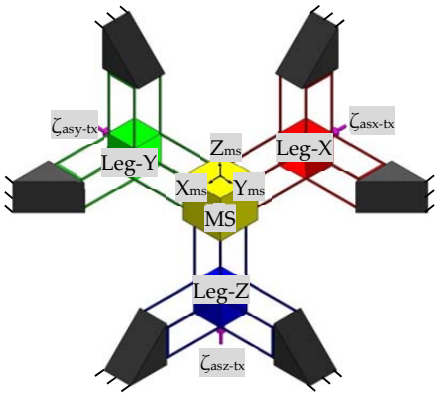

Figure 4.7 Reconfigured XYZ CPM with smaller parasitic motions

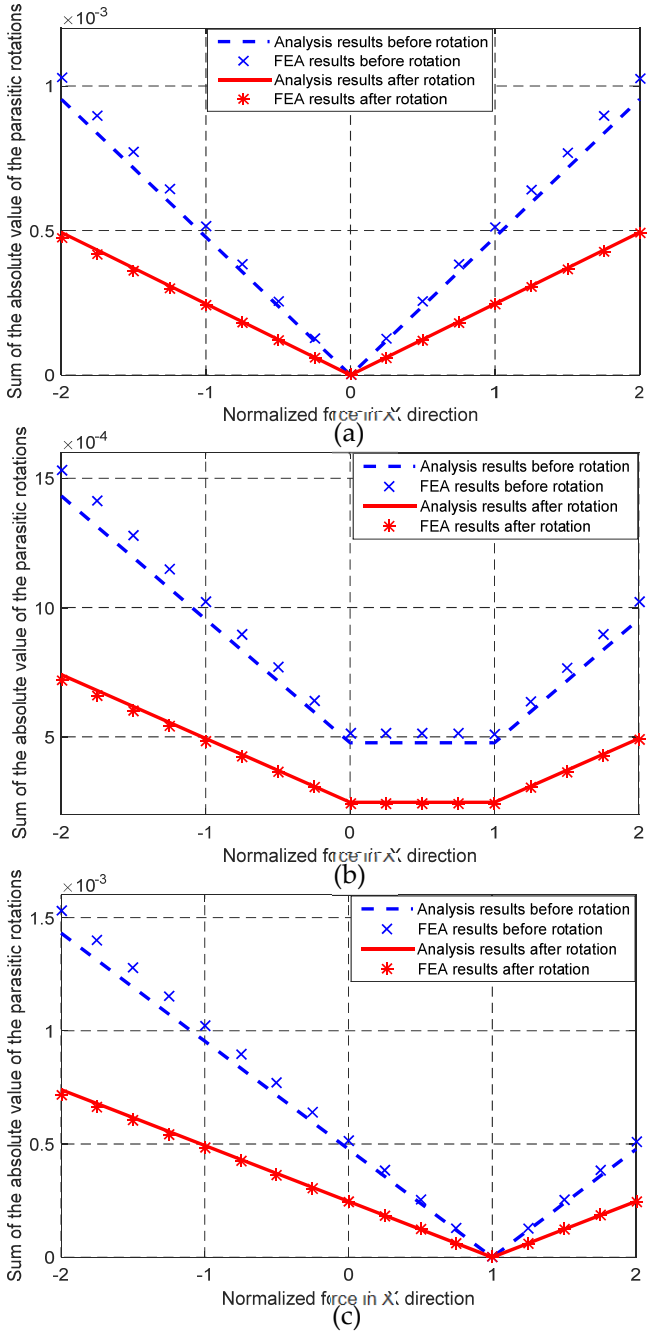

Figure 4.8 Analysis and FEA results: (a) $\zeta_{asy\text{-}tx} = 0$ and $\zeta_{asz\text{-}tx} = 0$, (b) $\zeta_{asy\text{-}tx} = 1$ and $\zeta_{asz\text{-}tx} = 0$, and (c) $\zeta_{asy\text{-}tx} = 1$ and $\zeta_{asz\text{-}tx} = 1$

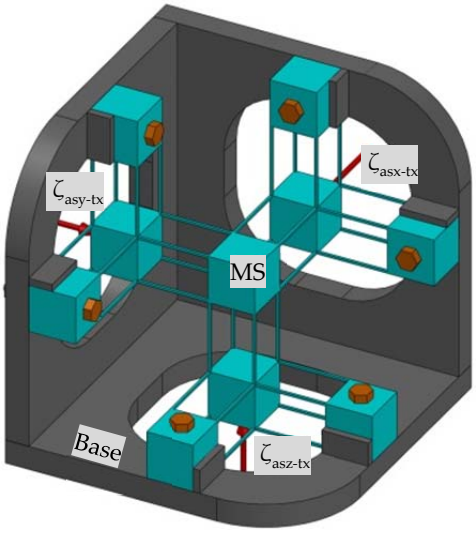

Figure 4.9 An optimal design based on the reconfigured XYZ CPM

4.3 Discussion

In Section 4.2, an XYZ CPM was reconfigured without considering the effects of the translations of the ICMs. As described in Section 4.1, any ICM can translate in three-dimensional space, and the parasitic motions of a compliant mechanism may be reduced through translating the ICMs of the compliant mechanism, as done in [99]. It can be seen that the XYZ CPM shown in Figure 4.9 consists of basic spatial four-beam parallelogram compliant mechanisms. The stiffness centre of the basic spatial four-beam parallelogram compliant mechanism is located at its geometrical centre. Based on the stiffness centre concept, one possible optimized design can be obtained by translating the spatial four-beam basic parallelogram compliant mechanisms, so that each of the actuation forces of the XYZ CPM goes through the stiffness centres of the associated basic parallelogram compliant mechanisms [99].

In this section, an XY compliant mechanism, as shown in Figure 4.10(a), is taken as an example for additional discussion. The XY compliant mechanism can be decomposed into ICMs and rigid stages, as illustrated in Figure 4.10(b). Module-X_1, Module-Y_1, Module-X_2 and Module-Y_2 are the basic ICMs of the XY compliant mechanism.

The XY compliant mechanism can be reconfigured by translating the four basic ICMs, as shown in Figure 4.11 (a stacked design). The stiffness centres of the two passive modules, Module-X_2 and Module-Y_2, overlap, and each actuation force passes through the stiffness centre of the actuated module, Module-X_1 or Module-Y_1, and through the overlapping stiffness centre of the two passive modules [93]. The parasitic motion of the XY compliant mechanism in Figure 4.11 has been significantly reduced compared with the original one, as shown by the FEA simulation verification. Therefore, the parasitic motions of a compliant mechanism can be reduced through the translations of the ICMs.

The structure of the XY compliant mechanism in Figure 4.10 can also be optimized to have a smaller parasitic rotation through rotating the ICMs, Module-X_1 and Module-Y_1, in their position spaces. The resulting optimal design with a reduced parasitic rotation is shown in Figure 4.12. When Aluminium alloy 6061 is selected as material (Young's modulus is 69000MPa, Poisson's ratio is 0.33) and the dimension of the identical beams and identical cubes of the XY compliant mechanisms are defined as follows: the beam length, beam in-plane thickness, beam out-plane thickness, cube out-plane height and cube in-plane width are 50mm, 1mm, 10mm, 10mm and 25mm, respectively, the FEA results of the parasitic rotations of the two XY compliant mechanisms can be seen in Figure 4.13. Figure 4.13 shows that the parasitic rotation of the XY compliant mechanism shown in Figure 4.12 is approximately 50% of that of the XY compliant mechanism shown in Figure 4.10.

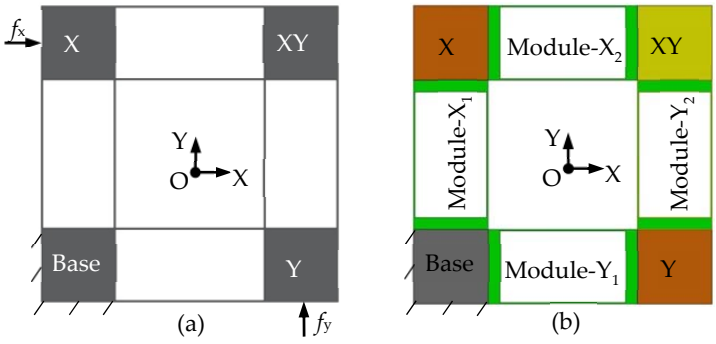

Figure 4.10 An XY compliant mechanism and its basic composition pattern: (a) the XY compliant mechanism, and (b) the basic composition pattern

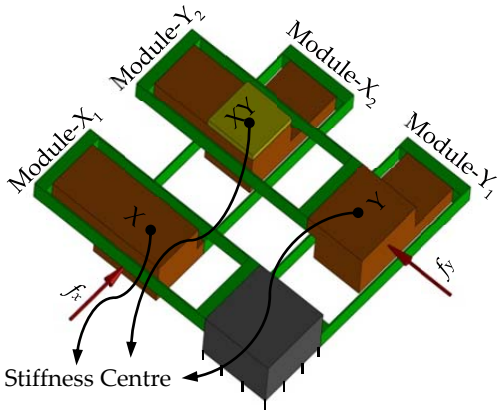

Figure 4.11 An XY compliant mechanism reconfigured from the XY compliant mechanism shown in Figure 4.10(a), via the translations of the ICMs

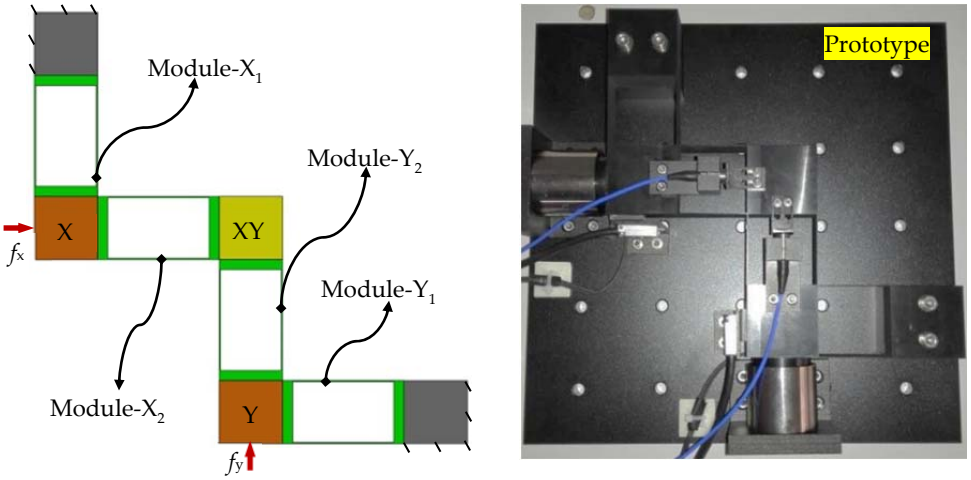

Figure 4.12 The CAD model and prototype of an XY compliant mechanism which is reconfigured from the XY compliant mechanism shown in Figure 4.10(a) by rotating the ICMs (Courtesy of Prof. Wei Wei, in BTBU, China)

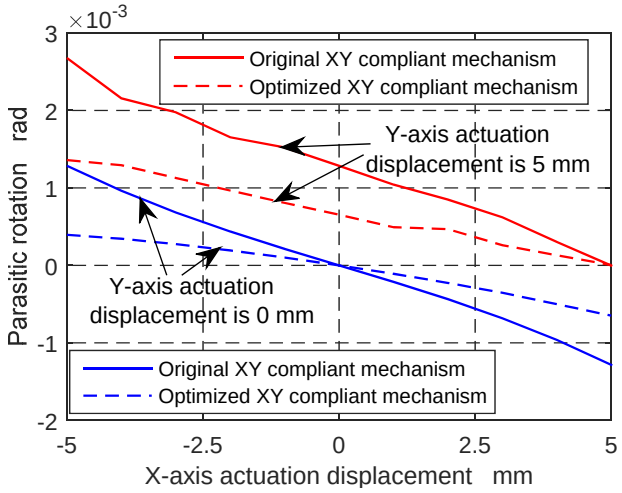

Figure 4.13 Comparison between the parasitic rotations of the XY compliant mechanisms shown in Figure 4.10(a) and Figure 4.12

4.4 Summary

A novel compliant mechanism reconfiguration approach, the PSR approach, has been proposed in this chapter. The PSR approach allows the reconfiguration of a compliant mechanism into many alternative compliant mechanisms, with different geometrical structures and motion characteristics. Therefore, the PSR approach can be used to improve the manufacturability, increase the load transmissibility, minimize the cross-axis couplings and lost motions, and increase the motion ranges through changing the stress distribution. Based on the PSR theory, the PSR-RPM approach is detailed in this chapter.

The PSR-RPM approach reduces parasitic motions of a compliant mechanism by optimizing the positions of the compliant modules of the compliant mechanism. The following three main tasks for reducing parasitic motions of a compliant mechanism, when using the PSR-RPM approach, have also been detailed: (a) decomposing the compliant mechanism into ICMs and rigid stages, (b) identifying the position spaces of the ICMs based on screw theory, and (c) obtaining the permitted positions for the ICMs from their position spaces where the parasitic motions of the compliant mechanism are minimized. In addition, a case study has been presented in which an XYZ CPM was reconfigured to a new XYZ CPM with approximately 50% reduction of parasitic motions (rotations of the output MS) based on the PSR-RPM approach, as validated by the FEA results.

5 PSR-BASED OPTIMIZATION APPROACH FOR THE DESIGN OF SYMMETRIC COMPLIANT MECHANISMS

The position-space-based reconfiguration (PSR) approach has been introduced in Chapter 4. Based on the PSR approach, two compliant mechanism optimization approaches, PSR-RPM and PSR-SCM approaches, are presented in this thesis. The PSR-RPM approach has been detailed in Chapter 4. In this chapter, the PSR-SCM approach is introduced with explanations of its principle and example demonstrations.

5.1 Principle and Procedure of PSR-SCM Approach

Symmetry enables excellent motion performance of compliant mechanisms, such as minimized parasitic motions. Traditionally, a symmetric compliant mechanism is designed by adding redundant compliant modules on a non-symmetric compliant mechanism [4, 55]. Therefore, traditional symmetric compliant mechanisms are highly over-constrained, leading to issues such as high actuation stiffness and large lost motions. However, the proposed PSR-SCM approach designs a symmetric compliant mechanism, by rearranging the compliant modules of a non-symmetric compliant mechanism within their position spaces and adding minimal redundant compliant modules. The PSR-SCM approach reconfigures a non-symmetric compliant mechanism into a symmetric compliant mechanism with the addition of minimal over-constraints (or without the addition of any over-constraints). Therefore, to design a symmetric compliant mechanism using the proposed PSR-SCM approach, over-constraints can be minimized, ensuring that the resulting compliant mechanism

not only has minimized parasitic motions but also can have greatly reduced actuation stiffness, minimized cross-axis coupling and decreased lost motions.

Using the PSR-SCM approach to reconfigure a non-symmetric compliant mechanism into a symmetric compliant mechanism under the following:

i. Decomposing the compliant mechanism into rigid stages and compliant modules in a decomposition pattern. In this step, the decomposition of a non-symmetric compliant mechanism is mainly dependent on designers' rational intuition, with consideration of reconfiguring this non-symmetric compliant mechanism into a symmetric compliant mechanism through rearranging the positions of the obtained compliant modules.

ii. Changing the positions of the compliant modules within their position spaces [20, 28], so that the non-symmetric compliant mechanism can be reconfigured into a symmetric compliant mechanism by adding zero or very few redundant compliant modules. If changing the positions of the compliant modules cannot successfully reconfigure the non-symmetric compliant mechanism into a symmetric compliant mechanism directly (without adding other over-constraints) under the decomposition patterns obtained in Step (i), another decomposition pattern may be considered in Step (i). Note that the derivation of the position spaces of the compliant modules is not detailed in this Chapter. If a compliant module is an ICM (independent compliant module, as defined in Chapter 4), the position space of the compliant module can be achieved using screw theory, as studied in Chapter 4. If a compliant module is not an ICM, the position space of the compliant module can be obtained by trial and error, which is not detailed in this thesis.

iii. Adding redundant compliant modules if needed, which enables the final design to be a symmetric compliant mechanism. A redundant compliant module of a compliant module should be placed at a possible permitted

position within the position space of the compliant module, as stated in Section 1.4.3.

iv. Checking if the obtained symmetric compliant mechanism is as desired. If not, other symmetric compliant mechanisms can be designed, via repeating Steps (i) – (iii) with other different decomposition patterns. One of these symmetric compliant mechanisms can be selected as the final design.

The proposed PSR-SCM approach can be employed to reconfigure any one compliant mechanism into a symmetric compliant mechanism. An original non-symmetric XYZ CPM is reconfigured into a symmetric XYZ CPM in Section 5.2.

5.2 Case Study

5.2.1 A symmetric XYZ CPM design

In this section, an original non-symmetric XYZ CPM (as shown in Figure 5.1(a)) is reconfigured into a symmetric XYZ CPM (Figure 5.1(h)). The non-symmetric XYZ CPM was presented by Hao in [77], which is a 3PPPRR (P: Prismatic, R: Revolute) mechanism. It is an exactly-constrained design in its general construction, without over-constraints in its compositional modules. The non-symmetric XYZ CPM can provide decoupled translations along the X_{ms}-, Y_{ms}- and Z_{ms}-axes, but its parasitic motions and lost motions are relative large. Therefore, a symmetric XYZ CPM, with minimized parasitic motions and reduced lost motions, is designed using the PSR-SCM approach, based on the following steps.

i. Decompose the non-symmetric XYZ CPM into rigid stages and compliant modules. Figure 5.1(b) shows that the rigid stages are an MS and BSs, and the compliant modules are actuated compliant modules (AMs: AM-X, AM-Y and AM-Z) and passive compliant modules (PMs: PM-X, PM-Y and PM-Z).

ii. Further decompose each of the AMs into two DTBCMs (double-two-beam compliant modules, as defined in Chapter 1). Figure 5.1(c) illustrates that the AM-X is decomposed into two DTBCMs, AM-X-1 and AM-X-2; the AM-Y is decomposed into two DTBCMs, AM-Y-1 and AM-Y-2; the AM-Z is decomposed into two DTBCMs, AM-Z-1 and AM-Z-2.

iii. Reconfigure the AM-X via translating the AM-X-1 (within its position space) and its adjacent BSs along the X_{ms}-axis, as shown in Figure 5.1(d), so that the MS is located at an intermediate position between the AM-X-1 and the AM-X-2. As can be seen, a RL-X is needed to link the AM-X-1 and the AM-X-2.

iv. Add redundant compliant modules, AM-X-1-R and AM-X-2-R, as shown in Figure 5.1(e), so that the AM-X is a mirror-symmetric compliant module about the MS. As described in Section 1.4.3 in Chapter 1, a redundant copy of a compliant module can be added at any one position within the position space of the compliant module. Therefore, the positions of the AM-X-1-R and the AM-X-2-R should be within the position spaces of the AM-X-1 and the AM-X-2, respectively.

v. Add a redundant PM, PM-X-R (Figure 5.1(e)), which is the reflection of the PM-X about the MS. In this case, the PM-X cannot be reconfigured to be symmetrical about the MS, so a redundant PM should be added (the redundant PM is placed within the position space of the PM). By this step, the leg of the XYZ CPM associated with the X_{ms}-axis translation has been reconfigured.

vi. Reconfigure the other two legs of the XYZ CPM associated with the translations along the Y_{ms}- and Z_{ms}-axes, following the same reconfiguration process of the leg associated with the translation along the X_{ms}-axis. The resulting design can be seen in Figure 5.1(f).

vii. Re-design the BSs, as shown in Figure 5.1(g).

viii. Combine all the rigid stages and compliant modules together (Figure 5.1(h)), which is the inverse process of decomposing the compliant

mechanism. The symmetric XYZ CPM shown in Figure 5.1(h) is the resulting symmetric XYZ CPM.

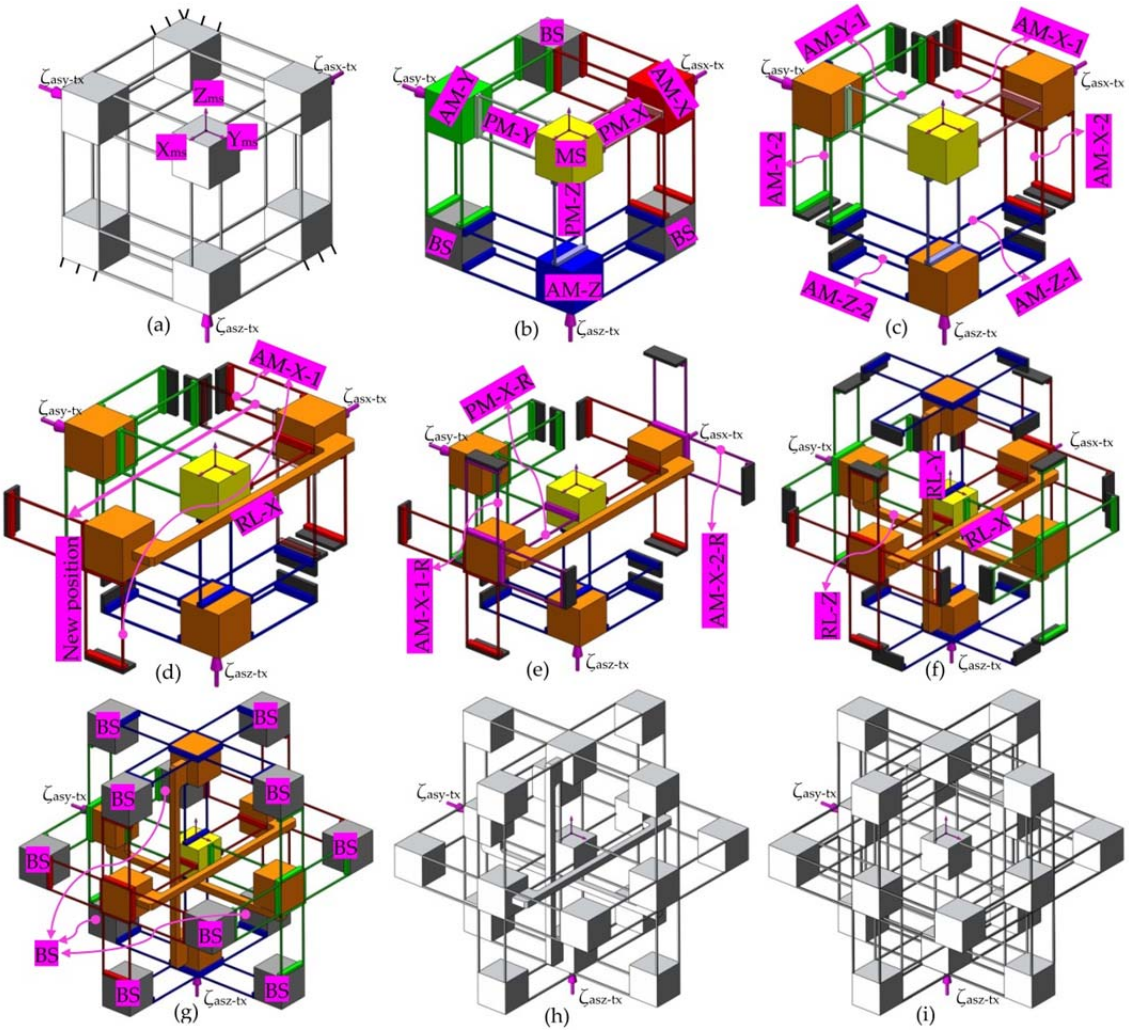

Figure 5.1 Symmetric XYZ CPM designed via reconfiguring a non-symmetric XYZ CPM: (a) the original non-symmetric XYZ CPM [30], (b) decomposition of the non-symmetric XYZ CPM, (c) further decomposition of the AMs of the non-symmetric XYZ CPM, (d) AM-X-1 translated to a new permitted position, (e) adding redundant compliant modules (over-constraints), (f) reconfiguration of the legs associated with the translations along the Y_{ms}- and Z_{ms}-axes, (g) BS design, (h) resulting symmetric XYZ CPM, and (i) another symmetric XYZ CPM designed by traditional approach, by adding redundant compliant modules on another three legs

Another symmetric XYZ CPM (Figure 5.1(i)) is designed by directly adding redundant compliant modules to the non-symmetric XYZ CPM (Figure 5.1(a)). It can be seen that the symmetric XYZ CPM shown in Figure 5.1(i) has more over-constraints, compared with the symmetric XYZ CPM that is shown in

Figure 5.1(h).

5.2.2 Kinetostatic modelling and analysis

The designed symmetric XYZ CPM, as shown in Figure 5.1(i), is modelled and analysed in this section. It can be known that the parasitic rotations and the parasitic translations of the symmetric XYZ CPM should be much smaller than the primary translations, due to the symmetric structure. Therefore, only the force-displacement relationships and the lost motions, of the XYZ CPM along the X_{ms}-, Y_{ms}- and Z_{ms}-axes, are modelled (using the CFB approach proposed in Chapter 3) and analysed in this section. The analysis results can be used to estimate the actuation stiffness, and to identify the parameters of the associated control system.

Suppose that the primary translations are performed at very small velocities. Therefore, dynamic contribution is not taken into account in the modelling. Additionally, the tiny parasitic motions are also ignored in the modelling.

Each PM of the symmetric XYZ CPM can be referred to as a two-beam compliant module (TBCM) as shown in Figure 5.2(a), and each AM of the symmetric XYZ CPM can be regarded as a combination of TBCMs. Therefore, the motions of the symmetric XYZ CPM are performed through the deformation of the TBCMs, so the modelling of the TBCM is carried out before modelling the symmetric XYZ CPM. Note that all the beams of the symmetric XYZ CPM are identical with square cross sections, and the cubes of the rigid stages are also identical.

The reaction forces produced by the deformation of the four-beam compliant module (FBCM), as shown in Figure 5.2(b), was first reported in [78]. The FBCM is a combination of two TBCMs shown in Figure 5.2(a). If ignoring the rotations of the TBCM, the reaction forces produced by the deformation of the TBCM along the X_{cm}-, Y_{cm}- and Z_{cm}-axes are half of the reaction forces produced by the

deformation of the FBCM along X_{cm}-, Y_{cm}- and Z_{cm}-axes, respectively. Therefore, the reaction force produced by the deformation of the TBCM along the X_{cm}-, Y_{cm}- and Z_{cm}-axes can be obtained, as shown in Equations (5.1) – (5.3), respectively.

$$\zeta_{\text{cm-tx}} = -\frac{840\left(5\xi_{\text{cm-tx}} + 3\left(\xi_{\text{cm-ty}}^2 + \xi_{\text{cm-tz}}^2\right)\right)}{175t^2 + 3\xi_{\text{cm-ty}}^2 + 3\xi_{\text{cm-tz}}^2} \tag{5.1}$$

$$\zeta_{\text{cm-ty}} = -\frac{24\xi_{\text{cm-ty}}\left(175t^2 + 210\xi_{\text{cm-tx}} + 129\xi_{\text{cm-ty}}^2 + 129\xi_{\text{cm-tz}}^2\right)}{175t^2 + 3\xi_{\text{cm-ty}}^2 + 3\xi_{\text{cm-tz}}^2} \tag{5.2}$$

$$\zeta_{\text{cm-tz}} = -\frac{24\xi_{\text{cm-tz}}\left(175t^2 + 210\xi_{\text{cm-tx}} + 129\xi_{\text{cm-ty}}^2 + 129\xi_{\text{cm-tz}}^2\right)}{175t^2 + 3\xi_{\text{cm-ty}}^2 + 3\xi_{\text{cm-tz}}^2} \tag{5.3}$$

where t is the normalized thickness of the beam. The $\xi_{\text{cm-tx}}$, $\xi_{\text{cm-ty}}$ and $\xi_{\text{cm-tz}}$ denote the translational displacements of the TBCM. Additionally, $\zeta_{\text{cm-tx}}$, $\zeta_{\text{cm-ty}}$ and $\zeta_{\text{cm-tz}}$ represent the reaction forces along the X_{cm}-, Y_{cm}- and Z_{cm}-axes, respectively, produced by the TBCM due to the deformation of the TBCM.

A TBCM can be regarded as a three-dimensional translational spring. The complete symmetric XYZ CPM can be modelled based on the analytical model of the TBCM. The motion performance of the symmetric XYZ CPM along the X_{ms}-, Y_{ms}- and Z_{ms}-axes is isotropic (O_{ms}-$X_{ms}Y_{ms}Z_{ms}$ is the global coordinate system). Therefore, only the primary translations along one of the three directions need to be studied. In this chapter, the derivation of the force-displacement relationship, associated with only the translations along the X_{ms}-axis, is detailed. Given any displacements, $\xi_{\text{asy-tx}}$ and $\xi_{\text{asz-tx}}$, of the RL-Y and RL-Z, respectively, the XYZ CPM can be simplified to the model shown in Figure 5.3 if only the force-displacement relationship in X_{ms}-axis is concerned.

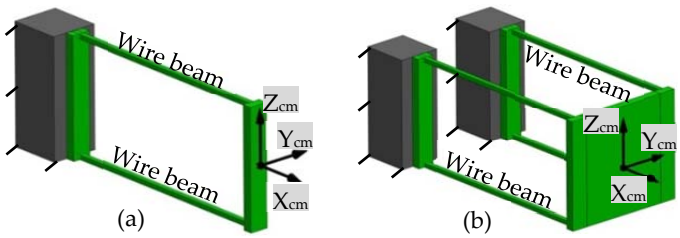

Figure 5.2 (a) A TBCM and its coordinate system, and (b) a FBCM and its coordinate system

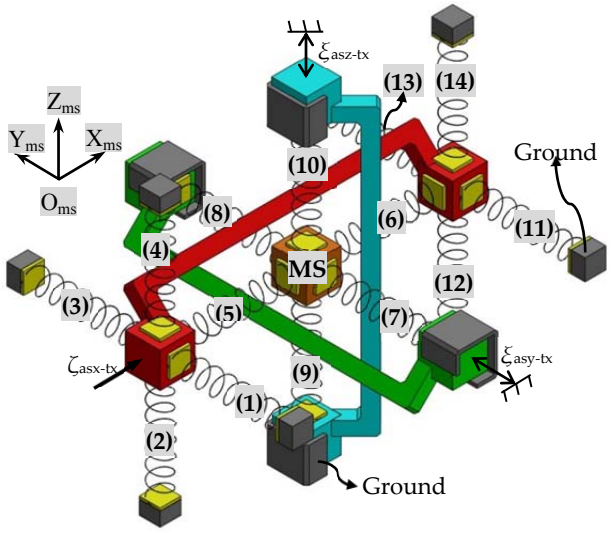

Figure 5.3 Simplified spring model of the symmetric XYZ CPM (RL-X is red in color, RL-Y is green in color, and RL-Z is blue in color)

Assume that the lost motions along the X_{ms}-, Y_{ms}- and Z_{ms}-axes are δ_x, δ_y and δ_z, respectively, which can be written as shown in Equation (5.4).

$$\delta_x = \xi_{asx\text{-}tx} - \xi_{ms\text{-}tx},\ \delta_y = \xi_{asy\text{-}tx} - \xi_{ms\text{-}ty} \text{ and } \delta_z = \xi_{asz\text{-}tx} - \xi_{ms\text{-}tz} \tag{5.4}$$

where $\xi_{ms\text{-}tx}$, $\xi_{ms\text{-}ty}$ and $\xi_{ms\text{-}tz}$ are the values of the primary translations of the MS along the X_{ms}-, Y_{ms}- and Z_{ms}-axes, respectively. The values of the primary translations of the RL-X, the RL-Y and the RL-Z are represented by $\xi_{asx\text{-}tx}$, $\xi_{asy\text{-}tx}$ and $\xi_{asz\text{-}tx}$, respectively. The model, as shown in Figure 5.3, contains 14 TBCMs in each axis, which are termed as TBCM-1 to TBCM-14, respectively. If all the parasitic rotations and parasitic translations of the symmetric XYZ CPM are ignored, the deformation displacements of each of the TBCMs can be obtained easily according to the primary translations and lost motions. The reaction forces of the TBCMs can also be calculated based on Equations (5.1) – (5.3).

Taking the TBCM-1 as an example, the TBCM-1 is linked to the RL-X, so the deformation displacements of the TBCM-1 can be derived from the motion displacements of the RL-X. If ignoring all the parasitic rotations and parasitic translations of the RL-X, the deformation displacements of the TBCM-1 equal to $\xi_{\text{asx-tx}}$, zero and zero along the X_{ms}-, Y_{ms}- and Z_{ms}-axes, respectively. Therefore, the reaction force, ζ_a, of the TBCM-1 along the X_{ms}-axis can be obtained, as shown in Equation (5.5), by substituting the deformation displacements of the TBCM-1 into Equations (5.2) and (5.3). Note that when substituting the deformation displacements into Equation (5.2), $\xi_{\text{cm-tx}}$, $\xi_{\text{cm-ty}}$ and $\xi_{\text{cm-tz}}$ in Equation (5.2) equal to zero, $\xi_{\text{asx-tx}}$ and zero, respectively; when substituting the deformation displacements into Equation (5.3), $\xi_{\text{cm-tx}}$, $\xi_{\text{cm-ty}}$ and $\xi_{\text{cm-tz}}$ in Equation (5.3) equal to zero, zero and $\xi_{\text{asx-tx}}$, respectively. Similarly, the reaction force of the TBCM-2, TBCM-3, TBCM-4, TBCM-11, TBCM-12, TBCM-13 or TBCM-14, to the RL-X along the X_{ms}-axis, can also be obtained as shown in Equation (5.5). The reaction forces of the TBCM-5, TBCM-6, TBCM-7, TBCM-8, TBCM-9 and TBCM-10, to the MS along the X_{ms}-axis, can be derived from Equations (5.6) – (5.11), respectively, which are represented as wrenches ζ_b, ζ_c, ζ_d, ζ_e, ζ_f and ζ_g, as shown below.

$$\zeta_{\text{a}} = -\frac{24\xi_{\text{asx-tx}}\left(129\xi_{\text{asx-tx}}^2 + 175t^2\right)}{3\xi_{\text{asx-tx}}^2 + 175t^2} \tag{5.5}$$

$$\zeta_{\text{b}} = \frac{840\left(3\left(\xi_{\text{ms-ty}}^2 + \xi_{\text{ms-tz}}^2\right) - 5\delta_{\text{x}}\right)}{3\xi_{\text{ms-ty}}^2 + 3\xi_{\text{ms-tz}}^2 + 175t^2} \tag{5.6}$$

$$\zeta_{\text{c}} = -\frac{840\left(3\left(\xi_{\text{ms-ty}}^2 + \xi_{\text{ms-tz}}^2\right) + 5\delta_{\text{x}}\right)}{3\xi_{\text{ms-ty}}^2 + 3\xi_{\text{ms-tz}}^2 + 175t^2} \tag{5.7}$$

$$\zeta_{\text{d}} = -\frac{24\xi_{\text{ms-tx}}\left(-210\delta_{\text{y}} + 129\xi_{\text{ms-tx}}^2 + 129\xi_{\text{ms-tz}}^2 + 175t^2\right)}{3\xi_{\text{ms-tx}}^2 + 3\xi_{\text{ms-tz}}^2 + 175t^2} \tag{5.8}$$

$$\zeta_e = -\frac{24\xi_{ms-tx}\left(210\delta_y + 129\xi_{ms-tx}^2 + 129\xi_{ms-tz}^2 + 175t^2\right)}{3\xi_{ms-tx}^2 + 3\xi_{ms-tz}^2 + 175t^2} \tag{5.9}$$

$$\zeta_f = -\frac{24\xi_{ms-tx}\left(-210\delta_z + 129\xi_{ms-ty}^2 + 129\xi_{ms-tx}^2 + 175t^2\right)}{3\xi_{ms-ty}^2 + 3\xi_{ms-tx}^2 + 175t^2} \tag{5.10}$$

$$\zeta_g = -\frac{24\xi_{ms-tx}\left(210\delta_z + 129\xi_{ms-ty}^2 + 129\xi_{ms-tx}^2 + 175t^2\right)}{3\xi_{ms-ty}^2 + 3\xi_{ms-tx}^2 + 175t^2} \tag{5.11}$$

When the MS is at static equilibrium, all the reaction forces on the MS along the X_{ms}-axis should be balanced, so Equation (5.12) can be obtained. When substituting Equations (5.6) – (5.11) into Equation (5.12), Equation (5.13) can be derived. Furthermore, the actuation force, $\zeta_{asx\text{-}tx}$, should be equal to the sum of the reaction forces of all the TBCMs except TBCM-5 and TBCM-6, along the X_{ms}-axis. Therefore, the relationship between the actuation force $\zeta_{asx\text{-}tx}$ and the primary translations of the MS can be obtained, as shown in Equation (5.14). Similarly, the lost motions along the Y_{ms}- and Z_{ms}-axes and the force-displacement relationships associated with the actuation forces, $\zeta_{asy\text{-}tx}$ and $\zeta_{asz\text{-}tx}$, can be derived, as shown in Equations (5.15) – (5.18). Note that the actuation forces, $\zeta_{asy\text{-}tx}$ and $\zeta_{asz\text{-}tx}$, are applied on the RL-Y and RL-Z, respectively.

$$\zeta_b + \zeta_c + \zeta_d + \zeta_e + \zeta_f + \zeta_g = 0 \tag{5.12}$$

$$\begin{aligned}\delta_x = {} & \frac{6\xi_{ms-tx}^3\xi_{ms-tyz}\left(129\xi_{ms-ty}^2 + 129\xi_{ms-tz}^2 + 7700t^2\right)}{175\xi_{ms-txy}\xi_{ms-txz}} \\ & + \frac{6\xi_{ms-tx}\xi_{ms-ty}^2\xi_{ms-tyz}\left(129\xi_{ms-tz}^2 + 3850t^2\right)}{175\xi_{ms-txy}\xi_{ms-txz}} \\ & + \frac{2\xi_{ms-tx}\xi_{ms-tyz}\left(66t^2\xi_{ms-tz}^2 + 175t^4\right)}{\xi_{ms-txy}\xi_{ms-txz}} \\ & + \frac{774\xi_{ms-tx}^5\xi_{ms-tyz}}{175\xi_{ms-txy}\xi_{ms-txz}}\end{aligned} \tag{5.13}$$

$$
\begin{aligned}
&\xi_{\text{ms-txy}} = 3\xi_{\text{ms-tx}}^2 + 3\xi_{\text{ms-ty}}^2 + 175t^2 \\
\text{where}\quad &\xi_{\text{ms-txz}} = 3\xi_{\text{ms-tx}}^2 + 3\xi_{\text{ms-tz}}^2 + 175t^2 \\
&\xi_{\text{ms-tyz}} = 3\xi_{\text{ms-ty}}^2 + 3\xi_{\text{ms-tz}}^2 + 175t^2
\end{aligned}
$$

$$
\begin{aligned}
\zeta_{\text{asx-tx}} = &\frac{48\xi_{\text{ms-tx}}\left(129\xi_{\text{ms-tx}}^2 + 129\xi_{\text{ms-tz}}^2 + 175t^2\right)}{3\xi_{\text{ms-tx}}^2 + 3\xi_{\text{ms-tz}}^2 + 175t^2} \\
&+ \frac{48\xi_{\text{ms-tx}}\left(129\xi_{\text{ms-tx}}^2 + 129\xi_{\text{ms-ty}}^2 + 175t^2\right)}{3\xi_{\text{ms-tx}}^2 + 3\xi_{\text{ms-ty}}^2 + 175t^2} \\
&+ \frac{192\xi_{\text{ms-tx}}\left(129\xi_{\text{ms-tx}}^2 + 175t^2\right)}{3\xi_{\text{ms-tx}}^2 + 175t^2}
\end{aligned}
\tag{5.14}
$$

$$
\begin{aligned}
\delta_{\text{y}} = &\frac{6\xi_{\text{ms-ty}}^3\xi_{\text{ms-txz}}\left(129\xi_{\text{ms-tx}}^2 + 129\xi_{\text{ms-tz}}^2 + 7700t^2\right)}{175\xi_{\text{ms-txy}}\xi_{\text{ms-tyz}}} \\
&+ \frac{6\xi_{\text{ms-ty}}\xi_{\text{ms-tx}}^2\xi_{\text{ms-txz}}\left(129\xi_{\text{ms-tz}}^2 + 3850t^2\right)}{175\xi_{\text{ms-txy}}\xi_{\text{ms-tyz}}} \\
&+ \frac{2\xi_{\text{ms-ty}}\xi_{\text{ms-txz}}\left(66t^2\xi_{\text{ms-tz}}^2 + 175t^4\right)}{\xi_{\text{ms-txy}}\xi_{\text{ms-tyz}}} \\
&+ \frac{774\xi_{\text{ms-ty}}^5\xi_{\text{ms-txz}}}{175\xi_{\text{ms-txy}}\xi_{\text{ms-tyz}}}
\end{aligned}
\tag{5.15}
$$

$$
\begin{aligned}
\zeta_{\text{asy-tx}} = &\frac{48\xi_{\text{ms-ty}}\left(129\xi_{\text{ms-ty}}^2 + 129\xi_{\text{ms-tz}}^2 + 175t^2\right)}{3\xi_{\text{ms-ty}}^2 + 3\xi_{\text{ms-tz}}^2 + 175t^2} \\
&+ \frac{48\xi_{\text{ms-ty}}\left(129\xi_{\text{ms-tx}}^2 + 129\xi_{\text{ms-ty}}^2 + 175t^2\right)}{3\xi_{\text{ms-tx}}^2 + 3\xi_{\text{ms-ty}}^2 + 175t^2} \\
&+ \frac{192\xi_{\text{ms-ty}}\left(129\xi_{\text{ms-ty}}^2 + 175t^2\right)}{3\xi_{\text{ms-ty}}^2 + 175t^2}
\end{aligned}
\tag{5.16}
$$

$$
\begin{aligned}
\delta_{\text{z}} = &\frac{6\xi_{\text{ms-tz}}^3\xi_{\text{ms-txy}}\left(129\xi_{\text{ms-ty}}^2 + 129\xi_{\text{ms-tx}}^2 + 7700t^2\right)}{175\xi_{\text{ms-tyz}}\xi_{\text{ms-txz}}} \\
&+ \frac{6\xi_{\text{ms-tz}}\xi_{\text{ms-ty}}^2\xi_{\text{ms-txy}}\left(129\xi_{\text{ms-tx}}^2 + 3850t^2\right)}{175\xi_{\text{ms-tyz}}\xi_{\text{ms-txz}}} \\
&+ \frac{2\xi_{\text{ms-tz}}\xi_{\text{ms-txy}}\left(66t^2\xi_{\text{ms-tx}}^2 + 175t^4\right)}{\xi_{\text{ms-tyz}}\xi_{\text{ms-txz}}} \\
&+ \frac{774\xi_{\text{ms-tz}}^5\xi_{\text{ms-txy}}}{175\xi_{\text{ms-tyz}}\xi_{\text{ms-txz}}}
\end{aligned}
\tag{5.17}
$$

$$\begin{aligned}\zeta_{\text{asz-tx}} &= \frac{48\xi_{\text{ms-tz}}\left(129\xi_{\text{ms-tx}}^2+129\xi_{\text{ms-tz}}^2+175t^2\right)}{3\xi_{\text{ms-tx}}^2+3\xi_{\text{ms-tz}}^2+175t^2} \\ &+\frac{48\xi_{\text{ms-tz}}\left(129\xi_{\text{ms-tz}}^2+129\xi_{\text{ms-ty}}^2+175t^2\right)}{3\xi_{\text{ms-tz}}^2+3\xi_{\text{ms-ty}}^2+175t^2} \\ &+\frac{192\xi_{\text{ms-tz}}\left(129\xi_{\text{ms-tz}}^2+175t^2\right)}{3\xi_{\text{ms-tz}}^2+175t^2}\end{aligned} \tag{5.18}$$

Using Equations (5.14) – (5.18), the actuation forces, $\zeta_{\text{asx-tx}}$, $\zeta_{\text{asy-tx}}$ and $\zeta_{\text{asz-tx}}$, and the lost motions, δ_x, δ_y and δ_z, can be obtained when specific translational displacements of the MS, $\xi_{\text{ms-tx}}$, $\xi_{\text{ms-ty}}$ and $\xi_{\text{ms-tz}}$, are required. Furthermore, the primary translational displacements of the RLs, $\xi_{\text{asx-tx}}$, $\xi_{\text{asy-tx}}$ and $\xi_{\text{asz-tx}}$, can also be obtained according to Equation (5.4).

The derived nonlinear analytical models are applicable for any geometrical dimension and material. In order to verify the analytical models using FEA simulations, one can let the wire-beam length be 50mm, the cross sectional dimension of each wire-beam be 1mm×1mm, the dimension of the motion stage be 25mm × 25mm × 25mm, the Young's modulus of the selected material be 69000MPa, and the Poisson's ratio of the material be 0.33. Based on these predefined values of the parameters, the analytical results and the FEA results, in terms of the X_{ms}-axis actuation force and the X_{ms}-axis lost motion rate (represented by R_{lm}), can be seen in Figure 5.4, under the following actuation conditions: (a) $\xi_{\text{asx-tx}}$ varies from −0.05 to +0.05, $\xi_{\text{asy-tx}}$=0 and $\xi_{\text{asz-tx}}$=0, (b) $\xi_{\text{asx-tx}}$ varies from −0.05 to +0.05, $\xi_{\text{asy-tx}}$=0.05 and $\xi_{\text{asz-tx}}$=0, and (c) $\xi_{\text{asx-tx}}$ varies from −0.05 to +0.05, $\xi_{\text{asy-tx}}$=0.05 and $\xi_{\text{asz-tx}}$=0.05. The commercial software, COMSOL MULTIPHYSICS, is selected for the nonlinear FEA simulations, using the 10-node tetrahedral element and fine meshing technology.

Figure 5.4(a) shows that the analytical results and the FEA results of the X_{ms}-axis actuation force match very well, with less than 2.58% difference. Figure 5.4(b) illustrates that the maximum difference between the analytical results and the FEA results of the X_{ms}-axis lost motion rate is less than 12.18%, but the trend of

the analytical results of R_{lm} are the same as that of the FEA results of R_{lm}. The difference rises as cross-axis input displacements increase. It can also be seen that the maximum lost motion rate is less than 0.82%, which is tiny compared with the primary translation.

Based on the analytical models of the symmetric XYZ CPM, the lost motion rate and the X_{ms}-axis primary translation of the MS are analysed, the results of which can be seen in Figure 5.5. When $\xi_{asy\text{-}tx}= 0$ and $\xi_{asz\text{-}tx}= 0$, Figure 5.5(a) shows that the R_{lm} decreases with decreasing t and $\xi_{asx\text{-}tx}$. Figure 5.5(b) illustrates R_{lm} increases with increasing $\xi_{asx\text{-}tx}$, $\xi_{asy\text{-}tx}$ and $\xi_{asz\text{-}tx}$. The actuation force, $\zeta_{asx\text{-}tx}$, increases with increasing $\xi_{asy\text{-}tx}$ and $\xi_{asz\text{-}tx}$, which is shown in Figure 5.5(c). It can be derived that the actuation stiffness increases along the X_{ms}-axis, when the primary translations along the other directions increase.

A prototype of the symmetric XYZ CPM is shown in Figure 5.6 (the material and dimension of the prototype are the same as the FEA model). The fabrication of the prototype is described in Appendix G. The input displacements of the ASs of the prototype are actuated and measured by three micrometres, respectively. Additionally, the displacements of the MS along the X_{ms}- and Y_{ms}-axes are measured by two digital dial gauges with a resolution of 1μm (the displacement of the MS along the X_{ms}-axis is not measured).

The relationships of the input and output translations along the X-axis are experimentally tested on the prototype. The maximum difference between the experimental results and the analytical results is less than 0.52%, as shown in Figure 5.7. The difference mainly arises from analytical modelling, machining and assembly errors, as well as the undesired deformation of rigid linkages. It is hard to check how much the machining and assembly errors affect the experimental results, but it is sure that the experimental results are affected by the machining and assembly errors. The reason is that the bolted linkages can reduce the stiffness (It can be seen from [77] that stiffness can reduce by

approximately 30% by bolted linkages). If the rigid cubes and the RLs are made of a material with higher Young's modulus, the experimental results can match the analytical results better. It can also be observed from the experimental results that the cross-axis coupling rate and the lost motion are less than 0.13% and 0.63%, respectively.

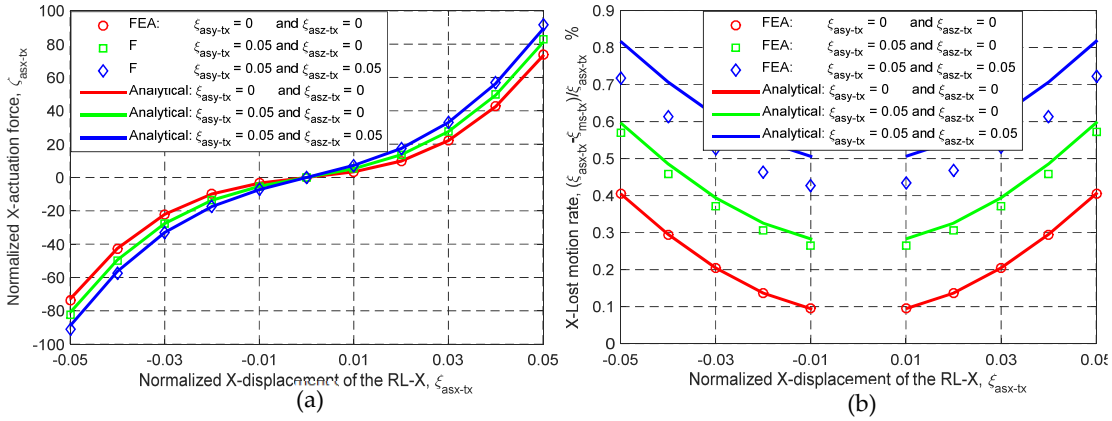

Figure 5.4 Comparison between the analytical results and the FEA results: (a) force-displacement relationship and (b) lost motion rate

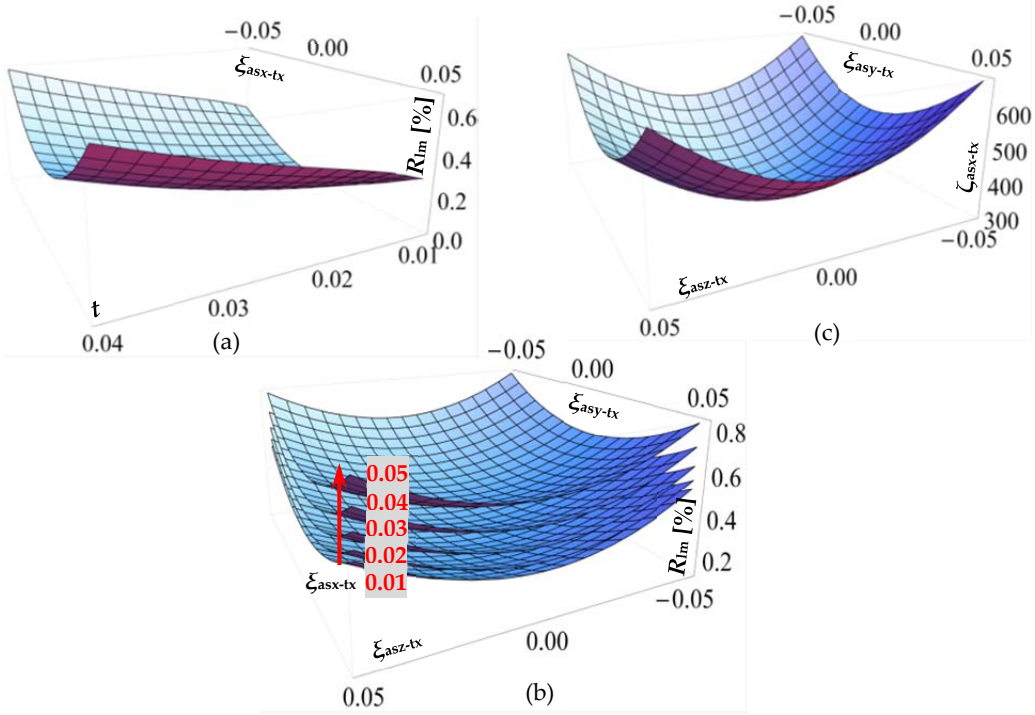

Figure 5.5 Analysis of lost motion and actuation force based on the analytical models: (a) lost motion rate (represented by R_{lm}) variation with ξ_{asx-tx} and t, when ξ_{asy-tx}= 0 and ξ_{asz-tx}= 0, (b) lost motion rate (represented by R_{lm}) variation with ξ_{asy-tx} and ξ_{asz-tx}, when ξ_{asx-tx} is equal to 0.01, 0.02, 0.03, 0.04 and 0.05, respectively, and (c) actuation force, ζ_{asx-tx}, variation with ξ_{asy-tx} and ξ_{asz-tx}, when ξ_{asx-tx}= 0

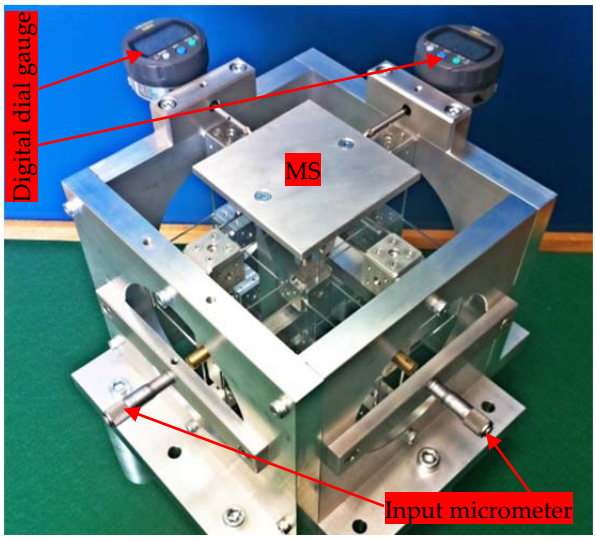

Figure 5.6 A prototype of the symmetric XYZ CPM

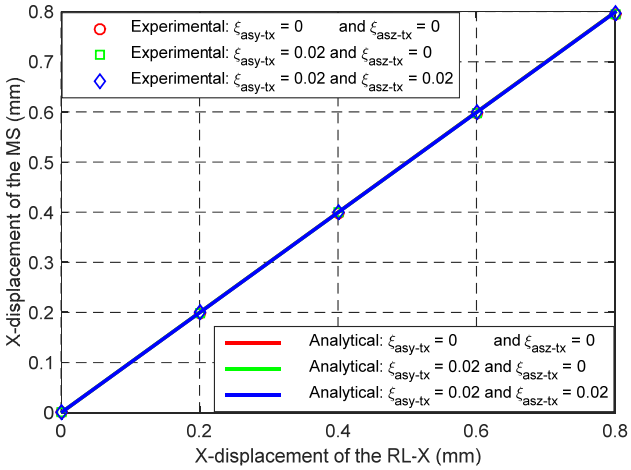

Figure 5.7 Relationship between the input displacement and the output displacement along the X_{ms}-axis

Compared with the XYZ CPM shown in Figure 5.1(a), the proposed XYZ CPM has reduced parasitic motions because of its symmetric configuration. Moreover, the lost motions and cross-axis coupling of the symmetric XYZ CPM are also reduced due to the three rigid linkages. Therefore, the XYZ CPM is an ideal candidate to build a high-precision XYZ positioning system. For a high-precision positioning system (such as nano-/micro-precision positioning system), a control system is always desired. In Appendix H, a semi-closed-loop control system is introduced for the prototype, with experimental tests. Note

that the asymmetric XYZ CPM shown in Figure 5.1(a) has less complex structure, so the asymmetric XYZ CPM is also a desirable candidate in some applications which are required to be manufactured easily.

5.3 Summary

A PSR-SCM approach is detailed in this chapter. The PSR-SCM approach can improve the motion characteristics of a non-symmetric compliant mechanism by reconfiguring the compliant mechanism into a symmetric compliant mechanism. The PSR-SCM approach reconfigures a non-symmetric compliant mechanism through replacing the compliant modules within their position spaces and adding a small number of redundant compliant modules, so that the non-symmetric compliant mechanism can be reconfigured into a symmetric compliant mechanism. The symmetric compliant mechanisms designed using the PSR-SCM approach are less over-constrained.

The basic procedure of the PSR-SCM approach has been presented. In order to demonstrate the PSR-SCM approach, a non-symmetric XYZ CPM is reconfigured into a symmetric XYZ CPM in this chapter. The designed symmetric XYZ CPM not only has minimized parasitic motions because of its symmetric structure, but also has minimized cross-axis coupling, reduced actuation stiffness and decreased lost motions.

6 DISCUSSION

The CPI synthesis approach, the CFB modelling approach and the PSR-based optimization approaches are newly proposed in this thesis. As a result, the main approaches, including the existing approaches, to the synthesis, modelling and optimization of XYZ CPMs can be listed below.

Synthesis approaches:

(a) The constraint-based synthesis approach,
(b) The screw-theory-based synthesis approach,
(c) The FACT synthesis approach,
(d) The rigid-body-replacement-based synthesis approach, and
(e) The CPI synthesis approach (proposed in this thesis).

Modelling approaches:

(a) The free-body-diagram (FBD)-based modelling approach,
(b) The energy-based modelling approach using the virtual work principle, and
(c) The CFB-based modelling approach (proposed in this thesis).

Optimization approaches:

(a) The stiffness-centre-based geometrical shape optimization approach,
(b) The geometrical dimension optimization approach, and
(c) The PSR-based geometrical shape and dimension optimization approaches (proposed in this thesis).

As mentioned in Chapter 1, the design process of a compliant mechanism is a combination of the synthesis, modelling and optimization. Therefore, in such a design process, one synthesis approach, one modelling approach and one optimization approach need to be selected from the associated approach lists, respectively. The combination of the CPI synthesis approach, the CFB modelling approach and the PSR-based optimization approaches can form a desirable process for designing XYZ CPMs, because, using these three approaches, both beginners and experts are able to design a variety of XYZ CPMs for different applications.

The advantages and disadvantages of the already existing approaches have been detailed in Chapter 1. This chapter shows how the proposed approaches overcome the challenges of the existing approaches, especially for designing XYZ CPMs. The main strengths and weaknesses of the proposed CPI synthesis approach, the CFB modelling approach and the PSR-based optimization approaches compared with the existing approaches are also discussed in this chapter. Furthermore, in this chapter, some possible combinations of the synthesis, modelling and optimization approaches, for designing other types of compliant mechanisms other than XYZ CPMs, are discussed. Additionally, the possible development of the proposed approaches is finally discussed in the end of this chapter.

Among the listed synthesis approaches, the rigid-body-replacement-based synthesis approach is mainly based on the development of rigid-body mechanisms. The rigid-body-replacement-based synthesis approach is a straightforward approach to synthesize compliant mechanisms. However, this approach heavily depends on the development of rigid-body mechanisms as well as design experience. The other synthesis approaches in the list, except for the rigid-body-replacement-based synthesis approach, are actually based on the following two concepts: (a) the mobility of a given rigid stage is determined by the locations and orientations of the constraint elements, such as wire-beams,

applied on it; and (b) one non-redundant 1-DOC constraint element removes one DOF from the given rigid stage.

Based on the concepts, the constraint-based synthesis approach can be used to synthesize any type of compliant mechanisms including XYZ CPMs. Using the constraint-based synthesis approach to synthesize a compliant mechanism, the designer needs to identify the locations and orientations of the selected constraint elements based on his/her design experience. Therefore, it is very hard to synthesize a variety of compliant mechanisms for different applications due to the design experience limitation. Because of this, the screw-theory-based synthesis approach and the FACT synthesis approach were proposed. The locations and orientations of constraint elements, in these two approaches, are derived by mathematical operations. Additionally, the locations and orientations of constraint elements are represented by screw vectors in the screw-theory-based synthesis approach and by geometrical shapes in the FACT synthesis approach. However, both the screw-theory-based synthesis approach and the FACT synthesis approach have their own limitations for the design of XYZ CPMs.

An XYZ CPM is a complex compliant mechanism, which includes several rigid stages and constraint elements. If using screw vectors to represent the locations and orientations of the constraint elements, the mathematical expression would be very complicated. The constraint elements used in the FACT approach are mainly wire-beams, because such a wire-beam provides the most basic constraint, and any constraint can be represented by a specific combination of wire-beams. Based on the FACT approach, one can visualize and determine the general shape of a compliant mechanism, through identifying the location and orientation of the wire-beams. The FACT approach is a desirable approach to synthesize compliant modules, but it is not a desirable approach to synthesize compliant mechanism systems such as XYZ CPMs because actuation coupling is not considered in the FACT approach.

The CPI synthesis approach proposed in this thesis decomposes an XYZ CPM into compliant modules. Moreover, the constraints and positions (including locations and orientations) of the compliant modules are derived using the screw theory. Additionally, the geometrical structures of the compliant modules can be identified using the FACT approach. Therefore, the CPI synthesis approach has the advantages of the screw-theory-based synthesis approach and the FACT synthesis approach. However, the CPI approach is limited to the synthesis of XYZ CPMs, which is the disadvantage of the CPI approach.

In order to further improve the motion characteristics of the XYZ CPMs synthesized using the synthesis approaches, the XYZ CPMs can be modelled and then optimized based on the models. The free-body-diagram (FBD)-based modelling approach and the energy-based modelling approach are mainly used approaches to model compliant mechanisms. However, these two modelling approaches are not ideal approaches to model complex compliant mechanisms such as XYZ CPMs due to their disadvantages. The energy-based modelling approach cannot take all internal geometrical parameters into account, the FBD-based nonlinear modelling approach needs to obtain the deformed configuration, and the FBD-based linear modelling approach cannot obtain results for large motion ranges. The CFB-based modelling approach proposed in this thesis can be employed to model a complex compliant mechanism such as an XYZ CPM linearly and nonlinearly, with consideration of all internal and external geometrical parameters. Moreover, when using the CFB-based modelling approach to model a compliant mechanism, the deformed configuration is not needed. Additionally, the mathematical expression of the CFB-based modelling approach can be understood easily. Therefore, the proposed CFB-based modelling approach is an ideal approach to model XYZ CPMs.

Based on the analytical models of an XYZ CPM, the XYZ CPM can be optimized to have minimized parasitic motions, reduced cross-axis coupling and decreased lost motions. The PSR-based optimization approaches proposed in this thesis can optimize both the geometrical shape and the geometrical dimension of a compliant mechanism including an XYZ CPM simultaneously, which is the main advantage of the PSR-based optimization approaches over the Stiffness-centre-based optimization approach and the geometrical dimension optimization approach.

As a result, the combination of the CPI synthesis approach, the CFB modelling approach and the PSR-based optimization approaches can form a desirable design process of XYZ CPMs. However, this combination is limited to the design of XYZ CPMs, which is its main disadvantage. Additionally, using this design process to design an XYZ CPM, the other synthesis approaches are also needed to synthesize the associated compliant modules.

For designing other types of compliant mechanisms, the CFB modelling approach and the PSR-based optimization approaches are also applicable and desirable. Unlike these approaches, the CPI synthesis approach can be employed to synthesize only XYZ CPMs. However, the CPI synthesis approach can be extended to synthesize all types of compliant mechanisms. For example, if the CPI synthesis approach is extended to synthesize XY CPMs, the following works should be done: (a) obtaining the topological structure of the basic XY CPM, (b) identifying the possible permitted constraints (or constraint spaces) of the associated compliant modules, and (c) identifying the possible permitted positions (or position spaces) of the compliant modules. Based on the derived topological structure, constraint spaces and position spaces, a great number of XY CPMs can be designed with diverse structures for different applications. It can be seen that similar work has been described for the synthesis of XYZ CPMs. Therefore, following the similar way, the CPI synthesis approach can be

extended to synthesize all types of compliant mechanisms. The development of the CPI approach is my future work.

7 CONCLUSIONS AND FUTURE WORK

7.1 Conclusions

This thesis focuses mainly on the design of compliant mechanisms, especially XYZ CPMs. Such a design requires a combination of type synthesis, analytical modelling and structure optimization. Therefore, the CPI synthesis approach, the CFB modelling approach and the PSR-based optimization approaches (PSR-RPM and PSR-SCM) have been presented and applied in this thesis. The proposed approaches form the main contributions of this thesis.

Three-legged XYZ CPMs are basic XYZ CPMs. In the CPI approach, a three-legged XYZ CPM is decomposed into compliant modules (AM-X, AM-Y, AM-Z, PM-X, PM-Y and PM-Z) and rigid stages (MS, AS-X, AS-Y, AS-Z, BS-X, BS-Y and BS-Z). The topological structure of the compliant modules and rigid stages has been obtained. This shows the interconnection of the compliant modules and rigid stages. Moreover, the constraint spaces of the compliant modules have been derived based on screw theory. When each of the compliant modules selects one possible permitted constraint from the constraint spaces, the compliant modules can be obtained in different geometrical forms, and can be placed in different positions. The possible permitted geometrical forms of the compliant modules can be derived using existing approaches such as the FACT approach. The derivation of the position spaces of the compliant modules is also presented in the CPI approach. Therefore, a large number of three-legged XYZ CPMs can be synthesized through connecting the compliant modules to the rigid stages, based on the topological structure of the three-legged XYZ

CPM, the geometrical forms and the position spaces of the compliant modules.

Additionally, XYZ CPMs, with more than three-legs, can be obtained through adding redundant legs to three-legged XYZ CPMs. XYZ CPMs, synthesized using the CPI approach, can provide decoupled translations, can be actuated by ground-mounted linear actuators, and can also provide a diversity of geometrical shapes for different applications.

A compliant module can provide elastic forces due to its deformation. Such an elastic force is defined as a variable constraint force in the CFB approach. In addition, the CFB approach defines an external force as a constant constraint force. The variable constraint forces produced by a BCM can be derived based on the previously obtained force-displacement relationship of the BCM. Any one NBCM can be decomposed into BCMs and rigid linkages. Therefore, the variable constraint forces produced by a NBCM can be obtained based on the variable constraint forces produced by the associated BCMs. In the CFB approach, a complex compliant mechanism (the complex compliant mechanism can be an XYZ CPM) can be decomposed into BCMs and/or NBCMs. When the complex compliant mechanism is in a state of equilibrium under the influence of some constant constraint forces (or external forces), the analytical model of the complex compliant mechanism can be derived based on the variable and constant constraint forces, using the CFB approach. The CFB approach can model compliant mechanisms (including XYZ CPMs) both linearly and nonlinearly. The derived analytical model of a compliant mechanism can be used to estimate the motion characteristics of the compliant mechanism.

As stated, a compliant module in a compliant mechanism has many possible permitted positions within its position space. Using the proposed PSR approach, a compliant mechanism can be reconfigured by rearranging the positions of the associated compliant modules within their position spaces. Such a reconfiguration of a compliant mechanism can be used to improve the motion

characteristics of the compliant mechanism. In this thesis, two PSR-based approaches, the PSR-RPM and PSR-SCM approaches, are proposed. The PSR-RPM is employed to reduce parasitic motions of compliant mechanisms. In order to improve the motion characteristics of a non-symmetric compliant mechanism, the PSR-SCM can be used to reconfigure the non-symmetric compliant mechanism into a symmetric compliant mechanism.

In order to simplify the derivation of position spaces, compliant modules must be ICMs, in the PSR-RPM approach. The parasitic motions of a compliant mechanism are modelled by taking the position spaces of the ICMs into account. Based on the models of the parasitic motions, the optimized positions of the ICMs can be derived, and then a new compliant mechanism with reduced parasitic motions is obtained through placing the ICMs at the optimized positions.

In the PSR-SCM approach, a non-symmetric compliant mechanism is decomposed into compliant modules and rigid stages. This decomposition is mainly based on designers' experience, so that a symmetric compliant mechanism can be obtained through rearranging the positions of the compliant modules, with the addition of a small number of redundant compliant modules.

Compared with existing optimization approaches, the PSR-based approaches (PSR-RPM and PSR-SCM approaches) can optimize a compliant mechanism by adding a small number of redundant compliant modules, and can consider both the geometrical dimension and shape of the compliant mechanism simultaneously. Note that the PSR, PSR-RPM and PSR-SCM approaches can be used to optimize any compliant mechanisms that include XYZ CPMs.

In this thesis, the principles of the proposed approaches have been presented, and the procedures of the approaches have been introduced and demonstrated by case studies. The case studies are also verified by FEA simulations and/or experimental tests. Several decoupled XYZ CPMs, with different structures,

have been synthesized using the CPI approach. These synthesized XYZ CPMs can be fabricated monolithically using a CNC milling machine. One of synthesized XYZ CPMs has also been modelled using the CFB approach and optimized using the PSR-RPM approach. The sum of the parasitic rotations of the optimized XYZ CPM is shown to be reduced by approximately 50%. Additionally, a non-symmetric XYZ CPM has been reconfigured into a symmetric XYZ CPM using the PSR-SCM approach. The symmetric XYZ CPM has desirable motion characteristics due to its symmetric structure and minimized over-constraints. A prototype of this symmetric XYZ CPM was fabricated, and an open-loop control system has also been presented for the prototype.

7.2 Future Work

The CFB approach and the PSR-based optimization approaches can be used to model and optimize all compliant mechanisms, including XYZ CPMs. However, the CPI approach focuses on the synthesis of XYZ CPMs. Therefore, it would be desirable to extend the CPI approach to the synthesis of other types of compliant mechanisms.

In this thesis, compliant mechanisms are modelled using the CFB approach without taking the dynamic effects into account. In the future, such dynamic effects will be considered in the CFB approach.

The PSR-based optimization approaches, as proposed in this thesis, are used to reduce parasitic motions of compliant mechanisms and to reconfigure a non-symmetric compliant mechanism into a symmetric compliant mechanism. One part of the future work being considered is to use the PSR approach to improve other motion characteristics, such as cross-axis coupling and lost motions, of a compliant mechanism. Additionally, it will not be required that the compliant modules in the PSR-RPM approach must be ICMs, so that more optimized designs can be obtained. Furthermore, position space identification in the PSR-

SCM approach will be based on a mathematical tool, rather than mainly on design experience.

The manufacture and nonlinear control of compliant mechanisms will also form part of the future work building on the foundation provided by this thesis.

This page is intentionally left blank.

REFERENCES

[1] R. V. Jones, "Instruments and experiences: papers on measurement and instrument design," *Wiley Series in Measurement Science and Technology, Chichester, New York: Wiley, 1988*, vol. 1, 1988.

[2] A. G. Erdman, and G. N. Sandor, *Mechanism design (3rd ed.): analysis and synthesis (Vol. 1)*, New Jersey, USA: Prentice-Hall, Inc., 1997.

[3] L. L. Howell, *Compliant mechanisms*, New York: John Wiley & Sons, 2001.

[4] N. Lobontiu, *Compliant mechanisms: design of flexure hinges*: CRC press, 2002.

[5] S. T. Smith, *Foundations of ultra-precision mechanism design*, Philadelphia: Gordon and Breach Science Publishers, 2003.

[6] J. J. Uicker, G. R. Pennock, and J. E. Shigley, *Theory of machines and mechanisms*: Oxford University Press Oxford, 2011.

[7] L. L. Howell, *Handbook of compliant mechanisms*, New York: John Wiley & Sons, 2013.

[8] D. Kim, D. Y. Lee, and D. G. Gweon, "A new nano-accuracy AFM system for minimizing Abbe errors and the evaluation of its measuring uncertainty," *Ultramicroscopy,* vol. 107, no. 4–5, pp. 322–328, 2007.

[9] G. Schitter, P. J. Thurner, and P. K. Hansma, "Design and input-shaping control of a novel scanner for high-speed atomic force microscopy," *Mechatronics*, vol. 18, pp. 282–288, 2008.

[10] L. Clark, B. Shirinzadeh, Y. Tian, and B. Yao, "Development of a passive compliant mechanism for measurement of micro/nano-scale planar three DOF motions," *IEEE/ASME Transactions on Mechatronics*, no. 99, pp. 1222-1232, 10.1109/TMECH.2015.2503728, 2015.

[11] M. L. Culpepper, and G. Anderson, "Design of a low-cost nano-manipulator which utilizes a monolithic, spatial compliant mechanism," *Precision Engineering*, vol. 28, no. 4, pp. 469–482, 2004.

[12] J. J. Gorman, and N. G. Dagalakis, "Force control of linear motor stages for microassembly," in ASME International Mechanical Engineering Conference and Exposition, Washington, D.C., 2003, pp. 615–623.

[13] J. Hesselbach, A. Raatz, and H. Kunzmann, "Performance of pseudo-elastic flexure hinges in parallel robots for micro-assembly tasks," *CIRP Annals - Manufacturing Technology,* vol. 53, no. 1, pp. 329–332, 2004.

[14] T. R. Hicks, and P. D. Atherton, *The nanopositioning book: Moving and measuring to better than a nanometre*: Queensgate Instruments Limited, 2000.

[15] H. Kozuka, J. Arata, K. Okuda, A. Onaga, M. Ohno, A. Sano, and H. Fujimoto, "A bio-inspired compliant parallel mechanism for high-precision robots," in IEEE International Conference on Robotics and Automation (ICRA), 2012, pp. 3122-3127.

[16] Y. Li, and Q. Xu, "A totally decoupled piezo-driven XYZ flexure parallel micropositioning stage for micro/nanomanipulation," *IEEE Transactions on Automation Science and Engineering,* vol. 8, no. 2, pp. 265–279, 2011.

[17] J. Yu, S. Bi, G. Zong, and X. Liu, "On the design of compliant-based micro-motion manipulators with a nanometer range resolution," in IEEE/ASME International Conference on Advanced Intelligent Mechatronics, Banff, Alberta, Canada, 2003, pp. 149-154.

[18] Y. K. Yong, S. O. R. Moheimani, B. J. Kenton, and K. K. Leang, "Invited review article: high-speed flexure-guided nanopositioning: mechanical design and control issues," *Review of Scientific Instruments,* vol. 83, no. 12, pp. 121101, 2012.

[19] M. L. Culpepper, S.-C. Chen, and S. Korb, "Design and manufacture of monolithic, 3D compliant mechanisms for nanomanipulation equipment," *Proceedings of the ASPE, Orlando*, pp. 1-4, 2004.

[20] S. Awtar, "Synthesis and analysis of parallel kinematic XY flexure mechanisms," PhD thesis, Mechanical Engineering, Massachusetts Institute of Technology, 2003.

[21] L. Zhou, A. E. Marras, H.-J. Su, and C. E. Castro, "DNA origami compliant nanostructures with tunable mechanical properties," *ACS Nano,* vol. 8, no. 1, pp. 27-34, 2014.

[22] S. Kota, J. Joo, Z. Li, S. Rodgers, and J. Sniegowski, "Design of compliant mechanisms: applications to MEMS," *Analog Integrated Circuits and Signal Processing,* vol. 29, no. 1–2, pp. 7–15, 10.1023/A:1011265810471, 2001.

[23] B. Krijnen, and D. M. Brouwer, "Flexures for large stroke electrostatic actuation in MEMS," *Journal of Micromechanics and Microengineering,* vol. 24, no. 1, pp. 015006, 2014.

[24] L. Prandi, C. Caminada, L. Coronato, G. Cazzaniga, F. Biganzoli, R. Antonello, and R. Oboe, "A low-power 3-axis digital-output MEMS gyroscope with single drive and multiplexed angular rate readout," in Solid-State Circuits Conference Digest of Technical Papers (ISSCC), 2011 IEEE International, 2011, pp. 104-106.

[25] N. Tolou, V. A. Henneken, and J. L. Herder, "Statically balanced compliant micro mechanisms (SB-MEMS): Concepts and simulation," in ASME International Design Engineering Technical Conferences & Computers and Information in Engineering Conference, Montreal, Quebec, Canada, 2010, pp. 447-454.

[26] G. M. Rebeiz, "RF MEMS switches: status of the technology," in 12th International Conference on Transducers, Solid-State Sensors, Actuators and Microsystems, 2003, pp. 1726-1729.

[27] M. L. C. d. Laat, H. H. P. Garza, J. L. Herder, and M. K. Ghatkesar, "A review on in situ stiffness adjustment methods in MEMS," *Journal of Micromechanics and Microengineering,* vol. 26, no. 6, pp. 063001, 2016.

[28] B. Krijnen, D. M. Brouwer, L. Abelmann, and J. L. Herder, "Vacuum behavior and control of a MEMS stage with integrated thermal displacement sensor," *Sensors and Actuators A: Physical,* vol. 234, pp. 321-330, 2015.

[29] B. Ando, S. Baglio, C. Trigona, N. Dumas, L. Latorre, and P. Nouet, "Nonlinear mechanism in MEMS devices for energy harvesting applications," *Journal of Micromechanics and Microengineering,* vol. 20, no. 12, pp. 125020, 2010.

[30] R. L. Harne, and K. W. Wang, "A review of the recent research on vibration energy harvesting via bistable systems," *Smart Materials and Structures,* vol. 22, no. 2, pp. 023001, 2013.

[31] P. D. Mitcheson, E. M. Yeatman, G. K. Rao, A. S. Holmes, and T. C. Green, "Energy harvesting from human and machine motion for wireless electronic devices," *Proceedings of the IEEE,* vol. 96, no. 9, pp. 1457-1486, 10.1109/JPROC.2008.927494, 2008.

[32] R. Andosca, T. G. McDonald, V. Genova, S. Rosenberg, J. Keating, C. Benedixen, and J. Wu, "Experimental and theoretical studies on MEMS piezoelectric vibrational energy harvesters with mass loading," *Sensors and Actuators A: Physical,* vol. 178, pp. 76-87, 2012.

[33] Z. Gao, and D. Zhang, "Design, analysis and fabrication of a multidimensional acceleration sensor based on fully decoupled compliant parallel mechanism," *Sensors and Actuators A: Physical,* vol. 163, no. 1, pp. 418-427, 2010.

[34] M. Boudaoud, and S. Régnier, "An overview on gripping force measurement at the micro and nano-scales using two-fingered microrobotic systems," *International Journal of Advanced Robotic Systems*, 2014, 46400, 2014.

[35] C. J. Rupp, A. Evgrafov, K. Maute, and M. L. Dunn, "Design of piezoelectric energy harvesting systems: a topology optimization approach based on multilayer plates and shells," *Journal of Intelligent Material Systems and Structures,* vol. 20, no. 16, pp. 1923-1939, 2009.

[36] M. I. Frecker, R. Powell Km Fau - Haluck, and R. Haluck, "Design of a multifunctional compliant instrument for minimally invasive surgery," *Journal of Biomechanical Engineering*, pp. 990-993, 2005.

[37] E. Sung, J. A. H. Slocum, R. Ma, J. F. Bean, and M. L. Culpepper, "Design of an ankle rehabilitation device using compliant mechanisms," *Journal of Medical Devices,* vol. 5, no. 1, pp. 011001, 10.1115/1.4002901, 2011.

[38] G. Chen, and S. Zhang, "Fully-compliant statically-balanced mechanisms without prestressing assembly: concepts and case studies," *Mechanical Sciences,* vol. 2, no. 2, pp. 169-174, 2011.

[39] S. Jun, X. Zhou, D. K. Ramsey, and V. N. Krovi, "Smart knee brace design with parallel coupled compliant plate mechanism and pennate elastic band spring," *Journal of Mechanisms and Robotics,* vol. 7, no. 4, pp. 041024, 2015.

[40] J. P. Khatait, D. M. Brouwer, J. P. Meijaard, R. G. K. M. Aarts, and J. L. Herder, "Flexible multibody modeling of a surgical instrument inside an endoscope," *Journal of Computational and Nonlinear Dynamics,* vol. 9, no. 1, pp. 011018, 10.1115/1.4026059, 2013.

[41] J. Mattheijer, J. L. Herder, G. J. M. Tuijthof, and E. R. Valstar, "Docking robustness of patient specific surgical guides for joint replacement surgery," *Journal of Mechanical Design,* vol. 137, no. 6, pp. 062301, 2015.

[42] L. A. Shaw, and J. B. Hopkins, "A shape-controlled compliant microarchitectured material," in ASME 2015 International Design Engineering Technical Conferences and Computers and Information in Engineering Conference, Boston, USA, 2015, pp. V05AT08A010.

[43] B. Haghpanah, H. Ebrahimi, D. Mousanezhad, J. Hopkins, and A. Vaziri, "Programmable elastic metamaterials," *Advanced Engineering Materials*, pp. 643-649, 10.1002/adem.201500295, 2015.

[44] S. Kota, R. Osborn, G. Ervin, D. Maric, P. Flick, and D. Paul, "Mission adaptive compliant wing–design, fabrication and flight test," in RTO Applied Vehicle Technology Panel (AVT) Symposium, 2009.

[45] M. Santer, and S. Pellegrino, "Concept and design of a multistable plate structure," *Journal of Mechanical Design,* vol. 133, no. 8, pp. 081001, 2011.

[46] P. Ghabezi, and M. Golzar, "Mechanical analysis of trapezoidal corrugated composite skins," *Applied Composite Materials,* vol. 20, no. 4, pp. 341-353, 10.1007/s10443-012-9267-6, 2012.

[47] M. Goldfarb, and N. Celanovic, "A flexure-based gripper for small-scale manipulation," *Robotica,* vol. 17, no. 02, pp. 181-187, 1999.

[48] F. Lotti, and G. Vassura, "A novel approach to mechanical design of articulated fingers for robotic hands," in IEEE/RSJ International Conference on Intelligent Robots and Systems, 2002, pp. 1687-1692.

[49] R. T. Schroer, M. J. Boggess, R. J. Bachmann, R. D. Quinn, and R. E. Ritzmann, "Comparing cockroach and Whegs robot body motions," in 2004 IEEE International Conference on Robotics and Automation, 2004, pp. 3288-3293.

[50] M. Hafez, M. D. Lichter, and S. Dubowsky, "Optimized binary modular reconfigurable robotic devices," *IEEE/ASME Transactions on Mechatronics,* vol. 8, no. 1, pp. 18-25, 10.1109/TMECH.2003.809156, 2003.

[51] R. J. Wood, "The first takeoff of a biologically inspired at-scale robotic insect," *IEEE Transactions on Robotics,* vol. 24, no. 2, pp. 341-347, 10.1109/TRO.2008.916997, 2008.

[52] J. B. Hopkins, J. Rivera, C. Kim, and G. Krishnan, "Synthesis and analysis of soft parallel robots comprised of active constraints," *Journal of Mechanisms and Robotics,* vol. 7, no. 1, pp. 011002, 10.1115/1.4029324, 2015.

[53] S. Perai, "Methodology of compliant mechanisms and its current developments in applications: a review," *American Journal of Applied Sciences,* vol. 4, no. 3, pp. 160-167, 2007.

[54] R. V. Jones, and I. R. Young, "Some parasitic deflexions in parallel spring movements," *Journal of Scientific Instruments,* vol. 33, no. 1, pp. 11, 1956.

[55] S. Awtar, and A. H. Slocum, "Constraint-based design of parallel kinematic XY flexure mechanisms," *Journal of Mechanical Design,* vol. 129, no. 8, pp. 816–830, 10.1115/1.2735342, 2006.

[56] S. Awtar, A. H. Slocum, and E. Sevincer, "Characteristics of beam-based flexure modules," *Journal of Mechanical Design,* vol. 129, no. 6, pp. 625–639, 10.1115/1.2717231, 2006.

[57] J. C. Maxwell, *The scientific papers of James Clerk Maxwell*, New York: Dover, 1890.

[58] D. L. Blanding, *Exact Constraint: Machine Design Using Kinematic Principles*, New York: ASME, 1999.

[59] L. C. Hale, "Principles and Techniques for Designing Precision Machines," PhD thesis, Massachusetts Institute of Technology, 1999.

[60] H. Su, "Mobility analysis of flexure mechanisms via screw algebra," *Journal of Mechanisms and Robotics,* vol. 3, no. 4, pp. 041010, 10.1115/1.4004910, 2011.

[61] H. Su, D. V. Dorozhkin, and J. M. Vance, "A screw theory approach for the conceptual design of flexible joints for compliant mechanisms," *Journal of Mechanisms and Robotics,* vol. 1, no. 4, pp. 041009, 2009.

[62] H. Su, and H. Tari, "On line screw systems and their application to flexure synthesis," *Journal of Mechanisms and Robotics,* vol. 3, no. 1, pp. 011009, 10.1115/1.4003078, 2011.

[63] H. Su, and C. Yue, "Type synthesis of freedom and constraint elements for design of flexure mechanisms," *Mechanical Sciences,* vol. 4, no. 2, pp. 263–277, 10.5194/ms-4-263-2013, 2013.

[64] J. Yu, S. Li, H. Su, and M. L. Culpepper, "Screw theory based methodology for the deterministic type synthesis of flexure mechanisms," *Journal of Mechanisms and Robotics,* vol. 3, no. 3, pp. 031008, 10.1115/1.4004123, 2011.

[65] C. Yue, Y. Zhang, H. Su, and X. Kong, "Type synthesis of three-degree-of-freedom translational compliant parallel mechanisms," *Journal of Mechanisms and Robotics,* vol. 7, no. 3, pp. 031012, 10.1115/1.4028758, 2015.

[66] J. B. Hopkins, and M. L. Culpepper, "Synthesis of multi-degree of freedom, parallel flexure system concepts via freedom and constraint

topology (FACT)-Part I: principles," *Precision Engineering,* vol. 34, no. 2, pp. 259–270, 2010.

[67] J. B. Hopkins, and M. L. Culpepper, "Synthesis of multi-degree of freedom, parallel flexure system concepts via freedom and constraint topology (FACT)-Part II: practice," *Precision Engineering,* vol. 34, no. 2, pp. 271–278, 2010.

[68] G. I. N. Rozvany, "Topology optimization in structural mechanics," *Structural and Multidisciplinary Optimization,* vol. 21, no. 2, pp. 89-89, 2014, 10.1007/s001580050173, 2014.

[69] S. R. Deepak, M. Dinesh, D. K. Sahu, and G. Ananthasuresh, "A comparative study of the formulations and benchmark problems for the topology optimization of compliant mechanisms," *Journal of Mechanisms and Robotics,* vol. 1, no. 1, pp. 011003, 2009.

[70] M. Frecker, G. Ananthasuresh, S. Nishiwaki, N. Kikuchi, and S. Kota, "Topological synthesis of compliant mechanisms using multi-criteria optimization," *Journal of Mechanical design,* vol. 119, no. 2, pp. 238-245, 1997.

[71] A. Saxena, "Topology design of large displacement compliant mechanisms with multiple materials and multiple output ports," *Structural and Multidisciplinary Optimization,* vol. 30, no. 6, pp. 477-490, 2005, 10.1007/s00158-005-0535-z, 2005.

[72] A. Saxena, and G. K. Ananthasuresh, "On an optimal property of compliant topologies," *Structural and Multidisciplinary Optimization,* vol. 19, no. 1, pp. 36-49, 10.1007/s001580050084, 2000.

[73] M. P. Bendsoe, and O. Sigmund, *Topology optimization: theory, methods, and applications*: Springer Science & Business Media, 2013.

[74] L. Cao, A. T. Dolovich, A. L. Schwab, J. L. Herder, and W. Zhang, "Toward a unified design approach for both compliant mechanisms and rigid-body mechanisms: module optimization," *Journal of Mechanical Design*, vol. 137, no. 12, pp. 122301, 10.1115/1.4031294, 2015.

[75] M. D. Murphy, A. Midha, and L. L. Howell, “The topological synthesis of compliant mechanisms,” *Mechanism and Machine Theory,* vol. 31, no. 2, pp. 185-199, 1996.

[76] E. G. Arthur, and G. N. Sandor, "Mechanism design analysis and synthesis," Ney Jersey: Prentice-Hall International, Inc, 1994.

[77] G. Hao, “Towards the design of monolithic decoupled XYZ compliant parallel mechanisms for multi-function applications,” *Mechanical Sciences,* vol. 4, pp. 291–302, 2013.

[78] G. Hao, X. Kong, and R. L. Reuben, “A nonlinear analysis of spatial compliant parallel modules: multi-beam modules,” *Mechanism and Machine Theory,* vol. 46, no. 5, pp. 680–706, 2011.

[79] S. Sen, and S. Awtar, “A closed-form nonlinear model for the constraint characteristics of symmetric spatial beams,” *Journal of Mechanical Design,* vol. 135, no. 3, pp. 031003, 10.1115/1.4023157, 2013.

[80] G. Hao, and X. Kong, “Design and modeling of a large-range modular XYZ compliant parallel manipulator using identical spatial modules,” *Journal of Mechanisms and Robotics,* vol. 4, no. 2, pp. 021009, 10.1115/1.4006188, 2012.

[81] G. Hao, and X. Kong, “Nonlinear analytical modeling and characteristic analysis of symmetrical wire beam based composite compliant parallel modules for planar motion,” *Mechanism and Machine Theory,* vol. 77, no. 0, pp. 122–147, 2014.

[82] L. L. Howell, A. Midha, and T. W. Norton, “Evaluation of equivalent spring stiffness for use in a pseudo-rigid-body model of large-deflection compliant mechanisms,” *Journal of Mechanical Design,* vol. 118, no. 1, pp. 126–131, 10.1115/1.2826843, 1996.

[83] G. Chen, and F. Ma, “Kinetostatic modeling of fully compliant bistable mechanisms using timoshenko beam constraint model,” *Journal of Mechanical Design,* vol. 137, no. 2, pp. 022301, 10.1115/1.4029024, 2015.

[84] Y. Yue, F. Gao, X. Zhao, and Q. Jeffrey Ge, "Relationship among input-force, payload, stiffness and displacement of a 3-DOF perpendicular parallel micro-manipulator," *Mechanism and Machine Theory,* vol. 45, no. 5, pp. 756–771, 2010.

[85] S. Sen, "Beam constraint model: Generalized nonlinear closed-form modeling of beam flexures for flexure mechanism design," PhD thesis, University of Michigan, 2013.

[86] G. Hao, M. Murphy, and X. Luo, "Development of a compliant-mechanism-based compact three-axis force sensor for high-precision manufacturing," in ASME 2015 International Design Engineering Technical Conferences and Computers and Information in Engineering Conference, 2015, pp. V009T07A082.

[87] S. Awtar, J. Ustick, and S. Sen, "An XYZ parallel-kinematic flexure mechanism with geometrically decoupled degrees of freedom," *Journal of Mechanisms and Robotics,* vol. 5, no. 1, pp. 015001, 10.1115/1.4007768, 2012.

[88] Y. K. Yong, and S. R. Moheimani, "A compact XYZ scanner for fast atomic force microscopy in constant force contact mode," in IEEE/ASME International Conference on Advanced Intelligent Mechatronics, 2010, pp. 225-230.

[89] G. Hao, "Simplified PRBMs of spatial compliant multi-beam modules for planar motion," *Mechanical Sciences,* vol. 4, pp. 311-318, 2013.

[90] N. Lobontiu, "Planar flexible hinges with curvilinear-axis segments for mechanisms of in-plane and out-of-plane operation," *Journal of Mechanical Design,* vol. 137, no. 1, pp. 012302, 10.1115/1.4028792, 2015.

[91] R. V. Jones, "Some uses of elasticity in instrument design," *Journal of Scientific instruments,* vol. 39, no. 5, pp. 193, 1962.

[92] S. T. Smith, *Flexures: elements of elastic mechanisms*, New York: Gordon and Breach Science Publishers, 2000.

[93] G. Hao, "A 2-legged XY parallel flexure motion stage with minimised parasitic rotation," *Proceedings of the Institution of Mechanical Engineers,*

Part C: Journal of Mechanical Engineering Science, vol. 228, no. 17, pp. 3156-3169, 2014.

[94] Z. Ni, D. Zhang, Y. Wu, Y. Tian, and M. Hu, "Analysis of parasitic motion in parallelogram compliant mechanism," *Precision Engineering,* vol. 34, no. 1, pp. 133–138, 2010.

[95] C. Yue, H. Su, and X. Kong, "Type synthesis of 3-dof translational compliant parallel mechanisms," in ASME International Design Engineering Technical Conferences, 2013.

[96] J. B. Hopkins, and M. L. Culpepper, "Synthesis of precision serial flexure systems using freedom and constraint topologies (FACT)," *Precision Engineering,* vol. 35, no. 4, pp. 638–649, 2011.

[97] J. B. Hopkins, "Design of parallel flexure systems via freedom and constraint topologies (FACT)," Master thesis, Massachusetts Institute of Technology, 2007.

[98] J. B. Hopkins, "Designing hybrid flexure systems and elements using freedom and constraint topologies," *Mechanical Sciences,* vol. 4, no. 2, pp. 319–331, 10.5194/ms-4-319-2013, 2013.

[99] G. Hao, and H. Li, "Design of 3-legged XYZ compliant parallel manipulators with minimised parasitic rotations [Online]," *Robotica,* vol. 33, no. 4, pp. 787-806, 2015.

[100] X. Kong, and C. M. Gosselin, *Type synthesis of parallel mechanisms*, Berlin Heidelberg: Springer-Verlag, 2007.

[101] G. Hao, and H. Li, "Conceptual designs of multi-degree of freedom compliant parallel manipulators composed of wire-beam based compliant mechanisms," *Proceedings of the Institution of Mechanical Engineers, Part C: Journal of Mechanical Engineering Science*, pp. 0954406214535925, 2014.

[102] J. S. Dai, and J. Rees Jones, "Interrelationship between screw systems and corresponding reciprocal systems and applications," *Mechanism and Machine Theory,* vol. 36, no. 5, pp. 633–651, 2001.

[103] S. Awtar, "Synthesis and analysis of parallel kinematic XY flexure mechanisms," PhD thesis, Massachusetts Institute of Technology, Cambridge, MA, 2004.

[104] G. Hao, "Cross-section considerations for wire-beam based translational compliant parallel manipulators," in The 31st International Manufacturing Conference, Cork, Ireland, 2014.

[105] J. Yu, S. Li, H.-j. Su, and M. L. Culpepper, "Screw theory based methodology for the deterministic type synthesis of flexure mechanisms," *Journal of Mechanisms and Robotics,* vol. 3, no. 3, pp. 031008, 10.1115/1.4004123, 2011.

[106] Y. Li, and Q. Xu, "Kinematic analysis and design of a new 3-DOF translational parallel manipulator," *Journal of Mechanical Design,* vol. 128, no. 4, pp. 729-737, 10.1115/1.2198254, 2005.

[107] J. S. Dai, D. Li, Q. Zhang, and G. Jin, "Mobility analysis of a complex structured ball based on mechanism decomposition and equivalent screw system analysis," *Mechanism and Machine Theory,* vol. 39, no. 4, pp. 445-458, 2004.

APPENDIX A: XYZ CPM WITH COUPLED PMS

The decomposition method used in this thesis is an effective way of analysing compliant modules of an XYZ CPM, which is suitable for designing most decoupled XYZ CPMs, with a consideration of actuator isolation. However, there is a limitation resulting from the decomposition assumption, as mentioned in Section 2.1 of Chapter 2. The assumption is that the PMs and AMs of an XYZ CPM are regarded as ICMs (independent compliant modules). Taking an AS which is constrained by one PM and one AM as an example, if the PM and the AM are ICMs, any one DOF of the AS can be constrained by the PM and/or the AM, but is not constrained by the combination of the PM and the AM. Due to this assumption, one type of decoupled XYZ CPMs cannot be synthesized using this CPI approach. These decoupled XYZ CPMs have the following characteristics: (a) the PMs in different legs are combined together to constraint a DOF of the MS, but any one of the PMs cannot resist the DOF. and/or (b) the AM and the PM in a leg are combined together to constrain a DOF of the AS, but the AM or the PM cannot resist the DOF of the AS separately. One specific example is shown below.

If two redundant constraint beams are added for each AM of the XYZ CPM as shown in Figure 2.13(c), the XYZ CPM-1 as demonstrated in Figure A. 1(a) can be obtained. The XYZ CPM-2 as illustrated in Figure A. 1(b) can be obtained by rotating the three PMs of the XYZ CPM-1 each by 45 degrees. The decoupled translations of the XYZ CPM-2 can be seen in Figure A. 1(c) – Figure A. 1(e).

Each of the PM in the XYZ CPM-2 system cannot constrain any one of the rotations of the MS of the XYZ CPM-2 about the X-, Y- and Z-axes with respect to the coordinate system O-XYZ. However, the combination of the three PMs can be resisted all the rotations of the MS. Therefore, the constraints of the PMs in XYZ CPM-2 system are not independent to each other.

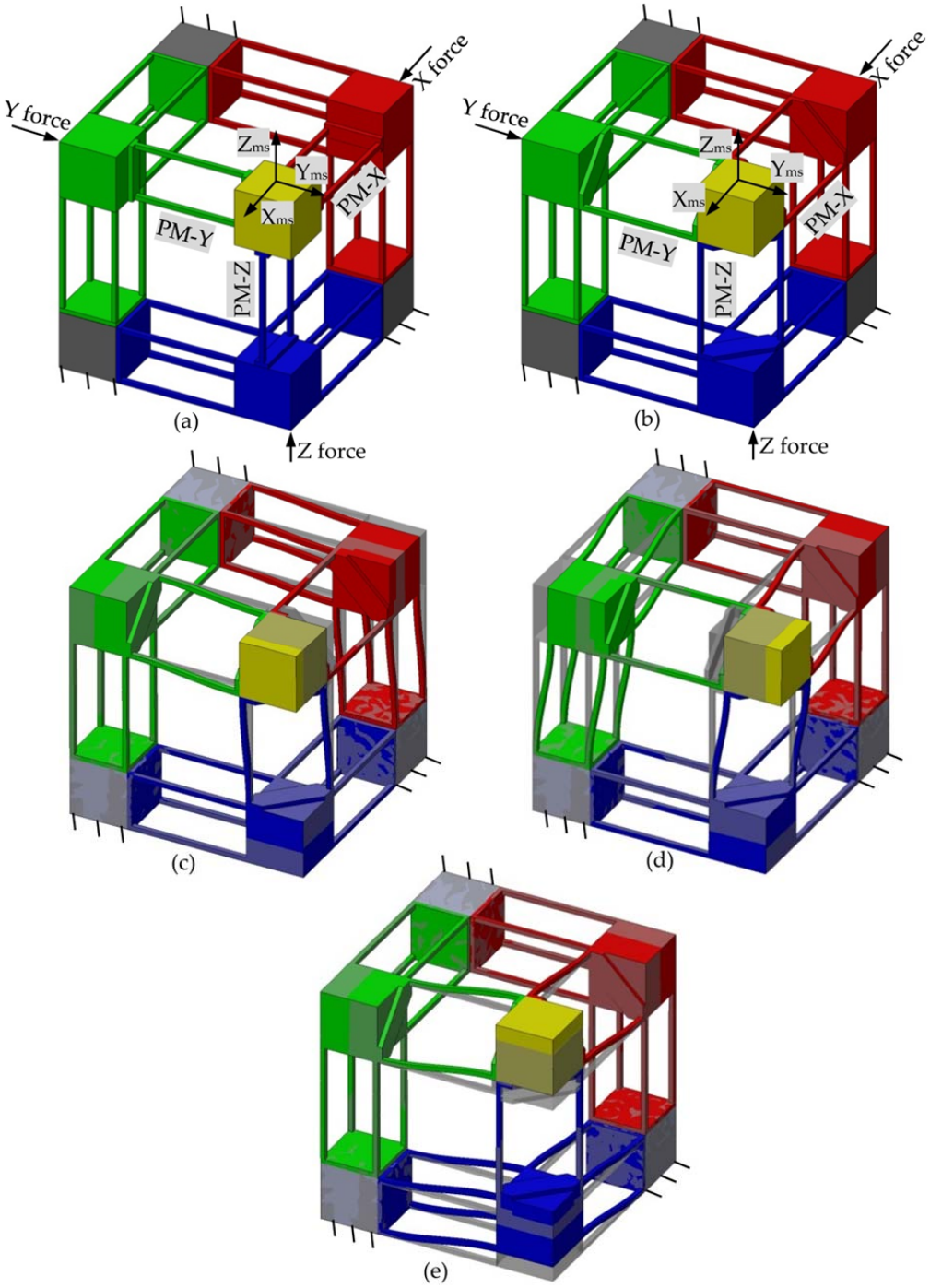

Figure A. 1 Decoupled XYZ CPM designs: (a) decoupled XYZ CPM-1, (b) decoupled XYZ CPM-2, (c) X direction motion of the decoupled XYZ CPM-2, (d) Y direction motion of the decoupled XYZ CPM-2, and (e) Z direction motion of the decoupled XYZ CPM-2

APPENDIX B: CONSTRAINT SPACES OF PMS AND AMS

B-constraint space is represented in Table B. 1, where T and R correspond to translational constraint and rotational constraint, respectively. The subscripts px, py and pz indicate the three PM local coordinate systems, and the subscripts ax, ay and az indicate the three AM local coordinate systems. The subscripts -tx, -ty and -tz represent the translational constraints along the three axes of each local coordinate system, and -rx, -ry and -rz indicate the rotational constraints about the three axes of each local coordinate system. The underlined rotational constraints can be transmitted from the AMs to the PMs.

The T-constraint space can be derived via transmitting some of the underlined rotational constraints from the AMs to PMs. The S-constraint space can be obtained through adding redundant rotational constraints to the AMs and PMs in the B-constraint space and T-constraint space. The B-constraint space, T-constraint space and S-constraint space form the constraint spaces of the compliant modules.

Table B. 1 B-constraint space

Comb-ination	Module	Constraints of the compliant modules in the three legs in the local coordinate systems		
		X	**Y**	**Z**
1	PMs	$T_{px\text{-}tx}R_{px\text{-}rx}R_{px\text{-}ry}R_{px\text{-}rz}$	$T_{py\text{-}tx}$	$T_{pz\text{-}tx}$
	AMs	$T_{ax\text{-}ty}T_{ax\text{-}tz}R_{ax\text{-}rx}R_{ax\text{-}ry}R_{ax\text{-}rz}$	$T_{ay\text{-}ty}T_{ay\text{-}tz}R_{ay\text{-}rx}R_{ay\text{-}ry}R_{ay\text{-}rz}$	$T_{az\text{-}ty}T_{az\text{-}tz}R_{az\text{-}rx}R_{az\text{-}ry}R_{az\text{-}rz}$
2	PMs	$T_{px\text{-}tx}R_{px\text{-}rx}R_{px\text{-}ry}$	$T_{py\text{-}tx}R_{py\text{-}rz}$	$T_{pz\text{-}tx}$
	AMs	$T_{ax\text{-}ty}T_{ax\text{-}tz}R_{ax\text{-}rx}R_{ax\text{-}ry}\underline{R_{ax\text{-}rz}}$	$T_{ay\text{-}ty}T_{ay\text{-}tz}\underline{R_{ay\text{-}rx}R_{ay\text{-}ry}}R_{ay\text{-}rz}$	$T_{az\text{-}ty}T_{az\text{-}tz}R_{az\text{-}rx}R_{az\text{-}ry}R_{az\text{-}rz}$
3	PMs	$T_{px\text{-}tx}R_{px\text{-}rx}R_{px\text{-}ry}$	$T_{py\text{-}tx}$	$T_{pz\text{-}tx}R_{pz\text{-}rx}$
	AMs	$T_{ax\text{-}ty}T_{ax\text{-}tz}R_{ax\text{-}rx}R_{ax\text{-}ry}\underline{R_{ax\text{-}rz}}$	$T_{ay\text{-}ty}T_{ay\text{-}tz}R_{ay\text{-}rx}R_{ay\text{-}ry}R_{ay\text{-}rz}$	$T_{az\text{-}ty}T_{az\text{-}tz}R_{az\text{-}rx}\underline{R_{az\text{-}ry}R_{az\text{-}rz}}$
4	PMs	$T_{px\text{-}tx}R_{px\text{-}rx}R_{px\text{-}rz}$	$T_{py\text{-}tx}R_{py\text{-}rx}$	$T_{pz\text{-}tx}$
	AMs	$T_{ax\text{-}ty}T_{ax\text{-}tz}R_{ax\text{-}rx}\underline{R_{ax\text{-}ry}}R_{ax\text{-}rz}$	$T_{ay\text{-}ty}T_{ay\text{-}tz}R_{ay\text{-}rx}\underline{R_{ay\text{-}ry}R_{ay\text{-}rz}}$	$T_{az\text{-}ty}T_{az\text{-}tz}R_{az\text{-}rx}R_{az\text{-}ry}R_{az\text{-}rz}$
5	PMs	$T_{px\text{-}tx}R_{px\text{-}rx}$	$T_{py\text{-}tx}R_{py\text{-}rx}R_{py\text{-}rz}$	$T_{pz\text{-}tx}$
	AMs	$T_{ax\text{-}ty}T_{ax\text{-}tz}R_{ax\text{-}rx}\underline{R_{ax\text{-}ry}R_{ax\text{-}rz}}$	$T_{ay\text{-}ty}T_{ay\text{-}tz}R_{ay\text{-}rx}\underline{R_{ay\text{-}ry}}R_{ay\text{-}rz}$	$T_{az\text{-}ty}T_{az\text{-}tz}R_{az\text{-}rx}R_{az\text{-}ry}R_{az\text{-}rz}$
6	PMs	$T_{px\text{-}tx}R_{px\text{-}rx}$	$T_{py\text{-}tx}R_{py\text{-}rx}$	$T_{pz\text{-}tx}R_{pz\text{-}rx}$
	AMs	$T_{ax\text{-}ty}T_{ax\text{-}tz}R_{ax\text{-}rx}\underline{R_{ax\text{-}ry}R_{ax\text{-}rz}}$	$T_{ay\text{-}ty}T_{ay\text{-}tz}R_{ay\text{-}rx}\underline{R_{ay\text{-}ry}R_{ay\text{-}rz}}$	$T_{az\text{-}ty}T_{az\text{-}tz}R_{az\text{-}rx}\underline{R_{az\text{-}ry}R_{az\text{-}rz}}$
7	PMs	$T_{px\text{-}tx}R_{px\text{-}rx}R_{px\text{-}rz}$	$T_{py\text{-}tx}$	$T_{pz\text{-}tx}R_{pz\text{-}ry}$
	AMs	$T_{ax\text{-}ty}T_{ax\text{-}tz}R_{ax\text{-}rx}\underline{R_{ax\text{-}ry}}R_{ax\text{-}rz}$	$T_{ay\text{-}ty}T_{ay\text{-}tz}R_{ay\text{-}rx}R_{ay\text{-}ry}R_{ay\text{-}rz}$	$T_{az\text{-}ty}T_{az\text{-}tz}\underline{R_{az\text{-}rx}}R_{az\text{-}ry}\underline{R_{az\text{-}rz}}$
8	PMs	$T_{px\text{-}tx}R_{px\text{-}rx}$	$T_{py\text{-}tx}R_{py\text{-}rz}$	$T_{pz\text{-}tx}R_{pz\text{-}ry}$
	AMs	$T_{ax\text{-}ty}T_{ax\text{-}tz}R_{ax\text{-}rx}\underline{R_{ax\text{-}ry}R_{ax\text{-}rz}}$	$T_{ay\text{-}ty}T_{ay\text{-}tz}\underline{R_{ay\text{-}rx}R_{ay\text{-}ry}}R_{ay\text{-}rz}$	$T_{az\text{-}ty}T_{az\text{-}tz}\underline{R_{az\text{-}rx}}R_{az\text{-}ry}\underline{R_{az\text{-}rz}}$
9	PMs	$T_{px\text{-}tx}R_{px\text{-}rx}$	$T_{py\text{-}tx}$	$T_{pz\text{-}tx}R_{pz\text{-}rx}R_{pz\text{-}ry}$

Comb-ination	Module	Constraints of the compliant modules in the three legs in the local coordinate systems		
		X	Y	Z
	AMs	$T_{ax\text{-}ty}T_{ax\text{-}tz}R_{ax\text{-}rx}\underline{R_{ax\text{-}ry}R_{ax\text{-}rz}}$	$T_{ay\text{-}ty}T_{ay\text{-}tz}R_{ay\text{-}rx}R_{ay\text{-}ry}R_{ay\text{-}rz}$	$T_{az\text{-}ty}T_{az\text{-}tz}R_{az\text{-}rx}R_{az\text{-}ry}\underline{R_{az\text{-}rz}}$
10	PMs	$T_{px\text{-}tx}R_{px\text{-}ry}R_{px\text{-}rz}$	$T_{py\text{-}tx}R_{py\text{-}ry}$	$T_{pz\text{-}tx}$
	AMs	$T_{ax\text{-}ty}T_{ax\text{-}tz}\underline{R_{ax\text{-}rx}}R_{ax\text{-}ry}R_{ax\text{-}rz}$	$T_{ay\text{-}ty}T_{ay\text{-}tz}\underline{R_{ay\text{-}rx}}R_{ay\text{-}ry}\underline{R_{ay\text{-}rz}}$	$T_{az\text{-}ty}T_{az\text{-}tz}R_{az\text{-}rx}R_{az\text{-}ry}R_{az\text{-}rz}$
11	PMs	$T_{px\text{-}tx}R_{px\text{-}ry}$	$T_{py\text{-}tx}R_{py\text{-}ry}R_{py\text{-}rz}$	$T_{pz\text{-}tx}$
	AMs	$T_{ax\text{-}ty}T_{ax\text{-}tz}\underline{R_{ax\text{-}rx}}R_{ax\text{-}ry}\underline{R_{ax\text{-}rz}}$	$T_{ay\text{-}ty}T_{ay\text{-}tz}\underline{R_{ay\text{-}rx}}R_{ay\text{-}ry}R_{ay\text{-}rz}$	$T_{az\text{-}ty}T_{az\text{-}tz}R_{az\text{-}rx}R_{az\text{-}ry}R_{az\text{-}rz}$
12	PMs	$T_{px\text{-}tx}R_{px\text{-}ry}$	$T_{py\text{-}tx}R_{py\text{-}ry}$	$T_{pz\text{-}tx}R_{pz\text{-}rx}$
	AMs	$T_{ax\text{-}ty}T_{ax\text{-}tz}\underline{R_{ax\text{-}rx}}R_{ax\text{-}ry}\underline{R_{ax\text{-}rz}}$	$T_{ay\text{-}ty}T_{ay\text{-}tz}\underline{R_{ay\text{-}rx}}R_{ay\text{-}ry}\underline{R_{ay\text{-}rz}}$	$T_{az\text{-}ty}T_{az\text{-}tz}R_{az\text{-}rx}\underline{R_{az\text{-}ry}R_{az\text{-}rz}}$
13	PMs	$T_{px\text{-}tx}R_{px\text{-}rz}$	$T_{py\text{-}tx}R_{py\text{-}rx}R_{py\text{-}ry}$	$T_{pz\text{-}tx}$
	AMs	$T_{x\text{-}ty}T_{x\text{-}tz}\underline{R_{x\text{-}rx}R_{x\text{-}ry}}R_{x\text{-}rz}$	$T_{ay\text{-}ty}T_{ay\text{-}tz}R_{ay\text{-}rx}R_{ay\text{-}ry}\underline{R_{ay\text{-}rz}}$	$T_{az\text{-}ty}T_{az\text{-}tz}R_{az\text{-}rx}R_{az\text{-}ry}R_{az\text{-}rz}$
14	PMs	$T_{px\text{-}tx}$	$T_{py\text{-}tx}R_{py\text{-}rx}R_{py\text{-}ry}R_{py\text{-}rz}$	$T_{pz\text{-}tx}$
	AMs	$T_{ax\text{-}ty}T_{ax\text{-}tz}R_{ax\text{-}rx}R_{ax\text{-}ry}R_{ax\text{-}rz}$	$T_{ay\text{-}ty}T_{ay\text{-}tz}R_{ay\text{-}rx}R_{ay\text{-}ry}R_{ay\text{-}rz}$	$T_{az\text{-}ty}T_{az\text{-}tz}R_{az\text{-}rx}R_{az\text{-}ry}R_{az\text{-}rz}$
15	PMs	$T_{px\text{-}tx}$	$T_{py\text{-}tx}R_{py\text{-}rx}R_{py\text{-}ry}$	$T_{pz\text{-}tx}R_{pz\text{-}rx}$
	AMs	$T_{ax\text{-}ty}T_{ax\text{-}tz}R_{ax\text{-}rx}R_{ax\text{-}ry}R_{ax\text{-}rz}$	$T_{ay\text{-}ty}T_{ay\text{-}tz}R_{ay\text{-}rx}R_{ay\text{-}ry}\underline{R_{ay\text{-}rz}}$	$T_{az\text{-}ty}T_{az\text{-}tz}R_{az\text{-}rx}\underline{R_{az\text{-}ry}R_{az\text{-}rz}}$
16	PMs	$T_{px\text{-}tx}R_{px\text{-}rz}$	$T_{py\text{-}tx}R_{py\text{-}ry}$	$T_{pz\text{-}tx}R_{pz\text{-}ry}$
	AMs	$T_{ax\text{-}ty}T_{ax\text{-}tz}\underline{R_{ax\text{-}rx}R_{ax\text{-}ry}}R_{ax\text{-}rz}$	$T_{ay\text{-}ty}T_{ay\text{-}tz}\underline{R_{ay\text{-}rx}}R_{ay\text{-}ry}\underline{R_{ay\text{-}rz}}$	$T_{az\text{-}ty}T_{az\text{-}tz}\underline{R_{az\text{-}rx}}R_{az\text{-}ry}\underline{R_{az\text{-}rz}}$
17	PMs	$T_{px\text{-}tx}$	$T_{py\text{-}tx}R_{py\text{-}ry}R_{py\text{-}rz}$	$T_{pz\text{-}tx}R_{pz\text{-}ry}$
	AMs	$T_{ax\text{-}ty}T_{ax\text{-}tz}\underline{R}_{ax\text{-}rx}\underline{R}_{ax\text{-}ry}\underline{R}_{ax\text{-}rz}$	$T_{ay\text{-}ty}T_{ay\text{-}tz}\underline{R_{ay\text{-}rx}}R_{ay\text{-}ry}R_{ay\text{-}rz}$	$T_{az\text{-}ty}T_{az\text{-}tz}\underline{R_{az\text{-}rx}}R_{az\text{-}ry}\underline{R_{az\text{-}rz}}$
18	PMs	$T_{px\text{-}tx}$	$T_{py\text{-}tx}R_{py\text{-}ry}$	$T_{pz\text{-}tx}R_{pz\text{-}rx}R_{pz\text{-}ry}$
	AMs	$T_{ax\text{-}ty}T_{ax\text{-}tz}R_{ax\text{-}rx}R_{ax\text{-}ry}R_{ax\text{-}rz}$	$T_{ay\text{-}ty}T_{ay\text{-}tz}\underline{R_{ay\text{-}rx}}R_{ay\text{-}ry}\underline{R_{ay\text{-}rz}}$	$T_{az\text{-}ty}T_{az\text{-}tz}R_{az\text{-}rx}R_{az\text{-}ry}\underline{R_{az\text{-}rz}}$
19	PMs	$T_{px\text{-}tx}R_{px\text{-}ry}R_{px\text{-}rz}$	$T_{py\text{-}tx}$	$T_{pz\text{-}tx}R_{pz\text{-}rz}$
	AMs	$T_{ax\text{-}ty}T_{ax\text{-}tz}\underline{R_{ax\text{-}rx}}R_{ax\text{-}ry}R_{ax\text{-}rz}$	$T_{ay\text{-}ty}T_{ay\text{-}tz}R_{ay\text{-}rx}R_{ay\text{-}ry}R_{ay\text{-}rz}$	$T_{az\text{-}ty}T_{az\text{-}tz}\underline{R_{az\text{-}rx}R_{az\text{-}ry}}R_{az\text{-}rz}$
20	PMs	$T_{px\text{-}tx}R_{px\text{-}ry}$	$T_{py\text{-}tx}R_{py\text{-}rz}$	$T_{pz\text{-}tx}R_{pz\text{-}rz}$
	AMs	$T_{ax\text{-}ty}T_{ax\text{-}tz}\underline{R_{ax\text{-}rx}}R_{ax\text{-}ry}\underline{R_{ax\text{-}rz}}$	$T_{ay\text{-}ty}T_{ay\text{-}tz}\underline{R_{ay\text{-}rx}R_{ay\text{-}ry}}R_{ay\text{-}rz}$	$T_{az\text{-}ty}T_{az\text{-}tz}\underline{R_{az\text{-}rx}R_{az\text{-}ry}}R_{az\text{-}rz}$
21	PMs	$T_{px\text{-}tx}R_{px\text{-}ry}$	$T_{py\text{-}tx}$	$T_{pz\text{-}tx}R_{pz\text{-}rx}R_{pz\text{-}rz}$
	AMs	$T_{ax\text{-}ty}T_{ax\text{-}tz}\underline{R_{ax\text{-}rx}}R_{ax\text{-}ry}\underline{R_{ax\text{-}rz}}$	$T_{ay\text{-}ty}T_{ay\text{-}tz}R_{ay\text{-}rx}R_{ay\text{-}ry}R_{ay\text{-}rz}$	$T_{az\text{-}ty}T_{az\text{-}tz}R_{az\text{-}rx}\underline{R_{az\text{-}ry}}R_{az\text{-}rz}$
22	PMs	$T_{px\text{-}tx}R_{px\text{-}rz}$	$T_{py\text{-}tx}R_{py\text{-}rx}$	$T_{pz\text{-}tx}R_{pz\text{-}rz}$
	AMs	$T_{ax\text{-}ty}T_{ax\text{-}tz}\underline{R_{ax\text{-}rx}R_{ax\text{-}ry}}R_{ax\text{-}rz}$	$T_{ay\text{-}ty}T_{ay\text{-}tz}R_{ay\text{-}rx}\underline{R_{ay\text{-}ry}R_{ay\text{-}rz}}$	$T_{az\text{-}ty}T_{az\text{-}tz}\underline{R_{az\text{-}rx}R_{az\text{-}ry}}R_{az\text{-}rz}$
23	PMs	$T_{px\text{-}tx}$	$T_{py\text{-}tx}R_{py\text{-}rx}R_{py\text{-}rz}$	$T_{pz\text{-}tx}R_{pz\text{-}rz}$
	AMs	$T_{ax\text{-}ty}T_{ax\text{-}tz}R_{ax\text{-}rx}R_{ax\text{-}ry}R_{ax\text{-}rz}$	$T_{ay\text{-}ty}T_{ay\text{-}tz}R_{ay\text{-}rx}\underline{R_{ay\text{-}ry}}R_{ay\text{-}rz}$	$T_{az\text{-}ty}T_{az\text{-}tz}\underline{R_{az\text{-}rx}R_{az\text{-}ry}}R_{az\text{-}rz}$
24	PMs	$T_{px\text{-}tx}$	$T_{py\text{-}tx}R_{py\text{-}rx}$	$T_{pz\text{-}tx}R_{pz\text{-}rx}R_{pz\text{-}rz}$
	AMs	$T_{ax\text{-}ty}T_{ax\text{-}tz}R_{ax\text{-}rx}R_{ax\text{-}ry}R_{ax\text{-}rz}$	$T_{ay\text{-}ty}T_{ay\text{-}tz}R_{ay\text{-}rx}\underline{R_{ay\text{-}ry}R_{ay\text{-}rz}}$	$T_{az\text{-}ty}T_{az\text{-}tz}R_{az\text{-}rx}\underline{R_{az\text{-}ry}}R_{az\text{-}rz}$
25	PMs	$T_{px\text{-}tx}R_{px\text{-}rz}$	$T_{py\text{-}tx}$	$T_{pz\text{-}tx}R_{pz\text{-}ry}R_{pz\text{-}rz}$
	AMs	$T_{ax\text{-}ty}T_{ax\text{-}tz}\underline{R_{ax\text{-}rx}R_{ax\text{-}ry}}R_{ax\text{-}rz}$	$T_{ay\text{-}ty}T_{ay\text{-}tz}R_{ay\text{-}rx}R_{ay\text{-}ry}R_{ay\text{-}rz}$	$T_{az\text{-}ty}T_{az\text{-}tz}\underline{R_{az\text{-}rx}}R_{az\text{-}ry}R_{az\text{-}rz}$
26	PMs	$T_{px\text{-}tx}$	$T_{py\text{-}tx}R_{py\text{-}rz}$	$T_{pz\text{-}tx}R_{pz\text{-}ry}R_{pz\text{-}rz}$
	AMs	$T_{ax\text{-}ty}T_{ax\text{-}tz}R_{ax\text{-}rx}R_{ax\text{-}ry}R_{ax\text{-}rz}$	$T_{ay\text{-}ty}T_{ay\text{-}tz}\underline{R_{ay\text{-}rx}R_{ay\text{-}ry}}R_{ay\text{-}rz}$	$T_{az\text{-}ty}T_{az\text{-}tz}\underline{R_{az\text{-}rx}}R_{az\text{-}ry}R_{az\text{-}rz}$
27	PMs	$T_{px\text{-}tx}$	$T_{py\text{-}tx}$	$T_{pz\text{-}tx}R_{pz\text{-}rx}R_{pz\text{-}ry}R_{pz\text{-}rz}$
	AMs	$T_{ax\text{-}ty}T_{ax\text{-}tz}R_{ax\text{-}rx}R_{ax\text{-}ry}R_{ax\text{-}rz}$	$T_{ay\text{-}ty}T_{ay\text{-}tz}R_{ay\text{-}rx}R_{ay\text{-}ry}R_{ay\text{-}rz}$	$T_{az\text{-}ty}T_{az\text{-}tz}R_{az\text{-}rx}R_{az\text{-}ry}R_{az\text{-}rz}$

APPENDIX C: NON-MONOLITHIC DECOUPLED XYZ CPMS

Based on the position space concept, each of the PMs in the XYZ CPM, as shown in Figure 2.17(a), can rotate as a whole about the X-axis of the PM local coordinate system. Figure C. 1(a) shows an XYZ CPM obtained by rotating the PMs of the XYZ CPM each by 45 degree about the X-axes of the PM local coordinate system. The decoupled translational motions of the XYZ CPM are derived using the FEA method, as demonstrated in Figure C. 1(b) – Figure C. 1(d). Another XYZ CPM illustrated in Figure C. 2 can be designed by rotating the PM-X of the XYZ CPM shown in Figure 2.17(a) at 90 degrees about the X-axis of the PM local coordinate system.

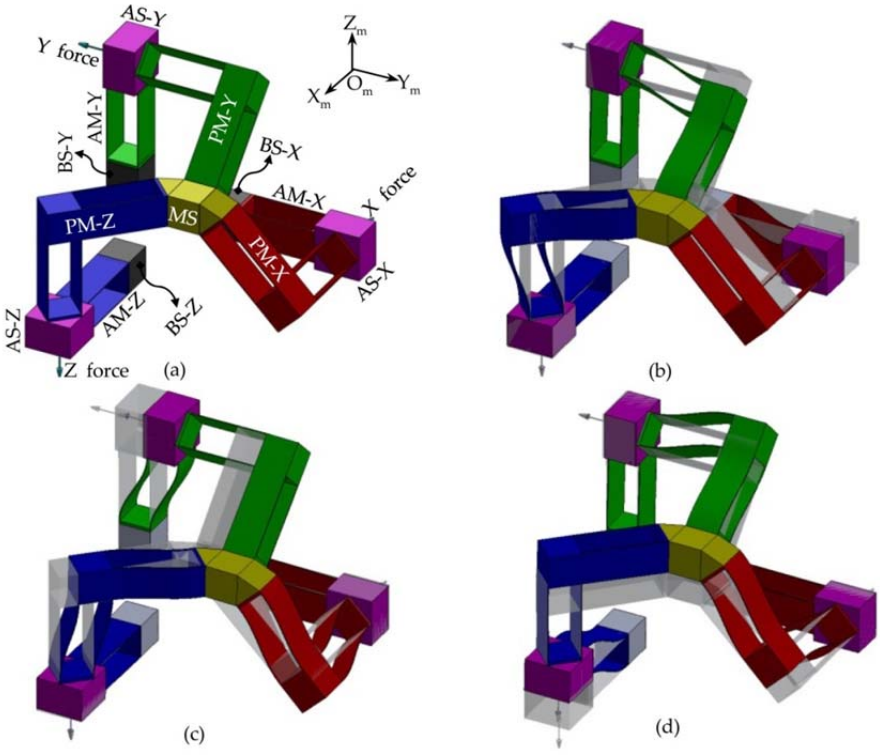

Figure C. 1 An XYZ CPM with PMs of the XYZ CPM shown in Fig. 17(a) rotated by 45 degrees about the X-axes of the PM local coordinate systems: (a) XYZ CPM without motion, (b) X motion only, (c) Y motion only, and (d) Z motion only

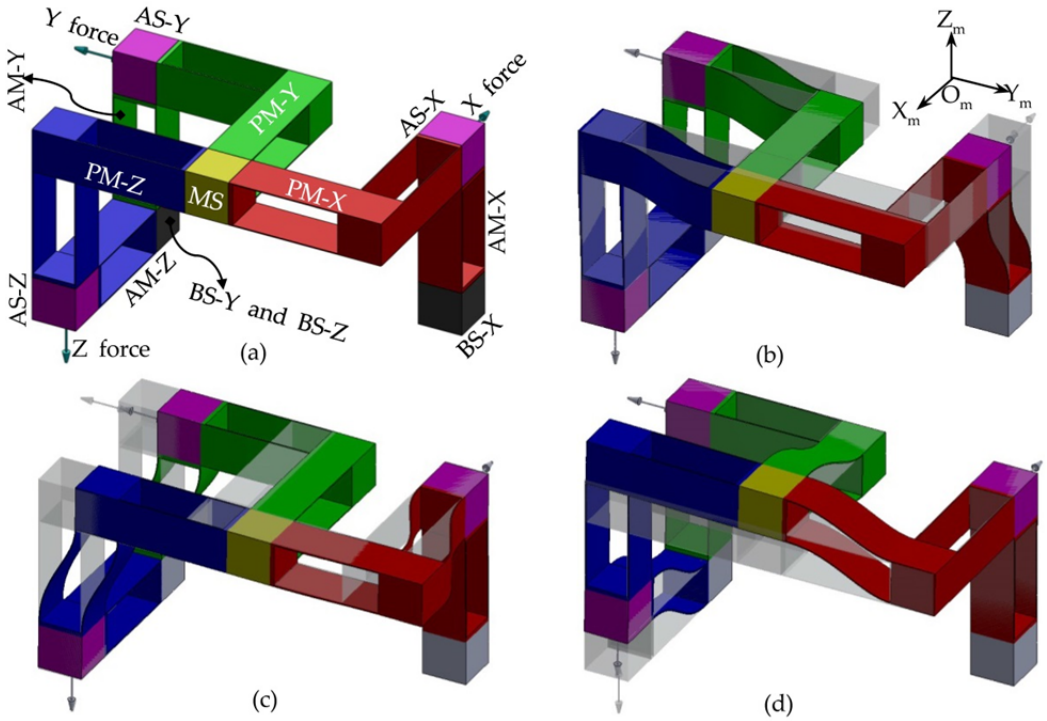

Figure C. 2 An XYZ CPM with PM-X of the XYZ CPM shown in Fig. 17(a) rotated by 90 degrees about the X-axis of the PM local coordinate system: (a) XYZ CPM without translations, (b) X translation only, (c) Y translation only, and (d) Z translation only

APPENDIX D: COUPLED XYZ CPM

The CPI approach does not focus on designing coupled XYZ CPMs, but a number of coupled XYZ CPMs can be obtained through making appropriate modifications to the decoupled XYZ CPMs synthesized using the CPI approach. The modification is usually based on the position space concept, with one typical example demonstrated below.

Figure D. 1(a) shows a decoupled XYZ CPM, which is also illustrated in Figure 2.17(a). If the decoupled XYZ CPM is decomposed into one motion stage (MS) and three legs, each of the legs has three translational DOF along the X-, Y- and Z-axes of the coordinate system O-XYZ. Therefore, each of the legs can constrain the three rotational DOF of the MS. Based on the method of identifying the position space of a compliant module, as studied in Section 2.3 of Chapter 2, each of the legs can freely rotate and translate along and about the X-, Y- and Z-axes without affecting the MS's three-axis translations. However, in order to make the MS controllable by the three actuation forces to have a spatial motion, the directions of any two of the three actuation forces cannot be parallel or collinear. This is as a result of the fact that when any two actuation forces are parallel or collinear, there is at least one leg to be redundant.

Consequently, the coupled XYZ CPM shown in Figure D. 1(b) is obtained by rotating the three legs about the specific axes, through the following steps: the Leg-X rotates about the Z-axis by −45 degrees and then rotates about the Y-axis by −45 degrees; the Leg-Y rotates about the X-axis by 45 degrees and then rotates about the Y-axis by 45 degrees; and the Leg-Z rotates about the Y-axis by −45 degrees and then rotates about the X-axis by −45 degrees. These rotations result in coupled actuation forces for the MS's motion. When only one of the three forces is applied, the MS will translate along the X-, Y- and Z-axes at the same time, as represented in Figure D. 1(c) – Figure D. 1(e). When actuation forces along the Y- and Z-axes are applied, the motions of the MS can be seen in

Figure D. 1(f). In other words, if only one of the three motions along the X-, Y- and Z-axes is needed, the three forces should be exerted simultaneously.

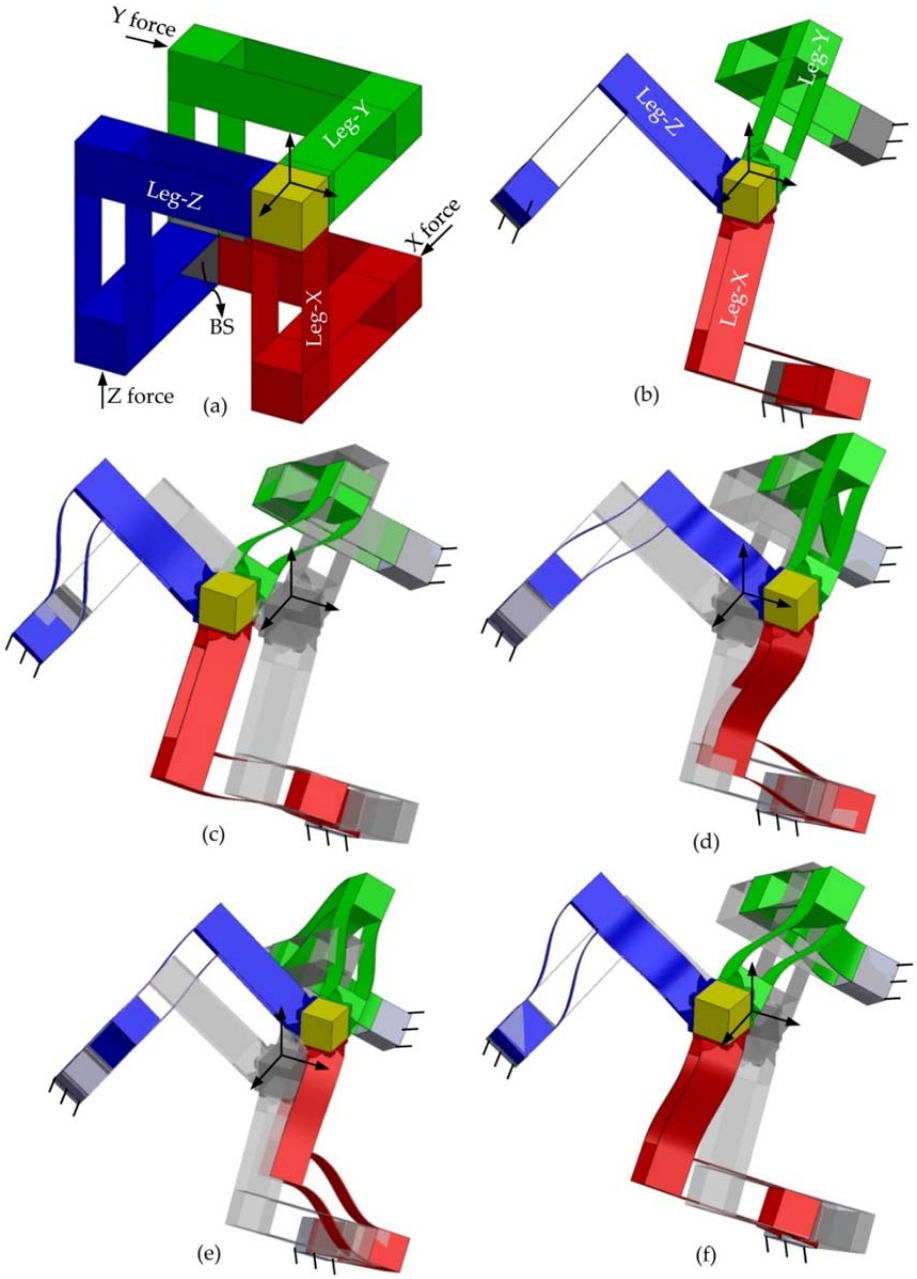

Figure D. 1 A coupled XYZ CPM designed via some appropriate modification on the decoupled XYZ CPM, as shown in Figure 2.17(a): (a) the decoupled XYZ CPM also shown in Figure 2.17(a), (b) the coupled XYZ CPM, (c) X-axis actuation force applied only, (d) Y-axis actuation force applied only, (e) Z-axis actuation force applied only, and (f) actuation forces along the X- and Y-axes both applied

APPENDIX E: TRANSFORMATION MATRICES

$$\mathbf{T}_{\text{pax-pmx}} = \begin{bmatrix} 1 & 0 & 0 & 0 & 0 & 0 \\ 0 & 1 & 0 & 0 & 0 & 0 \\ 0 & 0 & 1 & 0 & 0 & 0 \\ 0 & \xi_{\text{m-tz}} & -\xi_{\text{m-ty}} & 1 & 0 & 0 \\ -\xi_{\text{m-tz}} & 0 & -\xi_{\text{asx-tx}} + \xi_{\text{m-tx}} + 1 & 0 & 1 & 0 \\ \xi_{\text{m-ty}} & \xi_{\text{asx-tx}} - \xi_{\text{m-tx}} - 1 & 0 & 0 & 0 & 1 \end{bmatrix} \tag{E.1}$$

$$\mathbf{T}_{\text{pay-pmy}} = \begin{bmatrix} 1 & 0 & 0 & 0 & 0 & 0 \\ 0 & 1 & 0 & 0 & 0 & 0 \\ 0 & 0 & 1 & 0 & 0 & 0 \\ 0 & \xi_{\text{m-tx}} & -\xi_{\text{m-tz}} & 1 & 0 & 0 \\ -\xi_{\text{m-tx}} & 0 & -\xi_{\text{asy-tx}} + \xi_{\text{m-ty}} + 1 & 0 & 1 & 0 \\ \xi_{\text{m-tz}} & \xi_{\text{asy-tx}} - \xi_{\text{m-ty}} - 1 & 0 & 0 & 0 & 1 \end{bmatrix} \tag{E.2}$$

$$\mathbf{T}_{\text{paz-pmz}} = \begin{bmatrix} 1 & 0 & 0 & 0 & 0 & 0 \\ 0 & 1 & 0 & 0 & 0 & 0 \\ 0 & 0 & 1 & 0 & 0 & 0 \\ 0 & \xi_{\text{m-ty}} & -\xi_{\text{m-tx}} & 1 & 0 & 0 \\ -\xi_{\text{m-ty}} & 0 & -\xi_{\text{asz-tx}} + \xi_{\text{m-tz}} + 1 & 0 & 1 & 0 \\ \xi_{\text{m-tx}} & \xi_{\text{asz-tx}} - \xi_{\text{m-tz}} - 1 & 0 & 0 & 0 & 1 \end{bmatrix} \tag{E.3}$$

$$\mathbf{T}_{\text{pmx-pax}} = \begin{bmatrix} 1 & 0 & 0 & 0 & 0 & 0 \\ 0 & 1 & 0 & 0 & 0 & 0 \\ 0 & 0 & 1 & 0 & 0 & 0 \\ 0 & -\xi_{\text{m-tz}} & \xi_{\text{m-ty}} & 1 & 0 & 0 \\ \xi_{\text{m-tz}} & 0 & \xi_{\text{asx-tx}} - \xi_{\text{m-tx}} - 1 & 0 & 1 & 0 \\ -\xi_{\text{m-ty}} & -\xi_{\text{asx-tx}} + \xi_{\text{m-tx}} + 1 & 0 & 0 & 0 & 1 \end{bmatrix} \tag{E.4}$$

$$\mathbf{T}_{\text{pmy-pay}} = \begin{bmatrix} 1 & 0 & 0 & 0 & 0 & 0 \\ 0 & 1 & 0 & 0 & 0 & 0 \\ 0 & 0 & 1 & 0 & 0 & 0 \\ 0 & -\xi_{\text{m-tx}} & \xi_{\text{m-tz}} & 1 & 0 & 0 \\ \xi_{\text{m-tx}} & 0 & \xi_{\text{asy-tx}} - \xi_{\text{m-ty}} - 1 & 0 & 1 & 0 \\ -\xi_{\text{m-tz}} & -\xi_{\text{asy-tx}} + \xi_{\text{m-ty}} + 1 & 0 & 0 & 0 & 1 \end{bmatrix} \tag{E.5}$$

$$\mathbf{T}_{\text{pmz-paz}} = \begin{bmatrix} 1 & 0 & 0 & 0 & 0 & 0 \\ 0 & 1 & 0 & 0 & 0 & 0 \\ 0 & 0 & 1 & 0 & 0 & 0 \\ 0 & -\xi_{\text{m-ty}} & \xi_{\text{m-tx}} & 1 & 0 & 0 \\ \xi_{\text{m-ty}} & 0 & \xi_{\text{asz-tx}} - \xi_{\text{m-tz}} - 1 & 0 & 1 & 0 \\ -\xi_{\text{m-tx}} & -\xi_{\text{asz-tx}} + \xi_{\text{m-tz}} + 1 & 0 & 0 & 0 & 1 \end{bmatrix} \tag{E.6}$$

$$\mathbf{T}_{\text{pmx-m}} = \begin{bmatrix} 1 & 0 & 0 & 0 & 0 & 0 \\ 0 & 1 & 0 & 0 & 0 & 0 \\ 0 & 0 & 1 & 0 & 0 & 0 \\ 0 & w/2 & 0 & 1 & 0 & 0 \\ -w/2 & 0 & w/2 & 0 & 1 & 0 \\ 0 & -w/2 & 0 & 0 & 0 & 1 \end{bmatrix} \tag{E.7}$$

$$\mathbf{T}_{\text{pmy-m}} = \begin{bmatrix} 0 & 0 & 1 & 0 & 0 & 0 \\ 1 & 0 & 0 & 0 & 0 & 0 \\ 0 & 1 & 0 & 0 & 0 & 0 \\ w/2 & -w/2 & 0 & 0 & 0 & 1 \\ 0 & 0 & -w/2 & 1 & 0 & 0 \\ 0 & 0 & w/2 & 0 & 1 & 0 \end{bmatrix} \tag{E.8}$$

$$\mathbf{T}_{\text{pmz-m}} = \begin{bmatrix} 0 & 1 & 0 & 0 & 0 & 0 \\ 0 & 0 & 1 & 0 & 0 & 0 \\ 1 & 0 & 0 & 0 & 0 & 0 \\ 0 & 0 & w & 0 & 1 & 0 \\ 0 & -w & 0 & 0 & 0 & 1 \\ 0 & 0 & 0 & 1 & 0 & 0 \end{bmatrix} \tag{E.9}$$

$$\mathbf{T}_{\text{pax-asx}} = \begin{bmatrix} 1 & 0 & 0 & 0 & 0 & 0 \\ 0 & 1 & 0 & 0 & 0 & 0 \\ 0 & 0 & 1 & 0 & 0 & 0 \\ 0 & 0 & 0 & 1 & 0 & 0 \\ 0 & 0 & -w & 0 & 1 & 0 \\ 0 & w & 0 & 0 & 0 & 1 \end{bmatrix} \tag{E.10}$$

$$\mathbf{T}_{\text{pay-asy}} = \begin{bmatrix} 1 & 0 & 0 & 0 & 0 & 0 \\ 0 & 1 & 0 & 0 & 0 & 0 \\ 0 & 0 & 1 & 0 & 0 & 0 \\ 0 & 0 & 0 & 1 & 0 & 0 \\ 0 & 0 & -w & 0 & 1 & 0 \\ 0 & w & 0 & 0 & 0 & 1 \end{bmatrix} \tag{E.11}$$

$$\mathbf{T}_{\text{paz-asz}} = \begin{bmatrix} 1 & 0 & 0 & 0 & 0 & 0 \\ 0 & 1 & 0 & 0 & 0 & 0 \\ 0 & 0 & 1 & 0 & 0 & 0 \\ 0 & 0 & 0 & 1 & 0 & 0 \\ 0 & 0 & -w & 0 & 1 & 0 \\ 0 & w & 0 & 0 & 0 & 1 \end{bmatrix} \tag{E.12}$$

$$\mathbf{T}_{\text{amx-asx}} = \begin{bmatrix} 1 & 0 & 0 & 0 & 0 & 0 \\ 0 & 1 & 0 & 0 & 0 & 0 \\ 0 & 0 & 1 & 0 & 0 & 0 \\ 0 & 0 & 0 & 1 & 0 & 0 \\ 0 & 0 & -w/2 & 0 & 1 & 0 \\ 0 & w/2 & 0 & 0 & 0 & 1 \end{bmatrix} \tag{E.13}$$

$$\mathbf{T}_{\text{amy-asy}} = \begin{bmatrix} 1 & 0 & 0 & 0 & 0 & 0 \\ 0 & 1 & 0 & 0 & 0 & 0 \\ 0 & 0 & 1 & 0 & 0 & 0 \\ 0 & 0 & 0 & 1 & 0 & 0 \\ 0 & 0 & -w/2 & 0 & 1 & 0 \\ 0 & w/2 & 0 & 0 & 0 & 1 \end{bmatrix} \tag{E.14}$$

$$\mathbf{T}_{\text{amz-asz}} = \begin{bmatrix} 1 & 0 & 0 & 0 & 0 & 0 \\ 0 & 1 & 0 & 0 & 0 & 0 \\ 0 & 0 & 1 & 0 & 0 & 0 \\ 0 & 0 & 0 & 1 & 0 & 0 \\ 0 & 0 & -w/2 & 0 & 1 & 0 \\ 0 & w/2 & 0 & 0 & 0 & 1 \end{bmatrix} \tag{E.15}$$

where w is the edge length of the rigid stages, while $\xi_{\text{ms-tx}}$, $\xi_{\text{ms-ty}}$ and $\xi_{\text{ms-tz}}$ are used to represent the translations of the MS along the X_{ms}-, Y_{ms}- and Z_{ms}-axes,

respectively. Additionally, $\xi_{asx\text{-}tx}$, $\xi_{asy\text{-}tx}$ and $\xi_{asz\text{-}tx}$ represent the X-axis translational displacements of AS-X, AS-Y and AS-Z in their own local coordinate systems, respectively. The translations of the MS and the X-axis translations of the AS-X, AS-Y and AS-Z are the primary translations of the XYZ CPM. The other translations and rotations of the MS, AS-X, AS-Y and AS-Z are the parasitic motions of the XYZ CPM. The parasitic motions are much smaller than the primary translations, so the parasitic motions are not taken into account in the transformation matrices. If the $\xi_{ms\text{-}tx}$, $\xi_{ms\text{-}ty}$, $\xi_{ms\text{-}tz}$, $\xi_{asx\text{-}tx}$, $\xi_{asy\text{-}tx}$ and $\xi_{asz\text{-}tx}$, in the transformation matrices can be neglected, the transformation matrices above can be simplified to linear transformation matrices of the XYZ CPM corresponding to the un-deformed configuration of the XYZ CPM.

APPENDIX F: CONSTRAINT FORCE EQUILIBRIUM EQUATIONS

$$\zeta_{pmx-tx} = \frac{1680\left(5\left(\xi_{ms-tx}-\xi_{asx-tx}\right)+3\left(\left(\xi_{ms-ty}-\xi_{asx-ty}\right)^2+\left(\xi_{ms-tz}-\xi_{asx-tz}\right)^2\right)\right)}{3\left(\xi_{ms-ty}-\xi_{asx-ty}\right)^2+3\left(\xi_{ms-tz}-\xi_{asx-tz}\right)^2+175t^2} \tag{F.1}$$

$$\zeta_{pmx-ty} = \left(48\left(\xi_{m-ty}-\xi_{asx-ty}\right)\begin{pmatrix}210\left(\xi_{ms-tx}-\xi_{asx-tx}\right)+129\left(\xi_{ms-ty}-\xi_{asx-ty}\right)^2\\+129\left(\xi_{ms-tz}-\xi_{asx-tz}\right)^2+175t^2\end{pmatrix}\right)/\begin{pmatrix}3\left(\xi_{ms-ty}-\xi_{asx-ty}\right)^2\\+3\left(\xi_{ms-tz}-\xi_{asx-tz}\right)^2+175t^2\end{pmatrix} \tag{F.2}$$

$$\zeta_{pmx-tz} = \left(48\left(\xi_{ms-tz}-\xi_{asx-tz}\right)\begin{pmatrix}210\left(\xi_{ms-tx}-\xi_{asx-tx}\right)+129\left(\xi_{ms-ty}-\xi_{asx-ty}\right)^2\\+129\left(\xi_{ms-tz}-\xi_{asx-tz}\right)^2+175t^2\end{pmatrix}\right)/\begin{pmatrix}3\left(\xi_{ms-ty}-\xi_{asx-ty}\right)^2\\+3\left(\xi_{ms-tz}-\xi_{asx-tz}\right)^2+175t^2\end{pmatrix} \tag{F.3}$$

$$\zeta_{pmx-rx} = 4\begin{pmatrix}\delta\left(\xi_{ms-rx}-\xi_{asx-rx}\right)\left(3\left(\xi_{ms-ty}-\xi_{asx-ty}\right)^2+3\left(\xi_{ms-tz}-\xi_{asx-tz}\right)^2+175t^2\right)\\-210\left(5t^2-3tw+3w^2\right)\begin{pmatrix}\left(\xi_{ms-ry}-\xi_{asx-ry}\right)\left(\xi_{ms-ty}-\xi_{asx-ty}\right)\\+\left(\xi_{ms-rz}-\xi_{asx-rz}\right)\left(\xi_{ms-tz}-\xi_{asx-tz}\right)\end{pmatrix}\end{pmatrix}/\begin{pmatrix}3\left(\xi_{ms-ty}-\xi_{asx-ty}\right)^2\\+3\left(\xi_{ms-tz}-\xi_{asx-tz}\right)^2\\+175t^2\end{pmatrix} \tag{F.4}$$

$$\zeta_{pmx-ry} = 4\begin{pmatrix}175\left(4t^2-3tw+3w^2\right)\left(\xi_{ms-ry}-\xi_{asx-ry}\right)\\+6\left(\xi_{ms-tz}-\xi_{asx-tz}\right)\begin{pmatrix}35\left(\xi_{ms-tx}-\xi_{asx-tx}\right)+24\left(\xi_{ms-ty}-\xi_{asx-ty}\right)^2\\+24\left(\xi_{ms-tz}-\xi_{asx-tz}\right)^2+175t^2\end{pmatrix}\end{pmatrix}/\begin{pmatrix}3\left(\xi_{ms-ty}-\xi_{asx-ty}\right)^2\\+3\left(\xi_{ms-tz}-\xi_{asx-tz}\right)^2\\+175t^2\end{pmatrix} \tag{F.5}$$

$$\zeta_{pmx-rz} = 4\begin{pmatrix}175\left(4t^2-3tw+3w^2\right)\left(\xi_{ms-rz}-\xi_{asx-rz}\right)\\-6\left(\xi_{ms-ty}-\xi_{asx-ty}\right)\begin{pmatrix}35\left(\xi_{ms-tx}-\xi_{asx-tx}\right)+24\left(\xi_{ms-ty}-\xi_{asx-ty}\right)^2\\+24\left(\xi_{ms-tz}-\xi_{asx-tz}\right)^2+175t^2\end{pmatrix}\end{pmatrix}/\begin{pmatrix}3\left(\xi_{ms-ty}-\xi_{asx-ty}\right)^2\\+3\left(\xi_{ms-tz}-\xi_{asx-tz}\right)^2\\+175t^2\end{pmatrix} \tag{F.6}$$

$$\zeta_{amx-tx} = \frac{96\xi_{asx-tx}\left(35\left(3\left(\xi_{asx-tz}-\frac{1}{2}w\xi_{asx-ry}\right)+3\left(\frac{1}{2}w\xi_{asx-rz}+\xi_{asx-ty}\right)+5t^2\right)+129\xi_{asx-tx}^2\right)}{3\xi_{asx-tx}^2+175t^2} \tag{F.7}$$

$$\zeta_{amx-ty} = \frac{1}{3\xi_{asx-tx}^2+175t^2}24\begin{pmatrix}w\xi_{asx-rx}\left(35\left(6\left(\xi_{asx-tz}-\frac{1}{2}w\xi_{asx-ry}\right)+5t^2\right)+129\xi_{asx-tx}^2\right)\\+70\left(\frac{1}{2}w\xi_{asx-rz}+\xi_{asx-ty}\right)\left(6\left(\xi_{asx-tz}-\frac{1}{2}w\xi_{asx-ry}\right)+5t^2+5\right)\\+6\xi_{asx-tx}^2\left(43\left(\frac{1}{2}w\xi_{asx-rz}+\xi_{asx-ty}\right)+35\right)\end{pmatrix} \tag{F.8}$$

$$\zeta_{\mathrm{amx-tz}} = -\frac{1}{3\xi_{\mathrm{asx-tx}}^2 + 175t^2} 24 \left(\begin{array}{l} w\xi_{\mathrm{asx-rx}} \left(35\left(6\left(\frac{1}{2} w\xi_{\mathrm{asx-rz}} + \xi_{\mathrm{asx-ty}} \right) + 5t^2 \right) + 129\xi_{\mathrm{asx-tx}}^2 \right) \\ -2 \left(\begin{array}{l} 35\left(\xi_{\mathrm{asx-tz}} - \frac{1}{2} w\xi_{\mathrm{asx-ry}} \right) \left(6\left(\frac{1}{2} w\xi_{\mathrm{asx-rz}} + \xi_{\mathrm{asx-ty}} \right) + 5t^2 + 5 \right) \\ +3\xi_{\mathrm{asx-tx}}^2 \left(43\left(\xi_{\mathrm{asx-tz}} - \frac{1}{2} w\xi_{\mathrm{asx-ry}} \right) + 35 \right) \end{array} \right) \end{array} \right) \tag{F.9}$$

$$\zeta_{\mathrm{amx-rx}} = \frac{1}{3\xi_{\mathrm{asx-tx}}^2 + 175t^2} 4 \left(\begin{array}{l} \xi_{\mathrm{asx-rx}} \left(35\left(\begin{array}{l} 3w\left(6w+1\right)\left(\xi_{\mathrm{asx-tz}} - \frac{1}{2} w\xi_{\mathrm{asx-ry}} \right) + 3w\left(6w+1\right)\left(\frac{1}{2} w\xi_{\mathrm{asx-rz}} + \xi_{\mathrm{asx-ty}} \right) \\ +10\left(t^2\left(3w^2+3w+4\right) - 3tw + 3w^2 \right) \end{array} \right) \right. \\ \left. +18w\left(43w+8\right)\xi_{\mathrm{asx-tx}}^2 \right) \\ +6\left(3\left(43w+8\right)\xi_{\mathrm{asx-tx}}^2 + 175t^2\left(w+1\right) \right) \left(\frac{1}{2} w\xi_{\mathrm{asx-ry}} + \frac{1}{2} w\xi_{\mathrm{asx-rz}} + \xi_{\mathrm{asx-ty}} - \xi_{\mathrm{asx-tz}} \right) \end{array} \right) \tag{F.10}$$

$$\zeta_{\mathrm{amx-ry}} = -\frac{1}{3\xi_{\mathrm{asx-tx}}^2 + 175t^2} 4 \left(\begin{array}{l} 6\xi_{\mathrm{asx-tx}} \left(\begin{array}{l} 35\left(5t^2 - 3tw + 3w^2 \right) \xi_{\mathrm{asx-rx}} + 35 \left(\begin{array}{l} \left(6w+1\right)\left(\xi_{\mathrm{asx-tz}} - \frac{1}{2} w\xi_{\mathrm{asx-ry}} \right) \\ +5t^2\left(w+1\right) \end{array} \right) \\ +3\left(43w+8\right)\xi_{\mathrm{asx-tx}}^2 \end{array} \right) \\ -\xi_{\mathrm{asx-ry}} \left(3\delta\xi_{\mathrm{asx-tx}}^2 + 175\left(\left(\delta+4\right)t^2 - 3tw + 3w^2 \right) \right) \end{array} \right) \tag{F.11}$$

$$\zeta_{\mathrm{amx-rz}} = \frac{1}{3\xi_{\mathrm{asx-tx}}^2 + 175t^2} 4 \left(\begin{array}{l} 6\xi_{\mathrm{asx-tx}} \left(\begin{array}{l} -35\left(5t^2 - 3tw + 3w^2 \right) \xi_{\mathrm{asx-rx}} + 35 \left(\begin{array}{l} \left(6w+1\right)\left(\frac{1}{2} w\xi_{\mathrm{asx-rz}} + \xi_{\mathrm{asx-ty}} \right) \\ +5t^2\left(w+1\right) \end{array} \right) \\ +3\left(43w+8\right)\xi_{\mathrm{asx-tx}}^2 \end{array} \right) \\ +\xi_{\mathrm{asx-rz}} \left(3\delta\xi_{\mathrm{asx-tx}}^2 + 175\left(\left(\delta+4\right)t^2 - 3tw + 3w^2 \right) \right) \end{array} \right) \tag{F.12}$$

$$0 = -\zeta_{\mathrm{amx-tx}} + \zeta_{\mathrm{asx-tx}} + \zeta_{\mathrm{pmx-tx}} \tag{F.13}$$

$$0 = -\zeta_{\mathrm{amx-ty}} + \zeta_{\mathrm{asx-ty}} + \zeta_{\mathrm{pmx-ty}} \tag{F.14}$$

$$0 = -\zeta_{\mathrm{amx-tz}} + \zeta_{\mathrm{asx-tz}} + \zeta_{\mathrm{pmx-tz}} \tag{F.15}$$

$$0 = -\zeta_{\mathrm{amx-rx}} + \zeta_{\mathrm{asx-rx}} + \zeta_{\mathrm{pmx-rx}} + \zeta_{\mathrm{pmx-tz}}\xi_{\mathrm{ms-ty}} - \zeta_{\mathrm{pmx-ty}}\xi_{\mathrm{ms-tz}} \tag{F.16}$$

$$0 = -\zeta_{\mathrm{amx-ry}} + \zeta_{\mathrm{asx-ry}} + \zeta_{\mathrm{pmx-ry}} + \frac{1}{2} w\zeta_{\mathrm{amx-tz}} - w\zeta_{\mathrm{pmx-tz}} + \zeta_{\mathrm{pmx-tz}}\left(\xi_{\mathrm{asx-tx}} - \xi_{\mathrm{ms-tx}} - 1 \right) + \zeta_{\mathrm{pmx-tx}}\xi_{\mathrm{ms-tz}} \tag{F.17}$$

$$0 = -\zeta_{\mathrm{amx-rz}} + \zeta_{\mathrm{asx-rz}} + \zeta_{\mathrm{pmx-rz}} - \frac{1}{2} w\zeta_{\mathrm{amx-ty}} + w\zeta_{\mathrm{pmx-ty}} + \zeta_{\mathrm{pmx-ty}}\left(-\xi_{\mathrm{asx-tx}} + \xi_{\mathrm{ms-tx}} + 1 \right) - \zeta_{\mathrm{pmx-tx}}\xi_{\mathrm{ms-ty}} \tag{F.18}$$

$$\zeta_{\mathrm{pmy-tx}} = \frac{1680\left(5\left(\xi_{\mathrm{ms-ty}} - \xi_{\mathrm{asy-tx}} \right) + 3\left(\left(\xi_{\mathrm{ms-tx}} - \xi_{\mathrm{asy-tz}} \right)^2 + \left(\xi_{\mathrm{ms-tz}} - \xi_{\mathrm{asy-ty}} \right)^2 \right) \right)}{3\left(\xi_{\mathrm{ms-tx}} - \xi_{\mathrm{asy-tz}} \right)^2 + 3\left(\xi_{\mathrm{ms-tz}} - \xi_{\mathrm{asy-ty}} \right)^2 + 175t^2} \tag{F.19}$$

$$\zeta_{\mathrm{pmy-ty}} = \left(48\left(\xi_{\mathrm{ms-tz}} - \xi_{\mathrm{asy-ty}}\right) \begin{pmatrix} 210\left(\xi_{\mathrm{ms-ty}} - \xi_{\mathrm{asy-tx}}\right) + 129\left(\xi_{\mathrm{ms-tx}} - \xi_{\mathrm{asy-tz}}\right)^2 \\ +129\left(\xi_{\mathrm{ms-tz}} - \xi_{\mathrm{asy-ty}}\right)^2 + 175t^2 \end{pmatrix} \right) / \begin{pmatrix} 3\left(\xi_{\mathrm{ms-tx}} - \xi_{\mathrm{asy-tz}}\right)^2 \\ +3\left(\xi_{\mathrm{ms-tz}} - \xi_{\mathrm{asy-ty}}\right)^2 + 175t^2 \end{pmatrix} \tag{F.20}$$

$$\zeta_{\mathrm{pmy-tz}} = \left(48\left(\xi_{\mathrm{ms-tx}} - \xi_{\mathrm{asy-tz}}\right) \begin{pmatrix} 210\left(\xi_{\mathrm{ms-ty}} - \xi_{\mathrm{asy-tx}}\right) + 129\left(\xi_{\mathrm{ms-tx}} - \xi_{\mathrm{asy-tz}}\right)^2 \\ +129\left(\xi_{\mathrm{ms-tz}} - \xi_{\mathrm{asy-ty}}\right)^2 + 175t^2 \end{pmatrix} \right) / \begin{pmatrix} 3\left(\xi_{\mathrm{ms-tx}} - \xi_{\mathrm{asy-tz}}\right)^2 \\ +3\left(\xi_{\mathrm{ms-tz}} - \xi_{\mathrm{asy-ty}}\right)^2 + 175t^2 \end{pmatrix} \tag{F.21}$$

$$\zeta_{\mathrm{pmy-rx}} = \left(4 \begin{pmatrix} \delta\left(\xi_{\mathrm{ms-ry}} - \xi_{\mathrm{asy-rx}}\right)\left(3\left(\xi_{\mathrm{ms-tx}} - \xi_{\mathrm{asy-tz}}\right)^2 + 3\left(\xi_{\mathrm{ms-tz}} - \xi_{\mathrm{asy-ty}}\right)^2 + 175t^2\right) \\ -210\left(5t^2 - 3tw + 3w^2\right) \begin{pmatrix} \left(\xi_{\mathrm{ms-rx}} - \xi_{\mathrm{asy-rz}}\right)\left(\xi_{\mathrm{ms-tx}} - \xi_{\mathrm{asy-tz}}\right) \\ +\left(\xi_{\mathrm{ms-rz}} - \xi_{\mathrm{asy-ry}}\right)\left(\xi_{\mathrm{ms-tz}} - \xi_{\mathrm{asy-ty}}\right) \end{pmatrix} \end{pmatrix} \right) / \begin{pmatrix} 3\left(\xi_{\mathrm{ms-tx}} - \xi_{\mathrm{asy-tz}}\right)^2 \\ +3\left(\xi_{\mathrm{ms-tz}} - \xi_{\mathrm{asy-ty}}\right)^2 \\ +175t^2 \end{pmatrix} \tag{F.22}$$

$$\zeta_{\mathrm{pmy-ry}} = 4 \begin{pmatrix} 175\left(4t^2 - 3tw + 3w^2\right)\left(\xi_{\mathrm{ms-rz}} - \xi_{\mathrm{asy-ry}}\right) \\ +6\left(\xi_{\mathrm{ms-tx}} - \xi_{\mathrm{asy-tz}}\right) \begin{pmatrix} 35\left(\xi_{\mathrm{ms-ty}} - \xi_{\mathrm{asy-tx}}\right) + 24\left(\xi_{\mathrm{ms-tx}} - \xi_{\mathrm{asy-tz}}\right)^2 \\ +24\left(\xi_{\mathrm{ms-tz}} - \xi_{\mathrm{asy-ty}}\right)^2 + 175t^2 \end{pmatrix} \end{pmatrix} / \begin{pmatrix} 3\left(\xi_{\mathrm{ms-tx}} - \xi_{\mathrm{asy-tz}}\right)^2 \\ +3\left(\xi_{\mathrm{ms-tz}} - \xi_{\mathrm{asy-ty}}\right)^2 \\ +175t^2 \end{pmatrix} \tag{F.23}$$

$$\zeta_{\mathrm{pmy-rz}} = 4 \begin{pmatrix} 175\left(4t^2 - 3tw + 3w^2\right)\left(\xi_{\mathrm{ms-rx}} - \xi_{\mathrm{asy-rz}}\right) \\ -6\left(\xi_{\mathrm{ms-tz}} - \xi_{\mathrm{asy-ty}}\right) \begin{pmatrix} 35\left(\xi_{\mathrm{ms-ty}} - \xi_{\mathrm{asy-tx}}\right) + 24\left(\xi_{\mathrm{ms-tx}} - \xi_{\mathrm{asy-tz}}\right)^2 \\ +24\left(\xi_{\mathrm{ms-tz}} - \xi_{\mathrm{asy-ty}}\right)^2 + 175t^2 \end{pmatrix} \end{pmatrix} / \begin{pmatrix} 3\left(\xi_{\mathrm{ms-tx}} - \xi_{\mathrm{asy-tz}}\right)^2 \\ +3\left(\xi_{\mathrm{ms-tz}} - \xi_{\mathrm{asy-ty}}\right)^2 \\ +175t^2 \end{pmatrix} \tag{F.24}$$

$$\zeta_{\mathrm{amy-tx}} = \frac{96\xi_{\mathrm{asy-tx}}\left(35\left(3\left(\xi_{\mathrm{asy-tz}} - \frac{1}{2}w\xi_{\mathrm{asy-ry}}\right) + 3\left(\frac{1}{2}w\xi_{\mathrm{asy-rz}} + \xi_{\mathrm{asy-ty}}\right) + 5t^2\right) + 129\xi_{\mathrm{asy-tx}}^2\right)}{3\xi_{\mathrm{asy-tx}}^2 + 175t^2} \tag{F.25}$$

$$\zeta_{\mathrm{amy-ty}} = \frac{1}{3\xi_{\mathrm{asy-tx}}^2 + 175t^2} 24 \begin{pmatrix} w\xi_{\mathrm{asy-rx}}\left(35\left(6\left(\xi_{\mathrm{asy-tz}} - \frac{1}{2}w\xi_{\mathrm{asy-ry}}\right) + 5t^2\right) + 129\xi_{\mathrm{asy-tx}}^2\right) \\ +70\left(\frac{1}{2}w\xi_{\mathrm{asy-rz}} + \xi_{\mathrm{asy-ty}}\right)\left(6\left(\xi_{\mathrm{asy-tz}} - \frac{1}{2}w\xi_{\mathrm{asy-ry}}\right) + 5t^2 + 5\right) \\ +6\xi_{\mathrm{asy-tx}}^2\left(43\left(\frac{1}{2}w\xi_{\mathrm{asy-rz}} + \xi_{\mathrm{asy-ty}}\right) + 35\right) \end{pmatrix} \tag{F.26}$$

$$\zeta_{\mathrm{amy-tz}} = -\frac{1}{3\xi_{\mathrm{asy-tx}}^2 + 175t^2} 24 \begin{pmatrix} w\xi_{\mathrm{asy-rx}}\left(35\left(6\left(\frac{1}{2}w\xi_{\mathrm{asy-rz}} + \xi_{\mathrm{asy-ty}}\right) + 5t^2\right) + 129\xi_{\mathrm{asy-tx}}^2\right) \\ -2\begin{pmatrix} 35\left(\xi_{\mathrm{asy-tz}} - \frac{1}{2}w\xi_{\mathrm{asy-ry}}\right)\left(6\left(\frac{1}{2}w\xi_{\mathrm{asy-rz}} + \xi_{\mathrm{asy-ty}}\right) + 5t^2 + 5\right) \\ +3\xi_{\mathrm{asy-tx}}^2\left(43\left(\xi_{\mathrm{asy-tz}} - \frac{1}{2}w\xi_{\mathrm{asy-ry}}\right) + 35\right) \end{pmatrix} \end{pmatrix} \tag{F.27}$$

$$\zeta_{amy-rx}=\frac{1}{3\xi_{asy-tx}^2+175t^2}4\left(\begin{array}{l}\xi_{asy-rx}\left(\begin{array}{l}35\left(\begin{array}{l}3w(6w+1)\left(\xi_{asy-tz}-\frac{1}{2}w\xi_{asy-ry}\right)+3w(6w+1)\left(\frac{1}{2}w\xi_{asy-rz}+\xi_{asy-ty}\right)\\+10\left(t^2\left(3w^2+3w+4\right)-3tw+3w^2\right)\end{array}\right)\\+18w(43w+8)\xi_{asy-tx}^2\end{array}\right)\\+6\left(3(43w+8)\xi_{asy-tx}^2+175t^2(w+1)\right)\left(\frac{1}{2}w\xi_{asy-ry}+\frac{1}{2}w\xi_{asy-rz}+\xi_{asy-ty}-\xi_{asy-tz}\right)\end{array}\right) \quad (F.28)$$

$$\zeta_{amy-ry}=-\frac{1}{3\xi_{asy-tx}^2+175t^2}4\left(\begin{array}{l}6\xi_{asy-tx}\left(\begin{array}{l}35\left(5t^2-3tw+3w^2\right)\xi_{asy-rx}+35\left(\begin{array}{l}(6w+1)\left(\xi_{asy-tz}-\frac{1}{2}w\xi_{asy-ry}\right)\\+5t^2(w+1)\end{array}\right)\\+3(43w+8)\xi_{asy-tx}^2\end{array}\right)\\-\xi_{asy-ry}\left(3\delta\xi_{asy-tx}^2+175\left((\delta+4)t^2-3tw+3w^2\right)\right)\end{array}\right) \quad (F.29)$$

$$\zeta_{amy-rz}=\frac{1}{3\xi_{asy-tx}^2+175t^2}4\left(\begin{array}{l}6\xi_{asy-tx}\left(\begin{array}{l}-35\left(5t^2-3tw+3w^2\right)\xi_{asy-rx}\\+35\left((6w+1)\left(\frac{1}{2}w\xi_{asy-rz}+\xi_{asy-ty}\right)+5t^2(w+1)\right)+3(43w+8)\xi_{asy-tx}^2\end{array}\right)\\+\xi_{asy-rz}\left(3\delta\xi_{asy-tx}^2+175\left((\delta+4)t^2-3tw+3w^2\right)\right)\end{array}\right) \quad (F.30)$$

$$0=-\zeta_{amy-tx}+\zeta_{asy-tx}+\zeta_{pmy-tx} \quad (F.31)$$

$$0=-\zeta_{amy-ty}+\zeta_{asy-ty}+\zeta_{pmy-ty} \quad (F.32)$$

$$0=-\zeta_{amy-tz}+\zeta_{asy-tz}+\zeta_{pmy-tz} \quad (F.33)$$

$$0=-\zeta_{amy-rx}+\zeta_{asy-rx}+\zeta_{pmy-rx}-\zeta_{pmy-ty}\xi_{ms-tx}+\zeta_{pmy-tz}\xi_{ms-tz} \quad (F.34)$$

$$0=-\zeta_{amy-ry}+\zeta_{asy-ry}+\zeta_{pmy-ry}+\frac{1}{2}w\zeta_{amy-tz}-w\zeta_{pmy-tz}+\zeta_{pmy-tx}\xi_{ms-tx}+\zeta_{pmy-tz}\left(\xi_{asy-tx}-\xi_{ms-ty}-1\right) \quad (F.35)$$

$$0=-\zeta_{amy-rz}+\zeta_{asy-rz}+\zeta_{pmy-rz}-\frac{1}{2}w\zeta_{amy-ty}+w\zeta_{pmy-ty}+\zeta_{pmy-ty}\left(-\xi_{asy-tx}+\xi_{ms-ty}+1\right)-\zeta_{pmy-tx}\xi_{ms-tz} \quad (F.36)$$

$$\zeta_{pmz-tx}=\frac{1680\left(3\left(\left(\xi_{ms-tx}-\xi_{asz-ty}\right)^2+\left(\xi_{ms-ty}-\xi_{asz-tz}\right)^2\right)+5\left(\xi_{ms-tz}-\xi_{asz-tx}\right)\right)}{3\left(\xi_{ms-tx}-\xi_{asz-ty}\right)^2+3\left(\xi_{ms-ty}-\xi_{asz-tz}\right)^2+175t^2} \quad (F.37)$$

$$\zeta_{pmz-ty}=\left(48\left(\xi_{ms-tx}-\xi_{asz-ty}\right)\left(\begin{array}{l}129\left(\xi_{ms-tx}-\xi_{asz-ty}\right)^2+210\left(\xi_{ms-tz}-\xi_{asz-tx}\right)\\+129\left(\xi_{ms-ty}-\xi_{asz-tz}\right)^2+175t^2\end{array}\right)\right)/\left(\begin{array}{l}3\left(\xi_{ms-tx}-\xi_{asz-ty}\right)^2\\+3\left(\xi_{ms-ty}-\xi_{asz-tz}\right)^2+175t^2\end{array}\right) \quad (F.38)$$

$$\zeta_{pmz-tz}=\left(48\left(\xi_{ms-ty}-\xi_{asz-tz}\right)\left(\begin{array}{l}129\left(\xi_{ms-tx}-\xi_{asz-ty}\right)^2+210\left(\xi_{ms-tz}-\xi_{asz-tx}\right)\\+129\left(\xi_{ms-ty}-\xi_{asz-tz}\right)^2+175t^2\end{array}\right)\right)/\left(\begin{array}{l}3\left(\xi_{ms-tx}-\xi_{asz-ty}\right)^2\\+3\left(\xi_{ms-ty}-\xi_{asz-tz}\right)^2+175t^2\end{array}\right) \quad (F.39)$$

$$\zeta_{\mathrm{pmz-rx}} = 4\begin{pmatrix} \delta\left(\xi_{\mathrm{ms-rz}} - \xi_{\mathrm{asz-rx}}\right)\left(3\left(\xi_{\mathrm{ms-tx}} - \xi_{\mathrm{asz-ty}}\right)^2 + 3\left(\xi_{\mathrm{ms-ty}} - \xi_{\mathrm{asz-tz}}\right)^2 + 175t^2\right) \\ -210\left(5t^2 - 3tw + 3w^2\right)\begin{pmatrix}\left(\xi_{\mathrm{ms-rx}} - \xi_{\mathrm{asz-ry}}\right)\left(\xi_{\mathrm{ms-tx}} - \xi_{\mathrm{asz-ty}}\right) \\ +\left(\xi_{\mathrm{ms-ry}} - \xi_{\mathrm{asz-rz}}\right)\left(\xi_{\mathrm{ms-ty}} - \xi_{\mathrm{asz-tz}}\right)\end{pmatrix} \end{pmatrix} / \begin{pmatrix} 3\left(\xi_{\mathrm{ms-tx}} - \xi_{\mathrm{asz-ty}}\right)^2 \\ +3\left(\xi_{\mathrm{ms-ty}} - \xi_{\mathrm{asz-tz}}\right)^2 \\ +175t^2 \end{pmatrix} \tag{F.40}$$

$$\zeta_{\mathrm{pmz-ry}} = 4\begin{pmatrix} 175\left(4t^2 - 3tw + 3w^2\right)\left(\xi_{\mathrm{ms-rx}} - \xi_{\mathrm{asz-ry}}\right) \\ +6\left(\xi_{\mathrm{ms-ty}} - \xi_{\mathrm{asz-tz}}\right)\begin{pmatrix}24\left(\xi_{\mathrm{ms-tx}} - \xi_{\mathrm{asz-ty}}\right)^2 + 35\left(\xi_{\mathrm{ms-tz}} - \xi_{\mathrm{asz-tx}}\right) \\ +24\left(\xi_{\mathrm{ms-ty}} - \xi_{\mathrm{asz-tz}}\right)^2 + 175t^2\end{pmatrix} \end{pmatrix} / \begin{pmatrix} 3\left(\xi_{\mathrm{ms-tx}} - \xi_{\mathrm{asz-ty}}\right)^2 \\ +3\left(\xi_{\mathrm{ms-ty}} - \xi_{\mathrm{asz-tz}}\right)^2 + 175t^2 \end{pmatrix} \tag{F.41}$$

$$\zeta_{\mathrm{pmz-rz}} = 4\begin{pmatrix} 175\left(4t^2 - 3tw + 3w^2\right)\left(\xi_{\mathrm{ms-ry}} - \xi_{\mathrm{asz-rz}}\right) \\ -6\left(\xi_{\mathrm{ms-tx}} - \xi_{\mathrm{asz-ty}}\right)\begin{pmatrix}24\left(\xi_{\mathrm{ms-tx}} - \xi_{\mathrm{asz-ty}}\right)^2 + 35\left(\xi_{\mathrm{ms-tz}} - \xi_{\mathrm{asz-tx}}\right) \\ +24\left(\xi_{\mathrm{ms-ty}} - \xi_{\mathrm{asz-tz}}\right)^2 + 175t^2\end{pmatrix} \end{pmatrix} / \begin{pmatrix} 3\left(\xi_{\mathrm{ms-tx}} - \xi_{\mathrm{asz-ty}}\right)^2 \\ +3\left(\xi_{\mathrm{ms-ty}} - \xi_{\mathrm{asz-tz}}\right)^2 + 175t^2 \end{pmatrix} \tag{F.42}$$

$$\zeta_{\mathrm{amz-tx}} = \frac{96\xi_{\mathrm{asz-tx}}\left(35\left(3\left(\xi_{\mathrm{asz-tz}} - \frac{1}{2}w\xi_{\mathrm{asz-ry}}\right) + 3\left(\frac{1}{2}w\xi_{\mathrm{asz-rz}} + \xi_{\mathrm{asz-ty}}\right) + 5t^2\right) + 129\xi_{\mathrm{asz-tx}}^2\right)}{3\xi_{\mathrm{asz-tx}}^2 + 175t^2} \tag{F.43}$$

$$\zeta_{\mathrm{amz-ty}} = \frac{1}{3\xi_{\mathrm{asz-tx}}^2 + 175t^2} 24\begin{pmatrix} w\xi_{\mathrm{asz-rx}}\left(35\left(6\left(\xi_{\mathrm{asz-tz}} - \frac{1}{2}w\xi_{\mathrm{asz-ry}}\right) + 5t^2\right) + 129\xi_{\mathrm{asz-tx}}^2\right) \\ +70\left(\frac{1}{2}w\xi_{\mathrm{asz-rz}} + \xi_{\mathrm{asz-ty}}\right)\left(6\left(\xi_{\mathrm{asz-tz}} - \frac{1}{2}w\xi_{\mathrm{asz-ry}}\right) + 5t^2 + 5\right) \\ +6\xi_{\mathrm{asz-tx}}^2\left(43\left(\frac{1}{2}w\xi_{\mathrm{asz-rz}} + \xi_{\mathrm{asz-ty}}\right) + 35\right) \end{pmatrix} \tag{F.44}$$

$$\zeta_{\mathrm{amz-tz}} = -\frac{1}{3\xi_{\mathrm{asz-tx}}^2 + 175t^2} 24\begin{pmatrix} w\xi_{\mathrm{asz-rx}}\left(35\left(6\left(\frac{1}{2}w\xi_{\mathrm{asz-rz}} + \xi_{\mathrm{asz-ty}}\right) + 5t^2\right) + 129\xi_{\mathrm{asz-tx}}^2\right) \\ -2\begin{pmatrix}35\left(\xi_{\mathrm{asz-tz}} - \frac{1}{2}w\xi_{\mathrm{asz-ry}}\right)\left(6\left(\frac{1}{2}w\xi_{\mathrm{asz-rz}} + \xi_{\mathrm{asz-ty}}\right) + 5t^2 + 5\right) \\ +3\xi_{\mathrm{asz-tx}}^2\left(43\left(\xi_{\mathrm{asz-tz}} - \frac{1}{2}w\xi_{\mathrm{asz-ry}}\right) + 35\right)\end{pmatrix} \end{pmatrix} \tag{F.45}$$

$$\zeta_{\mathrm{amz-rx}} = \frac{1}{3\xi_{\mathrm{asz-tx}}^2 + 175t^2} 4\begin{pmatrix} \xi_{\mathrm{asz-rx}}\begin{pmatrix}35\begin{pmatrix}3w(6w+1)\left(\xi_{\mathrm{asz-tz}} - \frac{1}{2}w\xi_{\mathrm{asz-ry}}\right) + 3w(6w+1)\left(\frac{1}{2}w\xi_{\mathrm{asz-rz}} + \xi_{\mathrm{asz-ty}}\right) \\ +10\left(t^2\left(3w^2 + 3w + 4\right) - 3tw + 3w^2\right)\end{pmatrix} \\ +18w(43w+8)\xi_{\mathrm{asz-tx}}^2\end{pmatrix} \\ +6\left(3(43w+8)\xi_{\mathrm{asz-tx}}^2 + 175t^2(w+1)\right)\left(\frac{1}{2}w\xi_{\mathrm{asz-ry}} + \frac{1}{2}w\xi_{\mathrm{asz-rz}} + \xi_{\mathrm{asz-ty}} - \xi_{\mathrm{asz-tz}}\right) \end{pmatrix} \tag{F.46}$$

$$\zeta_{\mathrm{amz-ry}} = -\frac{1}{3\xi_{\mathrm{asz-tx}}^2 + 175t^2} 4 \left(\begin{array}{l} 6\xi_{\mathrm{asz-tx}} \left(\begin{array}{l} 35\left(5t^2 - 3tw + 3w^2\right)\xi_{\mathrm{asz-rx}} + 35\left(\begin{array}{l} \left(6w+1\right)\left(\xi_{\mathrm{asz-tz}} - \frac{1}{2}w\xi_{\mathrm{asz-ry}}\right) \\ +5t^2\left(w+1\right) \end{array} \right) \\ +3\left(43w+8\right)\xi_{\mathrm{asz-tx}}^2 \end{array} \right) \\ -\xi_{\mathrm{asz-ry}}\left(3\delta\xi_{\mathrm{asz-tx}}^2 + 175\left(\left(\delta+4\right)t^2 - 3tw + 3w^2\right)\right) \end{array} \right) \tag{F.47}$$

$$\zeta_{\mathrm{amz-rz}} = \frac{1}{3\xi_{\mathrm{asz-tx}}^2 + 175t^2} 4 \left(\begin{array}{l} 6\xi_{\mathrm{asz-tx}} \left(\begin{array}{l} -35\left(5t^2 - 3tw + 3w^2\right)\xi_{\mathrm{asz-rx}} + 35\left(\begin{array}{l} \left(6w+1\right)\left(\frac{1}{2}w\xi_{\mathrm{asz-rz}} + \xi_{\mathrm{asz-ty}}\right) \\ +5t^2\left(w+1\right) \end{array} \right) \\ +3\left(43w+8\right)\xi_{\mathrm{asz-tx}}^2 \end{array} \right) \\ +\xi_{\mathrm{asz-rz}}\left(3\delta\xi_{\mathrm{asz-tx}}^2 + 175\left(\left(\delta+4\right)t^2 - 3tw + 3w^2\right)\right) \end{array} \right) \tag{F.48}$$

$$0 = -\zeta_{\mathrm{amz-tx}} + \zeta_{\mathrm{asz-tx}} + \zeta_{\mathrm{pmz-tx}} \tag{F.49}$$

$$0 = -\zeta_{\mathrm{amz-ty}} + \zeta_{\mathrm{asz-ty}} + \zeta_{\mathrm{pmz-ty}} \tag{F.50}$$

$$0 = -\zeta_{\mathrm{amz-tz}} + \zeta_{\mathrm{asz-tz}} + \zeta_{\mathrm{pmz-tz}} \tag{F.51}$$

$$0 = -\zeta_{\mathrm{amz-rx}} + \zeta_{\mathrm{asz-rx}} + \zeta_{\mathrm{pmz-rx}} + \zeta_{\mathrm{pmz-tz}}\xi_{\mathrm{ms-tx}} - \zeta_{\mathrm{pmz-ty}}\xi_{\mathrm{ms-ty}} \tag{F.52}$$

$$0 = -\zeta_{\mathrm{amz-ry}} + \zeta_{\mathrm{asz-ry}} + \zeta_{\mathrm{pmz-ry}} + \frac{1}{2}w\zeta_{\mathrm{amz-tz}} - w\zeta_{\mathrm{pmz-tz}} + \zeta_{\mathrm{pmz-tx}}\xi_{\mathrm{ms-ty}} + \zeta_{\mathrm{pmz-tz}}\left(\xi_{\mathrm{asz-tx}} - \xi_{\mathrm{ms-tz}} - 1\right) \tag{F.53}$$

$$0 = -\zeta_{\mathrm{amz-rz}} + \zeta_{\mathrm{asz-rz}} + \zeta_{\mathrm{pmz-rz}} - \frac{1}{2}w\zeta_{\mathrm{amz-ty}} + w\zeta_{\mathrm{pmz-ty}} - \zeta_{\mathrm{pmz-tx}}\xi_{\mathrm{ms-tx}} + \zeta_{\mathrm{pmz-ty}}\left(-\xi_{\mathrm{asz-tx}} + \xi_{\mathrm{ms-tz}} + 1\right) \tag{F.54}$$

$$0 = \zeta_{\mathrm{m-tx}} - \zeta_{\mathrm{pmx-tx}} - \zeta_{\mathrm{pmz-ty}} - \zeta_{\mathrm{pmy-tz}} \tag{F.55}$$

$$0 = -\zeta_{\mathrm{pmy-tx}} + \zeta_{\mathrm{m-ty}} - \zeta_{\mathrm{pmx-ty}} - \zeta_{\mathrm{pmz-tz}} \tag{F.56}$$

$$0 = -\zeta_{\mathrm{pmz-tx}} - \zeta_{\mathrm{pmy-ty}} + \zeta_{\mathrm{m-tz}} - \zeta_{\mathrm{pmx-tz}} \tag{F.57}$$

$$0 = \zeta_{\mathrm{ms-rx}} - \zeta_{\mathrm{pmx-rx}} - \zeta_{\mathrm{pmz-ry}} - \zeta_{\mathrm{pmy-rz}} - \frac{1}{2}w\zeta_{\mathrm{pmy-tx}} - \frac{1}{2}w\zeta_{\mathrm{pmx-ty}} + \frac{1}{2}w\zeta_{\mathrm{pmy-ty}} - w\zeta_{\mathrm{pmz-tz}} \tag{F.58}$$

$$0 = -\zeta_{\mathrm{pmy-rx}} + \zeta_{\mathrm{ms-ry}} - \zeta_{\mathrm{pmx-ry}} - \zeta_{\mathrm{pmz-rz}} + \frac{1}{2}w\zeta_{\mathrm{pmx-tx}} + w\zeta_{\mathrm{pmz-ty}} - \frac{1}{2}w\zeta_{\mathrm{pmx-tz}} + \frac{1}{2}w\zeta_{\mathrm{pmy-tz}} \tag{F.59}$$

$$0 = -\zeta_{\mathrm{pmz-rx}} - \zeta_{\mathrm{pmy-ry}} + \zeta_{\mathrm{ms-rz}} - \zeta_{\mathrm{pmx-rz}} + \frac{1}{2}w\zeta_{\mathrm{pmx-ty}} - \frac{1}{2}w\zeta_{\mathrm{pmy-tz}} \tag{F.60}$$

APPENDIX G: FABRICATION OF A SYMMETRIC XYZ CPM

The designed symmetric XYZ CPM, as shown in Figure 5.1(h), can provide translations along the X_{ms}-, Y_{ms}- and Z_{ms}-axes, with desired motion characteristics. However, the MS of the symmetric XYZ CPM is located at the centre of the whole structure, and the symmetric XYZ CPM cannot be fabricated monolithically. Therefore, a practical design of the symmetric XYZ CPM is desired, which can be fabricated by a traditional subtractive manufacturing method using a computer numeric control (CNC) milling machine.

Because the XYZ CPM cannot be fabricated monolithically, assembling accessories (components) are presented, as shown in Figure G.1. The accessories, with mounting holes, can be fabricated using a CNC milling machine. These accessories are assembled together using screws, as shown in Figure G.2(a) – Figure G.2(e). Figure G.2(f) – Figure G.2(i) show that three RLs (rigid linkages), one output platform, one supporting seat and four legs are added to the module shown in Figure G.2(e). The output platform is connected to the MS with a RL. Therefore, the motion of the MS can be transmitted to the output platform, i.e., the output platform can translate in the three orthogonal directions under the actuation of the three actuators. The rigid accessories and the compliant accessories can be fabricated using different materials. Moreover, if one of the accessories is broken, it is easy to replace it with a new one. In addition, the actuation stiffness of the XYZ CPM can be increased by increasing the in-plane thickness, t_{in}, of the compliant AM beams (see Figure G.3). Note that the accessories should be assembled together strongly using screws, in order to avoid stiffness reduction. It can be seen from [76] that stiffness can reduce by approximately 30% by bolted joints.

A prototype of the XYZ CPM, with three micrometres as displacement inputs, is fabricated, based on the practical design shown in Figure G.2(i). The prototype

is shown in Figure 5.6. All components of the prototype are made of Aluminium 6061 (Young's modulus is about 69000MPa and Poisson's ratio is about 0.33). The output displacements of the MS can be measured by digital dial gauges with a resolution of 1μm.

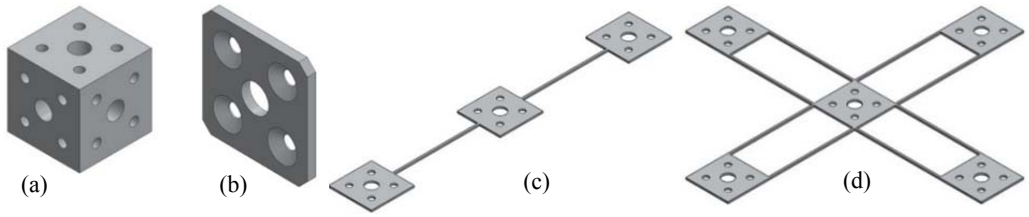

Figure G.1 Main assembling accessories: (a) rigid cube, (b) rigid washer, (c) compliant PM beam, and (d) compliant AM beam

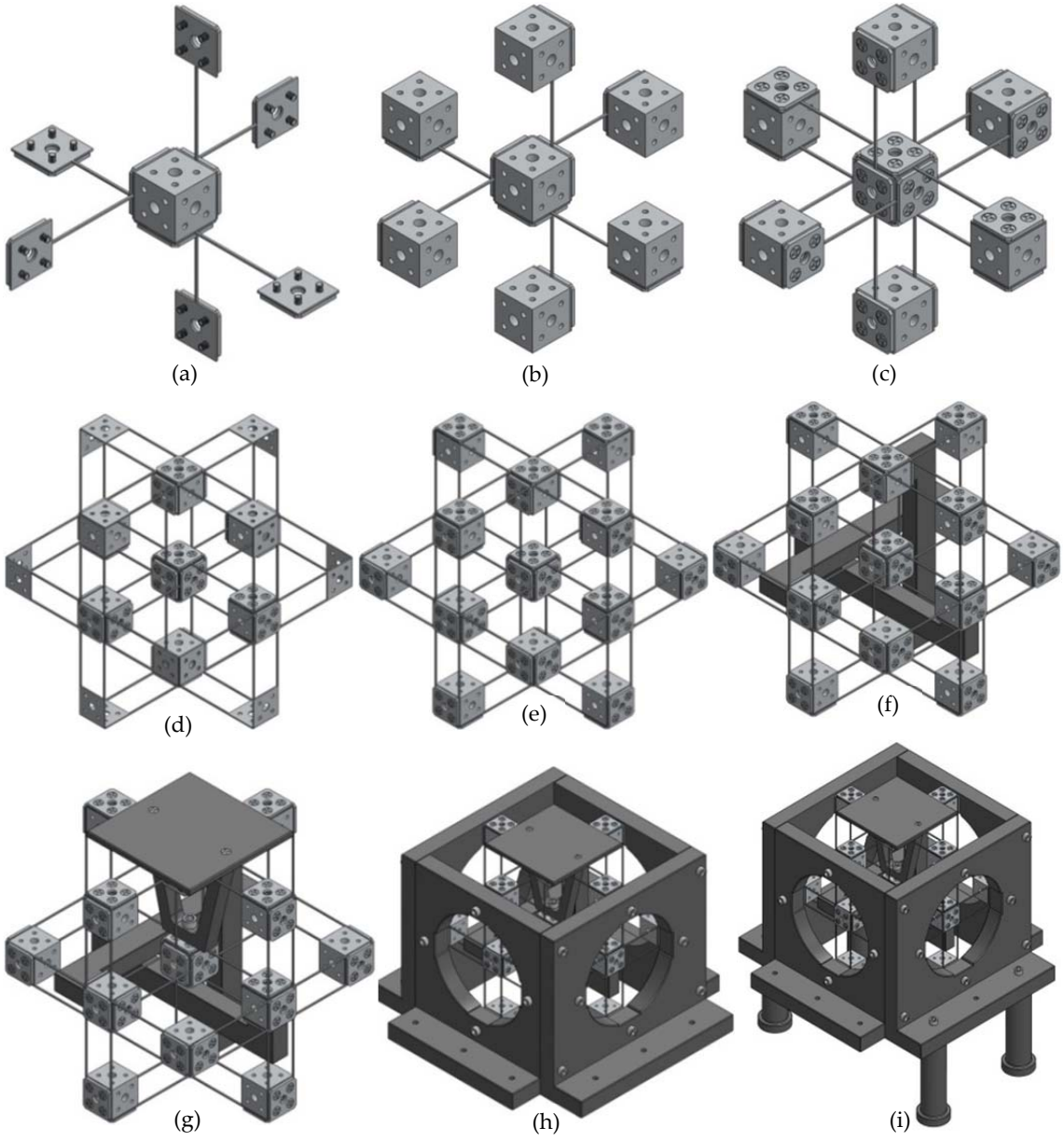

Figure G.2 Assembling process demonstration of the practical design

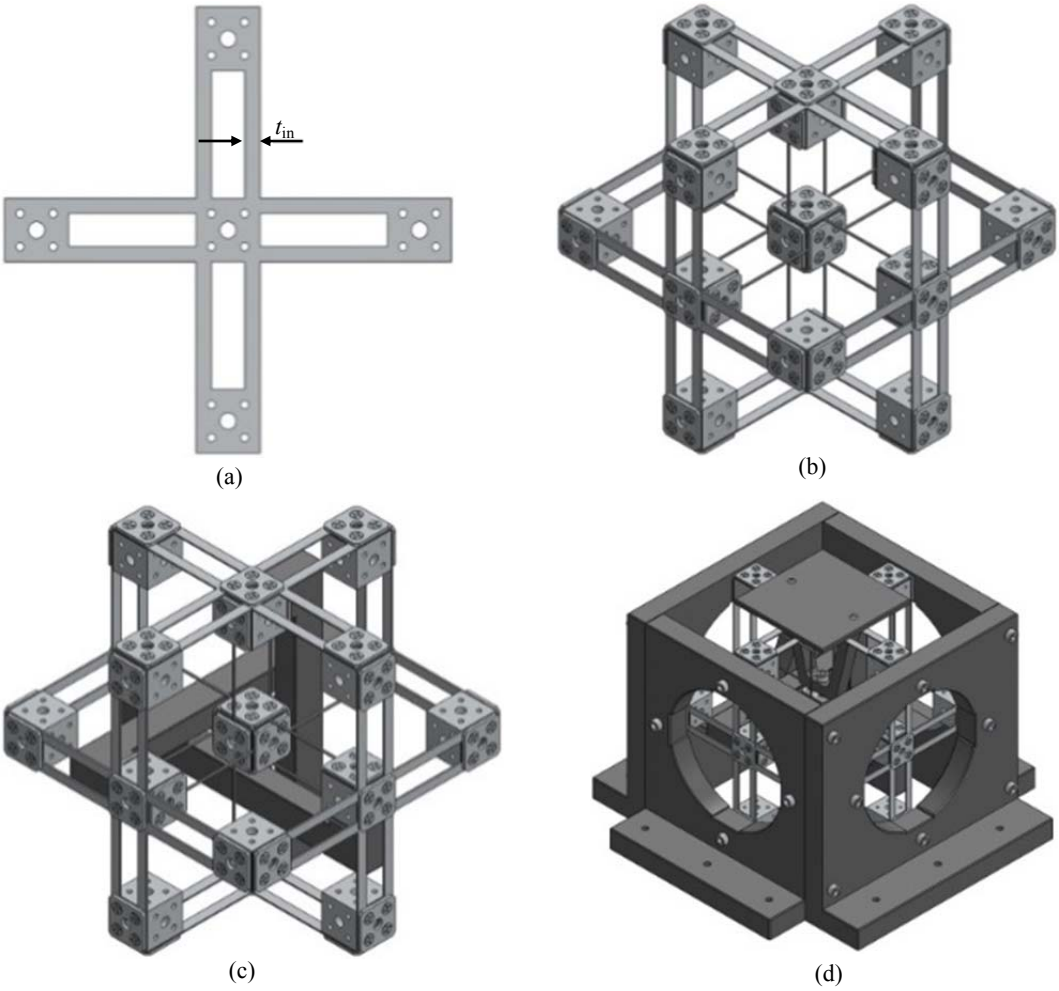

Figure G.3 A symmetric XYZ CPM with larger actuation stiffness

APPENDIX H: CONTROL SYSTEM FOR A SYMMETRIC XYZ CPM

The XYZ CPM (shown in Figure 5.1(h)) can be used in nano-/micro-positioning systems. Such a positioning system can be operated manually or automatically. The positioning system, as shown in Figure 5.6, is a manually operated positioning system (the translations are actuated by three micrometres and the displacements are measured by digital dial gauges). In this Appendix, a semi-closed-loop control system is introduced. This is used to control the XYZ CPM prototype shown in Figure 5.6.

In order to control the output platform of the XYZ CPM prototype to translate along the X_{ms}-, Y_{ms}- and Z_{ms}-axes with a desired resolution, the following three aspects should be emphasized: (a) actuator selection and assembling, (b) displacement sensor selection and assembling, and (c) control strategy. These three aspects are discussed in the following parts of this appendix.

(a) Actuator selection and assembling

According to Equation (3.61), the maximum motion range of the prototype should be smaller than 1.667mm. If a safety factor of two is assigned, the maximum motion range should be less than approximately 0.8mm. It can be calculated, using Equations (5.14), (5.16) and (5.18), that the maximum actuation force is approximately 17 N. Based on the maximum actuation force and motion range, different types of linear actuators, such as voice coils, linear motors and piezoelectric stacks, can be employed to actuate the XYZ CPM prototype. For this example, a cylindrical housed linear voice coil actuator (type number LAH16-23-000A-4E, shown in Figure H.1(a), made by BEI Kimco Company located in Vista, California, USA) can be selected to actuate one of the three translations of the XYZ CPM prototype. Such an actuator can offer a peak force

of 89N and a continuous stall force of 17N, with ±6.08mm motion range and virtually unlimited resolution (the resolution is limited only by the associated displacement sensors). However, three cylindrical frameless linear voice coil actuators (shown in Figure H.1(b), type number: LA30-48-000A, motion range: ±12.7mm, peak force: 445N and continuous stall force: 185N) are actually employed, due to the ready availability of these voice coil actuators.

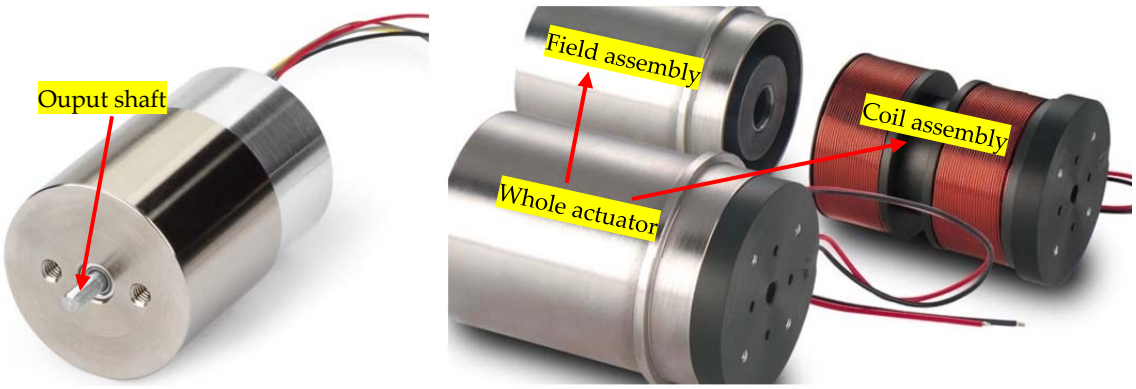

Figure H.1 Linear voice coil actuators: (a) cylindrical housed linear voice coil actuator, and (b) cylindrical frameless linear voice coil actuator

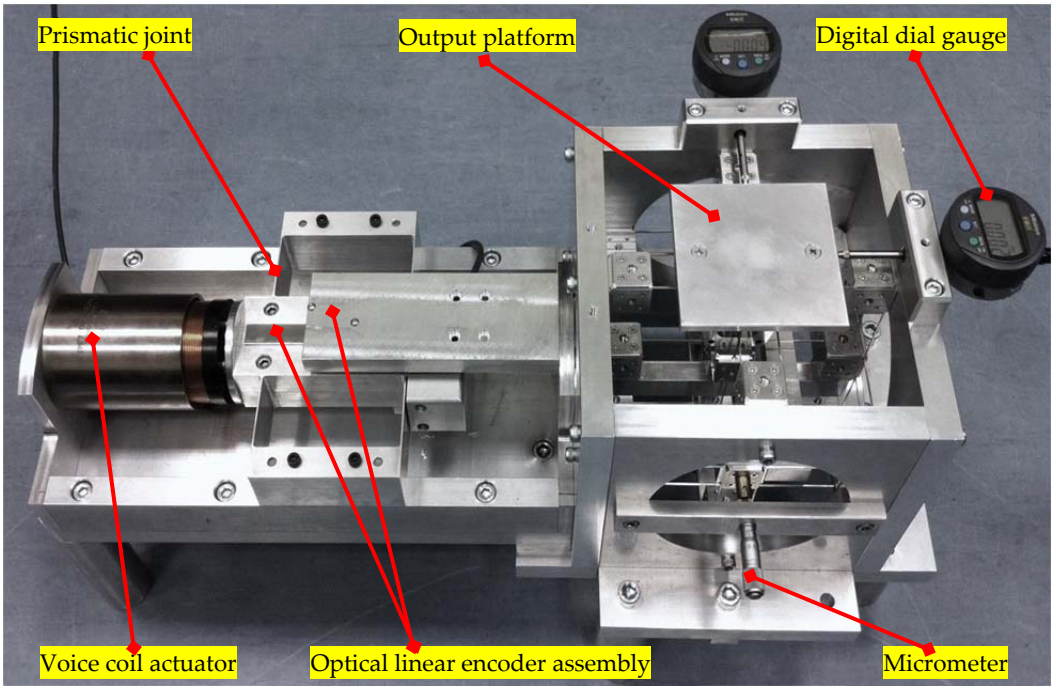

Figure H.2 Demonstration of the assembly of the XYZ CPM prototype, voice coil actuator, prismatic joint, optical linear encoder, micrometre input, and digital dial gauges

It can be seen from Figure H.1(a) that the translation of the output shaft of a cylindrical housed linear voice coil actuator is guided by the actuator, so the output shaft can be connected to an AS of the XYZ CPM prototype directly. However, the translation of the coil assembly of a cylindrical frameless linear voice coil actuator is not guided by the actuator, and the translation cannot be guided by an AS of the XYZ CPM prototype, because the coil assembly is heavy (0.744kg). Therefore, a prismatic joint is designed to guide the translation of the coil assembly of a cylindrical frameless linear voice coil actuator. In this example, a compliant prismatic joint is designed, as shown in Figure H.2.

(b) Displacement sensor selection and assembling

In order to control the output platform of the XYZ CPM prototype at a specific position, the translational displacements of the output platform along the X_{ms}-, Y_{ms}- and Z_{ms}-axes should be measured. The measurement can be achieved by a three-axis displacement sensor or three single-axis displacement sensors.

Three-axis displacement sensors (such as multi-axis laser interferometers) have complex structures. If using such a three-axis displacement sensor to measure the three translations of the XYZ CPM prototype, the XYZ CPM prototype control system will be bulky. If using three single-axis displacement sensors to measure the three translations, each of the three single-axis displacement sensors should be capable of tolerating the displacements of the other two translations.

In this example, the translational displacements of the three ASs of the XYZ CPM prototype are measured instead of the output platform of the XYZ CPM prototype, because the lost motions between the ASs and the output platform are less than 0.63% within a 0.8mm motion range, as studied in Section 5.2.2. Each of the ASs translates only along one specific direction, so the displacement sensor that is used to measure the displacement of the AS does not need to tolerate relative large transverse displacements along the other directions.

Therefore, an accurate optical linear encoder (as shown in Figure H.3) can be used to measure the translational displacement of one of the ASs. Such an optical linear encoder is comprised of a scale and a read head. The read head is used to read the encoded position from the scale. In this example, three optical linear encoders with a 5-nm resolution are used. Each of the optical linear encoders is modelled based on a SIGNUM™ (Renishaw Public Limited Company, Gloucestershire, UK) RSLM/RELM high accuracy linear encoder system (the type number of the read head is A-9572-1514, and the type number of the scale is A-9660-0130). The assembly of one of the optical linear encoders can be seen in Figure H.2.

Figure H.3 Optical linear encoder

(c) Control strategy

As stated in Chapter 5, the cross-axis coupling of the XYZ CPM prototype is tiny compared with the primary translations. Therefore, the three translations of the XYZ CPM prototype can be controlled separately. A control strategy is proposed in this appendix, which can be seen from the diagram flow chart shown in Figure H.4. It can also be seen from the diagram flow chart that the three translations of the XYZ CPM prototype are controlled separately, based on the same principle, so that only the control strategy relating to the X-axis translation is detailed. The procedure of the control strategy of the X-axis translation is shown in the steps below.

i. Input the required translational displacements of the XYZ CPM along the X_{ms}-, Y_{ms}- and Z_{ms}-axes.
ii. Calculate the lost motion along the X_{ms}-axis based on the required translational displacements, using Equation (5.13).
iii. Obtain the total X_{ms}-axis input, which equals the sum of the required displacement and lost motion along the X_{ms}-axis. The total X_{ms}-axis input is the position reference to be used by a dSPACE-based PID controller.
iv. Read the displacement of the X_{ms}-axis prismatic joint from the displacement sensor, and input the displacement to the dSPACE-based PID controller to act as the feedback position signal.
v. Calculate the output value of the dSPACE-based PID controller, based on both the total X_{ms}-axis input and the sensor reading.
vi. Amplify the output value of the dSPACE-based PID controller using the X_{ms}-axis driver.
vii. Use the amplified output of the driver to power the X_{ms}-axis actuator.
viii. Actuate the X_{ms}-axis prismatic joint and the AS-X, using the actuator.
ix. Repeat Steps (iv) – (viii), until the sensor reading matches the total X_{ms}-axis input.

Based on the statements above, a part of the described control system is set up as shown in Figure H.5, which is employed to control the X_{ms}-axis translation of the XYZ CPM prototype. Note that the Y_{ms}- and Z_{ms}-axes translations of the XYZ CPM prototype can be controlled by the micrometres and digital dial gauges.

Experimental tests are conducted on the XYZ CPM prototype system, and the results are shown in Figure H.6 – Figure H.8. It can be seen from the figures that the maximum error is less than 1%, over a 0.8mm motion range.

This semi-closed-loop control system cannot achieve a very high precision. If a nano-precision positioning system is desired, a closed-loop control system should be designed, with consideration of environment conditions such as

temperature and signal noise.

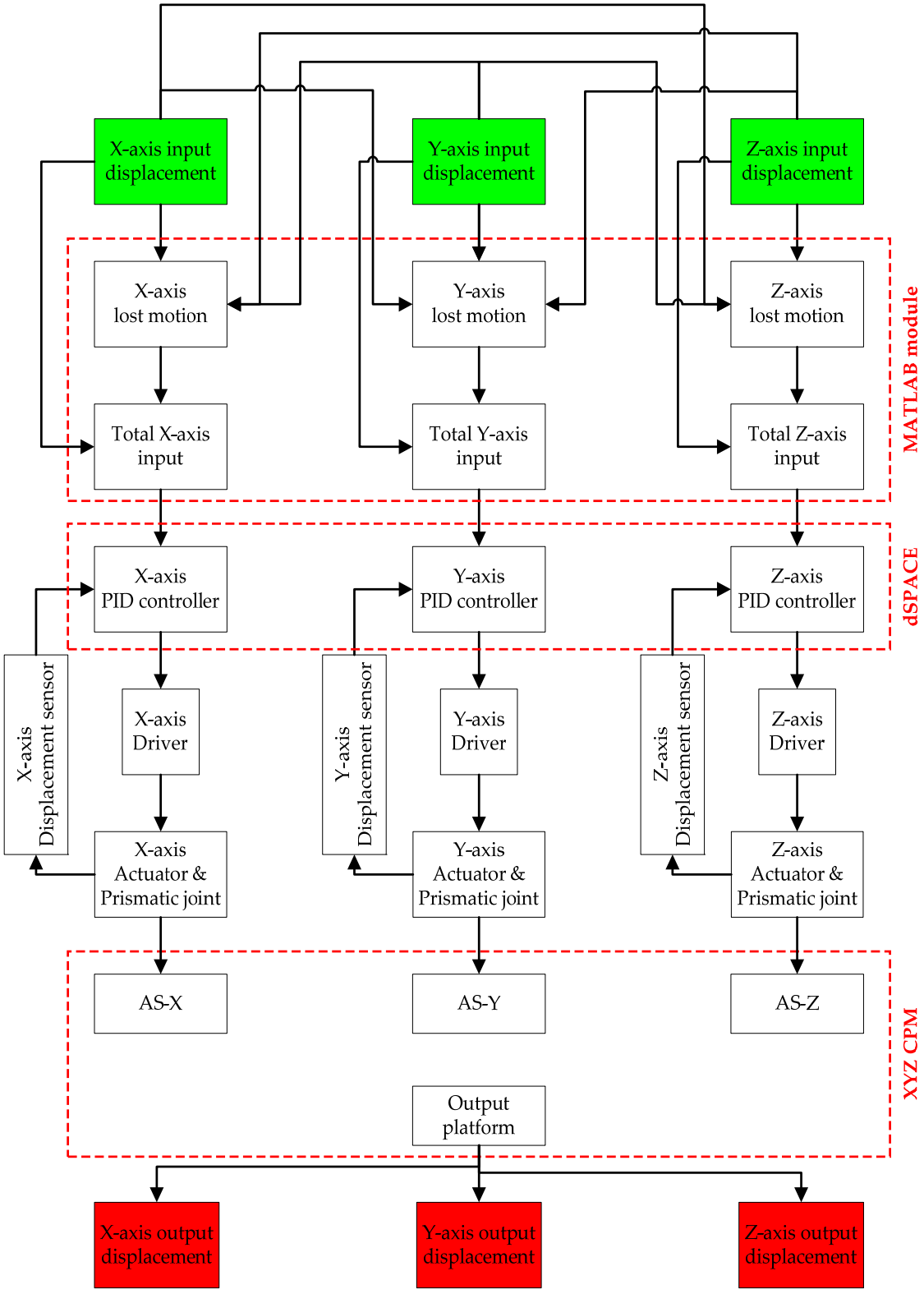

Figure H.4 Control principle of the X-axis displacement

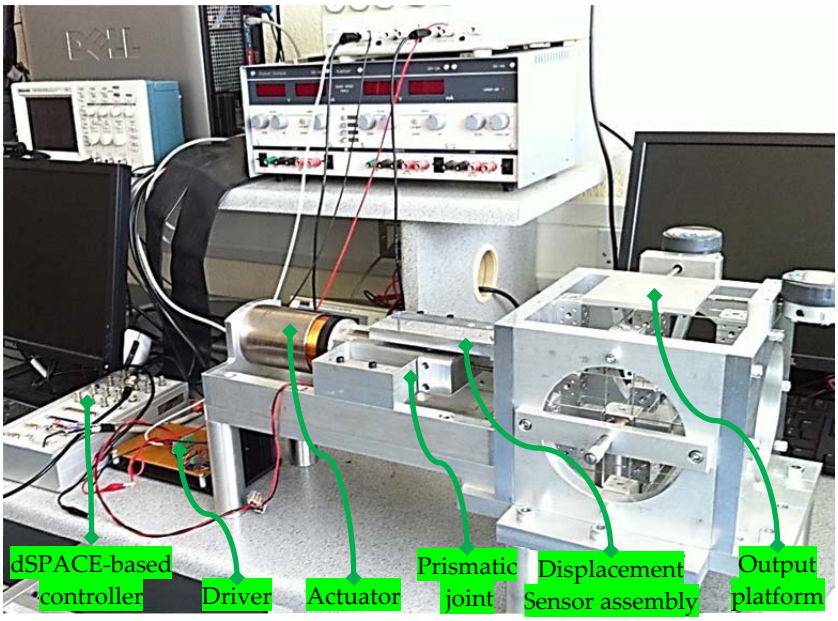

Figure H.5 Control system of a symmetric XYZ CPM

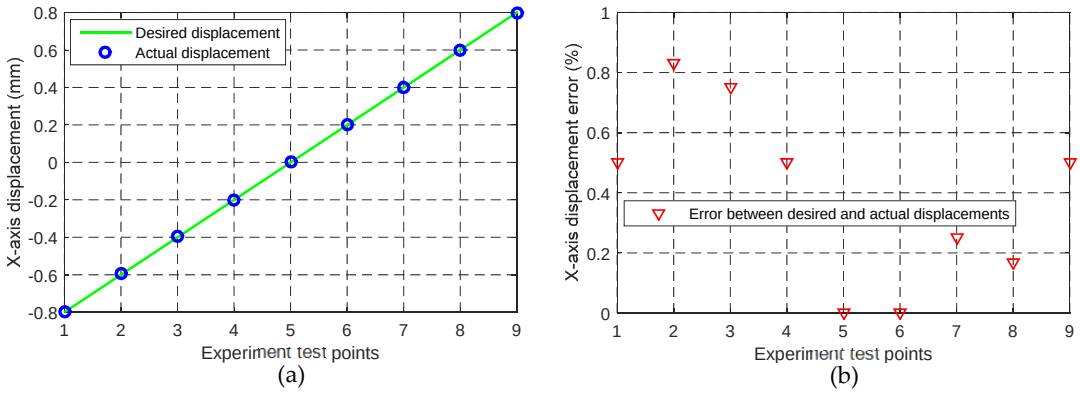

Figure H.6 Experimental results when the translational displacements along the Y_{ms}- and Z_{ms}-axes are both zero: (a) X-axis displacements, and (b) X-axis displacement errors

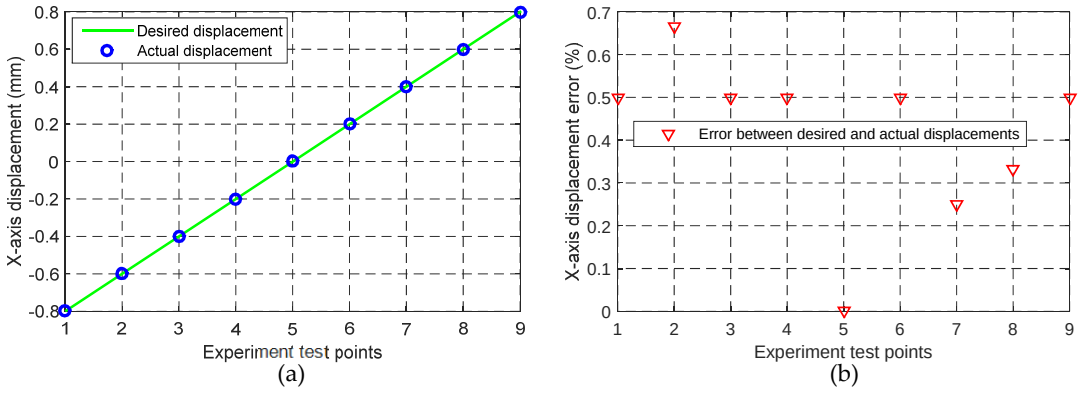

Figure H.7 Experimental results when the translational displacements along the Y_{ms}- and Z_{ms}-axes are 0.800mm and zero, respectively: (a) X-axis displacements, and (b) X-axis displacement errors

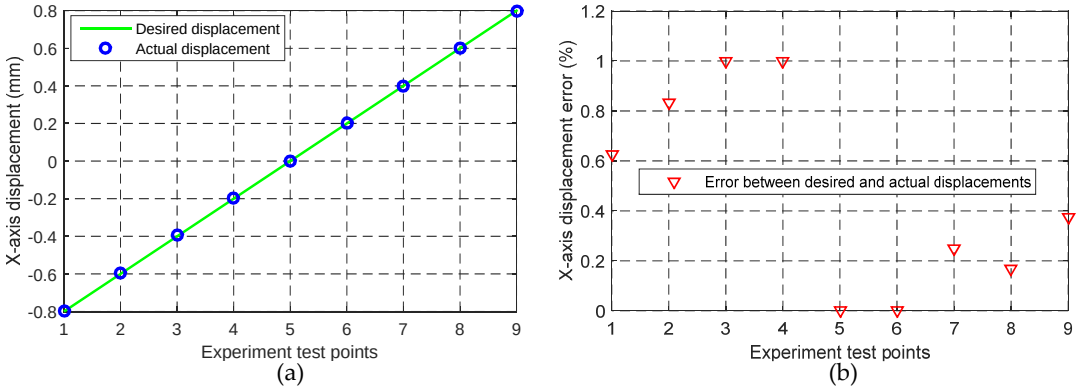

Figure H.8 Experimental results when the translational displacements along the Y_{ms}- and Z_{ms}-axes are both 0.800mm: (a) X-axis displacements, and (b) X-axis displacement errors